STUDIES ON
LASER INDUCED PHOTOTHERMAL PHENOMENA
IN SELECTED ORGANIC COMPOUNDS AND FULLERENES

BINDHU C.V.

THESIS SUBMITTED
IN PARTIAL FULFILMENT OF THE REQUIREMENTS
FOR THE DEGREE OF
DOCTOR OF PHILOSOPHY

LASER DIVISION
INTERNATIONAL SCHOOL OF PHOTONICS
COCHIN UNIVERSITY OF SCIENCE AND TECHNOLOGY
COCHIN - 682 022

JUNE 1998

Dedicated to
My Beloved Parents and Brother

INTERNATIONAL SCHOOL OF PHOTONICS
COCHIN UNIVERSITY OF SCIENCE AND TECHNOLOGY

Dr. C. P. GIRIJAVALLABHAN
PROFESSOR & DIRECTOR

COCHIN - 682 022
Kerala, India

CERTIFICATE

Certified that the research work presented in the thesis entitled, ***" Studies on Laser induced Photothermal Phenomena in Selected Organic Compounds and Fullerenes"*** is based on the original workdone by Ms. Bindhu C.V under my guidance in the International School of Photonics, Cochin University of Science & Technology, Cochin - 682 022 and has not been included in any other thesis submitted previously for the award of any degree.

Cochin - 682 022
22 June, 1998

Prof. C.P.Girijavallabhan

Tel. Off : (0484) 532848 Res : (0484) 346869 Fax : 0091-484-532495
Telex : 885 - 5019 CUIN Email : root @ cochin. ernet. in

DECLARATION

Certified that the work presented in the thesis entitled, "***Studies on Laser Induced Photothermal Phenomena in Selected Organic Compounds and Fullerenes***" is based on the original workdone by me under the guidance of Prof. C.P.Girijavallabhan in the International School of Photonics, Cochin University of Science & Technology, Cochin - 682 022, and has not been included in any other thesis submitted previously for the award of any degree.

CUSAT, Cochin- 682 022
22 June, 1998

Bindhu C.V

ACKNOWLEDGMENTS:

It is with great pleasure I express my sincere indebtedness and thankfulness to Prof. C.P.Girijavallabhan, Director, International School of Photonics, CUSAT for his efficient supervision, motivation and proficient advice all through my Ph.D. programme. I am strongly obliged to him for introducing me into this subject.

I am equally indebted to Prof. V. P. N. Nampoori for his keen interest and invaluable support in this work. I am very much grateful to him for the productive discussion and suggestions that were essential for the successful completion of this thesis.

I wish to acknowledge Prof. K. Babu Joseph (Former Head, Department of Physics, CUSAT) and Prof. M. Sabir, Head of the Department of Physics, CUSAT for providing the library facilities.

I am also thankful to Prof. V. M. Nandakumaran and Dr. P. Radhakrishnan for their encouragement.

My sincere thanks to:
Sri. P. Madhavan and Dr. Sivadas, CIFT, Cochin who have helped me a lot by providing the facilities for salinity and conductivity measurements in seawater.
Prof. Jacob Chacko, Head of the Department of Chemical Oceanography, CUSAT and Mr. Daniel Munga for their help in taking the absorption spectra.
Dr. P. V. Suresh and Dr. Edwin Xavier for the seawater and synthetic seawater samples.

Thanks are also due to Dr. Reji Philip and (late) Dr. P.Sathy for their help in the early stages of the present work.

Thanks to all the research scholars of ISP with special regards to Bindu, Seena, Shelly, Binoy and Pramod for their cooperation.

With deep sense of gratitude I thank Sudha Valavi and Preetha for the numerous helps they have rendered to me.

Financial assistance from University Grants Commission, Government of India in the form of junior as well as senior research fellowships is gratefully acknowledged. This work was partially supported by Department of Science & Technology, Government of India.

Achamma teacher has shown constant interest in my research career. I sincerely thank her.

With warm appreciation I thank Riju and Geetha for all that they have done for me.

No words can exhibit my gratefulness to my friend and colleague Hari. Whatever I have accomplished of any value in the long research career I owe to him. I am greatly indebted to him for his everlasting patience and continuing support.

(Bindhu)

Preface

Everything that we know about light comes from its interaction with matter. The effects produced by the interaction of high-power laser beams with matter is of considerable interst. Laser radiation from the ultraviolet to the infrared interacts primarily with the electrons of an atom or atomic system. Furthermore, the frequencies and energies associated with this reasonably extensive band of electromagnetic radiation do not induce nuclear disturbances, or even affect the energy levels of the inner core electrons of an atom at modest power levels. These photons do however readily interact with the outer valence electrons of the atoms. Clearly, the optical properties of any material will be mainly affected by the nature of its outermost electrons.

In the pre-laser era it was difficult to believe that the optical properties of a medium depend upon the intensity of the radiation incident on it. The basis for this conclusion is that the electric field strength associated with the conventional light sources used before the advent of lasers was much smaller than (10^3 V/cm) the field sttrengths of atomic or interatomic fields ($\simeq 10^7 - 10^{10}$ V/cm). The radiation with such low intensity is not able to affect atomic fields to the extent of changing optical parameters. The invention of laser in 1960 was a turning point. The high degree of coherence of the laser radiation provides high spatial concentration of optical power. With the availability of the femtosecond lasers it has become possible to get extremely high peak powers $\simeq 10^{18}$ W/cm^2). At such high fields, the relationship between electric polarization **P** and the electric field strength **E** ceases to be linear and several nonlinear effects begin to occur. Nonlinear absorption, a branch of nonlinear optics, refers to the interaction between radiation and matter accompanied by absorption of more than one photon. Nonlinear absorption has acquired great importance after the invention of high power lasers.

One of the objectives of the present work is to investigate the nonlinear absorption processes occurring in fullerene, selected organic solvents and laser dyes. Fullerenes and laser dyes were chosen because of their highly nonlinear behaviour. Fullerenes, the most beautiful among molecules, offer fascinating field of research owing to their significant structural properties. As toluene, benzene and carbon disulphide are the most widely used solvents for fullerenes, it seems important to study the nonlinear properties of these liquids as well. Like fullerenes, laser dyes also possess highly delocalized π electrons which are responsible for their nonlinear absorption. Dye lasers were the fulfillment of an experimenter's pipe dream - to have a laser that is easily tunable over a wide range of wavelengths. A better understanding

of the photophysical properties of laser dyes can significantly enhance the development and technology of dye lasers. We studied the nonlinear absorption properties of two rhodamine dyes to have some insight into their nonlinear optical properties.

When a medium is illuminated with laser raddiation, some of the incident energy will be absorbed by the molecules in the ground state, getting excited to higher energy states in the process. Following the absorption of a photon, the excess energy of a molecule can be dissipated in one of three ways. The molecule may (1) react photochemically, in which case the excess energy is used to break chemical bonds; (2) emit light, via fluorescence or phosphorescence, thereby reducing the internal energy; (3) or relax, in which case the internal (electronic or vibrational) energy of the molecule is converted to translational or thermal energy. It is the latter form of energy that is detected in photothermal spectroscopy. Absorption of a laser beam followed by nonradiative de-excitation in the sample results in the increase of temperature of the irradiated region. Typically, the sample is illuminated with a pulsed or chopped light source, producing periodic fluctuations in pressure, temperature or density with sample. By examining the magnitude of these fluctuations as a function of wavelength of the incident light, it is possible to obtain a photothermal spectrum of the sample under study.

The thermal fluctuations produced by nonradiative relaxations are typically monitored in one of two ways. If the compression-rarefaction pulse produced by the transient temperature jump is measured directly with a pressure transducer, such as a microphone or piezoelectric ceramic, the technique is termed optoacoustic or photoacoustic (PA) spectroscopy. Alternately, the temperature/pressure gradient may be probed optically, since the resulting density change will also produce a change in refractive index. Since the transient refractive index forms an effective lens, this technique is often called thermal lensing (TL), or thermal blooming spectroscopy.

Thermal lens formation results from absorption of the laser light. The absorption, which may be extremely weak, produces excited-state molecules which subsequently decay back to ground states. When the decay involves radiationless processes, localized temperature increases are produced in the sample. Since the refractive index depends on temperature, there is a resulting spatial variation of refractive index which is equivalent to the formation of a lens within the medium. For most liquids, the temperature coefficient of refractive index, dn/dT, is negative. Insertion of the liquid in a Gaussian-shaped beam therefore produces a concave lens and the beam diverges, or "blooms". Thus the thermal lens phenomenon is sometimes referred to as "thermal blooming". This thermal lens effect has been shown to

be a valuable spectroscopic tool. It has been used in the study of weak spectral transitions as well as for quantum yield measurements, lifetime measurements, for the study of thermal properties of various materials and in investigations of the rate and yield of a photochemical reaction, and of excited-state polarizabilities. The TL effect can be observed using moderate laser intensities in media with absorption length as low as $10^{-7}cm^{-1}$. Indeed, it holds great promise in many areas where sensitive spectroscopic probes are needed.

The PA effect is essentially an energy-conversion process i.e, light energy is converted into acoustic energy. On irradiation with an intensity modulated laser beam, a part of the absorbed energy is converted into translational energy of the molecules by nonradiative relaxation processes. This deexcitation channel finally results in the periodic heating of the sample which in turn results in the production of a pressure wave. Thus pulses of optical quanta are converted into acoustic pulses. The amplitudes of the acoustic signal obviously depends on the amount of energy absorbed. Of the several configurations of PA measurements, pulsed PA is the most sensitive as the high power delivered by a pulsed laser can generate acoustic signals of considerable magnitudes.

These thermo-optic techniques can be effectively utilized in nonlinear spectroscopy. We adopted both TL and PA techniques for the perusal of nonlinear properties of fullerenes and laser dyes. Another objective of the present research is to exploit the sensitivity and viability of TL and PA methods to determine absolute fluorescence quantum yield of laser dyes and thermal diffusivity of certain organic liquids.

The present thesis consisting of 9 chapters, describes the details of the work carried out and results obtained. A chapterwise summary of the thesis is given below:

Chapter 1 which is of an introductory nature, is divided into four sections. The first two sections discuss the basics of TL and PA techniques and a brief account of the theory underlying the TL and PA spectroscopy. The important aspects of fluorescence spectroscopy with particular emphasis on photophysical properties of laser dyes are presented in section 1.3, while a brief account of nonlinear absorption processes forms section 1.4.

Chapter 2 presents a detailed account of the experimental setups employed for the present series of studies. The thermal lens effect is studied using both continuous wave laser (CWTL) and pulsed laser (PTL). 532 nm radiation from a Q-switched pulsed Nd:YAG laser was used as the excitation beam in PTL experiments whereas chopped Argon ion laser beam was used in CWTL. He-Ne laser is used as the probe laser in both the TL configuration. Pulsed Photoacoustics (PPA) studies were carried out using the 532 nm radiation pulses from Q-switched Nd:YAG laser. Fluorescence experiments were also performed. For detection

and analysis of TL, PA and fluorescence signals, different instruments like Lock-in amplifier, Boxcar averager, Digital Storage Oscilloscope, Monochromator-PMT assembly etc. were used and the details of these are given in this chapter.

Chapter 3 presents an important application of TL for thermal diffusivity measurements. Among the various techniques, the thermal lens method is an excellent approach for the investigation of thermal properties. Thermal diffusivity is an important parameter in heat flow studies. It measures the rate of heat diffusion and like the optical absorption coefficient, it is unique for each material. We adopted pulsed double beam thermal lens method for thermal diffusivity measurements in certain organic liquids. We have also determined thermal diffusivity of sea water taken from different depths of sea.

Chapter 4 gives a detailed account of the investigation of nonlinear absorption processes occurring in laser dyes Rhodamine B and Rhodamine 6G using pulsed dual beam thermal lens method. In a typical dye laser system, several nonlinear effects like two-photon absorption, three photon absorption, excited state absorption etc. can occur in the pumped region of the dye soluiton since the pump intensities are normally of the order of $10^8 \mathrm{Wcm}^{-2}$ or higher. These processes reduce the effective stimulated emission cross section of laser dyes significantly. With PTL method we have noticed two photon absorption, three photon absorption along with excited state absorption processes in these laser dyes. We have also observed that Q_f decreases in the region of TPA. These aspects are discussed in detail in this chapter.

Chapter 5 focuses on one of the main applications of thermal lens effect, i.e, determination of fluorescence quantum yield (Q_f) of organic dyes. The Q_f of organic dyes is one of the important parameters in selecting efficient laser media. In this chapter we demonstrate that TL techniques can be very effectively employed to study the optical processes in highly fluorescing material. The TL method offers significant advantages over conventional methods because the absolute values of Q_f can be measured directly and no standard sample is required in this case. We determined Q_f of selected laser dyes like Rhodamine B and Rhodamine 6G using both CWTL and PTL. The fluorescence efficiency of organic dyes depends on the nature of excitation source, excitation wavelength, solvent used and concentration of the sample. We have studied the above aspects extensively and these are discussed in a detailed manner in this chapter. A comparison between PTL and CWTL is also attempted.

Chapter 6 gives an account of determination of Q_f of laser dyes using PA technique. For fluorescent materials, PA detection is sensitive to the total fluorescence emission. Any change in the emission characteristics will affect the PA signal. PA detection is very effective if small variations in Q_f of highly fluorescent matrerilas are to be studied because the change

in PA signal will be relatively much larger than that occurring in the fluorescence emission. A comparative study is made here between TL and PA studies in the determination of Quantum yiled.

Discovery of high molecular weight stable carbon clusters called fullerenes opened up a new and exciting field of research. It became possible to synthesise and isolate them in macroscopic quantities using simple and straight forward methods. It has been found that C_{60} and C_{70} exhibit optical nonlinearities leading to optical limiting. The optical limiting behaviour of C_{60} and C_{70} solutions in toluene is studied in **Chapter 7**. The causes for optical limiting are Reverse Saturable Absorption (RSA), Excited State Absorption (ESA), Two Photon Absorption (TPA), Nonlinear Scattering (NLS) etc. Using PA and TL techniques we have attempted to elucidate the role of these processes in the case of optical limiting in C_{60} and C_{70}.

Pulsed photoacoustic technique is an effective technique to study nonlinear processes in organic liquids like benzene, toluene, carbon disulphide etc. Laser ablation processes in liquid benzene, toluene and carbon disulphide have been investigated by pulsed photoacoustic technique using 532 nm radiation from a frequency doubled Q-switched Nd:YAG laser. These studies form the contents of **chapter 8**. The nature of variation of photoacoustic signal amplitude with laser energy clearly indicates that different phenomena like dissociation and ionisation are involved in the generation of photoacoustic effect and these are discussed in detail.

Chapter 9 gives the overall summary and conclusions drawn from the series of investigations presently carried out.

Part of the results contained in this thesis has been published/presented in the reputed international/national journals and symposium proceedings and the remaining results are communicated/to be communicated, the details of which are given below.

Papers published in International/National Journals:

[1] Thermal diffusivity measurements in seawater using transient thermal lens calorimetry
C. V. Bindhu, S. S. Harilal, V. P. N. Nampoori and C. P. G. Vallabhan,
Current Science **74**, 764-769 (1998).

[2] Thermal diffusivity measurements in organic liquids using thermal lens calorimetry,
C. V. Bindhu, S. S. Harilal, V. P. N. Nampoori and C. P. G. Vallabhan,
Optical Engineering (in press) (1998).

[3] Measurement of fluorescence quantum yield of Rhodamine B laser dye using thermal lens technique

C. V. Bindhu, S. S. Harilal, R. C. Issac, V. P. N. Nampoori and C. P. G. Vallabhan, *Journal Physics D: Applied Physics* **29**, 1074-1079, (1996).

[4] Determination of Fluorescence quantum yield of Rhodamine B laser dye by pulsed photoacoustic calorimetry

C. V. Bindhu, S. S. Harilal, R. C. Issac, V. P. N. Nampoori, and C. P. G. Vallabhan, *Modern Physics Letters B* 10, 1103-1110 (1996).

[5] Anomalous variation of thermal lens signal with concentration from rhodamine B in methanol solution

C. V. Bindhu, S. S. Harilal, R. C. Issac, V. P. N. Nampoori and C. P. G. Vallabhan, *Pramana - Journal of Physics*, **44**, 225-229, (1995).

[6] Observation of two photon absorption in toluene using pulsed photoacoustic technique

C. V. Bindhu, S. S. Harilal, R. C.Issac, V. P. N. Nampoori, and C. P. G. Vallabhan, *Pramana - Journal of Physics*, **44**, 231-235 (1995).

[7] Laser induced thermal lens effect in Rhodamine B - Signature of two photon absorption,

C. V. Bindhu, S. S. Harilal, R. C. Issac, V. P. N. Nampoori, and C. P. G. Vallabhan, *Modern Physics Letters B*, **9**, 1471-1477 (1995).

[8] A study of photoacoustic effect and optical limiting in the solution of C60 in toluene

R. C. Issac, S. S. Harilal, **C. V. Bindhu**, V. P. N. Nampoori, and C. P. G. Vallabhan, *Modern Physics Letters B*, **10**, 61-67 (1996).

[9] Photoacoustic saturation and optical limiting studies in C70

R. C. Issac, S. S. Harilal, **C. V. Bindhu**, G. K. Varier, V. P. N. Nampoori, and C. P. G. Vallabhan,

Optical Engineering, **36** 332-336 (1997).

[10] Study of laser ablation in liquids using pulsed photoacoustic technique

S. S. Harilal, R. C. Issac, **C. V. Bindhu**, V. P. N. Nampoori, and C. P. G. Vallabhan, *Modern Physics Letters B* **10**, 1053-1057 (1996).

[11]. Observation of multiphoton process in liquid CS_2 using pulsed photoacoustic technique

S. S. Harilal, R. C. Issac, **C. V. Bindhu**, V. P. N. Nampoori and C. P. G. Vallabhan, *Modern Physics Letters B*, **9**, 871-876.

[12]. Influence of ambient gas on the temperature and density of laser produced carbon plasma

S. S. Harilal, **C. V. Bindhu**, V. P. N. Nampoori, and C. P. G. Vallabhan,

Applied Physics Letters, **72**, 167-169 (1998)

[13]. Time evolution of electron density and temperature of laser produced YBa2Cu3O7 plasma

S. S. Harilal, **C. V. Bindhu**, V. P. N. Nampoori, and C. P. G. Vallabhan,

Applied Physics B : Lasers and Optics , **66**, 633-638.

[14]. Electron density and temperature measurements of laser induced YBa2Cu3O

S. S. Harilal, **C. V. Bindhu**, V. P. N. Nampoori, and C. P. G. Vallabhan,

Applied Spectroscopy **52(3)** (March issue) (in press) (1998).

[15].Time resolved study of CN band emission from plasma generated by laser irradiation of graphite

S. S. Harilal, **C. V. Bindhu**, V. P. N. Nampoori, and C. P. G. Vallabhan,

Spectrochimica Acta A: Molecular Spectroscopy, **53**, 1527-1537, (1997).

[16]. Optical emission studies of C2 species laser produced plasma from carbon

S. S. Harilal, R. C. Issac, **C. V. Bindhu**, V. P. N. Nampoori and Vallabhan,

*Journal of Physics D: Applied Physics***30**, 1703-1709, (1997).

[17].Time resolved analysis of C2 emission from a laser induced graphite plasma in helium atmosphere

S. S. Harilal, R. C. Issac, **C. V. Bindhu**, V. P. N. Nampoori and C. P. G. Vallabhan,

Japanese Journal of Applied Physics, **36**, 134-138 (1997).

[18]. Spatial analysis of C2 band emission from laser produced plasma

S. S. Harilal, R. C. Issac, **C. V. Bindhu**, V. P. N. Nampoori and C. P. G. Vallabhan,

Plasma Sources Science and Technology **6**, 317-322 (1997).

[19]. Fine structure in the time of flight distribution of C2 in laser produced plasma from graphite

S. S. Harilal, R. C. Issac, **C. V. Bindhu**, V. P. N. Nampoori and C. P. G. Vallabhan,

Pramana - Journal of Physics, **49**, 317-322 (1997).

[20].Anomalous profile of self reversed resonance Ba+ line in laser produced YBa2Cu3O7 plasma in air

R. C. Issac, S. S. Harilal, **C. V. Bindhu**, G. K. Varier, V. P. N. Nampoori and C. P. G. Vallabhan,

Spectrochimica Acta B: Atomic spectroscopy, **52**, 1791-1799 (1997).

[21]. Electron density and temperature measurements in laser produced carbon plasma

S. S. Harilal, **C. V. Bindhu**, R. C. Issac, V. P. N. Nampoori and C. P. G. Vallabhan,

Journal of Applied Physics, **82**, 2140-2146 (1997).

[22]. Emission and expansion dynamics of C2 species from laser produced carbon plasma

S. S. Harilal, R. C. Issac, **C. V. Bindhu**, V. P. N. Nampoori and C. P. G. Vallabhan,

Journal of Applied Physics, **81** 3637-3643 (1997).

[23]. Spatial and temporal evolution of C2 species in the laser induced plasma from graphite

S. S. Harilal, R. C. Issac, **C. V. Bindhu**, V. P. N. Nampoori and C. P. G. Vallabhan,

Journal of Applied Physics, **80**, 3561-3565 (1996).

[24]. Spatial and time resolved analysis of CN bands in the laser induced plasma from graphite

S. S. Harilal, R. C. Issac, **C. V. Bindhu**, V. P. N. Nampoori and C. P. G. Vallabhan,

Pramana - Journal of Physics, **46**, 145-151 (1996).

[25] Application of laser deflection technique for the study of diffusion process in electrolyte solutions

A. Kurien, **C. V. Bindhu**, S. S. Harilal, V. P. N. Nampoori, and C. P. G. Vallabhan,

Pramana - Journal of Physics, **43**, 401-405 (1994).

[26]. Pulsed photoacoustic studies in toluene

S. S. Harilal, R. C. Issac, **C. V. Bindhu.**, V. P. N. Nampoori and C. P. G. Vallabhan,

J. of Pure and Applied Ultrasonics, 17, 72-75 (1995).

Papers communicated/to be communicated:

[1] Multophoton absorption studies in rhodamine 6G laser dye in three solvents using transient thermal lens technique (communicated to *Optics Communications*)

[2] Solvent effects on fluorescence quantum yield of rhodamine 6G studied using thermal lens calorimetry (communicated to *Research in Chemical Intermediates*)

[3] Nonlinear absorption studies in rhodamine B by pulsed dual beam thermal lens technique (to be communicated to *Journal of Physics B*)

[4] Thermal lens measurements in C_{60} solutions (to be communicated to *Journal of Applied Physics*)

Papers presented at National Symposia:

[1] Use of thermal lens technique for the study of two photon processes in rhodamine B laser dye,

C. V. Bindhu, T. M. A. Rasheed, V. P. N. Nampoori and C. P. G. Vallabhan,

Proceedings of the National Laser Symposium, CAT, Indore, India, 161-162 (1994)

[2] Spectral features of ASE from rhodamine B laser dye pumped by 532 nm excitation

C. V. Bindhu, S. S. Harilal, R. C. Issac, V. P. N. Nampoori and C. P. G. Vallabhan,

Proceedings of the National Laser Symposium, IRDE, Dehradun, India, 237 (1995).

[3] Measurement of absolute fluorescence quantum yield of Rhodamine B solution using thermal lens technique

C. V. Bindhu, S. S. Harilal, R. C. Issac, V. P. N. Nampoori and C. P. G. Vallabhan,

Proceedings of the National Laser Symposium, IRDE, Dehradun, India, 237 (1995).

[4] Thermal lens calorimetry in rhodamine B solutions

C. V. Bindhu, S. S. Harilal, V. P. N. Nampoori and C. P. G. Vallabhan,

Proceedings of the National Laser Symposium at PRL, Ahmedabad, India, 110-111 (1997).

[5] Thermal diffusivity measurements in some organic liquids using transient thermal lens calorimetry

C. V. Bindhu, S. S. Harilal, V. P. N. Nampoori and C. P. G. Vallabhan,

Proceedings of the National Laser Symposium at PRL, Ahmedabad, India, 124-125 (1997).

[6] Laser induced plasma from graphite: Time dependence of vibrational temperature,

S. S. Harilal, R. C. Issac, **C. V. Bindhu**, V. P. N. Nampoori, and C. P.G. Vallabhan,

Proceedings of the National Laser Symposium at IRDE, Dehradun, India, 265-66 (1995).

[7] Spectral features of laser induced fluorescence emission from C70

S. S. Harilal, R. C. Issac, **C. V. Bindhu**, V. P. N. Nampoori and C. P. G. Vallabhan,

Proceedings of the National Laser Symposium at IRDE, Dehradun, India, 235-36 (1995).

[8]Characterization of C2 emission from laser ablated carbon plasma,

S. S. Harilal, R. C. Issac, **C. V. Bindhu**, V. P. N. Nampoori and C. P. G. Vallabhan,

Proceedings of the National Laser Symposium at BARC, Bombay, India, H15-16 (1996).

[9] Pulsed photoacoustic studies of laser ablation in liquids,

S. S. Harilal, R. C. Issac, **C. V. Bindhu**, V. P. N. Nampoori and C. P. G. Vallabhan,

Proceedings of Trombay Symposium on Radiation and Photochemistry at BARC, Bombay, India, 191-93 (1996).

[10] Temporal and spatial evolution of laser ablated carbon clusters from graphite plasma,
S. S. Harilal, R. C. Issac, **C. V. Bindhu**, V. P. N. Nampoori and C. P. G. Vallabhan,
Proceedings of the International Conference on Spectroscopy: Perspectives and Frontiers at BARC, Bombay, India, 146 (1996).

[11] Time evolution of electron temperature and density of laser produced plasma from YBa2 Cu3O7
S. S. Harilal, **C. V. Bindhu**, V. P. N. Nampoori and C. P. G. Vallabhan,
Proceedings of the National Laser Symposium at PRL, Ahmedabad, India, 221-222 (1997).

[12] Effect of ambient gas on the temperature and density of laser induced carbon plasma,
S. S. Harilal, **C. V. Bindhu**, V. P. N. Nampoori, and C. P. G. Vallabhan,
Proceedings of National Symposium on Plasma Science & Technology at IPR, Ahmedabad, India, OPI-03 (1997).

Contents

1 General Introduction **1**
1.1 Thermal Lens Spectroscopy 4
1.1.1 Thermal Lens Theory 5
1.1.2 Sensitivity and Temporal Characteristics 8
1.1.3 Measurement Approaches 10
1.1.4 Important Applications of Thermal lens 13
1.2 Photoacoustic Spectroscopy 16
1.2.1 Principle of Operation 16
1.2.2 Generation of Acoustic Waves 17
1.2.3 PA Generation 19
1.2.4 Simple Theory for Direct PA Generation 21
1.2.5 Simple Theory for Indirect PA Generation 22
1.2.6 PA Detection 25
1.2.7 Applications of PA Effect 25
1.3 Photophysical Properties of Laser dyes 28
1.3.1 Origin of Fluorescence 28
1.3.2 Quantitative Aspects of Light Absorption and Emission 31
1.3.3 An Overview of Dye Lasers 32
1.3.4 Requirements for a Dye to Act as a Laser Dye 33
1.3.5 Effect of solvent 35
1.3.6 Dye Aggregation 36
1.4 Nonlinear Absorption 37
1.4.1 Two Photon Absorption 38
1.4.2 Three Photon Absorption 40
1.4.3 Multiphoton Absorption 41
1.4.4 Excited State Absorption 41
1.4.5 Two-photon Assisted Excited State Absorption 42
1.5 References 43

2 Experimental Approach **51**
2.1 Introduction 52
2.2 Subsystems 52
2.2.1 Laser Sources 52
2.2.2 Chopper 54
2.2.3 Sample cell 54
2.2.4 Power Meters 54
2.2.5 Monochromators 55
2.2.6 The Photomultiplier 56
2.2.7 Digital Storage Oscilloscope 58
2.2.8 Boxcar averager/integrator 58
2.2.9 Chart Recorder 59
2.2.10 Lock-in amplifier 60
2.2.11 Photon Counter 61
2.2.12 Optical fibre 61

2.2.13 Vibration-free table 61
2.3 Experimental set up 62
2.3.1 Continuous Wave Thermal Lensing (CWTL) 62
2.3.2 Pulsed Thermal Lensing (PTL) 62
2.3.3 Pulsed Photoacoustics (PPA) 64
2.3.4 Fluorescence Studies 65
2.4 Summary 66
2.5 References 67

3 Thermal Diffusivity Measurements Using Transient Thermal Lens Calorimetry 69
3.1 Introduction 70
3.2 Experimental Set up 72
3.3 Theory 73
3.4 Thermal Diffusivity Measurements in Organic Liquids 74
3.5 Thermal Diffusivity Measurements in Seawater 77
3.6 Conclusion 81
3.7 References 82

4 Multiphoton Absorption Studies in Rhodamine 6G and Rhodamine B Laser Dyes in Different Solvents Using Transient Thermal Lens Technique 85
4.1 Introduction 86
4.2 Experimental 90
4.3 Principle of TL detection of MP processes 90
4.4 Results and discussion 91
4.4.1 Rhodamine 6G solutions 92
4.4.2 Thermal Lens Studies in Rhodamine B 104
4.5 Conclusion 109
4.6 References 109

5 Measurement of Absolute Fluorescence Quantum Yield of Rhodamine Dyes Using Dual Beam Thermal Lens Technique 114
5.1 Introduction 115
5.2 Methods of Measuring Quantum Yields 116
5.2.1 MgO_2 as a standard: 116
5.2.2 Comparison with Compounds of Known Quantum Yields 117
5.2.3 Photothermal methods 118
5.3 Q_f Measurements Using Thermal Lens Method 119
5.3.1 Theory 121
5.4 Experimental 124
5.5 Results and Discussion 124
5.5.1 Solvent Effects on Fluorescence Spectra 125
5.5.2 Q_f Measurements in Rhodamine 6G Using CWTL Technique 130
5.5.3 Q_f measurements in Rhodamine B Laser dye 137
5.5.4 Q_f Measurements Using Pulsed Thermal Lens 139
5.5.5 Energy Dependence of Q_f values 144
5.6 Conclusion 145

5.7 References 146

6 Pulsed Photoacoustic Determination of Absolute Fluorescent Quantum Yield of the Laser Dye Rhodamine B 151
6.1 Introduction 152
6.2 Experimental Set up 154
6.3 Results and Discussion 154
6.4 Conclusion 157
6.5 References 158

7 Optical Limiting and Photothermal Studies in Fullerenes 160
7.1 Introduction 161
7.2 Optical limiting 164
7.2.1 Reverse Saturable absorption 166
7.2.2 Two Photon Absorption 168
7.2.3 Nonlinear Refraction 170
7.2.4 Induced Scattering 170
7.3 Optical limiting in C_{60} and C_{70} 171
7.4 Thermal lensing in C_{60} and C_{70} toluene solutions 180
7.5 Photoacoustic Studies in C_{60} and C_{70} 185
7.6 Conclusions 190
7.7 References 191

8 Use of Pulsed Photoacoustic Technique for the Study of Nonlinear Processes in Liquids 197
8.1 Introduction 198
8.2 Experimental Setup 200
8.3 Results and Discussion 201
8.3.1 TPA Studies in Toluene 201
8.3.2 TPA Studies in Benzene 203
8.3.3 Multiphoton Absorption Studies in CS_2 204
8.4 Conclusions 207
8.5 References 207

9 Summary and Conclusions 211

INTERNATIONAL SCHOOL OF PHOTO

Chapter 1

General Introduction

This thesis describes the application of laser induced photothermal phenomena for the study of nonlinear phenomena in certain organic compounds. We attempted photothermal studies in laser dyes and fullerenes for a better understanding of the different nonlinear processes taking place in these molecules. Thermal lens and photoacoustic techniques were employed. First two sections of this chapter presents a brief introduction into different photothermal techniques like thermal lensing and photoacoustics. In the preceeding sections a brief description of the photophysical properties of laser dyes and different nonlinear absorption mechanisms are given.

Photothermal Phenomena

The warming effect of sunlight on a cool morning is perhaps one of most pleasurable experiences offered by nature. Observation of the thermal effects of electromagnetic radiation has played an important role in the discovery and understanding of many natural processes. In modern times, interest in the thermal effects of radiation developed with the invention of the laser. This is because of the special properties which laser beams possesses in contrast with ordinary light beams.

Lasers can provide highly directed, highly monochromatic radiations with high power densities. Following the invention of the laser, many of its striking applications to analytical measurements have been reported [1]. Improvements over conventional light sources have been possible when one takes advantage of special properties of laser light. High power levels can lead to larger signals in laser-excited fluorescence [2] and thermo-optical effects [3], as well as in new types of signals in, e.g., two photon excited fluorescence [4]. Coherence can enhance interferometric measurements [5]. High resolution can provide unique and accurate information in atomic spectroscopy [6]. Good collimation and polarization properties can improve polarimetric measurements [7]. Short pulse durations allow temporal resolution of events. In recent times ultrafast events have been successfully studied with femtosecond laser pulses.

During the past few years an optical technique, called photothermal technique has been developed to investigate the optical properties of materials that are unsuitable with the traditional spectrophotometry. In photothermal spectroscopy, the energy absorbed by the material as a result of its interaction with incident radiation is measured directly and the heat produced by nonradiative decay of excited species acts to modify the optical properties of the sample [8]. Photothermal effects are caused by the heating of a sample after the absorption of optical energy (or in general, the absorption of an energetic beam). After optical absorption, other deexcitation channels besides heating can also occur, as indicated in fig.1.1. These other deexcitation branches complement the heating branch in the sense that all branching ratios must add up to one. Photothermal heating of a sample is produced with the use of laser beams, xenon arcs or other intense light sources [9-14].

All photothermal techniques have a common origin in the use of electromagnetic radiation in the UV to IR region of the spectrum as probing radiation and in this respect are similar to conventional UV/VIS spectroscopies. Unlike these, however, the sample is not quantified by transmission or luminescence but rather by the nonradiative de-excitation of excited states,

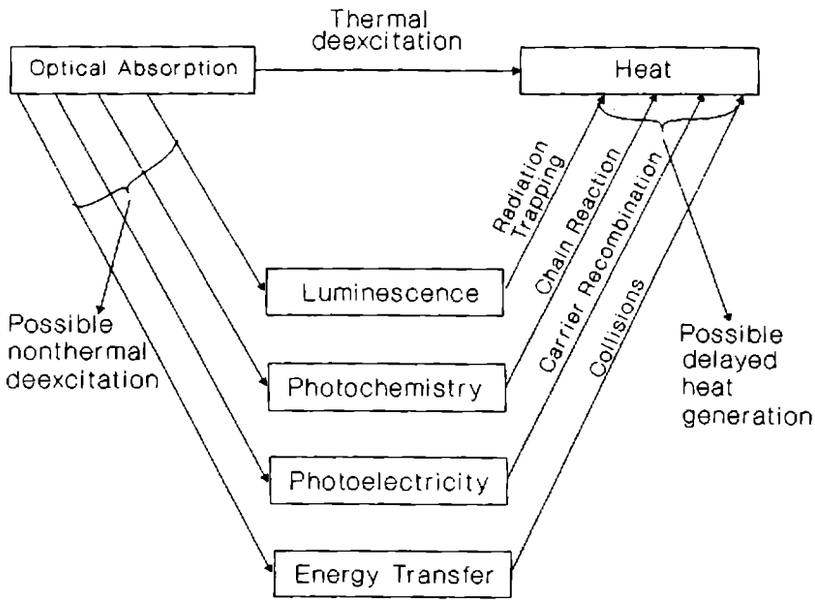

Figure 1.1: Possible consequences of optical absorption.

Table 1.1 Detection techniques for photothermal spectrometries

Technique	Detection principle
Photoacoustic spectrometry using -	
(a) Microphone	Pressure wave in a closed cell containing the sample, contacting gas and microphone
(b) Piezo or pyro-electric sensor	Attached sensor detects the thermal wave in the sample by deformation or temperature rise
Thermal lens spectrometry using -	
(a) Beam deflection	Off-axis thermal gradient induced deflection of a probe beam parallel to pumping beam.
(b) Co-axial probe beam detection	Symmetric lens detected by a probe coaxial with the pump beam.
Photothermal beam deflection -	
(a) Thermally induced	Beam deflection caused by a thermally induced refractive index gradient (dn/dT)
(b) Concentration induced	Beam deflection caused by a concentration induced refractive index gradient (dn/dC)
Photothermal radimetry -	
(a) Laser induced optothermal spectrometry	IR thermal emission

which results in a change in temperature of the substrate or contacting medium. Often these techniques employ a laser to provide a modulated or pulsed excitation beam which is tuned to the absorption maximum of a chromophore and focused into the sample. Subsequent non-radiative relaxation generates a thermal wave which can be detected in the sample or in the

contacting medium using any of several different detection schemes summarised in Table 1.1.

The advantages of photothermal techniques are: 1) photothermal heating can provide convenient and sensitive methods for detecting optical absorption in matter 2) information concerning deexcitation mechanisms can be obtained 3) very delocalized or very rapid photothermal heating can be achieved to provide novel measurements or produce new effects.

1.1 Thermal Lens Spectroscopy

The thermal lens (TL) effect or thermal blooming was discovered by Gordon and co-workers [15] only a few years after the invention of the continuous wave (cw) laser. While carrying out an intracavity excitation of a liquid sample for Raman spectroscopy, the authors observed time-dependent changes in the laser intensity which they could attribute to localized heating of the sample. They derived a theory for the thermal defocusing of the beam, which predicted the magnitude and time constant of the response.

The TL effect may be described as a change in the optical path of the sample induced by absorption of a laser beam. Fig.1.2 represents schematic of the TL effect. A laser beam passes from left to right through the sample having an optical length bounded by the vertical lines. The initial unheated sample and far-field beam profile are shown in fig.1.2 (a). A steady state TL and the beam profile are shown in fig.1.2 (b). In a typical TL experiment, the sample is illuminated with a laser beam having gaussian intensity distribution. Some of the incident energy is absorbed by the sample or by the chromophore within the sample. Excited states formed in this way may either lose energy radiatively e.g., fluorescence or phosphorescence or by nonradiative routes e.g., internal conversion or by interaction with other molecules in the sample which results in the generation of heat. The flow of heat from the region illuminated by the laser results in a thermal gradient that is proportional to the beam intensity profile in the sample. Heating is stronger at the centre of the beam profile than in the wings. The temperature gradient creates a refractive index gradient. The greater heat produced at the beam center raises the temperature and, for most liquids that expand upon heating, lowers the refractive index, n. This creates a shorter optical path, nl, along the center of the beam path, where l is the physical length of the sample. The resulting thermo-optical element has the shape of a negative lens which causes the laser beam to diverge. As the beam passes through the solution, it progressively diverges. The degree of divergence depends upon the power of the laser beam and the absorption coefficient of the sample. The increased divergence of the beam may be observed some distance beyond the sample as a larger spot size or a lower

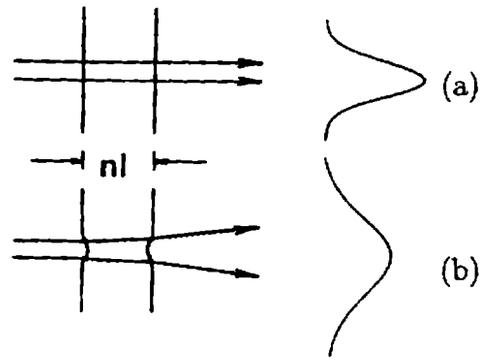

Figure 1.2: Diagram of the thermal lens effect

intensity at the beam center.

1.1.1 Thermal Lens Theory

In this section the theory of the TL effect is described, and this enables one to determine the absorbance of a sample by this technique. This theory also identifies the optical and sample-dependent factors that affect the measurement sensitivity. The TL effect has been theoretically treated under a variety of experimental conditions [16-30]. The existing theoretical models range from relatively simple formulations to complex and sophisticated derivations. These models cover TL effects which are generated under different excitation conditions (pulsed and cw excitation), different pump-probe geometries (single beam, dual beam, collinear and crossed beam configuration, pump and probe beam displacements) and different sample conditions (stationary and flowing samples).

Generation of temperature gradient inside the irradiated sample is common to all photothermal techniques. The first step in the derivation of a theoretical TL model is, therefore, the solution of the appropriate nonsteady thermal diffusion equation [30],

$$\frac{\partial T(r,t)}{\partial t} = D\nabla^2 T(r,t) - v_x \frac{\partial T(r,t)}{\partial x} + \frac{1}{\rho C_p} Q(r,t) \tag{1.1}$$

where T(r,t) is temperature, D is the thermal diffusivity, ρ is the density and C_p is the specific heat at the constant pressure of the medium of the uniform velocity v_x in the x direction. Q(r,t) is the source term which represents the heat produced per second per unit volume of the sample due to the absorption of pump beam light and the subsequent radiationless deexcitation of excited atoms or molecules in the sample. The source term depends mainly on the mode of excitation and other experimental parameters. These dependencies can be

written in simplified forms if the sample is optically thin (transmittance ≈ 1), which is usually in the case of TL measurements.

For pulsed excitation case, Q(r,t) during excitation ($0 \leq t \leq t_0$) is given as

$$Q(r,t) = \frac{2\ln(10)\alpha E_0}{\pi a^2 t_0} \exp\left(\frac{-2(x^2+y^2)}{a^2}\right) \tag{1.2}$$

where E_0 is the energy of the laser pulse, which is propagating in the z-direction, α is the decadic absorption of the medium per unit length, and a is the $1/e^2$ radius of the pump beam with Gaussian profile. After the excitation ($t > t_0$), Q(r,t) equals zero.

For the case of cw excitation Q(r,t) is given as

$$Q(r,t) = \frac{2\ln(10)\alpha P_{av}}{\pi a^2} \exp\left(\frac{-2(x^2+y^2)}{a^2}\right)(1+\cos\omega t) \tag{1.3}$$

where P_{av} is the average power of the beam, which is sinusoidally modulated at a frequency $F=\omega/2\pi$. As a result the power P of the beam oscillates between P=0 to $P=2P_{av}$.

When the source term is known, one can obtain time dependent temperature distribution inside the sample (T(r,t)). This can be evaluated for any particular case of excitation by substituting the appropriate expression for Q(r,t) into eqn. (1.1).

In pulse mode excitation case temperature distribution in the sample cell T(x,y,t) may be written as

$$T(x,y,t) = \frac{2\ln(10)\alpha E_0}{\pi t_0 \rho C_p} \int_0^{t_0} \frac{1}{8D(t-\tau)+a^2} \times \exp\left(\frac{-2[(x-v_x(t-\tau))^2+y^2]}{8D(t-\tau)+a^2}\right) d\tau \tag{1.4}$$

when $t > t_0$. Similarly, the solution of equation for cw excitation mode is given by

$$T(x,y,t) = \frac{\ln(10)\alpha P}{\pi \rho C_p} \int_0^{t} \frac{1+\cos\omega t}{8D(t-\tau)+a^2} \exp\left(\frac{-2[(x-v_x(t-\tau))^2+y^2]}{8D(t-\tau)+a^2}\right) d\tau \tag{1.5}$$

Due to nonuniform radial temperature distribution, time dependent refractive index gradient is formed inside the sample and can be described as

$$n(x,y,t) = n_0 + \left(\frac{\partial n}{\partial T}\right)_{T_A} T(x,y,t) \tag{1.6}$$

where n_0 is the unperturbed refractive index at ambient temperature T_A.

The irradiated sample acts like a lens, which affects the laser beam intensity profile by altering its radius w. Relative changes in the beam intensity which are proportional to the relative changes in the power of the beam reaching the detector are, therefore, a direct

measure of the TL strength. Since the change in beam radius is usually small (weak TL approximation), the TL signal s(t) for a laser beam with a Gaussian profile is given as

$$s(t) = \frac{w_2^2(t) - w_2^2(0)}{w_2^2(0)} \tag{1.7}$$

where $w_2(0)$ is the radius of the unperturbed beam at the detector site and $w_2(t)$ is the time dependent radius of a beam perturbed by a TL. $w_2(t)$ may be found by using an appropriate ray transformation matrix according to the so-called ABCD law [16, 31], which gives

$$w_2^2(t) = w_0^2 \left[\left(1 - \frac{z_2}{f(t)}\right)^2 + \frac{1}{z_0^2}\left(z_1 + z_2 - \frac{z_1 z_2}{f(t)}\right)^2 \right] \tag{1.8}$$

where z_2 is the distance between the sample and the detector, z_1 is the distance between the probe beam waist and the sample and w_0 is the radius of the probe beam at its waist, $z_0 = \pi w_0^2/\lambda$ is the confocal distance of the probe beam with a wavelength λ and f(t) is the focal distance of the TL.

Substituting eqn.(1.8), eqn.(1.7) can be simplified for weak TL case ($f(t) \gg z_1$ and z_0). Knowing that at t=0, f(0) = ∞, s(t) for the far field approximation ($z_2 \gg z_1$ and $z_2 \gg z_0$) can be written as

$$s(t) = -\frac{2z_1}{f(t)} \tag{1.9}$$

When calculating the focal distance of the TL, which is needed to evaluate the TL strength, it is necessary to consider different possible geometrical configurations of pump and probe beams. Most frequently collinear configuration is used, eventhough geometries of transverse [32] as well as obliquely crossed [33] TL were also utilized and treated theoretically.

The steady state focal length of the induced lens given in the parabolic approximation of the lens is given by [34]

$$f = \frac{\pi k \omega^2}{2.303 P(dn/dT) A} \tag{1.10}$$

where k is the thermal conductivity of the sample, P is the laser excitation power and A is the absorbance of the sample. Thus as P, dn/dT and A get larger then the focal length of the lens gets shorter and the beam divergence increases.

By combining eqns. (1.9) and (1.10) and by taking adequate derivatives of eqns. (1.4) and (1.5), expressions for TL signal under pulsed or cw excitation conditions can be obtained. It is however, much more convenient to use somewhat less complex expressions to illustrate the differences in the dependency of the TL signals on experimental parameters. The focus will placed on nonflowing samples (v_x=0) and on cases where displacement between the probe and

the pump beam beam is negligible. Since the TL signal is usually measured as the relative change in the probe beam center intensity, x = y = 0 can also be assumed.

For excitation with a very short laser pulse ($t_0 \rightarrow 0$; impulse approximation) the assumptions mentioned above yield the following expression for the TL signal [30]

$$s_p(t) = -\frac{4\ln(10)AE_0z_1}{\pi ka^2t_c}\frac{\partial n}{\partial T}\frac{1}{(1+2t/t_c)^2} \tag{1.11}$$

where $s_p(t)$ is the TL signal with pulsed mode excitation, $A = \alpha l$ is a the absorbance of the sample, $t_c = a^2\rho C_p/4k = a^2 4D$ is the characteristic time constant of the TL experiment, and k is the thermal conductivity of the sample.

Similarly TL signal s_c corresponding to cw excitation is given by

$$s_c(t) = -\frac{2\ln(10)APz_1}{\pi ka^2}\frac{\partial n}{\partial T}\frac{1}{(1+t_c/2t)} \tag{1.12}$$

It must be noted that eqns. (1.11) and (1.12) are subject to certain limitations, which originates from the approximations used during their derivations. From these equations it is found that the TL signal strength is strongly dependent on the energy of the pulsed laser or the power of a cw laser used for excitation. Eqns. (1.11) and (1.12) indicate that the TL signal also dependent on the size of the pump beam. Since t_c is related to the inverse square of the pump beam radius the pulsed excitation is advantageous, particularly in the case of small volume samples.

1.1.2 Sensitivity and Temporal Characteristics

The sensitivity of a pump-and-probe method depends on the relative positions of the two beams in the sample. If the pumping laser is much smaller than the probe, the fraction of the probe beam which is affected by the refractive index gradient would be small, resulting in a minimal effect on the probe beam divergence. If the spot size of the source beam is much larger than the probe, the entire probe beam is affected, but by a weaker refractive index gradient. As a result, the maximum effect on the probe beam divergence occurs when the pump laser beam within the sample is approximately the same size as the probe beam.

The relative change in the intensity induced by the TL reaches a steady state value after several time constants. The relative change in the beam centre intensity can be related to the absorbance through the relation [34]

$$\frac{\Delta I_{bc}}{I_{bc}} = 2.303EA + \frac{(2.303EA)^2}{2} \tag{1.13}$$

where E= [-P(dn/dT)λk] is the enhancement in sensitivity over transmission measurement that would produce a relative intensity change

$$\frac{I_0 - I}{I_0} = 1 - 10^{-A} \cong 2.303A \tag{1.14}$$

for small absorbances.

The sensitivity of a TL measurement, therefore, depends linearly on laser power. The choice of solvent can greatly influence the enhancement one observes for the laser power available [16]. Nonpolar solvents like carbon tetrachloride are particularly advantageous since they exhibit a large dn/dT and small thermal conductivity. The sensitivity of TL measurement made in water under similar conditions would be 30 times smaller. The time constant of the TL effect also varies with solvent to a lesser extent. The time constant depends quadratically on the beam spot size while the sensitivity is independent of spot size. This is somewhat surprising since the strength of the TL increases with decreasing spot size as shown by eqn. (1.10). This can be explained as follows. For a laser beam having gaussian intensity profile, in the far-field region of the beam at large distances from the waist, the spot size, ω increases linearly with propagation, or equivalently, the divergence angle ϕ becomes constant [16]

$$\phi = \tan^{-1}\frac{\omega}{Z} \cong \frac{\omega}{Z} = \frac{\lambda}{\pi\omega_0} \tag{1.15}$$

where ω_0 is the spot size at the beam waist. Hence, the concominant increase in the divergence angle of the beam, ϕ, with decreasing spot size, shown in eqn. (1.15), exactly cancels the effect of the stronger TL.

It is instructive to examine the refractive index and temperature sensitivity of the TL effect. Assuming a 1% change in the beam center intensity can be detected, the corresponding induced phase shift is $\theta = 0.01 = -2\pi\Delta nb/n\lambda_0$, where b is the sample path length and Δn is the refractive index change at the beam center compared with the edges. For a 1-cm path length and $\lambda_0 = 632.8$ nm, the relative change in the refractive index is only $\Delta n/n = -1.0 \times 10^{-7}$. For a solvent having a large dn/dT such as carbon tetrachloride, this refractive index change corresponds to a temperature difference of $\Delta T = 2.5 \times 10^{-4}$ K. The sensitivity of a spatially coherent laser beam to such small refractive index gradients is the basis of the detection capabilities of the TL effect.

1.1.3 Measurement Approaches

1.1.3.1 Single - Beam Measurements

Single-beam TL spectrometers are unique among the TL instruments because the same laser beam is used to excite the sample and simultaneously probe the TL formed. Single beam set up was used in the early stages of TL technique. Initially, they were applied to study the dependence of the TL effect on parameters such as laser power, beam divergence, sample length, concentration and flow [35-37]. Application of TL in the chemical analysis has not been realized until 1979 when Dovichi and Harris [38] used the technique to detect CuII at ppm levels. Authors still used the single beam configuration, despite the availability of dual beam instruments, which should provide better sensitivity. The reason for this, and for the relatively frequent use of single beam instruments is probably due to relative simplicity of such instrument and ease of operation compared to dual beam instruments ie., only one laser is used to generate and detect TL.

In single beam TL instrument, the laser beam is focused with a lens and modulated with a chopper or shutter. After passing through the sample, the beam center intensity is usually measured in the far field with a photodiode placed behind a pinhole. The photodiode output is amplified and fed into a storage oscilloscope which gives the transient change in the beam center intensity.

The single beam method of TL measurements can be used to produce a differential response by optical means [39]. Reference and unknown samples are located on opposite sides of the beam waist so that the TL strengths of the two samples are subtracted by their opposite effect on the far-field beam spot size. This differential configuration was found to exhibit immunity from laser power fluctuations, but is limited to sufficiently weak TL, so that the divergence of the beam responds linearly to the absorbance in each cell.

The positioning of the sample with respect to probe beam waist is essential to obtain high sensitivity of the TL measurements. As can be inferred from eqn. (1.12) the sample should be positioned as far as from the probe beam waist as possible in order to observe the largest effect of the TL on the beam. However, because the same beam is probing the TL, one must take into account the decrease in power density due to the increase in beam radius with distance. The TL signal should be maximum when the sample is positioned at one confocal distance from the beam waist ($z_1 = z_0$). For such a case eqn. (1.12) can be written as

$$s_c(t) = -\frac{\ln(10)AP}{\pi k}\frac{\partial n}{\partial T}\frac{1}{(1+t_c/2t)} \tag{1.16}$$

This expression was obtained under the assumption that the TL is a perfect thin lens (parabolic refractive index distribution) with no aberrations. Such an approximation gives a good qualitative description of the TL but is quantitatively inaccurate. Sheldon and co-workers [42] derived a more accurate theoretical model which takes into account the true aberrant nature of the TL. According to the aberrant TL model the sample should be placed at a distance $z_0/\sqrt{3}$ from the beam waist to obtain maximum TL signal which is given by

$$s_c(t) = -\frac{\ln(10)AP}{\pi k}\frac{\partial n}{\partial T}\tan^{-1}\left(\frac{1}{(1+t_c/t)\sqrt{3}}\right) \tag{1.17}$$

Nevertheless, the optimal position for the sample cell is most frequently found experimentally and not by calculation, which requires accurate data on beam radius that is difficult to obtain.

1.1.3.2 Dual-Beam Configurations

In dual-beam TL method, the generation and detection of the TL was achieved separately by a modulated pump beam and nonmodulated probe beam respectively. A high power cw or pulsed laser usually serves as the source of the pump beam, while the probe is derived from relatively weaker cw laser. By using separate lenses to focus the excitation beam directly onto the sample and to mismatch the beam waists of the pump and probe beam, the highest TL signal strength can be achieved. Good spatial overlapping of both beams inside the sample is necessary for optimal sensitivity. The alignment and combining of the two beams is facilitated by a beam splitter or dichroic mirror. The generated TL produces fluctuations in the intensity of the probe beam that can be sensitively monitored by signal averaging devices such as lock-in amplifiers and boxcars, provided that the excitation beam is filtered out before reaching the detector. Signal intensities in a dual beam TL experiment usually obtained from the differences (I(t) - I(0)) between the probe beam center intensities at the beginning (I(0)) and at the end (I(t)) of pump laser excitation.

The first report of dual beam TL measurements were the work of Grabiner et. al. [40]. They used a He-Ne probe laser beam to measure the time resolved formation of the TL as monitor of energy transfer in gas phase molecules pumped by a pulsed CO_2 laser. The first application of the dual beam TL technique to spectroscopic absorption measurements was the work of Long et. al [41]. Swofford and Morrel [27] have presented the mathematical analysis of the cw dual beam TL technique by extending the model of Gordon et. al [15] to account for the cumulative effect of the chopped heating beam. Fang and Swofford [43] have discussed in detail the various experimental requirements that are to be met in carrying out TL experiments in particular.

Modeling the response of a dual-beam TL experiment is more complicated than the single-beam theory presented since one must take into account the confocal parameters and spot sizes of both pumping and probing laser beams [43]. Using the simplifying assumption that the spot sizes of the two beams in the sample are approximately equal, which probably produces less than optimum sensitivity [44, 45], a numerical model for the dual beam experiment was developed [46]. An analytical solution to the frequency response was also published [47] and the results, expressed in terms of a reduced frequency, $\nu_0 = \pi\nu t_c$, where ν is the chopping frequency and t_c is the TL time constant. While the response is found to decrease markedly for chopping at frequencies, $\nu \geq 0.1 t_c^{-1}$, the signal-to-noise ratio over a similar range of ν_0 was found to be nearly constant [47].

1.1.3.3 Comparison of Single and Dual Beam Configurations

In single beam TL experiment, one uses a single laser source to provide both the sample excitation and the means for probing the heat produced by the absorption process. In many cases however, the use of separate laser sources for the pump and probe beams can provide significant benefits in performance. For example in absorption spectroscopy, where the pump laser is to be tuned over a wavelength range, the point by point measurement scheme of the single beam technique becomes very time consuming and cumbersome. In such cases the use of separate lasers to pump and to probe the TL will be more advantageous. Since only a single wavelength is always detected, the detection optics and detectors need to be optimized only for a single probe wavelength, one need not take into account the spectral response of the optical elements and the detector.

The principal advantage of single beam configuration over pump - and - probe is optical simplicity. No matching of beam spot sizes, coaxial alignment of beams, or careful overlap within the sample is required. The beam needs only to be focused through the sample and centred on the detector in the far field and the sample translated to find the position of maximum response. This greatly reduces the likelihood of spurious results due to drift in alignment as well as the cost of the experimental set up in optical mounts and alignment effort.

An experimental comparison of the dual-and single-beam TL methods was published [48]. Under the constraint of equal spot sizes at the sample, the ratio of the sensitivities was found to agree with the theoretical prediction:

$$\frac{E_p}{E_s} = \frac{(dn/dT)_p \lambda_s}{(dn/dT)_s \lambda_p} \tag{1.18}$$

where s and p subscripts corresponds to the single beam and probe beams, respectively. This result indicates a potential sensitivity advantage for probing with a shorter wavelength laser beam, which would be significant for improving the sensitivity of infrared absorption measurements made with a TL [49]. The reproducibilities and limits of detection for the single- and dual-beam configurations were found to be equivalent, probably affected by a common source of noise. Since the intensity noise of the two lasers was quite different, the sample must be contributing to the uncertainty in the two measurements, either from convection [50] and/or small particles [51].

1.1.4 Important Applications of Thermal lens

TL technique finds many applications in different fields of science and technology. An excellent review by Snook and Lowe [52] gives a detailed account of the applications of TL spectroscopy. Only a few important applications will be discussed in the preceeding sections.

1.1.4.1 Trace detection

The TL effect has begun to be developed as a new tool for trace-level determinations [53-57]. Grabiner and co-workers [58] suggested that the excellent sensitivity of the TL technique could prove to be valuable for the detection of trace concentrations of absorbing species in atmospheric samples. This work and that of Nieman and Colson [59], where TL spectroscopy was used in a study of the electronic states of *trans*-butadiene and SO_2, implies that TL spectroscopy is useful in the determination of characteristics of molecules in the gaseous phase. The change in refractive index with temperature of a typical gas at 1 atm pressure, nitrogen for example, is only 0.9×10^{-6} K^{-1}, which is a factor of 600 smaller than liquid CCl_4 [60]. Due to the small density and heat capacity, time constants for the TL effect in gases are very short. The short time constants in gases point to a significant sensitivity advantage for pulsed excitation, since the breakeven pulse energy, $E_t = P.t_c$, is proportional to t_c [16]. The above concepts were described in detail in the first analytical paper on gas-phase thermal measurements [54].

The first study of the application of the TL technique to trace solute determination was by Dovichi and Harris [38]. TL measurements have also been carried out for the determination of iron [61-66]. Spectrophotometric determination of nonmetals has also been accomplished using the TL. Nitrite [44] was detected at a 0.2 nM concentration using a single-beam TL experiment. Hu and Whinnery [65] first observed the anti-symmetric dependence of the TL

lens effect on the position of the induced TL relative to a waist in a Gaussian beam. Dovichi and Harris [39] constructed a differential TL spectrometer. If the value of for the sample is negative, then a diverging lens will ensue if the sample is placed beyond the waist in the beam. If the same sample is positioned an equal distance before the waist, a converging lens will result. Therefore, when two cells, filled with identical weakly absorbing samples, are placed symmetrically about a beam waist, a cancellation of $\sim$ 99% of the TL signal is observed. In this manner, the signal due to the sample matrix or the solvent, can be optically subtracted from that of the sample automatically, if one cell filled with a blank sample, is placed $3^{1/2}Z_c$ before the beam waist, and the sample cell is placed $3^{1/2}Z_c$ beyond the beam waist. Using this experimental arrangement, an improvement in the detection limits of more than an order of magnitude was reported [39]. Theoretical and experimental details of the use of TL on the kinetic determination of chemical reactions have been reported by various authors [44].

1.1.4.2 Measurement of Absolute Absorption Coefficients

The assumption that the signal generated by a TL spectrometric experiment is proportional to the absolute absorption coefficient was made in most of the initial publications on this technique [66-68]. Whinnery [68] assumed that the thermal energy absorbed from a laser beam passing through a nearly transparent material allowed the measurement of the absorption coefficient with sensitivities of $\leq 10^{-5}cm^{-1}$. Twarowski and Kliger [69] measured the two photon absorption spectrum of benzene with a pulsed nitrogen laser pumped dye head in the range 360-530 nm using a series of laser dyes. Carter and Harris [70] showed that the detection limits for the smaller sample volume (pathlength = 0.1 cm) reflect greater precision and a larger sensitivity compared with the greater sample volume (1cm).

1.1.4.3. Chromatographic Detection and Flow Injection Analysis

The sensitivity of the TL technique, the small volume characteristics of a focused laser beam, and the more general applicability of thermal rather than fluorescence detection have made this method an attractive detector for liquid chromatography and flow injection analysis [71, 72] . Given the need for selectivity in TL measurements, combining these methods would appear to be mutually beneficial. To use a TL as a detector of a flowing process, the effect of flow on the measurement needed to be considered [73].

The first application of TL detection to liquid chromatography employed a single-beam experiment [74]. A dual-beam instrument was tested with conventional [47] and microbore

HPLC [75]. The combination of TL detection and flow injection analysis is also mutually beneficial. Flow injection analysis has been advocated as a means of reducing contamination and carry over in ultra trace analysis with laser-based detectors [54].

1.1.4.4. Quantum Yields

Hu and Whinnery [65] were the first to point out that TL technique could be used to measure the fluorescence quantum yield of organic dyes. The total power absorbed by the dye solution can be measured spectrophotometrically, and then the power that is converted into heat is measured by TLS. More details about the fluorescence quantum yield measurements using TLS are discussed in Chapter 5 of this thesis. Terazima and Azumi [76-78] carried out a series of investigations to measure the quantum yield of triplet formation and the triplet lifetime of several different species in the liquid and solid phase, using time - resolved TL method. The quantum yield of photodissociation of iodine has been studied by Lebedkin and Klimov [79].

1.1.4.5 Heats of Reaction, Energetics and Kinetic Studies

Time resolved TL has been successfully employed to study heats of reaction and energetics [80] which highlights the potential for TL in fundamental studies of reaction kinetics and energetics. Since the time-resolved method detects time-dependent heat emitted through radiationless transitions metastable and excited state information can be obtained which is not obtainable by other techniques such as flash photolysis.

1.1.4.6 Thermal Lensing in Glass and Other Solid Laser Materials

The characterization of the transmission properties of laser beams through optical glasses, ruby, sapphire and lithium niobate crystals has been extensively studied for more than two decades. The existence of undesirable thermal effects associated with the generation of laser light is a basic problem in the design, and operation of any efficient solid-state laser device. In 1968, Dabby and Whinnery first termed these thermo-optical effects seen in solid samples, TL [81]. They observed that TLs were formed in common lead glasses, which decreased the natural laser beam divergence, demonstrating a positive value for dn/dT. They observed strong thermal self-focusing of an argon ion laser beam, when it was passed through a 15 cm length of lead glass. Baesso *et al* [82] measured the absolute thermal diffusivity of soda-lime glass using a time-resolved TL method and was in agreement with that found using photoacoustic spectroscopy [83] on an identical sample.

1.2 Photoacoustic Spectroscopy

The photoacoustic (PA) or optoacoustic (OA) effect is the generation of acoustic waves in a sample resulting from the absorption of photons. This process was first invented by Bell [84], Tyndall [85] and Rontgen [86] in 1881. Sunlight was focused onto a sample contained in a cell that was connected to a listening tube. When the sunlight was repeatedly blocked and unblocked, sound could be heard through the listening tube at the sunlight chopping frequency. Although the effect has been known for over 100 years, there has been a recent increased interest in the phenomenon, both in theoretical and experimental studies. This renewed interest stems from several possible reasons. Two of them are the availability of intense light sources such as lasers and development of high sensitivity detection tools for measuring acoustic waves. It has been used to study a variety of chemical and physical phenomena in a number of fields. PA techniques have been shown to be capable of detecting weak absorption features in gases as well as in condensed matter. Furthermore, PA methods are finding many unique applications, such as in spectroscopic studies of opaque or powdered materials, studies of energy conversion processes, and nondestructive evaluation or imaging of invisible subsurface defects in solids [87-91].

The essential feature of photoacoustic spectroscopy (PAS) is that the heat deposited in the sample by the absorption of a modulated light beam is detected. Thus PAS has the following advantages: (a) it can be used for strongly light scattering materials and (b) the PA signal is dependent on the excited state decay pathways resulting in acoustic generation. These features distinguish PAS from other spectroscopic methods.

This section is meant for describing the PA generation processes, the acoustic detection methods and a brief account of the applications of PA, but not to be an extensive review. Detailed reviews of the PA theory and applications have been discussed by various authors [92-99].

1.2.1 Principle of Operation

The basic theory behind PA detection is quite simple. Light absorbed by a sample will excite a fraction of the ground-state molecular population into higher energy levels. In general, following electronic excitation, a molecule has three channels open to it: (i) it may luminesce, leaving little or no heat in the sample; (ii) it may undergo photochemistry, again leaving little or no heat in the sample; or (iii) it may do nothing, i.e., cascade through the manifold of electronic-vibrational-rotational levels to finally reach its ground state with the surrounding

molecules concomitantly being heated. It is this part of the excitation energy, which is conventionally called the radiationless path way. The nonradiative component will ultimately generate heat in the localized region of the excitation light beam. If the incident radiation is modulated, the absorption of energy is interrupted at the frequency of modulation and consequently the heat produced in the sample after energy conversion also appears at this frequency. This temperature rise in a closed system of constant volume produces a periodic increase in pressure which follows the modulation frequency of the incident radiation. The pressure wave is then detected with a suitable sensor such as microphone transducer used for a gaseous sample. PA detection is unique in that it is a direct monitor of the nonradiative relaxation channel and, hence, it complements absorption and fluorescence spectroscopic techniques. It is also an extremely sensitive technique, with the ability to detect highly forbidden optical transitions and trace components in a mixture.

Indeed in the original work of Bell [84], using the sun as the source, distinctly audible signals were detected for various samples using only the unaided ear as the detector. It is apparent, even with the simple apparatus for the demonstration of the PA effect, that the amplitude of the signal is directly proportional to the intensity of the source. In addition, the amplitude of the signal is inversely proportional to the modulation frequency, since at high frequencies the radiant energy supplied to the sample per pulse decreases and thus results in less heat energy per pulse being available to cause the pressure change. It is also observed that the amplitude of the PA signal is greatest with samples of large surface area, e.g., fine powders [100], where the most efficient absorption of radiation by the solid and effective heat transfer to the surrounding gaseous atmosphere is possible.

1.2.2 Generation of Acoustic Waves

PA generation is generally due to photothermal heating effects. The mechanism of sound excitation by the interaction of laser radiation with matter are diverse. In principle there are five important interaction mechanisms which can be responsible for the generation of acoustic waves: dielectric breakdown, vapourization or material ablation, thermoelastic process, electrostriction, and the radiation pressure. Their contribution depends on the parameters of the incident laser beam as well as on the optical and thermal parameters of the medium.

The dielectric breakdown only occurs at laser intensities above $\sim$ 10 GWcm^{-2} which is easily obtainable from a pulsed laser in the focus of lens. This effect has been investigated experimentally and theoretically in detail for gases, liquids and solids [101-104]. The plasma

production related to the dielectric breakdown produces a shock wave which propagates initially at supersonic speed in the medium. The dielectric breakdown is the most efficient process for converting optical energy into acoustic energy. The conversion efficiency can reach up to 30% in liquids [105]. The dielectric breakdown dominates the interaction at high laser intensities, especially in transparent media where sound generation due to ordinary absorption does not occur [106].

The second interaction mechanism, i.e., explosive vaporization in the case of liquids [103] or material ablation on solids [107], is responsible for the acoustic wave generation if the laser energy density within the absorbing volume of the sample exceeds a certain threshold determined by the thermal properties of the medium. The material ablation on solids is usually accompanied by plasma formation. The ejection of material from the surface involves a recoil momentum which propagates into the bulk as an acoustic transient. For liquids the conversion efficiency in this case can reach 1 [108].

For absorbing media the thermoelastic process is important for the sound generation. This process is based on the transient heating of a restricted volume by the absorbed laser energy. The induced temperature gradient produces as a result of thermal expansion, a strain in the body. This causes an acoustic wave which propagates away from the heated zone. The thermoelastic process, i.e., heating without phase change, dominates the excitation of sound in absorbing matter at laser energies below the vapourization threshold. The conversion efficiency in this case is rather low, typically $< 10^{-4}$ for liquids [109].

The electrostriction as the fourth interaction mechanism is always present due to the electric polarizability of molecules in the sample which causes them to move into or out of regions of higher light intensity depending on positive or negative polarizability. These motions produce a density gradient and, consequently, a sound wave similar to that caused by the thermoelastic process [110]. Electrostriction as a sound generation mechanism is only important in very weakly absorbing media where it may limit the PA detection sensitivity. However, it has been demonstrated theoretically [111] and experimentally [95] that by using suitable time-gated detection of the acoustic signal, strong suppression of the electrostictive component is possible.

In comparison to other sound generating mechanisms the radiation pressure itself is negligible for acoustic wave generation. . For the case of total absorption of the laser radiation at the sample surface the amplitude of the radiation pressure is given by $p_{rad} = I/c$, where I is the laser intensity and c the light velocity in vacuum. For a laser intensity of 1 MW cm^{-2} one obtained $P_{rad} = 0.3$ mbar compared, for example, to a few bars in the case of thermoelastic

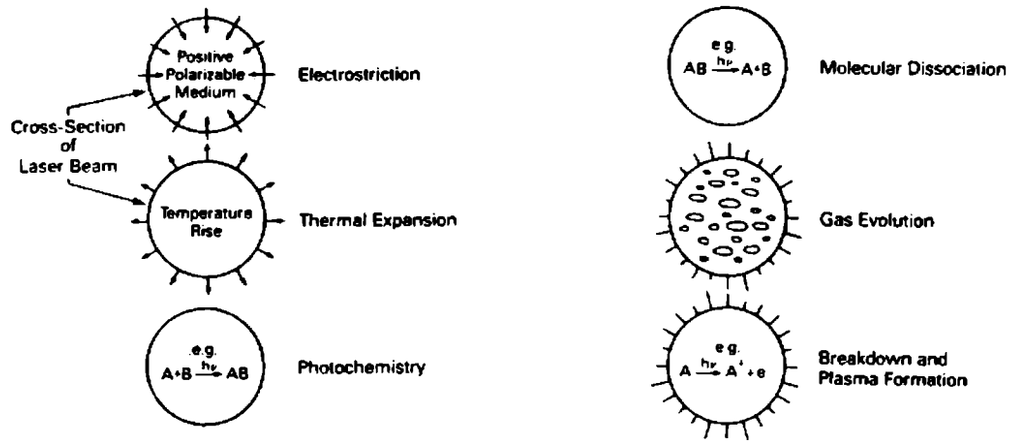

Figure 1.3: some common mechanisms of PA generation. The technique of PA spectroscopy always uses the thermal expansion mechanism

sound generation under identical conditions.

There are three further mechanisms that play a role only under specific circumstances. These are (a) photochemical effects where molecules AB are formed from the initial species A and B under the action of laser radiation (A+B+hν $\rightarrow$AB); (b) molecular dissociation where the opposite takes place (i.e., AB + hν $\rightarrow$ A+B); and (c) bubble formation [103, 112].

1.2.3 PA Generation

PA generation can be classified as either direct or indirect. Some of the possible PA generation mechanism are given in fig. 1.3. In the direct PA generation, the acoustic wave is produced in the sample where the excitation beam is absorbed [113-116]. In indirect PA generation [117-121], the excitation beam produces a modulated temperature at the surface of a solid or liquid sample. The sample is kept in contact with a transparent coupling medium and time dependent expansion of the coupling fluid is produced. This pressure wave can be sensed by a microphone. Here, the coupling medium is typically a gas or a liquid, and the sample is a solid or a liquid. Both direct and indirect PA generation are widely used for spectroscopic purposes.

PA generation can also be classified according to the two excitation modes: the continuous wave (cw) modulation mode and the pulsed mode. In the cw case, the signal is typically analyzed in the frequency domain; amplitude and phase of one or several Fourier components are measured and narrow-band filters can be used to suppress the noise. In cw modulated PA measurements, the modulation frequency is typically in the 1-1000 Hz regime and the acoustic propagation distance during a period is typically much larger than the sample cell. In such cases, we must first determine the acoustic eigen modes of the sample cell, and the excitation beam will excite an eigen mode to an amplitude depending on the magnitude of the overlap integral of the thermal source with the eigen mode [95]. When systematic noise (like noise to window, PA cell wall, or substrate absorption) dominates in the experimental system pulsed PA detection is usually preferred.

In the pulsed PA technique, the signal is acquired and analyzed in the time domain, making simple gating techniques for noise suppression possible. In pulsed PA measurements, the excitation pulse is typically short ($< \mu$s) and the acoustic propagation distance during the excitation pulse is typically much smaller than the dimension of the sample; hence in most cases, the PA pulse shape is independent of boundary reflections, and the sample can often be treated as infinite in extent.

The factors that affect and limit the ultimate sensitivity of PPA technique include (a) Optical absorption signals from windows, (b) scattering of light from the bulk of the liquid being absorbed by the transducer and (c) electrostriction. The signals arising from the first two can be minimized by the choice of of low-loss windows, reduction of scattering impurities in the liquid and an appropriate time gating of the acoustic signals. Time gating is very important since scattered light travels at the velocity of light in the medium while the acoustic signal generated in the bulk travels at the acoustic velocity in the medium. Thus the bulk acoustic signal will be delayed as compared to the acoustic signals generated from scattered light. On the other hand for the case of acoustic signals resulting from optical absorption by the windows, the acoustic pulse arrives after that originating from the sample.

The acoustic pulse generated due to electrostriction processes in the laser-irradiated region is of similar to that arising from the bulk absorption, and hence there is no reasonable way to distinguish between the two. The use of short laser pulse durations (giving rise to high optical intensities and correspondingly high electric fields) will increase the effects of electrostriction. It can be shown that the absorption coefficient α_1 at which the PA signal and the acoustic signal due to the electrostrictive effect become equal is inversely proportional to the diameter of the laser spot size [121]. For a laser pulse duration of 70 ns and beam spot size $\sim$3 mm

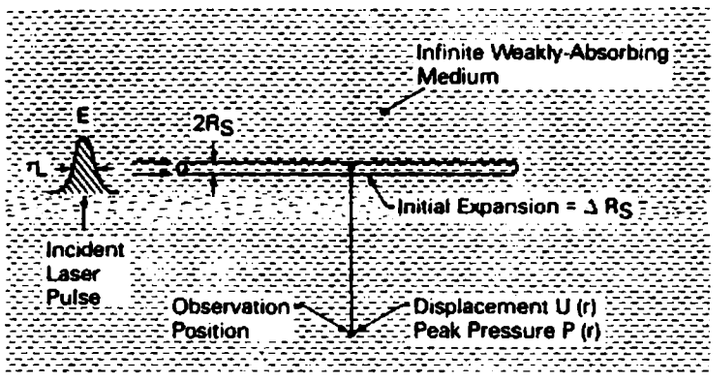

Figure 1.4: Schematic explanation of direct PA generation

the estimated value of $\alpha_1 \sim 6 \times 10^{-8}\text{cm}^{-1}$, and if the pulse width is longer, say 1 μs, then α_1 becomes $\sim 4 \times 10^{-9}\text{cm}^{-1}$. Further there is negligible dependence of the electrostriction effect on laser wavelength. Hence, even the $4 \times 10^{-9}\text{cm}^{-1}$ level does not represent a limitation on the smallest absorption coefficient that can be measured using pulse PA, if the material being studied has a wavelength dependent absorption. The detailed general theories of PA generation tend to be rather involved: to show the important parameters, we consider a simple case of direct and indirect PA generation.

1.2.4 Simple Theory for Direct PA Generation

The simplest case of direct thermal PA generation is indicated in fig. 1.4 for the case of an infinite weakly absorbing medium excited by a narrow pulsed beam producing PA source of radius R_s. It is assumed that the laser pulse width τ is sufficiently short so that the thermal diffusion effects can be neglected. The initial expansion ΔR_s of the source radius R_s immediately after the laser pulse is given by [98]

$$\pi(R_s + \Delta R_s)^2 l - \pi R_s^2 l = \beta V \Delta T \tag{1.19}$$

with the initial temperature rise

$$\Delta T = \frac{E\alpha l}{\rho V C_p} \tag{1.20}$$

where l is the length of the PA cell (assumed long), β is the expansion coefficient, $V=\pi R_s^2 l$ is the source volume, E is the laser pulse energy, α is the absorption length (with $\alpha l << 1$), ρ is the density and C_p is the specific heat at constant pressure. Combining eqns.(1.19) and

(1.20), and assuming $\Delta R_s << R_s$, we have [95]

$$\Delta R_s = \frac{\beta E \alpha}{2\pi R_s \rho C_p} \tag{1.21}$$

The peak displacement U(r) at the observation point at distance r from the PA source (for r << l) varies as $r^{1/2}$ because of conservation of acoustic energy, as described by Landau and Lifshitz for a cylindrical acoustic wave [122]

$$U(r) = \Delta R_s \left(\frac{R_s}{r}\right)^{1/2} = \frac{\beta E \alpha}{2\pi R_s^{1/2} \rho C_p r^{1/2}} \tag{1.22}$$

The peak acoustic pressure $P(r)$ at position r is related to the acoustic displacement U(r) and sound velocity c by

$$P(r) \approx \frac{c\rho U(r)}{\tau} \tag{1.23}$$

Substituting eqn.(1.22) in eqn.(1.23), we obtain the peak PA pressure observed at r for small source radius as

$$P(r) = \frac{\beta c E \alpha}{2\pi R_s^{1/2} C_p \tau r^{1/2}} \tag{1.24}$$

Eqn.(1.24) shows the basis of PA spectroscopy based on direct PA generation. It indicates that the normalized PA signal, defined as the detected acoustic pressure amplitude P divided by the laser pulse energy E is proportional to the absorption coefficient α with a proportionality constant K that depends on geometry and thermo-elastic properties. Thus, if the laser beam is tunable, the normalized PA spectrum provides an uncalibrated absorption spectrum if K is unknown. Absolute calibration is possible by calculating $K = \beta c/(2\pi R_s^{1/2} C_p \tau)^{1/2}$, or more practically, by measuring the normalized PA signal for a known absorber at one wavelength and thus empirically finding K. Eqn.(1.24) also indicates clearly the advantages and features of the PA spectroscopy of weak absorption by direct PA generation. For detecting small α, the signal magnitude P is increased by using intense laser pulses.

1.2.5 Simple Theory for Indirect PA Generation

A simple case of indirect PA generation is indicated in fig. 1.5. In general, indirect PA generation does not provide high sensitivity as the direct PA generation for detecting weak absorptions, basically because it is only a thin layer of a thermal diffusion length at the surface of the solid sample that is thermally coupled to the gas, producing the detected acoustic wave. However, PA generation is very valuable for the case opposite to weak absorption, that is, when the optical absorption is so strong that no light passes through the sample and hence

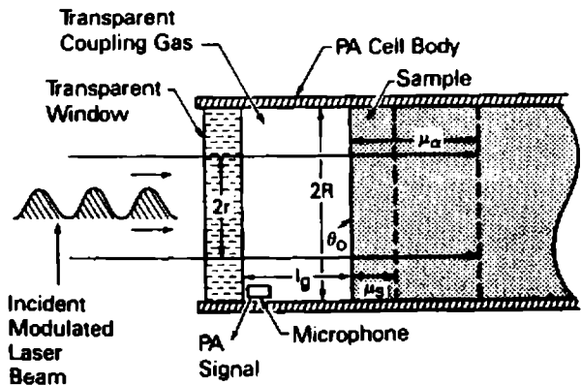

Figure 1.5: Schematic explanation of the indirect PA generation

conventional transmission monitoring fails. A detailed mathematical treatment of the indirect PA generation in solids has been given by Rosencwaig and Gersho, now commonly referred to as R-G theory [94]. R-G theory has been found to be very successful in interpreting most of the experimental results. This theory shows that in a gas-microphone PA cell, the acoustic wave generation depends on the pressure disturbance produced at the sample-coupling gas interface and the transport of this disturbance to the microphone. The generation of the acoustic pressure disturbance depends upon the temperature distribution at the sample surface. Thus the R-G theory could exactly predict the temperature distribution in the gas which directly depends on the absorption of light by the sample. A brief outline of the R-G theory is presented here. The detailed account of the theory is given elsewhere [94].

Let the incident laser beam of radius r and modulated at frequency f be incident on the sample of thickness l_s in a cylindrical cell of radius R and coupling gas thickness l_g. Let the sample optical attenuation coefficient be α at the excitation wavelength, and the optical absorption length be $\mu_\alpha = 1/\alpha$. The modulated component of the laser-induced heating is distributed over a diffusion length μ_s given by [98]

$$\mu_s = \left(\frac{D_s}{\pi f}\right)^{1/2} \tag{1.25}$$

where D_s is the thermal diffusivity of the sample. We assume that the optical wavelength and the modulation frequency are chosen so that the length l_s, μ_α and μ_s are in decreasing magnitudes. This represent one of the most interesting cases for PA spectroscopy. Let the

modulated laser beam intensity absorbed by the sample be represented by

$$I(t) = \frac{1}{2}I_0(1 + \sin 2\pi ft) \tag{1.26}$$

The modulated heat produced within the diffusion length μ_s, which is the depth in communication with the coupling gas, is only a fraction μ_s/μ_α of the power input I_0 that is absorbed over a depth μ_α. The heat conduction in the geometry of fig.1.5 can be described as follows: Thermal conductivity × thermal gradient = thermal power within the diffusion length, which means

$$k_s\frac{\theta_0}{\mu_s} \approx I_0\frac{\mu_s}{\mu_\alpha} \tag{1.27}$$

where k_s is the sample conductivity and θ_0 is the amplitude of the temperature variation on the sample surface, which is thermally coupled to an active volume V_{act} of the gas, given by (for $l_g > \mu_g$),

$$V_{act} \approx \pi r^2 \mu_g \tag{1.28}$$

where μ_g is the gas thermal diffusion length. Using the ideal-gas law, the amplitude δV of the volume change of V_{act} is

$$\delta V = \frac{V_{act}\theta_0}{T} \tag{1.29}$$

where T is the absolute temperature. Now the volume fluctuation δV causes a pressure fluctuation δP at the microphone. Assuming the adiabatic pressure-volume relation, we have

$$\delta P = \frac{\gamma P \delta V}{V} \tag{1.30}$$

where γ is the ratio of the specific heats and V is the total cell volume, given by

$$V = \pi R^2 l_g \tag{1.31}$$

Combining eqns. (1.27) to (1.31), we obtain the PA amplitude δP as

$$\delta P = \frac{\gamma P \mu_g \mu_s^2 I_0 r^2}{\mu_\alpha k_s l_g T R^2} \tag{1.32}$$

Eqn.(1.32) which agrees with the more detailed work of Rosencwaig and Gersho [94], indicates that the PA magnitude is proportional to the sample absorption coefficient $\alpha = 1/\mu_\alpha$, and the normalized PA signal $\delta P/I_0$ measured for a range of excitation wavelength λ can provide the absorption spectrum $\alpha(\lambda)$ as in the direct PA generation case. The unusual advantage here is that spectra of totally opaque or highly light-scattering materials can now be measured.

1.2.6 PA Detection

PA generation is caused by a modulated absorption which can be due to a modulated light beam. Modulation methods for the light source include Q- switching, mode locking, flash-lamp pumping, wavelength switching, mechanical chopping, electro-optic or acousto-optic modulating, wavelength modulating etc..

The PA cell is a container for the sample and for the microphone or transducer, such that the incident excitation beam is absorbed by the sample to produce an acoustic signal. Many designs of PA cells have been described in the literature [94, 95, 98, 123, 124], aiming at various aspects of signal improvement, noise reduction, and ease of use. PA cells can be classified into two general kinds: cells designed for gaseous samples [125], and those designed for condensed matter samples [123]. The former generally utilizes a microphone (with a relatively soft deflecting diaphragm) to sense the gaseous pressure fluctuations produced by the optical absorption. Besides microphone detection, fibre-optic detection [126] and optical probe-beam-deflection detection can also be used for gaseous samples [121]. In the second type of cells, for condensed matter, both microphones and piezoelectric transducers are in common use for detection. At low modulation frequencies or long enough pulse durations of the excitation beam, the exact geometry of the PA cell is important, since the acoustic wave can be reflected from the cell walls to produce interference and resonances. Hess [127] has reviewed the effects of acoustic resonance upon PA detection sensitivity. Noise can be reduced by locating the excitation beam entrance and exit positions at acoustic nodes in a resonant cell. On the other hand, at very high modulation frequency or very short pulse duration of the excitation beam, effects of reflections from cell walls are unimportant, and so is the geometry of the PA cell. Piezo-electric transducers are preferred over microphones for pulsed PA detection in condensed matter because of their much faster rise times and better acoustic impedance matching [128].

1.2.7 Applications of PA Effect

There exist several excellent reviews on applications of PA technique in various fields of physics chemistry, biology, engineering and medicine in the literature [92-95,97,105,121,129]. Only a brief account of the PA applications will be described here.

There are four general classes of applications of PA methods:

(1) PA spectroscopy: In this class of application, the PA signal amplitude is measured for a range of optical excitation wavelength, producing a PA spectrum; other factors (e.g., efficiency

in thermal deexcitation and in acoustic wave generation) are usually kept or assumed fixed while the PA spectrum is obtained. This is actually an excitation spectrum based on acoustic detection [124].

(2) PA monitoring of deexcitation processes: Here, the thermal decay branch is monitored to provide information on a competing decay branch. After optical excitation, four decay branches are generally possible: luminescence, photochemistry, photoelectricity, and heat that may be generated directly or through energy-transfer processes. For example, if luminescence and heat are the only two competing branching, PA monitoring of the heat branch can provide the quantum efficiency of luminescence under suitable circumstances [128, 129].

(3) PA probing of thermoelastic and other physical properties of materials: various information can be obtained conveniently with the help of the optical generation of thermal waves or acoustic waves. Such information includes sound velocity, elasticity, temperature, flow velocity, specific heat, thermal diffusivity, thickness of thin film, substrate defects and so on [87, 88, 130].

(4) PA generation of mechanical motions: PA effects can produce motions like liquid droplet ejection or structural vibrations.

PA detection techniques have been applied to a wide range of problems including many forms of spectroscopy in gases, liquids, and solids. A main attribute of acoustic detection is its high detection sensitivity. In addition, the energy deposited in the sample is measured directly. Several advantages result from this feature and PA spectroscopy often complements normal absorption and fluorescence spectroscopy. In the past two decades, PA effect has found many applications in spectroscopy of solids, liquids and gases, in medicine and biology, trace analysis, pollution monitoring, remote sensing, physics of semiconductors and amorphous materials, in thin films and so on. The application of PA effect has been so widely accepted that PA microscopy (PAM), Fourier transform PAS, PA trace analysis, PA magnetic resonance etc. are, by themselves areas of very strong research activity.

PA spectroscopic applications naturally divide into two categories, those utilizing chopped cw excitation sources and those using pulsed light sources. Considering only lasers, attributes of chopped cw sources are their inherent spectral purity (narrow frequency bandwidth) and high average power. Applications include high-resolution spectroscopy, thermal diffusivity measurements, the detection of 'forbidden' transitions such as singlet to triplet electronic transitions or vibrational overtone absorptions. Trace analysis and detection also falls into the category of weak absorption spectroscopy [131].

Pulsed excitation sources have a high peak light intensity or power which is advanta

geous for enhancing nonlinear photoprocesses. Nonlinear photoprocesses which have been detected acoustically include two photon visible/UV absorption spectroscopy, stimulated Raman spectroscopy and infrared multiphoton absorption. Pulsed PA also provide time domain discrimination allowing real time monitoring of photoinduced relaxation processes [132].

The PA effect can be observed only when the incident radiation is absorbed by the sample. Thus, if the wavelength of the ultraviolet, visible or near infrared radiation incident upon the sample is varied, the amplitude of the PA signal observed at a given wavelength will provide a measure of the ability of the sample to absorb the incident radiation, i.e., the absorption spectrum of the sample will be obtained. The PA power spectrum obtained by measurement of the signal amplitude vs wavelength of the incident radiation should therefore resemble the electronic absorption spectrum of the sample and be complementary in this way for the examination of solid samples should have a number of advantages over conventional optical absorption or diffuse reflectance spectroscopy.

Due to its high sensitivity, PA detection is ideally suited for measuring weak vibrational overtone absorptions. Vibrational overtone spectroscopy promises to provide much greater insight into the processes which control the photophysics of highly excited vibrational levels. Overtone absorption in liquids was detected by many PA researchers, the first reported in benzene [133, 134]. These studies have been extended to water and D_2O to study the weak absorption in water in the visible region, which is important for underwater laser communication studies [135]. The fluorescence quantum yield of laser dyes also has been determined using PA technique [136, 137]. PA studies have been extensively applied to the study of biological and medical processes [138, 139]. Recently, the technique of Pulsed PA was used to investigate the diffusion of chromophores in human skin [140]. The photochemical reactions, which necessarily occurs in all plants, can be studied by PA technique due to the fact that if a fraction of the absorbed energy is consumed by the photochemical process, then the PA spectra differs from the absorption spectra. These measurements can be performed by comparing the PA spectra obtained for a calibrated PA cell for the sample before and after the photochemical process has taken place. Extensive studies were performed on chloroplasts using this technique

PA technique has been widely applied to gas phase studies, especially in the areas of spectroscopy, trace analysis and pollution monitoring [141]. In gases, the absorption measurement capacity of $\sim 10^{-10}$ cm^{-1} with a cell length of $\sim$10 cm, using a continuously modulated laser for excitation, has been reported [142].

1.3 Photophysical Properties of Laser dyes

Fluorescence is the result of the rapid emission of light energy from a molecule which has become excited by light absorption. Fluorescence occurs following the radiative transition of the excited molecules from the first excited singlet state to the ground state. Such transitions are quantum mechanically 'allowed' and the emissive rates are typically 10^{8} sec^{-1}. These high emissive rates result in fluorescence lifetimes $\sim$ ns. The lifetime is the average period of time a fluorophore remains in the excited state. Substances which emit significant fluorescence possess delocalized electrons formally present in conjugated double bonds. Laser dyes contain an extended system of conjugate bonds, i.e., alternating single and double bonds. Laser dyes are characterized by a strong absorption band in the visible region of the electromagnetic spectrum. Dyes are large molecules (with molecular weight ranging from about 175 to 1000) that can absorb light from a wide spectral region and fluoresce at longer wavelengths. This section describes some fundamental aspects of fluorescence emission from laser dyes. In addition the section is intended to give an insight into the different optical processes taking place in a dye after light absorption along with the lasing characteristics of organic dyes.

1.3.1 Origin of Fluorescence

At room temperature most molecules are in the lowest vibrational level of the ground electronic state and from here transitions take place upwards on absorption of light. A dye molecule raised to an upper vibrational level of higher excited state rapidly loses its energy by collisions with surrounding molecules. This process indicated by the wavy lines in the fig.1.6, is known as internal conversion. It is found that a dye molecule when raised to higher electronic excited states, undergo internal conversion whereby it decays nonradiatively from a low vibrational level of the upper state to a high vibrational level of the lower state having the same total energy. Once internal conversion has occurred, the molecule again rapidly loses its excess vibrational energy by collision with solvent molecules. The net result of all these processes is that molecules raised to levels higher than the lowest vibrational level of the first excited state (i.e. level 0 of S_1) rapidly fall to the latter. Some substances may undergo photochemical reaction when raised to upper excited states but the processes leading to such reaction (e.g. dissociation) must take place rapidly to compete with the internal conversion and loss of vibrational energy by collisions. Similarly for light emission from these upper states to be appreciable, it also would have to a much more rapid process than it normally is, and consequently in solution the observation of light emission due to transitions from upper

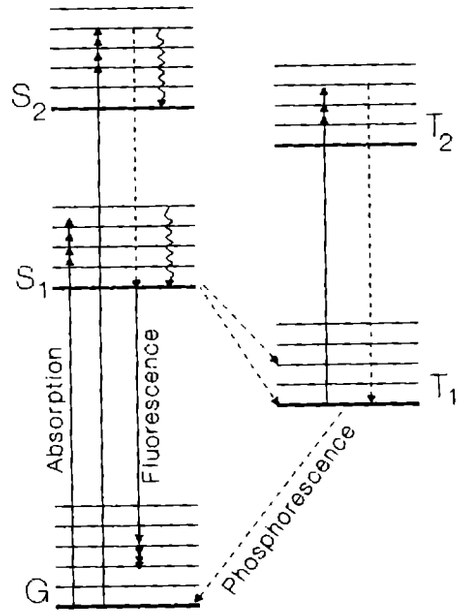

Figure 1.6: Typical energy level diagram of dye molecule

excited states is very rare.

From level 0 of S_1, the molecule can return to any one of the vibration-rotation levels of the ground state with the emission of fluorescence. If all the molecules that absorb light return to the ground state in this way, the solution will fluoresce with a quantum yield of unity. A fraction of the excited molecules may return to the ground state by other mechanisms, for example by intersystem crossing to the triplet manifold. The lowest vibrational level of the lowest triplet state is generally situated some way below that of the lowest excited state. Intersystem crossing occurs by the molecule crossing over to one of the upper vibrational levels of the lowest triplet state. From here the molecule rapidly loses its excess vibrational energy and falls to near the lowest vibrational level of the triplet state. The quantum efficiency of fluorescence then will be less than unity.

There are two possible ways, at least in principle, of using the dye solution as an active medium in dye laser: one might utilize either the fluorescence or the phoshorescence emission. At first sight the long lifetime of the triplet state makes phosphorescence look more attractive. On the other hand, due to strongly forbidden transition, a very high concentration of the active species is required to obtain an amplification factor large enough to overcome the inevitable cavity losses [143]. In fact, for many dyes this concentration would be higher than

the solubility of the dyes in any solvent. A further unfavourable property of these systems is that there will almost certainly be losses due to triplet-triplet absorption. It must be remembered that triplet-triplet absorption bands are generally very broad and diffuse and the probability that they would overlap the phosphorescence bands is high. Because of these difficulties no laser using the phosphorescence of a dye has been reported. The possibility cannot be ruled out because further study of phosphorescence and triplet-triplet absorption in molecules of different types of chemical constitution might eventually lead to a laser operating, for example, at the temperature of liquid nitrogen.

The fact that at room temperature absorption takes place almost exclusively from the lowest vibrational level of the ground state, while the emission takes place exclusively from the lowest vibrational level of the first excited state explains why only one transition, namely the 0-0 transition, is common to both the absorption and emission spectra. Frequently the emission spectrum is an approximate mirror-image of the first absorption band because the distribution of vibrational levels in the first excited state, which determines the shape of the first absorption band, is often similar to the distribution of vibrational levels in the ground state, which determines the shape of the fluorescence emission spectrum.

Energy losses between excitation and emission are observed universally for fluorescing molecules, except in the vapour phase. This phenomenon was first observed by Stokes in 1952 [144] and Stokes law states that the wavelength of the fluorescence is always longer than that of the exciting light. One common cause of Stokes shift is the rapid decay to the lowest vibrational level of S_1. Furthermore, fluorophores generally decay to excited vibrational levels of S_0, resulting in loss of vibrational energy. In addition to these effects, fluorophores can display further Stokes' shifts due to solvent effects and excited state reactions. In the gas phase, atoms and molecules do not always show Stokes' shifts. An unshifted emission is observed when the gas concentrations are sufficiently small so that the excited molecule does not collide with any other molecules prior to emission. Such encounters are a source of relaxation. In the fluid phase such collisions are continuous.

The fluorescence spectrum is generally observed irrespective of the excitation wavelength. Upon excitation into higher electronic and vibrational levels, the excess energy is quickly dissipated, leaving the fluorophore in the lowest vibrational level of S_1. This relaxatior occurs in about 10^{-12} sec, and is presumably a result of a strong overlap among numerou states of nearly equal energy. Because of this rapid relaxation, emission spectra are usuall independent of the excitation wavelength. Exceptions exist, such as azulene [145] which m emit both from S_2 and S_1.

1.3.2 Quantitative Aspects of Light Absorption and Emission

Consider a parallel beam of light of intensity I_0 directed on a parallel sided specimen. Then,

$$I_0 = I_R + I_R' + I_S + I_A + I_T \tag{1.33}$$

where I_R and I_R' are the intensity of light reflected at each interface; I_s, the scattered part; I_A, the intensity of absorbed light and I_T, the part that is transmitted.

At some point within the medium bounded by the infinitely thin layer dl, let the light intensity be I. The intensity of light absorbed, dI_A, in traversing the thin layer is thus equal to the product of the incident intensity, I, on the layer, and the total effective cross-section of the molecules per cm^2 of the beam in the layer, i.e.

$$dI_A = -dI = Ikc'dl \tag{1.34}$$

where c is the number of molecules/cc and k is the effective cross-section of one molecule in cm^2. On integration between 0 and l', the above equation gives the Beer-Lambert law.

$$I_T = I_0 e^{-kc'l} \tag{1.35}$$

A more practical form of the the above equation is as follows:

$$\log_{10} \frac{I_0}{I} = \epsilon cl \tag{1.36}$$

in which c is now measured in moles/litre and ϵ is known as the molecular extinction coefficient.

The quantity $\log_{10} \frac{I_0}{I}$ is known as the optical density or absorbance of the solution and is proportional to the concentration of the absorbing species. If more than one absorbing species is present the optical density of the mixture is equal to the sum of the optical densities of the separate components.

Absorption spectra consist simply of a plot of ϵ, or of $\log \epsilon$, against the wavelength or frequency of the light being absorbed. Fluorescence emission spectra are normally plotted in one of three ways. In the first method the number of quanta emitted per second within a unit wavelength interval at the wavelength concerned is plotted against the wavelength λ. In the second method the number of quanta emitted per second within a unit frequency interval is plotted against frequency. A third method is to plot energy emitted per second within unit wavelength interval against wavelength. The fluorescence is emitted from the specimen in all directions, but it is rarely necessary to plot the intensity scale in absolute units, relative values are all that are usually needed.

Because emission almost takes place exclusively from the lowest vibrational level of the first excited state, the fluorescence emission spectrum is always the same, no matter what the wavelength of the exciting radiation. This is a most useful rule in practical spectrofluorimetry because if it is found that the shape of the emission spectrum of a solution does change when the wavelength of the exciting light is varied, the presence of more than one fluorescence species should be suspected.

The relationship between the intensity of fluorescence and the extinction coefficient can be derived from the Beer-Lambert law. The rate of fluorescence emission, Q is equal to the product of the rate of light absorption (measured in quanta per sec) and the fluorescence quantum efficiency, Q_f [146]

$$Q = I_A Q_f \tag{1.37}$$

and from eqn.(1.35) therefore

$$Q = I_0(1 - e^{-kc'l)}Q_f \tag{1.38}$$

$$Q = I_0\left(kc'l - \frac{(kc'l)^2}{2} + \frac{(kc'l)^3}{6} - \ldots\ldots\ldots\ldots\right)Q_f \tag{1.39}$$

Taking the concentration in moles/litre, and changing into molecular extinction coefficient, we have:

$$Q = I_0(2.3\epsilon cl)\left(1 - \frac{2.3\epsilon cl}{2} + \frac{(2.3\epsilon cl)^2}{6} - \ldots\ldots\ldots\right)Q_f \tag{1.40}$$

For weakly absorbing solutions for which the optical density, ϵcl is small, and the equation simplifies to

$$Q = I_0(2.3\epsilon cl)Q_f \tag{1.41}$$

The above equation indicate that for a given substance in dilute solution contained in a particular cuvette, the intensity of the fluorescence observed is proportional to the product of concentration and the intensity of the exciting light.

1.3.3 An Overview of Dye Lasers

The first report of dye laser action was that of Sorokin and Lankard [147] who observed laser emission from a solution of chloroaluminium pthalocyanine. Independently, Schafer, Schmidt and Volze [148] obtained laser action in the infrared from a number of cyanine-type dyes. The uniqueness of these contributions was that they were the first reports of laser action from broad, diffuse energy bands rather a set of discrete energy levels, typical of gas and rare earth lasers. The tunability of the dye laser is a consequence of the broadened electronic levels characteristic of organic dyes.

Dye lasers are perhaps the most versatile and one of the most successful lasers available today. The most important attribute of the dye laser is its tunability, which gives the user access to essentially any wavelength. In the dye laser's region of operation, only a few lasers are competitive and those are only in limited parts of the dye laser's spectral region. A few new tunable lasers are beginning to threaten some of the traditional domains of the dye laser [149]. These include semiconductor, color-center, Ti-sapphire, alexandrite, and a few optically pumped solid state lasers. Other nontunable lasers exist that oscillate in the visible and near-visible region of the spectrum; for example, the Kr-ion and Ar-ion lasers have many useful lasing lines, and the optically pumped dimer lasers (sodium, lithium, iodine, etc.) have hundreds of lines, but the lines are relatively narrow and, even when combining all of these lasers, the actual fractional coverage of the available spectrum is small.

Dye lasers offer to researchers both pulsed and continuous wave (cw) operation that is tunable from the near-UV to the near-IR. A number of photophysical properties such as absorptivity, fluorescence yield, Stokes' shift, triplet population formation influence threshold determine the laser characteristics. The influence of solvent medium on laser-dye photophysics also plays significant role in determining the laser qualities [150, 151]. The cw dye laser is a well-established tool of optical science. This laser has a unique set of capabilities that include broad tunability, high power, and the ability for extremely high resolution. No other optical source can provide a comparable combination of tunability, resolution and power. The power levels available from cw dye lasers are generally more than adequate for spectroscopic applications. The output power of cw dye lasers varies with dye. Special high power cw dye lasers systems have been developed that can produce tens of watts of tunable visible radiation. With broad tuning ranges and narrow line widths, single-mode cw dye lasers can provide impressively large resolution. Continued improvements in the pump lasers, the dyes, and the nonlinear optical materials will undoubtedly provide higher output powers and extended spectral coverage. The spectral characteristics of cw dye lasers are both good and bad: good with respect to their line widths, and hence, spectral resolving capabilities, but generally poor with respect to their amplitude noise properties. Because of necessity, techniques have been developed to reduce the problems associated with this amplitude noise.

1.3.4 Requirements for a Dye to Act as a Laser Dye

The fact that out of thousands of commercially available dyes, only a few are good laser dyes, indicates that these must meet some special requirements to qualify as laser dyes. As

discussed in earlier sections, radiative process (i.e. fluorescence) is responsible for stimulated emission in the case of these dyes. Nonradiative processes always compete with fluorescence pathway and these can diminish the laser output and sometimes they may be prominent that the laser action may be completely diminished. Hence a good laser dye should have the following features .

1. As the fluorescence is responsible for stimulated emission, a laser dye should have very high fluorescence yield. Also it should have a wide fluorescence band so as to tunable over a broad spectral range.
2. As non-radiative processes deactivate the excited state and thus reduce the fluorescence quantum yield, the dye structure should be such that these processes are not favoured.
3. Because of the relatively long lifetime of the triplet molecules (in the order of microseconds) the dye accumulates during the pumping process in the triplet state T_1, which often has considerable absorption for the laser light. Thus some of the molecules are taken away from the lasing process. Moreover, due to triplet-triplet absorption, they cause an additional loss in the laser.
4. An efficient laser dye in its first excited singlet state should have negligible absorption at the excitation and lasing wavelength. Otherwise, losses would occur, as in triplet-triplet absorption, because the decay to the first excited singlet or triplet level is nonradiative.
5. The absorption spectrum of the dye should match with the spectral distribution of the pump source in order to take full advantage of the pump source.
6. During the lasing process a certain amount of thermal energy is released, giving rise to temperature gradients in the solution that may cause optical inhomogeneities. Hence the dye should be soluble in solvents having good thermal properties such as water, methanol etc..
7. An ideal laser should possess very good photochemical stability, otherwise not only the dye is depleted but sometimes the photo-products can quench the laser output.

Of the thousands of organic dyes available, only a few classes of dyes meet the stringent criteria for becoming useful laser dyes. The various classes of dyes and the region of the spectrum they cover are illustrated in elsewhere [152].

Many of these dyes may be viewed as having a benzene ring as the base chromophore, substituted with a number of electron donating groups - such structures generally increases the transition moment for optical absorption and also fluorescence emission. The light absorption of dyes on a semi quantitative basis has been explained by Kuhn [153, 154]. Factors increasing the fluorescence efficiency will increase the efficiency of dye lasers. It is known that a rigid planar molecular structure favours high fluorescence efficiency [155]. Generally,

a freely rotating group attached to the molecule reduces the fluorescence efficiency. In rhodamine B having two freely rotating diethylamino groups, the fluorescence efficiency is highly sensitive to change in temperature. But rhodamine 101 in which rigidization of the latter diethylamino group increases fluorescence substantially, is independent of temperatures [155].

Electron donating substituents on the aromatic ring generally increase the fluorescence efficiency as they increase the π electron density on the ring and hence the oscillator strength is increased. Also a dye substituted with heavy atoms shows reduced fluorescence efficiency as heavy atoms introduce increased spin-orbit coupling and increase the intersystem crossing efficiency [145, 156]

1.3.5 Effect of solvent

The photophysical and chemical properties of dyes are influenced to a great extent by the solvent environment. Hence solvent plays a very important role in dye lasers. During the dye laser operation the solution is subjected to a very high intense field of radiation. Nonuniform heating of the solvent takes place which in turn generates temperature gradient that may cause optical inhomogeneities in the solution. Hence the solvent used in a dye laser should possess good thermo-optical properties like water and heavy water. The solvent should not help dimerization and other photochemical processes in the laser dyes. The solvent should be transparent to the pump and lasing wavelength.

There are many solvent introduced effects which lead to changes in fluorescence efficiency. There are no generalized effects on solvents for all these dyes, but they vary from dye to dye. It has been observed in many cases that there is a considerable shift in the absorption and emission wavelengths of the dyes. Hence change of solvent can be used as a method for tuning the laser dyes. The energy difference between the 0-0 transitions should be greatest for those molecules showing a large change in the dipole moment on excitation to the first excited state. For a given substance it should also be greater in more polar solvents [146]. There is a relationship connecting the 0-0 band shift, the polarity of the solvent and the change in the dipole moment of the solute on excitation. By measuring the 0-0 band shift in a series of solvents, the dipole moment in the excited state can be calculated [157].

The selection of solvent can affect the performance of laser dyes in terms of alteration of fluorescence yield and lifetime as well as fluorescence wavelength. This phenomenon is also related to the long-held observation that dyes perform better when rigidly fixed in planar geometries. This restriction of allowed constraints imposed by assembly of dye substituents

in rings. These findings can now be understood in terms of a confluence of effects associated with the creation of dye dipoles, the conformational mobility of substituent groups, and solvent stabilization of charged species. The effects of selected solvents on the fluorescence yield and lifetime parameters for coumarin XI have been reported by Jones and co-workers [150, 158]. Studies by Jones et. al [150] revealed the principal influence of increased solvent polarity on nonradiative rate constant, k_d. More over, this undesirable reduction of emission yield and lifetime can be reversed (1) on adoption of very viscous solvents like glycerol, (2) with operation at low temperatures (ideally below room temperature).

Acidity of the solvent is another important property that influences the dye laser emission especially when the pKa of the ground and excited states are different. Thus by changing the pH of the solution it is possible to get large tuning range [155].

Formation of donor-acceptor charge transfer complexes between excited dye molecules and solvent also plays a major role. If such an exciplex is non-fluorescent, its formation may quench the fluorescence [159]

1.3.6 Dye Aggregation

Aggregation that can occur for higher concentrations of dye in water or alcohol solutions is well known. Potential driving forces for this phenomenon include the freeing the solvent molecules from solvation (hydration) spheres surrounding individual dye structures. Weak intermolecular bonding involving dipole-dipole and other forces is also important. The results of dimerization, which can be suppressed at higher temperatures, include subtle shifts in absorption due to exciton interacton (the coupling of the electronic states of individual molecules - splitting of energy levels - due to mutual overlap of orbitals). Fluorescence in dimers or higher aggregates is completely suppressed. This unwelcome alteration in dye dynamics is connected to the reduced lifetime of aggregated forms of organic dyes. For example, using fast time resolved fluorescence and absorption methods, Smirl et al [160] have shown that rhodamine B monomer and dimer in water display excited state lifetimes of 1.6 ns and 100 psec, respectively, signaling a high rate of nonradiative decay for the dye dimer. Aggregation is not an important deterrent where very low concentrations can be accommodated ([dye] generally $< 10^{-4}$ M) or where dye molecules are isolated in microdomains such as those provided by detergents.

1.4 Nonlinear Absorption

The intense monochromatic radiation from a laser can induce profound changes in the optical properties of a material. Nonlinear absorption refers to the change in transmittance of a material absorbing more than one photon before relaxing to the ground state can be greatly enhanced. As early as 1931, Goppert-Mayer derived the two photon transition probability in a system using second order quantum perturbation theory [161]. Since the invention of the laser, not only has this phenomenon of the simultaneous absorption of two photons been observed in a wide variety of materials, multiphoton (> 2) absorption has also been widely studied. In addition, population redistribution induced by intense laser fields leads to interesting counter plays of stimulated emission and absorption, complicated energy transitions in complex molecular systems, and the generation of free carriers in solids. These phenomena are manifested optically in a reduced (saturable) or increased (reverse saturable) absorption.

All optical nonlinearities can be broadly classified into two groups: instantaneous and accumulative nonlinearities. For the former, the polarization density resulting from an applied electric field occurs essentially instantaneously. For such interactions, the polarization density amplitude is usually expanded in a Taylor series in the electric field amplitude, E, or:

$$P = \epsilon_0[\chi^{(1)}E + \chi^{(2)}EE + \chi^{(3)}EEE + \ldots\ldots], \tag{1.42}$$

$\chi^{(n)}$ is the complex susceptibility tensor of order n. The first term $\chi^{(1)}$ is responsible for linear absorption and refraction, while the remaining terms are associated with light-induced nonlinear effects. The $\chi^{(2)}$ term is present only in noncentrosymmetric materials, and it gives rise to sum and difference frequency mixing, optical rectification, and the electro-optic effect. The term most widely applied to optical limiting is that involving $\chi^{(3)}$. The most important $\chi^{(3)}$ processes for optical limiting are two photon absorption, which is associated with the imaginary part of $\chi^{(3)}$, and the electronic Kerr effect, which is associated with the real part of $\chi^{(3)}$.

In contrast with the instantaneous nonlinearities, accumulative nonlinearities arise from interactions with memory, i.e., the polarization density generated by an applied field either develops or decays on a time scale comparable to or longer than the period of the exciting radiation. Such interactions are dissipative, i.e., they require energy transfer from the field to the medium, and the nonlinearity is initiated by this energy transfer. In contrast with the instantaneous nonlinearities which depend on the instantaneous intensity in the medium, accumulative nonlinearities depend on the energy density deposited in the medium. Examples

of such accumulative nonlinearities include nonlinear absorptive processes such as excited state absorption and free carrier absoprtion, and nonlinear refractive processes associated with free carrier generation or optically induced heating. These nonlinearities can also be nonlocal, i.e., the polarisation density induced at position r may depend on the optical intensity at position r'. An important example of such a process is the photorefractive effect.

The many different effects produced by nonlinear absorption in the frequency dependent transmittance of a material have led to several applications in science and technology. These include such diverse areas as nonlinear spectroscopy and optical limiting. In the subsections that follow, several of the formulas and phenomenon pertinent to an understanding of simultaneous multiphoton absorption, cumulative multistep absorption and absorption effects associated with population redistributions are discussed.

1.4.1 Two Photon Absorption

Two photon absorption (TPA) involves a transition from the ground state of a system to a higher-lying state by the simultaneous absorption of two photons from an incident radiation field. This process involves different selection rules than those of single photon absorption. Hence TPA spectroscopy complements linear absorption spectroscopy in studying the excited states of systems.

Two possible situations are illustrated in fig.1.7. In the first, two photons from the same optical field oscillating at frequency ω are absorbed to make the transition, which is approximately resonant at 2ω. In the second situation, two optical fields at frequencies ω_e and ω_p are present, and one photon from each field is absorbed for the transition, which is approximately resonant at $\omega_e + \omega_p$. The first field in this case (ω_e) can be thought of as the pump or excitation beam, while the second (ω_p) can be thought of as the probe beam. In both cases, the intermediate (or virtual) state is not real (i.e., does not involve a real stationary state of the system). Hence the system must absorb the two photons simultaneously. This makes the process sensitive to the instantaneous optical intensity.

Although the transition does not involve a real intermediate state, often there are impurities present that will produce a small amount of linear absorption. It should be understood that this absorption does not contribute to the transition to the final state of the process but only serves as an additional loss mechanism. Two-step absorption involving a single photon pumped intermediate state is described as Excited State Absorption (ESA).

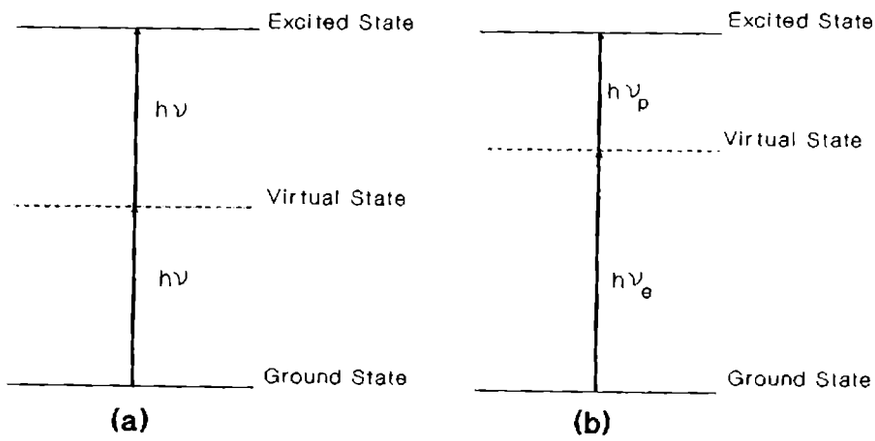

Figure 1.7: Two possible situations for TPA. (a) Self-TPA, (b) Pump-probe TPA

1.4.1.1 Single beam TPA

The nonlinear absorption in this case is proportional to the square of the instantaneous intensity. The differential equation describing the optical loss is given by [162]

$$\frac{dI}{dz} = -\alpha I - \beta I^2 \tag{1.43}$$

where α is the linear absorption coefficient due to the presence of impurities and β is the TPA coefficient.

The TPA coefficient β is a macroscopic parameter characterizing the material. Often, there is interest in the individual molecular TPA property that is described by the TPA cross-section σ_2. The relation between β and σ_2 is given by

$$\sigma_2 = \frac{\hbar\omega\beta}{N} \tag{1.44}$$

where N is the number density of molecules in the system, and $\hbar\omega$ is the energy of photons in the incident optical field. The TPA coefficient is also related to the third order susceptibility. This relation is [161]

$$\beta = \frac{3\pi}{\epsilon_0 n^2 c\lambda} Im\left[\chi^{(3)}_{xxxx}(-\omega;\omega,\omega,-\omega)\right] \tag{1.45}$$

Note that it is the imaginary part of $\chi^{(3)}$ that determines the strength of nonlinear absorption.

1.4.1.2 Two-beam Two-photon Absorption

This process, depicted in fig.1.7(b), involves the simultaneous absorption of two photons of different frequencies. These are designated as the pump or excitation frequency ω_e and the

probe frequency ω_p. The intensity in each of these beams can be comparable, but more often $I_p << I_e$.

The TPA coefficients involved in this process are again related to the third order susceptibility. The fact that the excitation and probe fields can have orthogonal polarization implies that this nonlinear process can lead to an induced dichroism in the material.

The differential equations describing the attenuation of the beams are [163, 164]

$$\frac{dI_e}{dz} = -\alpha_e I_e - 2\left[\frac{\omega_e}{\omega_p}\right]^{1/2} \beta_{ep} I_e I_p - \beta_{ee} I_e^2 \tag{1.46}$$

$$\frac{dI_p}{dz} = -\alpha_p I_p - 2\left[\frac{\omega_p}{\omega_e}\right]^{1/2} \beta_{pe} I_p I_e - \beta_{pp} I_p^2 \tag{1.47}$$

The first and last terms in these equations describe the linear and self-induced two-photon absorption, respectively, while the middle terms are what give rise to induced dichroism.

Two situations are considered. First, the excitation photon energy is less than half the energy of the first two-photon allowed transition. Thus the term involving β_{ee} can be ignored. Also, the self-induced absorption term involving β_{pp} is ignored since the probe is assumed to be weak relative to the excitation beam. In the second situation, self-induced TPA by the excitation beam is allowed, and the induced dichroism by the probe on the pump is assumed to be negligible. This implies that the excitation beam can pump allowed two-photon states both by itself (at $2\omega_e$) and in conjunction with the probe (at $\omega_e + \omega_p$). This is possible when there is a large density of two-photon allowed states, such as occurs in the conduction band of semiconductors and in the excited state spectrum of polyatomic molecules.

1.4.2 Three Photon Absorption

The phenomenon of resonant three photon absorption (3PA) is illustrated in fig.1.8. Three cases are shown involving one, two and three fields. Only the single field is treated here. Assuming that impurities introduce some background linear absorption, the equation describing the attenuation of a beam experiencing 3PA is given by

$$\frac{dI}{dz} = -\alpha I - \gamma I^3 \tag{1.48}$$

where γ is the 3PA coefficient. 3PA is a fifth order nonlinear process and γ is related to the fifth order susceptibility [163, 164]

$$\gamma = \frac{5\pi}{\epsilon_0^2 n^3 c^2 \lambda} Im[\chi^{(5)}_{xxxx}(-\omega;\omega,\omega,-\omega,-\omega)] \tag{1.49}$$

Again the beam is assumed to be linearly polarized and the medium is centrosymmetric.

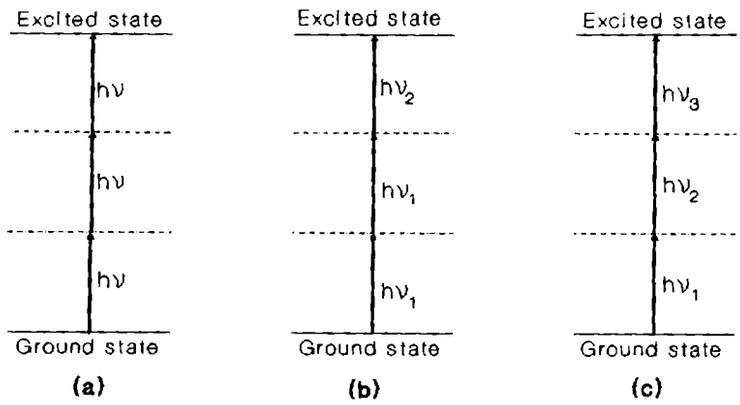

Figure 1.8: Schematic diagram of three photon absorption (3PA). (a) single beam self-3PA, (b) Two-beam 3PA, (c) Three-beam 3PA

1.4.3 Multiphoton Absorption

Multiphoton absorption (MPA) refers to the simultaneous absorption of photons from a single beam or multiple beams. The analogous to equations (1.43) and (1.48) for the absorption of n+1 photons from a single optical beam is [163]

$$\frac{dI}{dz} = -(\alpha + \gamma^{n+1} I^n) I \tag{1.50}$$

where $\gamma^{(n+1)}$ is the (n+1) photon absorption coefficient and has units of m^{2n-1}/W^n.

Nonresonant MPA is usually very weak for n $\geq$ 3. It can, however, be significant in semiconductors, especially narrow band gap materials.

Shen gives the transition probability rate per molecule for a nonresonant n-photon transition as [1]

$$W^{(n)} = \frac{\sigma^{(n)} I_1(\omega_1) I(\omega_2) \ldots\ldots\ldots I_n(\omega_n)}{\hbar^n \omega_1 \omega_2} \tag{1.51}$$

where $\sigma^{(n)}$ (assumed a scalar quantity) is the n-photon absorption cross-section.

For nonresonant transitions, $\sigma^{(n+1)}/\sigma^{(n)} \simeq 10^{-34}$ [163]. Therefore, $\sigma^{(n+1)} I/\hbar\omega \simeq 10^{-6}\sigma^{(n)}$ for I $\sim$1 GW/cm^2. Thus very high intensities are required to excite MPA. This is usually accompanied by avalanche ionization and breakdown in condensed matter.

1.4.4 Excited State Absorption

When the incident intensity is well above the saturation intensity, then the excited state can become significantly populated. In systems such as polyatomic molecules and semiconductors, there is a high density of states near the state involved in the excitation. The excited electron

can rapidly make a transition to one of these states before it eventually returns back to the ground state. There are also a number of higher-lying states that may be radiatively coupled to these intermediate states, and for which the energy differences are in near-resonance with the incident photon energy. Therefore before the electron completely relaxes to the ground state, it may experience absorption that promotes it to a higher - lying state. This process is called excited state absorption (ESA). It is observable when the incident intensity is sufficient to deplete the ground state significantly.

When the absorption cross-section of the ESA is smaller than that of the ground state, the transmission of the system will be increased when the system is highly excited. This process is called Saturable Absorption (SA). When the absorption cross-section of the excited state is larger than that of the ground state, then the system will be less transmissive when excited. This gives the opposite result as saturable absorption (SA) and is thus called Reverse Saturable Absorption (RSA).

In semiconductors, the absorption of a photon with energy greater than the band gap will promote an electron to the conduction band, where it is a free carrier and can contribute to current flow when a field is applied. The excited electron will rapidly thermalize and relax to the bottom of the conduction band. From there it will recombine with an excited hole in the valence band after a characteristic recombination time. However, at sufficiently high intensities, it can with high probability absorb another photon while it is still in the conduction band. This process is called free carrier absorption. It has similar qualitative characteristics to RSA.

1.4.5 Two-photon Assisted Excited State Absorption

When two-photon absorption is particularly strong in a material, it can lead to significant population of a two-photon allowed state. Often there are allowed radiative transitions from this state to higher-lying states of the system, i.e., excited state absorption can ensue from the two-photon pumped state. This occurs both in polyatomic molecules and in semiconductors.

The attenuation and excited state population equations are given by

$$\frac{\partial I}{\partial z} = -\alpha I - \beta I^2 - \sigma N I \tag{1.52}$$

and

$$\frac{\partial N}{\partial t} = \frac{\beta I^2}{2\hbar\omega} - \frac{N}{\tau_1} \tag{1.53}$$

where α is the linear absorption coefficient for impurity absorbers, and τ_1 represents the

lifetime of two-photon excited states. By solving these equation, the nonlinear transmittance of the system can be determined.

1.5 References

[1] G. M. Hieftje, J. C. Travis and F. E. Lytle (eds.) *Lasers in Chemical Analysis* (Humana : Clifton, New Jersey 1981).

[2] E. S. Yeung and M. J. Sepaniak, *Anal. Chem.*, **52**, 1465A (1980).

[3] J. Stone, *J. Opt. Soc. Am.*, **62**, 327 (1972).

[4] M. J. Sepaniak and E. S. Yeung, *Anal. Chem.*, **49**, 1554 (1997).

[5] S. D. Woodruff and E. S. Yeung, *Anal. Chem.*, **54**, 1174 (1982).

[6] W. G. Tong and E. S. Yeung, *Talanta*, **31**, 659 (1984).

[7] E. S. Yeung, L. E. Steenholk and J. C. Kuo, *Anal. Chem.*, **52**, 1399 (1980).

[8] A. Hordvik, *Appl. Opt.*, **16**, 2827 (1973).

[9] D. A. Cremers and R. A. Keller, *Appl. Opt.*, **21**, 1654 (1982).

[10] J. M. Harris and N. J. Dovichi, *Anal. Chem.*, **52**, 695A (1980).

[11] M. Franko and C. D. Tran, *Rev. Sci. Instrum.*, **67**, 1 (1996).

[12] A. C. Boccara, D. Fournier and J. Badog, *Appl. Phys. Letts.*, **36**, 130 (1980).

[13] T. I. Chen and M. D. Morris, *Anal. Chem.*, **56**, 19 (1984).

[14] M. J. Pelletier, H. R. Thorsheim and J. M. Harris, *Anal. Chem.*, **54**, 239 (1982).

[15] J. P. Gordon, R. C. C. Leite, R. S. Moore, S. P. S. Porto and J. R. Whinnery, *J. Appl. Phys.*, **36**, 3 (1965).

[16] J. M. Harris in *Analytical Applications of Lasers* (ed.) E. H. Piepmeir (John Wiley, New York, 1986).

[17] S. Wu and N. J. Dovichi, *J. Appl. Phys.*, **67**, 1170 (1990).

[18] F. W. Dabby, R. W. Boyko, and J. R. Whinnery, *IEEE J. Quant. Elect.*, **5**,516 (1969).

[19] M. Franko and C. D. Tran, *Rev. Sci. Instrum.*, **62,** 2430 (1991).

[20] M. Franko and C. D. Tran, *Rev. Sci. Instrum.*, **62,** 2439 (1991).

[21] J. R. Barker and T. Rothem, *Chem. Phys.*, **68,** 331 (1982).

[22] R. Vyas and R. Guptha, *Appl. Opt.*, **27,** 4701 (1988).

[23] C. A. Carter and J. M. Harris, *Appl. Opt.*, **476** (1984).

[24] C. Rojas, R. J. Silva, J. DF. Spear and R. E. Russo, *Anal. Chem.*, **63,**1927 (1991).

[25] S. Shen, A. J. Soroka and R. D. Snook, *J. Appl. Phys.*, **78,** 700 (1995).

[26] Q. He, R. Vyas and R. Guptha, *Appl. Opt.*, **36.**1841 (1997).

[27] R. L. Swofford and J. A. Morrell, *J. Appl. Phys.*, **49,**3667 (1978).

[28] R. T. Bailey, D. Pugh and W. Johnstone, *J. Chem. Soc. Far. Trans.* **76,**633 (1980).

[29] W. A. Weimer and N. J. Dovichi, *J. Appl. Phys.*, **59,** 225 (1986).

[30] R. Guptha *in Photothermal Investigations of Solids and Fluids* ed. J. A. Sell (Academic, New York, 1988).

[31] A. Yariv, *Optical Electronics* (Holt, Rinehart and Winston, New York, 1985).

[32] T. G. Nolan, D. J. Bornhop and N. J. Dovichi, *J. Chromat.*, **384,**189 (1987).

[33] J. R. Erskine and D. R. Babbitt, **43,**668 (1989).

[34] N. J. Dovichi and J. M. Harris, *Anal. Chem.*, **53**, 106 (1981).

[35] K. E. Rieckhoff, *Appl. Phys. Letts.*, **9,**87 (1966).

[36] J. R. Whinnery, D. T. Miller and F. Dabby, *IEEE J. Quant. Elect.*, **3.**282 (1967).

[37] S.A. Akhamov, D. P. Krindach, A. V. Migulin, A. P. Sukhorukov and R. V. Khokhlov, *IEEE J. Quant. Elect.*, **4,**568 (1968).

[38] N. J. Dovichi and J. M. Harris, *Anal. Chem.*, **51,**728 (1979).

[39] N. J. Dovichi and J. M. Harris, *Anal. Chem.*, **52,**2338 (1980).

[40] F. R. Grabiner, D. R. Siebert and G. W. Flynn, *Chem. Phys. Letts.*, **17,** 189 (1972)

[41] M. E. Long, R.L. Swofford, and A.C. Albrecht, *Science*, **191** 183 (1976).

[42] S. J. Sheldon, L. V. Knight, J. M. Thorne, *Appl. Opt.*, **21** 1663 (1982).

[43] H. L. Fang and R. L. Swofford in *Ultrasensitive Laser Spectroscopy,* ed. D. L. Kliger (Academic New York 1983)Ch3.

[44] J. P. Haushalter and M. D. Morris, *Appl. Spectr*, **34** 445 (1980).

[45] J. W. Perry, E. A. Ryabov and A. H. Zewail, *Laser Chem.,* **1** 9 (1982).

[46] H. L. Fang and R. L. Swofford, *J. Appl. Phys.*, **50** 6609 (1979).

[47] C. E. Buffet and M. D. Morris, *Anal. Chem.,* **54** 1824 (1982).

[48] C. A. Carter and J. M. Harris, *Anal. Chem.* **55** 1256 (1983).

[49] C. A. Carter, J. M. Brady and J. M. Harris, *Appl. Spectr.*, **36** 309 (1982).

[50] C. E. Buffet and M. D. Morris, *Appl. Spectr.,* **37** 455 (1983).

[51] R. Anthone, P. Flament, G. Gouesbet, and Me. Weill, *Appl. Opt.,* **21** 2 (1982).

[52] R. D. Snook and R. D. Lowe, *Analyst*, **120**, 2051 (1995).

[53] R. D. Snook, R. D. Lowe, and M. L. Baesso, *Analyst*, **123**, 587 (1998).

[54] K. Mori, T. Imasaka and N. Ishibashi, *Anal. Chem.,* **55** 1075 (1983).

[55] G. R. Ramos, B. W. Smith and N. Omenetto, *Appl. Spectr.*, **42** 341 (1988).

[56] G. R. Long and S. E. Bialyaeva, *Anal. Chem.,* **56** 2806 (1984).

[57] A. G. Abroskin, T. V. Belyaeva and Y. A. Barbalat, *Analyst,* **117** 1957 (1992).

[58] D.R.Siebert, F.R. Grabiner and G.W. Flynn, *J. Chem. Phys.*, **60** 1564 (1974).

[59] G. C. Nieman and S. D. Colson, *J. Chem. Phys.*, **68** 2994 (1978).

[60] R. A. Leach and J. M. Harris, *Anal. Chem.,* **56** 1481 (1984).

[61] K. Miyaishi, T. Imasaka and N. Ishibashi, *Anal. Chem.*, 54 2039 (1982).

[62] T. G. Nalan, W. A. Weimer and N. J. dovichi, *Anal. Chem.,* **56** 1706 (1984).

[63] K. Miyaishi, T. Imasaka and N. Ishibashi, *Anal. Chim. Acta,* **124** 381 (1981).

[64] R. A. Leach and J. M. Harris, *Anal. Chim. Acta.*, **164** 91 (1984).

[65] C. Hu and J. R. Whinnery, *Appl. Opt.*, **12**, 72 (1973).

[66] T. Berthoud, N. Delorme and P. Mauchien, *Anal. Chem.*, **57** 1216 (1985).

[67] J. Shen, R. D. Lowe and R. D. Snook, *Chem. Phys.*, **197** 255 (1992).

[68] J. R. Whinnery, Acc. *Chem. Res.*, **7** 225 (1974).

[69] A. J. Twarowski and D. S. Kliger, *Chem. Phys.*, **20** 259 (1977).

[70] C. A. Carter and J. M. Harris, *Anal. Chem.*, **56** 922 (1984).

[71] K. V. Skogerboe and E. S. Yeung, *Anal. Chem.* **58** 1014 (1986).

[72] C. E. Buffect and M. D. Morris, *Anal. Chem.*, **54** 1824 (1982).

[73] N. J. Dovichi and J. M. Harris, *Anal. Chem.*, **53** 689 (1981).

[74] R. A. Leach and J. M. Harris, *J. Chromat.*, **115** 218 (1981).

[75] C. E. Buffect and M. D. Morris, *Anal. Chem.*, **55** 376 (1983).

[76] M. Terazima and T. Azumi, *Chem. Phys. Letts.*, **141** 237(1987).

[77] M. Terazima and T. Azumi, *Chem. Phys. Letts.*, **145** 286(1988).

[78] M. Terazima and T. Azumi, *Chem. Phys. Letts.*, **153** 27 (1988).

[79] S. F. Lebedkin and A. D. Klimov, *Chem. Phys. Letts.*, **190** 313 (1992).

[80] T. Suzuki, Y. Kaji, K. Shibaya and K. Obi, *Bull. Chem. Soc. Jpn.*, **65** 1084 (1992).

[81] F. W. Dabby and J. R. Whinnery, *Appl. Phys. Letts.*, **13**, 284 (1968).

[82] M. L. Baesso, J. Shen and R. D. Snook, *J. Appl. Phys.*, **75** 3732 (1994).

[83] A. M. Mansanares, M. L. Baesso, E. C. da Silva H. Vargas and L. C. M. Miranda, *Phys. Rev. B*, **40**, 7912 (1989).

[84] A. G. Bell, *Philos. Mag.*, **11**, 510 (1881)

[85] J. Tyndall, *Proc. Roy. Soc. London.*, **31**, 307 (1881)

[86] W. C. Rontgen, *Philos. Mag.*, **11**, 308 (1881)

[87] S. S. Raman, V. P. N. Nampoori and C. P. G. Vallabhan, *Appl. Phys. Lett.*, **67**, 2939 (1995)

[88] S. S. Raman, V. P. N. Nampoori and C. P. G. Vallabhan, *J. Mat. Sci.*, **15**, 230 (1996)

[89] R. C. Issac, S. S. Harilal, C. V. Bindhu, G. K. Varier, V. P. N. Nampoori and C. P. G. Vallabhan, *Opt. Engg.*, **36**, 332 (1997)

[90] P. Sathy, R. Philip, V. P. N. Nampoori and C. P. G. Vallabhan, *Opt. Commn.*, **74**, 313 (1990)

[91] A. Philip, P. Radhakrishnan, V. P. N. Nampoori and C. P. G. Vallabhan, *J. Phys. D.*, **26**, 836 (1993)

[92] Y. H. Pao, *Optoacoustic Spectroscopy and Detection* (Academic, NY, 1975)

[93] A. Rosencwaig, *Anal. Chem.*, **47**, 5924 (1975)

[94] A. Rosencwaig, *Photoacoustics and Photoacoustic Spectroscopy,* (Wiley, NY, 1980)

[95] C. K. N. Patel and A. C. Tam, *Rev. Mod. Phys.*, **53**, 517 (1981).

[96] D. A. Hutchins, *Can. J. Phys.*, **64**, 1247 (1986).

[97] M. J. Colles, N. R. Geddes and E. Mehdizadeh, *Contem. Phys.*, **20**, 11 (1979).

[98] A. C. Tam *in Analytical Application of Lasers* (ed.) by E. H. Piepmeir (John Wiley & Sons, New York 1986)

[99] A. C. Tam *in Ultrasensitive Spectroscopy* (Academic, New York, 1983).

[100] M. J. Adams, A. A. King and G. F. Kirbright, *Analyst*, **101**, 73 (1976).

[101] J. F. Ready, *Effects of High Power Laser Radiation* (Academic, New York, 1971).

[102] S. S. Harilal, C. V. Bindhu, V. P. N. Nampoori and C. P. G. Vallabhan, *Appl. Phys. Letts.*, **72**, 167 (1998).

[103] S. S. Harilal, C. V. Bindhu, R. C. Issac, V. P. N. Nampoori and C. P. G. Vallabhan, *Mod. Phys. Letts.*, **10,** 1053 (1996).

[104] N. Bloembergan, *IEEE J. Quan. Electr.*, **10,** 375 (1974)

[105] L. M. Lyanshev and K. A. Naugol'nykh, *Sov. Phys. Acoust.*, **27,** 357 (1981)

[106] M. W. Sigrist, *J. Appl. Phys.*, **60,** 483 (1986)

[107] S. S. Harilal, C. V. Bindhu, R. C. Issac, V. P. N. Nampoori and C. P. G. Vallabhan, *J. Appl. Phys.*, **82,** 2140 (1997).

[108] M. W. Sigrist and F. K. Kneubuhl, *J. Acou. Soc. Am.*, **64,** 652 (1978)

[109] F. V. Bunkin and V. M. Komissarov, *Sov. Phys. Acous.*, **19,** 203 (1973).

[110] S. R. J. Brueck, H. Kildal and L. J. Belanger, *Opt.Comm.*, **34**,199 (1980).

[111] H. M. Lai and K. Young, *J. Acous .Soc. Am.*, **72,** 2000 (1982).

[112] S. S. Harilal, R. C. Issac, C. V. Bindhu, V. P. N. Nampoori and C. P. G. Vallabhan, *Mod. Phys. Letts.*, **9,** 871 (1995).

[113] R. M. White, *J. Appl. Phys.*, **34,** 3559 (1963).

[114] L. S. Gourney, *J. Acou. Soc. Am.*, **40,** 1322 (1966).

[115] B. Sullivan and A. C. Tam, *J. Acou. Soc. Am.*, **75,** 437 (1984).

[116] J. M. Heritier, *Opt. Commn.*, **44,** 267 (1983).

[117] A. Rosencwaig and A. Gersho, *J. Appl. Phys.*, **47,** 64 (1976).

[118] L. C. Aamodt and J. C. Murphy, *J. Appl. Phys.*, **48,** 3502 (1977).

[119] G. C. Wetsel Jr. and F. A. Mcdonald, *Appl. Phys. Lett.* **30,** 252 (1977).

[120] A. C. Tam and Y. H. Wong, *Appl. Phys. Letts.*, **36,** 471 (1980).

[121] A. C. Tam., *Rev. Mod. Phys.*, **58,** 381 (1986).

[122] L. D. Landau and E. M. Lifshitz, *Fluid Mechanics*, (Pergamon, Ney York, 1959).

[123] R. Philip, P. Sathy, V. P. N. Nampoori and C. P. G. Vallabhan, *J. Phys. B.*, **25**, 151 (1992).

[124] A. V. R. Kumar, *Ph. D. Thesis*, Cochin University of Science & Technology (1992).

[125] A. V. R. Kumar, G. Padmaja, V. P. N. Nampoori and C. P. G. Vallabhan, *Pramana*, **33**, L621 (1989).

[126] R. E. Russo, D. Rojas, P. Robouch and R. S. Silva, *Rev. Sci. Instrum.*, **61** 3729 (1990).

[127] P. Hess in *Topics in Current Physics* Vol 46,47 (Springer Verlag, 1989).

[128] P. Sathy, *Ph.D. Thesis*, Cochin University of Science & Technology (1992).

[129] J. B. Kinney, and R. H. Stately, *Ann. Rev. Mater. Sci.*, **12**, 295 (1982).

[130] C. V. Bindhu, S. S. Harilal, R. C. Issac, V. P. N. Nampoori and C. P. G. Vallabhan, *Pramana - J. Phys.*, **44**, 231 (1995).

[131] P. Satheeshkumar, *Ph. D. Thesis*, Cochin Uiversity of Science & Technology (1987).

[132] R. Philip, *Ph.D. Thesis*, Cochin University of Science & Technology (1993).

[133] C. K. N. Patel and A. C. Tam, *Appl. Phys. Letts..*, **34** 467 (1979).

[134] C. K. N. Patel and A. C. Tam, *J. Chem. Phys.*, **71** 1470 (1979).

[135] A. C. Tam and C. K. N. Patel, *Appl. Opt.*, **18** 3348 (1979).

[136] P. Sathy, R. Philip, V. P. N. Nampoori and C. P. G. Vallabhan, *Pramana*, **34**, 585 (1990).

[137] C. V. Bindhu, S. S. Harilal, R. C. Issac, V. P. N. Nampoori and C. P. G. Vallabhan, *Mod. Phys. Letts.*, **10** 1103 (1996).

[138] K. A. Giese, A. Nicolaus, B. Sennhelm and K. Kolmel, *Can. J. Phys.*, **64**, 1139 (1986)

[139] S. E. Braslavsky, *Photochem. Photobiol.*, **43**, 667 (1986).

[140] F. Lahjomri, G. Puccetti, R. M. Leblanc, V. Alard, A. Denis and J. F. Tranchant, *Photochem. Photobiol.*, **65**, 292 (1997).

[141] M. A. Gondal, *Appl. Opt.*, 3195 **36**, (1997).

INTERNATIONAL SCHOOL OF PHOTONICS LIBRARY

[142] Patel and Kerl R J, *Appl. Phys. Letts.*, **30,** 578 (1977).

[143] F. P. Schafer in *Dye Lasers* (ed.) F. P. Schafer, (Springer-Verlag, Berlin, 1977).

[144] G. G. Stokes, *Phil. Trans. Royal Soc. London*, **142** 463 (1852).

[145] J. B. Birks, *Photophysics of Aromatic Molecules* (Wiley-Interscience, London, 1970).

[146] C. A. Parker, *Photoluminescence of Solutions*, (Elsevier, Amsterdam, 1968).

[147] P. P. Sorokin, J. R. Lankard, *IBM J. Res. Develop.*, **10,** 162 (1966).

[148] F. P. Schafer, W. Schmidt and J. Volze, *Appl. Phys. Letts.*, **9,** 309 (1966).

[149] R. A. Meyers (ed.) *Encyclopeadia of Laser Technology* (Academic, NY, 1991).

[150] G. Jones II, W. R. Jackson and W. R. Bergmark, *J. Phys. Chem.*, **89,** 294 (1985)

[151] S. M. Grenchi, G. R. Bird and A. H. Zewail, *Laser Chem.*, **6,** 361 (1986).

[152] C. V. Shank, *Rev. Mod. Phys.*, **47,** 649 (1975).

[153] H. Kuhn, *Chimica*, **9,** 237 (1955).

[154] H. Kuhn, *Progress in the Chemistry of Organic Natural Products,* D. L. Zechmeister (ed.) (Springer, Wein, 1958).

[155] K. H. Drexhage in *Dye Lasers* (ed.) F. P. Schafer, (Spriger-verlag, Berlin, 1977).

[156] N. J. Turro, *Molecular Photochemistry* (Benjamin, New York, 1965).

[157] E. Lippert, *Z. Elektrochem.*, **61** 962 (1957).

[158] G. Jones II, W.R. Jackson and A.M. Halpern, *Chem. Phys. Letts.*, **72,** 391 (1970).

[159] A. Diens, C. V. Shank and A. M. Trozzolo, *Appl. Phys. Letts.*, **17,** 189 (1970).

[160] A. L. Smirl, J. B. Clark and B. R. Russel, *J. Chem. Phys.*, **77,** 631 (1982).

[161] G. Mayer, *Ann.Phys.*, **9** 273 (1931).

[162] L. W. Tutt and T. F. Bogges, *Prog. Quan. Elect.*, **17,** 299 (1993).

[163] Y. R. Shen, *The Principles of Nonlinear Optics*, (John Wiley, New York, 1984).

[164] R. W. Boyd, *Nonlinear Optics*, (Academic Press, New York, 1992).

Chapter 2

Experimental Approach

This chapter deals with the general experimental methods followed in the present research. Details of the experimental set up used for the thermal lens as well as photoacoustic studies are discussed separately. A brief description of subsystems like laser sources, monochromator, photomultiplier tube, lock-in amplifier, boxcar averager and storage oscilloscope used for the above measurements are presented.

2.1 Introduction

When light is absorbed by a sample, a fraction of the ground state molecules will get excited into higher energy levels. These excited states subsequently relax through a combination of radiative and nonradiative processes. The nonradiative component will generate heat in the localized region of the excitation beam or pressure wave that propagates away from the excited region. The change in refractive index along the beam path can effectively be monitored using the thermal lensing technique and the pressure wave can be detected by using a suitable sensor such as microphone or pressure transducer. The radiative component can be detected using fluorescence spectroscopic technique. This section gives a broad outline of the experimental techniques employed in the present investigations such as the cw and pulsed thermal lens, pulsed photoacoustics and fluorescence technique. Finer details of the respective experimental arrangements will be given in the following chapters.

Firstly, a brief description of the different subsystems, like laser sources, lock-in amplifier, box car averager etc. used for these experimental studies are given.

2.2 Subsystems

2.2.1 Laser Sources

The lamp/monochromator and the laser are the two types of light sources in use in photothermal spectroscopy. Lasers, with their nearly monochromatic beam of high spectral brightness, enjoy significant advantages over lamp/monochromator combination which account for the wider acceptance of the former as photothermal light sources.

In the present scheme of experiment, an argon ion laser and a Q-switched Nd:YAG laser were used as the pump source in cw and pulsed mode of thermal lensing respectively. In both cw and pulsed double beam thermal lens, the He-Ne laser source was used as the probe beam. For pulsed photoacoustic measurements the Q-switched Nd:YAG was used. A brief account of these laser sources are given in this section.

2.2.1.1 Argon ion laser

The cw laser source used in the present thermal lens experiment was a 12 Watt Argon ion laser (Spectra Physics model 171). It can be made to operate both in multiline and in single lines of wavelength 514.5, 496.5, 488, 476.5 and 456 nm. The discrete lines can be obtained by tuning the prism which is placed in the cavity. The laser output has a gaussian profile

and has a frequency stability of 60 MHz/°c and a stability of ± 0.5% when used in the light control mode [1]. The laser is also provided with power meter for continuous monitoring of the output power. The whole laser system and power supply system is equipped with an elaborated water cooling arrangement.

2.2.1.2 Nd:YAG laser

The pulsed laser used in our experiment was an electro-optically Q-switched Nd:YAG laser (Quanta Ray DCR 11) having a fundamental frequency of 1.06 μm.

The optical cavity in the DCR-11 is an unstable resonator. In a stable resonator the ray of light is traveling close to the optical axis and is reflected toward the optical axis by its cavity mirrors, so it is always contained along the primary axis of the laser. By contrast, a ray traveling in an unstable resonator can be reflected away from the axis by one of the cavity mirrors. Stable resonators can only extract energy from a small volume near the optical axis of the resonator, which limits the energy of the output. Conversely, unstable resonators can have large beam diameters. Thus they can efficiently extract energy from active media whose cross-sectional area is large, like that of typical Nd:YAG laser rods. The output coupler in an unstable resonator is a small high reflector mounted on a clear substrate which lies on the optical axis of the resonator. Energy escapes from the resonator by diffracting around this dot, which gives the "diffraction coupled resonator" (DCR) its name [2]. The laser provides pulses of FWHM 9 ns with a power stability of ± 4%. The laser beam has a typical line width of < 1 cm^{-1} with 220 MHz spacing between the longitudinal modes and a beam divergence of < 0.5 mrad.

The high peak power of the Q-switched pulses permit frequency conversion in nonlinear crystals like KD*P. By introducing appropriate crystals in the beam path, higher order harmonics can be obtained. The 1064 nm fundamental interacts with the crystal to produce 532 nm wavelength. The resultant 532 nm wave can be doubled again by passing it through a second crystal, which yields a 266 nm wave. It can also be mixed in KD*P with the residual 1064 nm to produce a 355 nm wave. The laser provides trigger outputs to synchronize oscilloscope, energy meter, boxcar etc..

2.2.1.3 He-Ne laser

The probe beam in thermal lens spectroscopy should preferably have a gaussian intensity profile and good stability. The 632 nm radiation from a He:Ne laser (Model 102 Spectra

Physics) was used as the probe in our thermal lens experiments. The output of the laser is 5 mW and is intensity stabilized [3].

2.2.2 Chopper

For double beam cw thermal lens measurements the argon ion laser beam was modulated using a mechanical chopper (EG&G Parc model 192 or SR540, Stanford Research systems). Mechanical chopper is the simplest form of a modulator consisting of a rotating slotted disk placed in the path of the light beam. It offers 100% modulation depths for frequencies from a few Hz to 5 - 8 KHz [4, 5].

2.2.3 Sample cell

For taking the liquid samples we have used 10 mm and 5 mm quartz cuvettes. Both four side polished and two side polished cuvettes were available.

2.2.4 Power Meters

2.2.4.1 EG & G Gamma Scientific

For measuring the laser power during the cw thermal lens experiment the EG&G laser power meter (EG&G Gamma Scientific model 460-1A) was used. This laser power meter incorporates an EG&G silicon photo voltaic detector with a circular sensitive area of 1 cm^2. The unique detector features high sensitivity, long-term stability, excellent linearity of response over a wide dynamic range, and ultra-low noise levels [6]. The windowless features of the detector eliminates errors caused by multiple reflections in parallel optics.

2.2.4.2 Scientech

This is a disc calorimeter that employs a calibrated thermopile which generates a voltage proportional to the heat that is liberated from the absorption of the input laser flux. Many thermoelectric junctions are arranged in series and sandwiched between an absorption surface producing heat which flows through the thermopile. The heat flow is accurately proportional to the laser beam power and substantially independent of the laser beam spatial distribution of power [7]. The thermopile output is a linear low impedance, dc signal of approximately 0.09 volts/W. The following are the major specifications of Scientech 362 : flat spectral response in the region of 400 nm to 1200 nm, a continuous power range (for cw lasers and average

power measurement of pulsed lasers) from 0 to 10 Watts, a maximum power density of 47 W cm^{-2} and a maximum pulse energy density of 3.3 J cm^{-2}.

2.2.5 Monochromators

Monochromators are widely used for analyzing the light emitted from another device or process, and for observing the effects of specific wavelengths of light transmitted through various materials. The specifications for the performance of a monochromator include the dispersion and the stray light levels. Generally the dispersion is given in nm/mm, where the slit width is expressed in mm. In selecting monochromator for emission spectroscopy, one looks for low stray light levels to avoid problems due to scattered stray light. Stray light is defined as any light which passes through the monochromator besides that of the desired wavelength. In addition, monochromators are chosen for high efficiency to maximize the ability to detect low light levels. The slit widths are generally variable and a typical monochromator will have both an entrance and an exit slit. The light intensity which passes through a monochromator is approximately proportional to the square of the slit width. Larger slit widths yield increased signal levels, and therefore higher signal to noise (S/N) ratios. Smaller slit widths yield higher resolution, but at the expense of light intensity. A small slit width is used to increase precision of the wavelength determination and to decrease the light intensity. Grating monochromators may have planar or concave gratings. Planar gratings are usually produced mechanically and may contain imperfections in some of the grooves. Concave gratings are usually produced by holographic and photoresist methods, and imperfections are rare. Imperfections of the gratings are major source of stray light transmission by the monochromators, and of ghost images from the grating. For this reason the holographic gratings are preferable for emission spectroscopy. Another important characteristic of the grating monochromators is that the transmission efficiency depends upon polarization of the light. Therefore the emission spectrum of the sample can be shifted in wavelength and altered in shape, depending upon the polarization conditions chosen to record. In the present work we used the following three monochromators:

2.2.5.1 Spex

Spex, Model 1704 is a 1 meter scanning spectrometer having a maximum resolution of 0.05 A [8]. The monochromator covers a spectral range 350-950 nm using a grating with 1200 grooves per mm blazed at 500 nm and spectral band pass 0.1 A . The entrance and exit

slits on the front of the spectrometer are controlled by micrometer type knob above the slits. The scan rate of the monochromator is adjusted by using microprocessor controlled Spex compudrive (CD2A) arrangement. Spex compudrive has got a key board control over the spectrometer which not only provides repeat scan over the spectral regions but also gives the scan status and spectrometer position. So using this system one can easily tie into a dialog with the detector electronics system. The main advantages of CD2A compudrive are, we can programme the start and end positions of the scan, rate, repetitions, delay between repetitions, recorder scale and marker frequency [9].

The output of the Spex monochromator is coupled to a thermoelectrically cooled photomultiplier tube (Thorn EMI, model KQB 9863, rise time 2 ns, quantum efficiency 22%).

2.2.5.2 Jarrell-Ash

Jarrell-Ash 82-000 is a 0.5 meter Ebert scanning monochromator having a maximum resolution of 0.02 nm [10]. The monochromator covers a spectral range of 200 nm to 1600 nm with tree interchangeable grating blazed at 180 nm, 500 nm and 750 nm respectively. This instrument provides a smooth scanning motion in eight speeds ranging from 0.2 nm/minute to 50 nm/min. The output from the Jarrell-Ash monochromator is detected by an EMI, model 9683 KQB photomultiplier tube that can be directly mounted at the exit face of the monochromator. Model 9683 is a head-on type PMT having an S-20 cathode, and performs well in the 300-800 region.

2.2.5.3 McPherson

McPherson model 275 is a 0.2 meter concave holographic grating monochromator [11]. It has two flat folding mirrors. The monochromators covers a spectral range of 185 nm to 4000 nm using different gratings. Due to its high light gathering power, this monochromator is suitable for high sensitivity fluorescence work.

2.2.6 The Photomultiplier

The photomultiplier tube (PMT) is a very versatile and sensitive detector of radiant energy in the ultra-violet, visible, and near-infrared regions of the electromagnetic spectrum. Among the oldest detector technologies (first developed in the mid-1930s), PMTs use vacuum rather than solid-state techniques to multiply electrons generated by photons. They are widely used

in research activities ranging from biomedicine to astronomy as well as in medical diagnostic technology, environmental monitoring and aerospace.

For a large number of applications the PMT is the most practical sensitive detector available. The basic reason for the superiority of the PMT is the secondary-emission amplification which makes them uniquely sensitive among photosensitive devices currently used. The basic radiation sensor is the photocathode which is located inside a vacuum envelope. Light passes through an input window and strikes the photocathode, leading to the emission of photoelectrons into an evacuated tube. Photoelectrons are emitted and directed by an appropriate electric field to an electrode or dynode within the envelope. A number of secondary electrons are emitted at this dynode for each impinging primary photoelectron. These secondary electrons in turn are directed to a second dynode and so on until a final gain of perhaps 10^6 is achieved [12]. The electrons from the last dynode are collected by an anode which provides the signal current that is read out.

The PMT has a photocathode in either a side-on or a head-on configuration. The side-on type receives incident light through the side of the glass bulb, while, in the head-on type, it is received through the end face of the glass bulb. The head-on type has a semitransparent photocathode (transmission-mode photocathode) and it provides better uniformity than the side-on type having a reflection-mode photocathode. A schematic representation and its operation of a typical photomultiplier tube is given in fig. 2.1. We have used the following Thron EMI PMT with S-20 cathode in our works

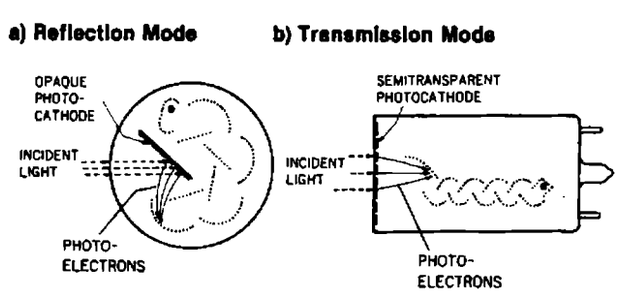

Figure 2.1: Schematic representation and operation of a typical photomultiplier tube

The exit slit of the Jarrall-Ash monochromator was coupled to a Thorn EMI PMT (Model 9683-KQB) with S-20 cathode. This Thron EMI PMT was operated in the range 1-1.3 kV. It has a fairly good quantum efficiency in the 300-800 nm spectral range. For the maintenance of a constant output voltage across the terminals, a highly stabilized power supply (Thorn

EMI PM28B was fed to the PMT. The tube has an air-cooled, RF shielded housing and was used in conjunction with the Jarrel Ash monochromators.

The Spex monochromator was coupled to a thermoelectrically cooled (-50^{0}C) Thron EMI photon counting PMT with S-20 cathode (quantum efficiency 22%). The operating voltage for this PMT was 1.7-2.1 kV.

2.2.7 Digital Storage Oscilloscope

A digital storage oscilloscope (DSO) was used to monitor the signal from the photomultiplier tube. The oscilloscope can be triggered both internally and externally. In the present work it was triggered externally using Nd:YAG laser pulses. It is provided with averaging facility. The pulse shapes can be digitally stored and plotted. The digital storage oscilloscope is a vital instrument for recording, storing and analyzing transient wave forms in a variety of experiments.

The storage oscilloscope is also required while setting the gate width and delay of the gated integrator. The DSO has facilities to capture and store the pulse shapes for later analysis and to obtain a hard copy using a plotter/printer. For the present studies we used two digital storage oscilloscopes: 1. 200 MHz, Iwatsu Model DS-8621 [13] and 2. 100 MHz, Tektronix, TDS 220, Maximum sampling rate 1GS/s [14].

2.2.8 Boxcar averager/integrator

In some experiments, it might be essential to recover a part or the whole of an output signal pulse so that the signal shape can be analyzed. To recover such a signal buried in noise, suitable averaging processes are required and for that, some kind of multi-point averager or a fourier transform analyzer is necessary. Signals of such transient nature, triggered by repetitive pulses from the excitation source can be analyzed in this fashion. This is achieved by a boxcar integrator, which essentially is an instrument used to recover complex repetitive signals hidden in noise.

The boxcar used here is a Stanford Research Systems (SR250) module. It essentially has a fast gated integrator and an averager. Triggered by the pulse from the laser, the gate provides an adjustable delay from few ns to 100 ms, before it generates a continuously adjustable gate of 2 ns to 15 ms [15]. The signal at the gate is integrated by the fast gated integrator and is normalized by the gate width to provide a voltage proportional to the part of the input signal pulse level at the gate. By fixing the delay and the gate width so that only the voltage

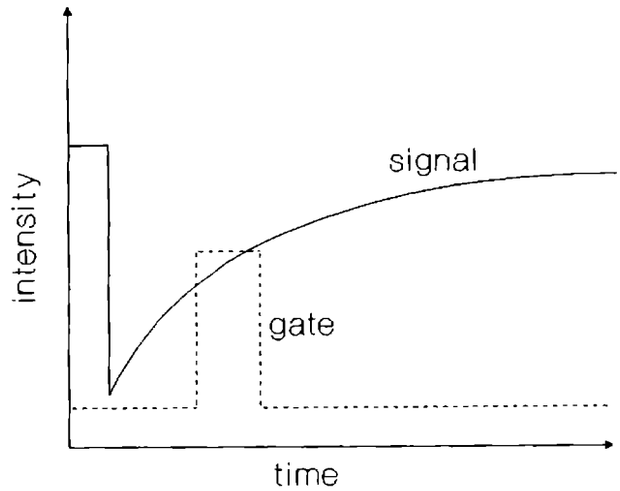

Figure 2.2: The typical PMT signal, the time delay and the gate width of the boxcar

from the part of the signal pulse alone is measured, it is possible temporally to separate out the PMT signal due to the emission of the particular species from the other unwanted signal components contained in the signal pulse, thus improving the signal to noise (S/N) ratio of the detection. The sensitivity control of the boxcar averager provides further amplification of the signal. The typical PMT signal, the time delay and the gate width of the boxcar are shown in fig. 2.2. A moving exponential average over 1 to 10,000 samples is available at the averaged output. This traditional averaging technique is useful for pulling out small signals from noisy backgrounds. Typically the signals are averaged over 10 pulses. Averaging over very large number of pulses does increase S/N ratio, but makes the system very sluggish in response to fast variations in the signal. In addition to the traditional technique, the averaging circuitry may be used to actively subtract a baseline drift or background from the signal.

2.2.9 Chart Recorder

The Analog-Digital X-Y plotter used in these experiments was manufactured by Rikadenki Kogyoco. Ltd., Japan. This is a high performance DC Servo system X-Y recorder with added digital plotter function [16]. In digital mode, title, scale, data etc. can be added to this recording. We used the chart recorder in its analog mode. In analog mode, the input analog signal is recorded directly by a pen writing.

In analog mode, the chart recorder provides high performance, high-speed X-Y recorder

function. The X-output and the averaged output sockets of the Boxcar averager/integrator were connected to the X and Y terminals of the Chart recorder respectively for recording the fluorescence emission spectrum.

2.2.10 Lock-in amplifier

Usually the output signal from an experimental set up employed for detecting very weak optical effects is immersed in various types of noises. Generally noise is generated due to the following reasons: (a) external light that may come through the collection optics, (b) scattered laser light from the sample, (c) dark current of the PMT which is a dc level of a few nA, (d) shot noise from the PMT whose periodicity is very low, (e) Johnson noise, (f) amplifier noise etc. Of these (a) and (b) can be minimised by proper positioning of the sample holder and optical components. Also PMTs are presently available with minimal dark current ratings. Synchronization using lock-in amplifier is more effective in reducing noises in these kinds of experimental measurements. Lock-in detection is particularly useful in eliminating noise in thermal lens experiments.

Lock-in amplifiers are used to detect and measure very small ac signals - all the way down to a few nanovolts. Accurate measurements may be made even when the small signal is obscured by noise sources many thousands of times larger. Lock-in amplifiers use a technique known as phase-sensitive detection to single out the component of the signal at a specific reference frequency and phase. Noise signals at frequencies other than the reference frequency are rejected and do not affect the measurement. In our experiment we have used the Stanford Research Systems SR850 DSP Lock-in Amplifier [17]. The functional block diagram of the SR850 is shown in fig. 2.3. All lock-in measurements require a reference signal. The SR850 generates its own sine wave as the lock-in reference. The lock-in reference is $V_L \sin(\omega_L t+\theta_{ref})$. The SRS amplifies the signal and then multiplies it by the lock-in reference using a phase-sensitive detector or multiplier. The output of the Phase Sensitive Detector (PSD) is simply the product of two sine waves.

$$\begin{aligned} V_{psd} &= V_{sig}V_L \sin(\omega_r t + \theta_{sig}) \sin(\omega_L t + \theta_{ref}) \\ &= 1/2V_{sig}V_L \cos([\omega_r - \omega_L]t + \theta_{sig} - \theta_{ref}) - 1/2V_{sig}V_L \cos([\omega_r + \omega_L]t + \theta_{sig} + \theta_{ref}) \end{aligned} \tag{2.1}$$

The PSD output is two AC signals,. one at the difference frequency (ω_r-ω_L) and the other at the sum frequency (ω_r+ω_L). if ω_r=ω_L, the difference frequency component will be a DC signal. In this case, the filtered PSD output will be V_{psd}=$1/2V_{sig}V_L \cos(\theta_{sig}$-$\theta_{ref})$. It is a DC signal proportional to the signal amplitude.

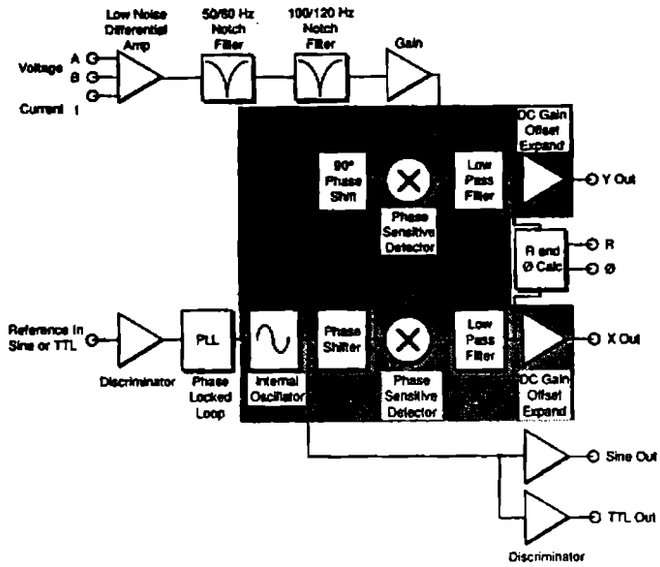

Figure 2.3: The fundamental block diagram of SR850

2.2.11 Photon Counter

For fluorescence measurements SR400 Gated Photon Counter was used [18]. The SR400 Photon Counter can be operated in Boxcar mode and Lock-in mode. In the boxcar mode, the gates are used to enable the counters only when the signal is present. If the gates are scanned, then the time profile of the signal is recorded. Background subtraction can be included by using one gate for the signal and an equal width gate on the background, either before or after the signal.

2.2.12 Optical fibre

The intensity variation of the probe beam caused by thermal lens effect of the medium has to be detected by a finite small aperture detector. We have chosen a fibre sensor for this purpose. The fibre tip acts as a finite aperture to collect the thermal lens signal. After passing through the filter the thermal lens signal enters through the fibre to the monochromator - PMT assembly. This arrangement provides considerable flexibility to the experimental set up and avoids the use of pin hole.

2.2.13 Vibration-free table

The whole experimental set up (both thermal lens and photoacoustics) was arranged on a home-made vibration isolated table so that errors due to any stray vibrations are a minimum.

2.3 Experimental set up

2.3.1 Continuous Wave Thermal Lensing (CWTL)

The argon ion laser based double-beam thermal lens calorimeter is schematically shown in fig. 2.4. The experimental set up for the present dual beam thermal lens study is identical with that reported previously [19] with some modifications. The 514 or 488 nm output from an argon ion laser (Spectra Physics, Model 171) was used as the pump source to generate the thermal lens in the medium. Radiation of wavelength 632.8 nm from a low power intensity stabilized He-Ne laser source (5 mW, Spectra Physics) was used as the probe beam. Pump beam was intensity modulated using a mechanical chopper. The intensity modulated Argon ion beam was focused by a lens 25 cm to the sample solution. Sample solution was taken in a quartz cuvette which is kept in the pump beam path. The He-Ne laser beam (probe beam) was focused by another convex lens and was made to pass collinearly through the sample with the help of a dichroic mirror. A filter was placed in the path of the emergent beams which allows only the 632.8 nm wavelength to reach the detector where the tip of an optical fibre serves as the finite aperture. The polished tip of long graded index optical fiber (200 μm core, NA = 0.22) placed at 90 cm away from the centre of the sample cuvette serves both as an aperture and as a light guide for the probe beam to a monochromator - PMT assembly. The multimode fibre which was mounted on a XYZ translator will also act as a pin hole. Using optical fibres to transmit the laser beams makes the thermal lens technique amenable to remote, in situ analysis. It also reduces the influence of mode and pointing variations in the probing laser. Here we used a multimode fibre which minimize alignment procedures and noise problems encountered with single mode fibres.The monochromator - PMT assembly tuned to the probe beam wavelength (632.8 nm) provides further filtering of the signal. The PMT output was directly connected to a digital lock-in amplifier for further analysis.

2.3.2 Pulsed Thermal Lensing (PTL)

The schematic diagram of the experimental set up used for the transient thermal lens studies is shown is shown in fig. 2.5. This experimental set up is analogous to cw thermal lens set up except the excitation laser and detection system. The 532 nm radiation from a frequency doubled Q-switched Nd:YAG laser was used as the pump beam. The probe laser used was the beam from an intensity stabilized He-Ne laser that produces linearly polarized TEM_{00} beam. The pump and probe beams are combined by using a dichroic mirror and made collinear by

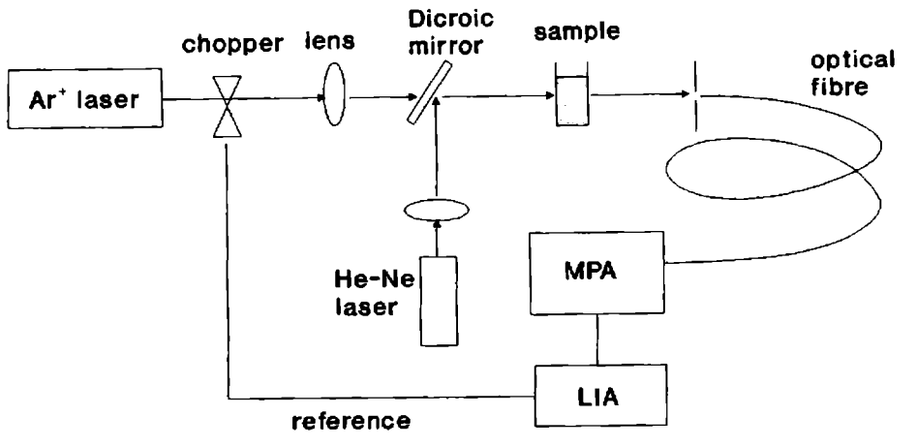

Figure 2.4: A block diagram of the experimental arrangement for the CW thermal lens spectrophotometry (MPA - Monochromator-PMT assembly, LIA - Lock-in amplifier)

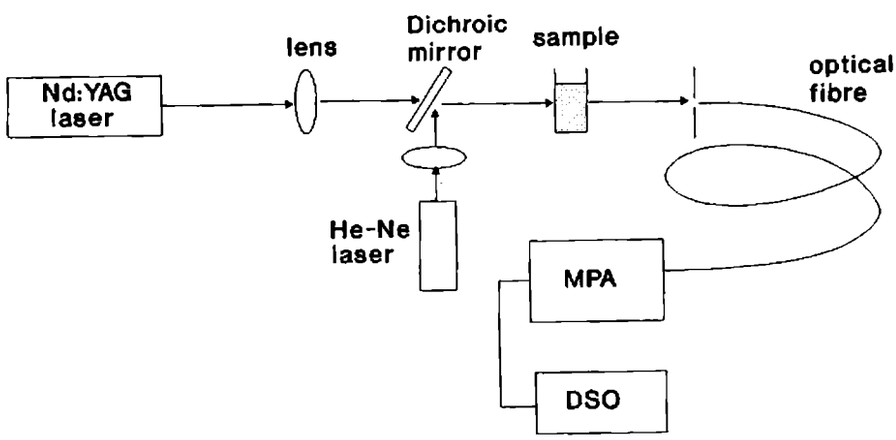

Figure 2.5: The schematic diagram of the pulsed thermal lens technique (MPA - Monochromator-PMT assembly, DSO - Digital storage oscilloscope)

carefully adjusting the optical components in thex-, y-, z- planes. As the 532 nm radiation was passed through the sample containing cuvette, the molecules absorb some of the incident energy and get excited to higher energy levels. The subsequent deexcitation process can occur radiatively or nonradiatively. It is the nonradiative part that gives rise to thermal lens formation. The resulting refractive index gradient follows the intensity distribution of the exciting pump beam. The position of the cuvette was adjusted to get maximum value for the thermal lens signal [20, 21]. The thermal lens signal was detected by sampling the intensity of the centre portion of the probe beam through a small aperture. In the present work the intensity of the center portion of the transmitted probe beam was detected by using an optical fiber. The output of the optical fiber entered into a Photomultiplier tube that was coupled to a McPerson monochromator which further filtered out the scattering of the excitation beam. The time dependent thermal lens signal is processed with a digital storage oscilloscope.

2.3.3 Pulsed Photoacoustics (PPA)

The schematic diagram of the photoacoustic (PA) cell along with transducer used in the present studies is shown in fig. 2.6(a). Except for minor variations, the design of the PA cell is similar to that described by Patel and Tam [22]. The PA cell is made of stainless steel and it is provided with glass windows for the entry and exit of the laser beam. The acoustic transducer that detects the laser induced PA signals consists of a lead-zirconate-titanate (PZT) disc of 4 mm thickness and 15 mm diameter, firmly mounted in a stainless steel chamber which is screwed onto the PA cell [23, 24]. The purpose of mounting the PZT disc inside the stainless steel casing is to minimize external electrical pick up and to prevent sample contamination by PZT (and vice versa). The diaphragm of the transducer chamber has a thickness of 0.5 mm and it is finely polished. A lead disc followed by a copper disc forms the backing of the PZT, which is spring loaded within the chamber. Spurious electrical pick-up is negligible, and signal ringing is reduced to a tolerable level.

Fig. 2. 6(b) represents the schematic representation of the pulsed photoacoutic experimental set up. The second harmonic output beam (532nm) from a Q-switched Nd:YAG laser was focused by a convex lens (focal length 5 cm) into the PA cell containing the sample at room temperature. The lens position was adjusted so that the beam focus was at the center of the cell. A dichroic filter oriented at 45^0 to the beam axis separates the fundamental frequency component (1064 nm) from the second harmonic. The incident power was monitored

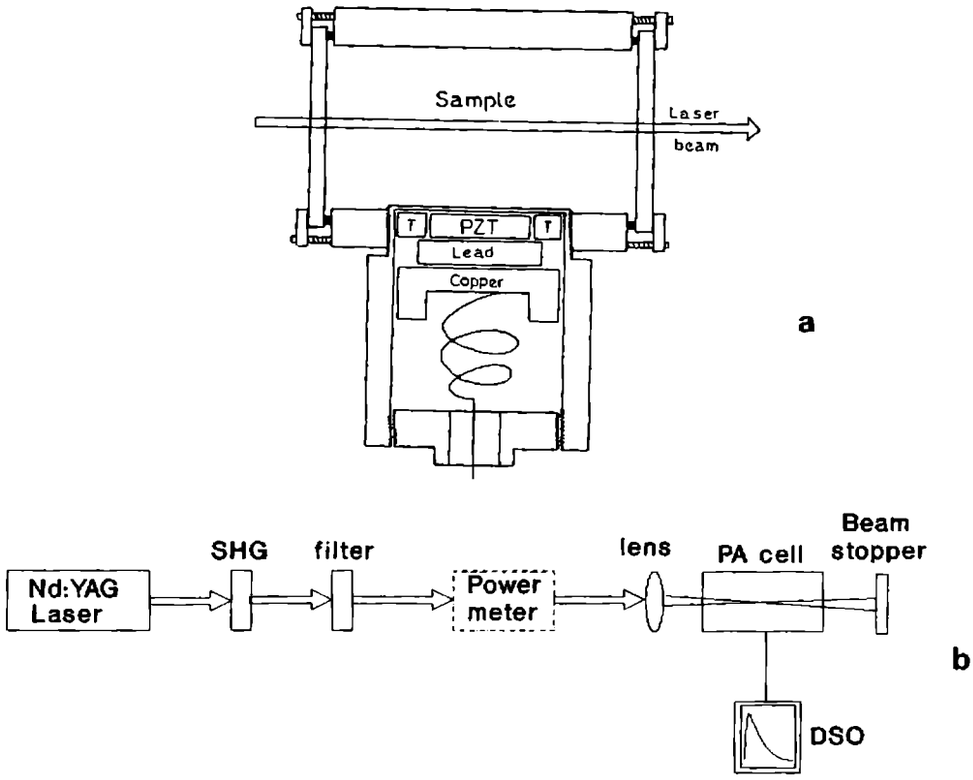

Figure 2.6: The schematic diagram of the (a) transducer and (b) photoacoustics experimental set up

by a laser power meter (Scientech model 362) and the transducer output was observed on a 200 MHz digital storage oscilloscope (Iwatsu model DS8621). The averaged amplitude of the first pulse in the PA signal trace was monitored as a function of laser power.

2.3.4 Fluorescence Studies

The successful application of fluorescence methods requires a good understanding of the instrumentation involved. Considerable attention to the experimetnal details is necessary. To obtain reliable spectral data one should be aware of and control numerous factors like the apparent fluorescence intensity and spectral distribution that can be dependent upon the optical density and the precise geometry of the sample. The most common geometry used for fluorescence is right angle observation of the center of a centrally illuminated cuvette. Other geometric arrangements include front-face and off-center illumination.

In a practical set up to observe weak fluorescence emission with moderate spectral resolution, the actual signal is usually immersed in various types of noises. Lock-in detection is particularly useful in eliminating the noise in cw fluorescence measurements and boxcar detection is efficient in avoiding unwanted noise for pulsed excitation. A gated photon counter

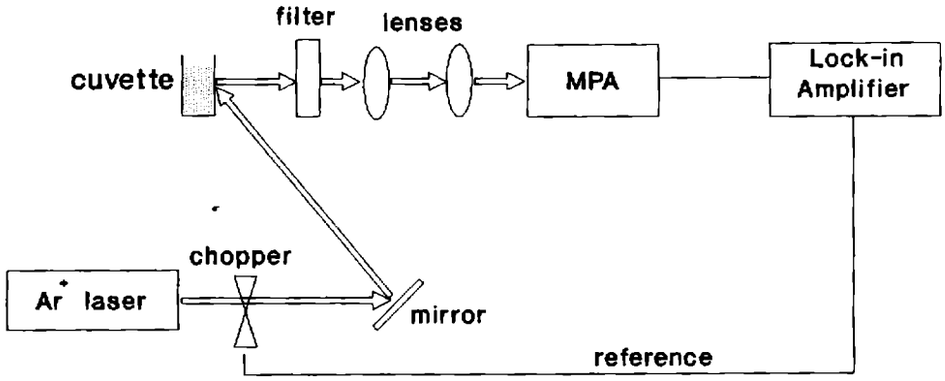

Figure 2.7: The Schematic diagram of cw fluorescence instrumentation

can also be used for these purposes, because it is operative both for cw and pulsed excitation mode.

Typical set up for the cw fluorescence measurements is given in fig. 2.7. The laser beam excites the fluorescence in the sample solution taken in a quartz cuvette. For recording the fluorescence spectra, front-surface emission geometry was employed in the present studies. The fluorescent emission photons were collected and focused using appropriate collimating and focussing lenses on to the tip of a multimode optical fibre, which acts as an optical guide. The other end of the fibre was attached to a monochromator - PMT assembly. Proper optical filters are used to avoid the entry of the scattered laser radiation into the monochromator. The emission was wavelength scanned in the desired region. The fluorescence spectra were charted in both pulsed and cw mode of excitation. In pulsed configuration, the signal from the PMT was gated and averaged using the gated integrator/boxcar averager and fed to chart recorder while the fluorescent emission was scanned using a Lock-in amplifier for the cw configuration of fluorescence recording.

2.4 Summary

In this chapter, different experimental aspects used for the present series of studies *viz.* Dual-beam thermal lensing, Pulsed Photoacoustics and fluorescence instrumentation were briefly discussed. A brief account of the different laser sources and detection systems used for the present series of investigations was also given.

2.5 References

[1] Instruction Manual, Argon ion laser, Spectra Physics, Model 171.

[2] Instruction Manual, Nd:YAG laser, Quanta Ray DCR 11.

[3] Instruction Manual, He-Ne laser, Spectra Physics, Model 102.

[4] Instruction Manual, Mechanical Chopper, EG&G Parc model 192.

[5] Instruction Manual, Mechanical Chopper, Standford Research sytems, SR540.

[6] Instruction Manual, EG&G Gamma Scientific model 460-1A.

[7] Instruction Manual, Scientech (model 362).

[8] Instruction Manual, Spex 1704 Spectrometer (Spex, USA).

[9] Instruction Manual, Spex CD2A Compudrive (Spex, USA).

[10] Instruction Manual, Jarrell-Ash monochromator.

[11] Instruction Manual, McPerson moniochromator.

[12] Photomultiplier tubes, Construction and operating charecteristics (Hamamatsu, Japan).

[13] Instruction Manual, Iwatsu DS8651 Oscilloscope, (Iwatsu, Japan)

[14] Instruction Manual, Tektronix Model TDS 220.

[15] Instruction Manual, Standford Research Systems Boxcar Averager and Gated Integrator Model SR 250.

[16] Instruction Manual, Rikadenki Chart Recorder

[17] Instruction Manual, Standford Research Systems Model SR850.

[18] Instruction Manual, Standford Research Systems Model SR400.

[19] H.L. Fang and R.L. Swofford in *Ultrasensitive Laser Spectroscopy* D.S.Kliger (ed.), (Academic Press, New York) (1983)

[20] C. V. Bindhu, S. S. Harilal, V. P. N. Nampoori and C. P. G. Vallabhan, *Curr. Sci.*, **74**, 764 (1998).

[21] C. V. Bindhu, S. S. Harilal, V. P. N. Nampoori and C. P. G. Vallabhan, *Opt. Engg.* (in press) (1998).

[22] C. K. N. Patel and A. C. Tam, *Rev. Mod. Phys.*, **53**, 517 (1981).

[23] C. V. Bindhu, S. S. Harilal, R. C. Issac, V. P. N. Nampoori and C. P. G. Vallabhan, *Pramana -J. Phys.*, **44**, 231 (1995).

[24] S. S. Harilal, R. C. Issac, C. V. Bindhu, V. P. N. Nampoori and C. P. G. Vallabhan, *Mod. Phys. Lett.*, **9**, 871 (1995).

Chapter 3

Thermal Diffusivity Measurements Using Transient Thermal Lens Calorimetry

Thermal diffusivity measurements were carried out in certain organic liquids as well as in seawater using pulsed dual beam thermal lens technique. 532 nm radiation from a frequency doubled Q-switched Nd:YAG laser was used as the heating source and an intensity stabilized He-Ne laser as the probe beam. Experiments were carried out to determine the characteristic time constant of the transient thermal lens signal. Measured thermal diffusivity values for the selected organic solvents are in excellent agreement with literature values. Similar measurements were carried out to determine the thermal diffusivity of seawater. Variation of the thermal diffusivity with depth from which the samples were taken was observed. The thermal diffusivity values of the seawater are found to vary with the salinity.

3.1 Introduction

There has been renewed interest in recent years for developing new laser-based methods of determining the thermal properties of materials in different forms [1-6]. This is mainly because of the availability of novel experimental techniques in the context of the rapid advances in materials technology and the many new applications of materials under very severe environmental conditions. A laser beam can deliver more energy to a small-area specimen than would be possible with a xenon flash lamp. Such a source of energy has the added advantage that it can operate from much greater distances. The beam can, for instance, pass through a window to be absorbed by a sample maintained at a high temperature within an evacuated enclosure. Furthermore, by using a Q-switching mode it becomes possible to reduce the dissipation times less than 1 μs.

The thermal characteristics of the sample affect the nature of the signal observed, and in particular the thermal diffusivity (D) of the sample. Thermal diffusivity is of direct importance in heat flow studies, as it determines the rate of periodic heating or transient heat propagation through the medium, a situation often encountered in experiments with pulsed or chopped laser radiation. Thermal diffusivity is the ratio of the thermal conductivity to the specific heat and density of a material and has dimensions characteristic of a diffusion coefficient *viz.* $(\text{length})^2 \times (\text{time})^{-1}$. The inverse of D is a measure of the time required to establish thermal equilibrium for a given sample. The value of D like the optical band gap, is also a unique parameter for each material but is extremely dependent upon the compositional and microstructural variables. Because of its controlling effect and common occurrence in heat-flow problems, its accurate determination is often necessary and a knowledge of D of a substance can be used to calculate thermal conductivity data. Although it is a derived quantity, D is regarded as an important physical quantity in that it determines the rate of heat propagation in transient-state processes. Furthermore, the development of improved measurement techniques and their application to transient experimental methods is leading to an increasing use of these methods as a means of deriving thermal conductivity values.

The use of time-resolved temperature measurement techniques for the evaluation of D of materials has been well documented and most methods are based upon the original work undertaken by Angstrom [7]. A flash method of measuring D was described by Parker and co-workers [8]. An extensive review of D of materials had been presented by Touloukian [9] where a number of methods for determining the diffusivity are discussed in detail. There exists a number of commonly used steady-state and non-steady state methods of measuring

thermal parameters [9-17]. However, there is some dissatisfaction with the length of the time required to make reliable measurements, and in some cases, the large sample sizes required by these techniques impose intolerable limitations. Just as with the determination of thermal conductivity, the methods employed for the determination of D are troubled by errors due to unwanted heat transfers as all materials conduct heat to a greater or lesser extent. These are naturally reduced when the experimental time is decreased, and much shorter times can be used in transient, variable-state experiments than when a static temperature distribution has to be established. This has long been realized, but the satisfactory application of transient methods has awaited technological developments which have allowed temperature changes to be more accurately determined over short measured time intervals. Improved technology has thus led to a revival of interest in transient methods for determining thermal properties, particularly at high temperatures.

Transient or steady periodic methods like transient hot wire method [11] should be capable of detecting and determining values time-dependent quantities for which only a final value will be obtained by steady state methods. However this approach requires that a very fine and fragile platinum wire be suspended in the sample and that it be connected to external electrical circuitry. Laser flash technique is also widely used for measurement of D of solid samples [12, 18, 19]. In this technique a flash of radiant energy is deposited on the surface of a homogeneous slab and the diffusivity is calculated from the time required for the temperature rise at the opposite surface to reach a known percentage of its maximum value. The temperature is measured by contacting a 1- or 2-mil-dia thermocouple at the centre, or by optical means; the results may need to be corrected for finite pulse time effect, heat losses, and nonuniform heating.

Methods based on photothermal effects are eminently suited for the measurement of thermal properties of materials. Most noncontact measurements are based on photothermal techniques utilizing modulated or pulsed laser beams for the determination of thermal diffusivities [20-23]. Methods based on photothermal phenomena like photoacoustic effect, photothermal refraction and thermal lens techniques can be effectively utilized for material characterization and nondestructive evaluation. Adams and Kirkbright [24] employed optoacoustic spectroscopy to obtain data concerning the spectral absorption characteristics and D of small solid samples. They developed theoretical expressions to relate the optical and thermal properties of such samples to the amplitude and phase of the photoacoustic signal.

Among the various photothermal spectroscopic methods based on the thermal relaxation of excited species, thermal lens spectroscopy has appeared to be very sensitive and powerful

[25-28]. The thermal lens technique can also be effectively utilized for multiphoton absorption studies [29, 30], determination of absolute fluorescence quantum yield [31], and for monitoring certain slow chemical reactions [32]. The sensitivity of this technique is higher than that of the conventional transmission and reflection techniques because in the former the absorbed energy is measured directly.

The TL method can be successfully employed for the determination of D especially in the liquid phase. With a pulsed laser as the excitation source we get a transient thermal lens and by monitoring this transient thermal lens, D can be determined. The work of Gordon et. al [28] on the thermo-optical effect in a liquid provides a basis for linking the rate of dissipation of the thermal lens to a quantitative measure of D. Using a single-beam thermal lens technique, Calmettes and Laj [22] measured D values for certain liquids and solid polymethacrylate. The single beam thermal lens technique is slow and also for liquids prolonged heating could cause additional errors because of convection currents. Gupta et. al. [27] developed double beam thermal lens technique for measuring D of transparent solids and liquids. In their technique a transient thermal lens was formed in the test specimen by using a dye laser pulse as a heating source and the thermal lens decay was monitored by means of a cw He-Ne laser. Their measured values of thermal diffusivitiy for water and a polycarbonate plastic were found to be in good agreement with literature values. Bailey et. al. [21] successfully determined gas phase thermal diffusivities of selected liquids using dual beam thermal lens method and extended their studies for measuring liquid phase thermal conductivities of certain liquids [20].

In the present chapter, we show that dual beam thermal lens technique can be effectively utilized for the determination of D of certain organic liquids and seawater.

3.2 Experimental Set up

The details of the experimental set up is given in chapter 2. The 532 nm radiation from a frequency doubled Q-switched Nd:YAG laser was used as the pump beam. An intensity stabilized He-Ne laser was used as the probe beam. The pump and probe beams were combined by using a dichroic mirror and made collinear by carefully adjusting the optical components in the x-, y-, z- planes. The sample was taken in a 5 mm quartz cuvette. The position of the cuvette was adjusted to get maximum value for the thermal lens signal. The thermal lens signal was detected by sampling the intensity of the centre portion of the probe beam through a small aperture. In the present work the intensity of the central portion of the transmitted

probe beam was detected by using an optical fiber. Here the optical fiber also serves as the limiting aperture. The output of the optical fiber was detected by a Photomultiplier tube that was coupled to a McPerson monochromator which further filtered out the scattered light from the excitation beam. The time dependent TL signal was processed with a digital storage oscilloscope. All the measurements were made at a room temperature of 24^0C.

3.3 Theory

In the case of pulsed laser excitation, the pulse width of the heating laser is very small and the rate of the radiationless transition is very fast in comparison with decay rate of the thermal lens effect. The signal strength reaches the maximum value almost instantly and it decays with a characteristic time constant. The pulsed thermal lens system has distinct advantages with respect to large enhancement factor and its background substraction capability. Quantitative analysis of this transient phenomenon is given by Twarowski and Kliger [29, 33] along with experimental verifications.

Assuming a gaussian intensity profile for the pump beam, the focal length of the induced thermal lens by pulsed laser irradiation is given by

$$\frac{1}{f} = \frac{1}{f_0}\left(1 + \frac{2nt}{t_c}\right)^{-2} \tag{3.1}$$

Here

$$\frac{1}{f_0} = \frac{4lDN\sigma h\nu Hn^2}{kJ\omega^{2n+2}}\frac{d\eta}{dT}\left(\frac{2}{\pi}\right)^n \tag{3.2}$$

where D = $\frac{k}{\rho c}$, H = $\int_0^t$P(t) dt; l, the thickness of the thermal lens; N, molecules per cc; D, thermal diffusivity; k, thermal conductivity; ρ, density; c, specific heat; η refractive index of the medium; ν, frequency of the pump beam; P(t) pulsed laser power as a function of time; ω, beam radius; J, Joule's constant; σ, cross section for n photon absorption and n, number of photons absorbed. Since the temperature coefficient of the refractive index is negative for most liquids, the eqns. (3.1) and (3.2) predict that the lens will be divergent.

If another laser is used to monitor this thermal lens, then the intensity at the beam center of the probe beam can be expressed by

$$S = \frac{I_t - I_\infty}{I_t} = S_{t=0}\frac{1}{\left(1 + 2n\frac{t}{t_c}\right)^2} \tag{3.3}$$

where

$$S_{(t=0)} = \frac{I_\infty - I_0}{I_0} \tag{3.4}$$

where I_∞, I_0, I_t are the steady state thermal lens signal, signal at time t = 0 and signal at time t respectively.

The characteristic time constant t_c is related to the thermal diffusivity D and beam radius (ω) through the relation

$$t_c = \frac{\omega^2}{4D} \tag{3.5}$$

To eliminate the uncertainty in the determination of beam radius, a reference sample with known D is used to determine the D of the unknown sample. In our case water was used as the reference sample. Thus,

$$D = D_{water}\frac{t_c^{water}}{t_c} \tag{3.6}$$

The time dependence of the lensing phenomenon gives a detailed account of the thermal history of the sample medium. Clearly the magnitude of the thermal lens effect depends on the competition between the rate of creation of the lens and the rate of decay of the lens, and these are related to the D of the medium.

3.4 Thermal Diffusivity Measurements in Organic Liquids

To demonstrate the applicability of the method, we have measured D of several transparent liquid samples. Using the present set up, the thermal diffusivities of different organic samples were determined with water as the reference. Trace amounts of dye rhodamine 6G were added in certain samples to increase the absorption of the pulsed laser beam thereby increasing the thermal lens signal intensity. This level of impurity will not affect the solvent thermal conductivity since adding trace amounts of dye affect only the optical properties and not the thermal properties of the solvent [34]. Typical transient thermal lens signal is given in fig.3.1 for different organic liquids. Eqn. (3.3) leads us to the prediction that a plot of $S^{-1/2}$ will be a linear function of time. Verification of this prediction is shown in fig. 3.2. From the slope and intercept, the value of n/t_c can be determined. One can determine the value of n from measurements of the dependence of thermal lens signal on laser energy E of the pump laser pulse, using the relationship [33]

$$\frac{I_t - I_{t=\infty}}{I_t} \propto E^n \tag{3.7}$$

The variation of TL signal with laser energy for all the liquids studied showed a linear dependence suggesting one photon absorption (n = 1). From these measurements we calculated the values of characteristic time constant t_c corresponding to each organic liquids. We have

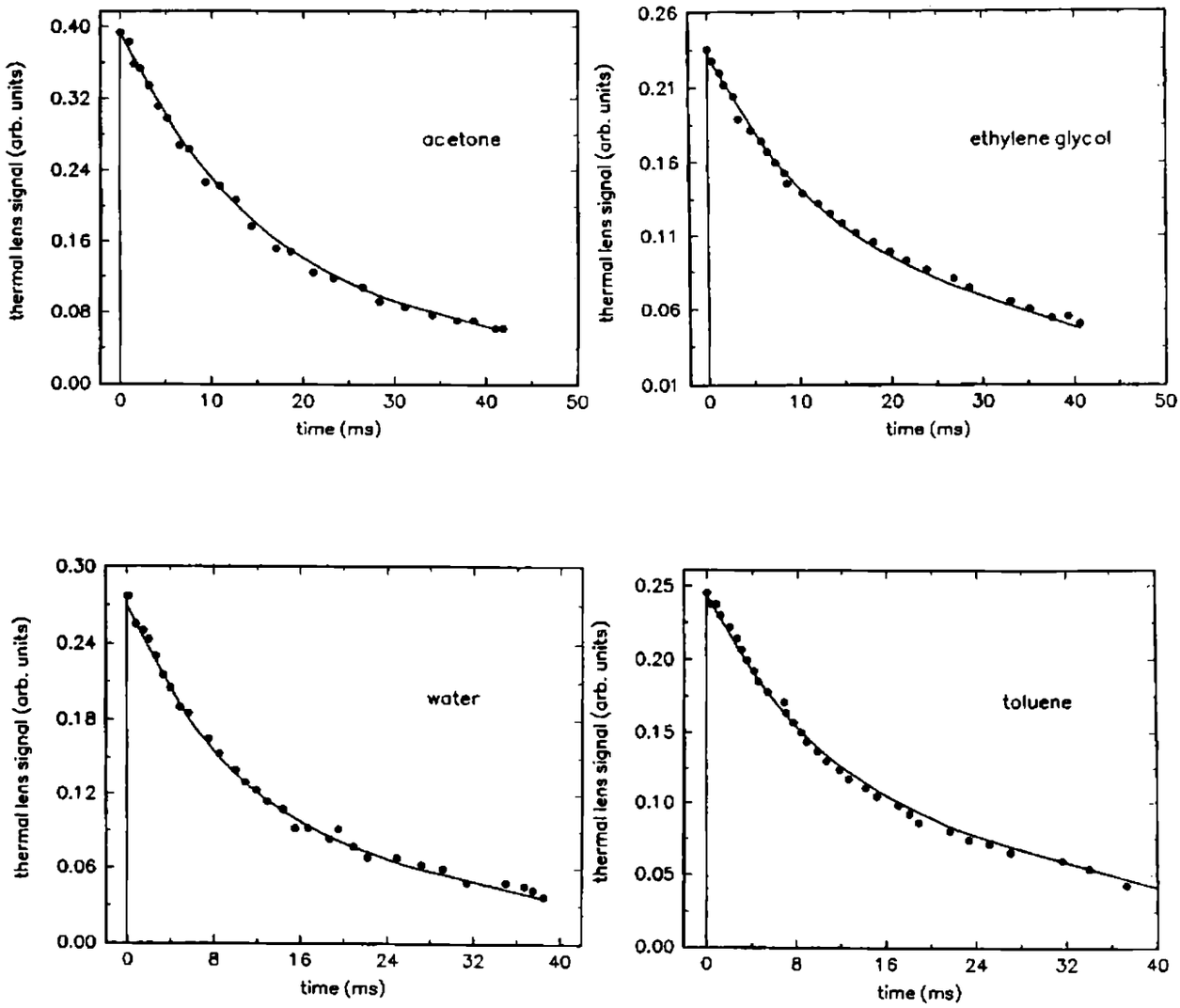

Figure 3.1: Transient decay curve measured by pulsed thermal lens technique. The points in the figures represent the experimental datas. The solid curves represent the theoretical fit obtained using eqn. 3.3. The theoretical fits were made with measured values of t_c obtained from figure 3.2 ($t_c^{acetone} = 60$ ms; $t_c^{toluene} = 59$ ms; $t_c^{ehyleneglycol} = 66.6$ ms; $t_c^{water} = 45$ ms).

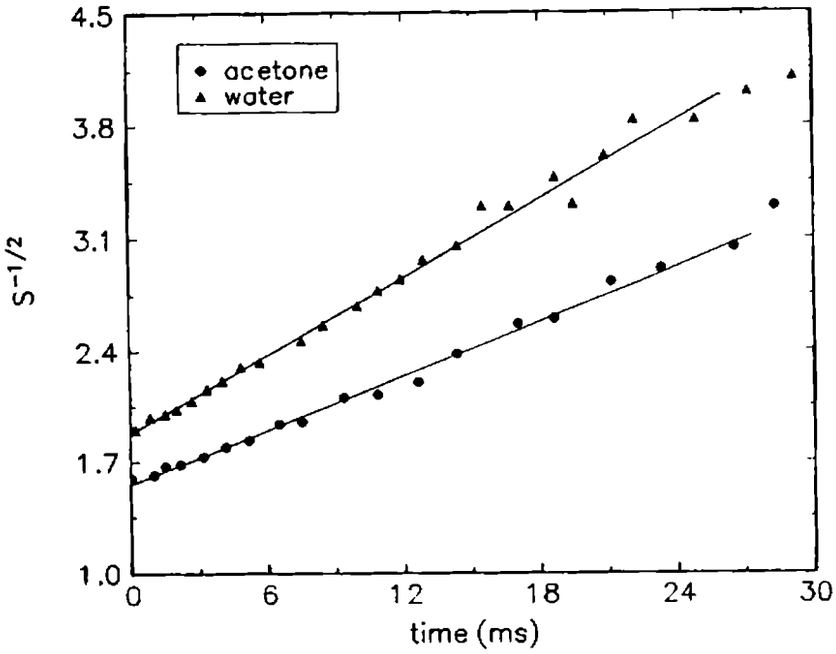

Figure 3.2: Typical linear plots of experimental data obtained using eqn. 3.3. From the slope and intercept of these plots value of t_c is evaluated.

verified measured t_c with theoretical fit using eqn. 3.3. The smooth curve in the fig.3.1 gives such a theoretical fit obtained from eqn.3.3, assuming t_c which was obtained from the slope and intercept of the linear plot (fig.3.2). The agreement between the theoretical and experimental data is good. The results also show that water reaches thermal equilibrium faster than all other liquids studied in the present work. Hence D of water ($1.43 \times 10^{-3} cm^2/sec$) should be higher than that of the other liquids. In table 3.1, we summarize the results for the thermal diffusivities for various samples. The D values obtained using the present experimental set up are in excellent agreement with reported literature values [35, 36] of the same for these organic liquids.

Table 3.1 Thermal diffusivity values for different organic liquids studied using dual beam transient thermal lens calorimetry. Reported literature values are also given.

sample	D obtained by using TL method	literature value
acetone	$(1.073 \pm 0.005) \times 10^{-3} cm^2 s^{-1}$	$1.07 \times 10^{-3} cm^2 s^{-1}$
toluene	$(1.091 \pm 0.008) \times 10^{-3} cm^2 s^{-1}$	$1.04 \times 10^{-3} cm^2 s^{-1}$
methanol	$(1.072 \pm 0.004) \times 10^{-3} cm^2 s^{-1}$	$1.08 \times 10^{-3} cm^2 s^{-1}$
benzene	$(9.952 \pm 0.006) \times 10^{-4} cm^2 s^{-1}$	$1.01 \times 10^{-3} cm^2 s^{-1}$
glycerol	$(9.987 \pm 0.006) \times 10^{-4} cm^2 s^{-1}$	$1.00 \times 10^{-3} cm^2 s^{-1}$
ethanol	$(9.471 \pm 0.009) \times 10^{-4} cm^2 s^{-1}$	$9.33 \times 10^{-4} cm^2 s^{-1}$
ethylene glycol	$(9.658 \pm 0.001) \times 10^{-4} cm^2 s^{-1}$	$9.71 \times 10^{-4} cm^2 s^{-1}$

3.5 Thermal Diffusivity Measurements in Seawater

The optical and thermal properties of seawater are the basic building blocks of the physical and chemical oceanography. Eventhough few reports are available on the optical properties of seawater [37, 38], little attention is given to understand the thermal properties of seawater. The upper surface of the sea is being heated by Sun's rays. During night, the upper layers get cooled down mainly due to heat conduction to lower layers. The temperature of the sea surface is determined by the rate of heat diffused from the upper layers to the deeper region and vice versa. Thus a knowledge of thermal diffusivity of seawater is of great importance in the field of oceanography. We have carried out these measurements in different samples of seawater taken from different depths of sea. These results are compared with that obtained from artificially made 'seawater'.

One of the foundations of chemical and physical oceangraphy is the hypothesis that so far as the major dissolved constituents are concerned, seawater has constant relative composition. Seawater is an aqueous solution of some dozen inorganic constituents (table 3.2), the determination of any single major element can be used as a measure of other elements and of salinity. Apparently sodium and chlorine constitute 85 solid substances of the seawater.

Table 3.2 Major constituents of seawater. [40]

Ion	gm/Kg of seawater of salinity 35 ‰)	proportion to sum %
Cl^-	18.98	55.04
Br^-	0.065	0.19
SO_4^-	2.649	7.68
HCO_3^-	0.14	0.41
F^-	0.001	0.00
H_3BO_3	0.026	0.07
Mg^{++}	1.272	3.69
Ca^{++}	0.4	1.16
Sr^{++}	0.013	0.04
K^+	0.38	1.1
Na^+	10.556	30.61

There are also elements of which minute traces have been identified in seawater and are a necessity of life to certain organisms. Radioactive matter also occurs naturally in the sea, for example, uranium is found in concentrations of 1-3 mg/cubic metre.

The most useful conservative property of seawater in circulation studies is salinity. For many purposes, it is not necessary to know the concentration of the individual elements in seawaterr, it is enough to know the total salt content or the salinity. It is defined as the total amount of solid material in grams contained in 1 kg of seawater when all the bromine and

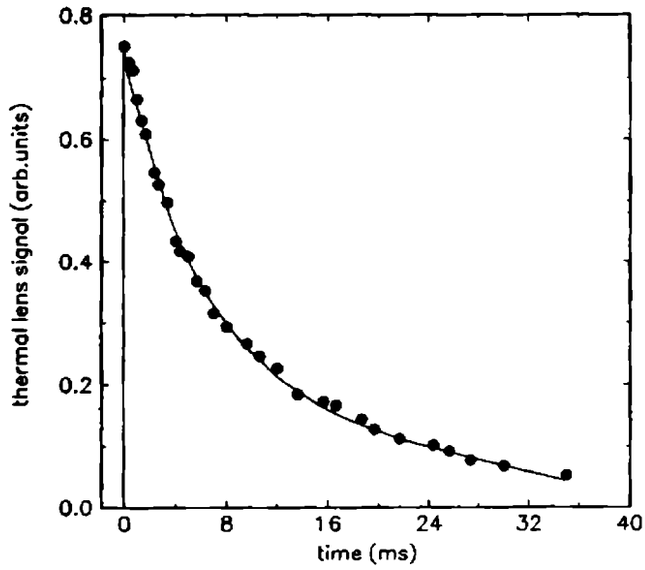

Figure 3.3: Transient decay curve measured by pulsed thermal lens technique for seawater sample taken from a depth of 300 ft. The points in the figures represent the experimental datas. The solid curves represent the theoretical fit obtained using eqn. 3.3.

iodine have been replaced by the equivalent amount of chlorine, all the carbonate has been converted to oxide, and all the organic matter has been completely oxidized. The salinity of seawater is usually expressed in parts per thousand or by the symbol "‰". In majority of places in the oceans, the salinity lies between 34 and 37‰. In places receiving a great deal of fresh water, the salinity may be less than 34‰. The salinity of the oceans is high wherever strong evaporation is continually extracting water from the ocean.

The dissolved components of seawater are transported from place to place by advective processes and move from water parcels of greater concentration to those of lesser concentration by diffusion processes. These agencies act equally on all dissolved constituents, and their effects can be traced by measuring the concentrations of any one of them [39].

For the present studies, the seawater samples were collected from the Arabian sea at a distance of 100 km away from the shore of Cochin in the summer season during which the sea is more or less calm. The sample collection was made upto a depth of 300 feet from the sea surface.

We performed D measurements in seawater samples using the pulsed double beam thermal lens technique. The sample was taken in a quartz cuvette. Trace amounts of dye rhodamine 6G were added to increase the absorption of the laser photons thereby increasing the thermal lens signal intensity. Thermal lens signals were obtained from water and different samples of seawater. Typical thermal lens transient for seawater sample is given in fig.3.3.

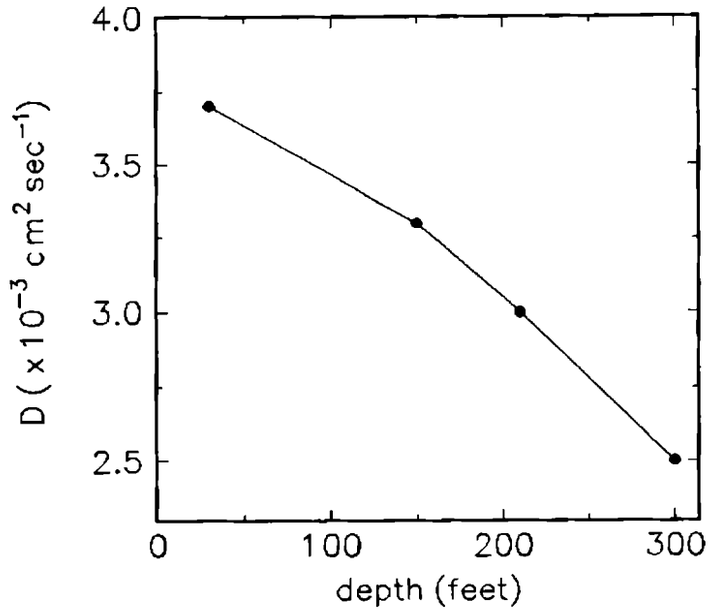

Figure 3.4: Variation of thermal diffusivity of seawater with depth

The variation of TL signal with laser energy for all the seawater samples studied showed a linear dependence suggesting one photon absorption. The charateristic time constant t_c corresponding to each sample were calculated. We have verified measured t_c with theoretical fit using eqn.3.3. The smooth curve in the fig.3.3 gives such a theoretical fit obtained using eqn.(3.3), taking t_c from the slope and intercept of the linear plot. The agreement between the theoretical and experimental data is good. Using pure water as reference with D = 1.43×10^{-3}cm^2/s, we calculated thermal diffusivities for the different seawater samples.

It is found that the D values of seawater varies with depth from which it is taken (fig.3.4). The values of D show decreasing tendency as the depth increases. The estimated D value for sea water at a depth of 30 ft is 3.65×10^{-3}cm^2/s and it is decreased to a lower value 2.53×10^{-3}cm^2/s at a depth of 300 ft. We measured salinity and conductivity of the seawater samples using salinity and conductivity meters respectively. The variation of these parameters with depth is shown in fig.3.5. The salinity and conductivity values of these samples are found to decrease with increasing depth. Salinity does appear to be important in determining the thermal diffusivity. The thermal characteristics of seawater are subjected to regional and seasonal variations. The seasonal change in wind direction and consequent reversal of ocean currents, together with the abrupt change in the pattern of precipitation may contribute towards large variations in the annual surface salinity. In order to verify the results obtained in seawater samples, we carried out similar measurements in artificially

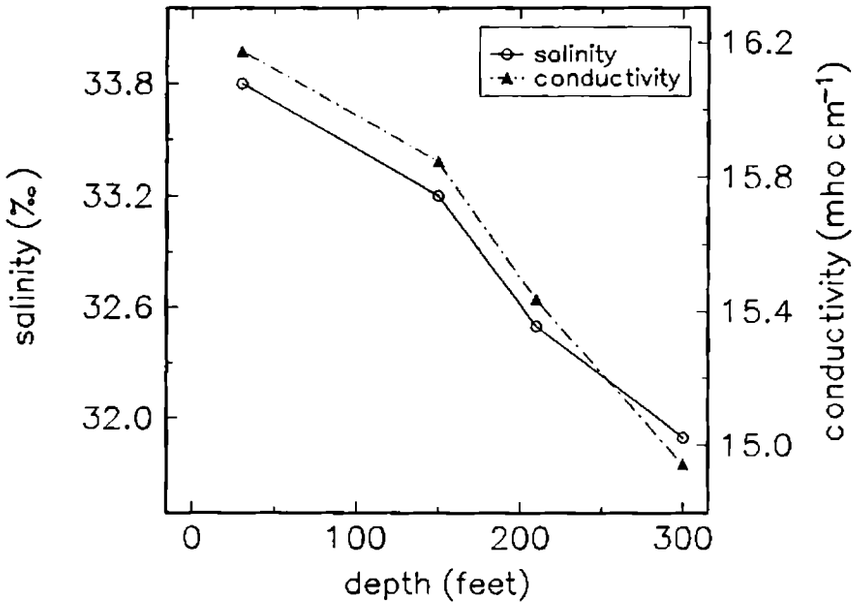

Figure 3.5: Variation of conductivity and salinity of seawater with depth

prepared seawater sample solutions. We have prepared artificial seawater in accordance with the reported method of Ott [41]. Artificial seawater of any salinity can be prepared by choosing appropriate quantities of individual salts. The ratio of the concentrations between the salts remains almost constant. The individual concentration varies linearly with salinity. The salinity of the artificial seawater was varied to study the effect of this parameter on thermal diffusivity. It is observed that the thermal lens signal strength is maximum for the sample with highest salinity. A possible explanation for the thermal lens enhancement upon increase in salinity is a change in the bulk refractive index which might alter the absorption coefficient of the solution. Fig.3.6 gives the variation of D with salinity of the artificial seawater. The D values obtained for artificial seawater also showed a similar trend with decreasing salinity. From fig.3.5 it is seen that salinity varies only from 34.1 to 31.6 ‰ and D varies from 3.7×10^{-3}cm^2/s to 2.5×10^{-3}cm^2/s. On the other hand from fig.3.6 for artificial seawater prepared in the laboratory, the variation in diffusivity for a variation in salinity from 3 to 25 ‰ is from 1.5×10^{-3}cm^2/s to 3.5×10^{-3}cm^2/s. Thus the D values for seawater and artificial seawater follow different trajectories. Obviously the exact chemical composition in terms of both organic and inorganic materials cannot be the same in both cases. It is also likely that seawater will contain some amount of suspended matter and microorganisms. This is borne out by the fact that the absorption coefficient of natural sea water (filtered) is 11×10^{-4} cm^{-1} while that of synthetic sea water is 8×10^{-4} cm^{-1} at 532 nm [42]. Hence it is to be expected

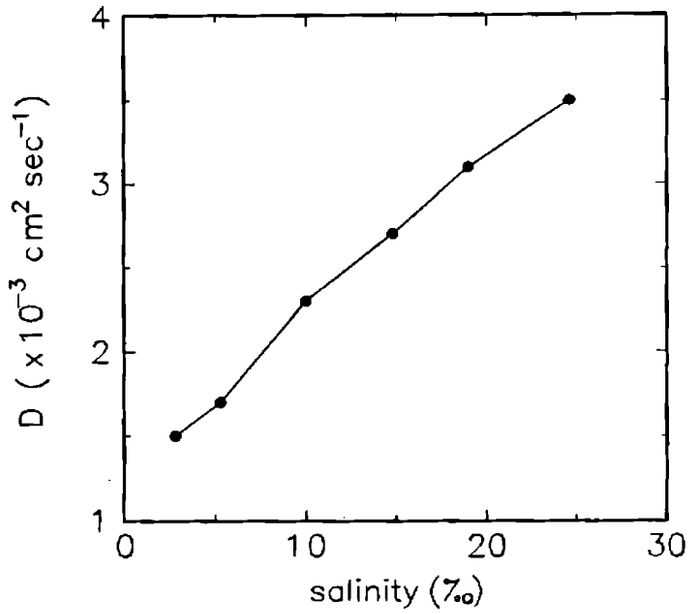

Figure 3.6: Variation of thermal diffusivity of artificial seawater with salinity

that the thermal diffusion coefficient of seawater and its synthetic analogue should follow different trajectories with respect to variation in salinity.

By comparing the above results and that obtained from the seawater samples, it is clear that D values of the seawater decreases with decreasing salinity. It can be inferred that the upper parts of the sea contain more salt than the deeper regions. When the sea gains heat by the absorption of solar radiation, most of the heat is absorbed in the first few meters. Molecular conductivity could provide only a very slow transport of heat downwards and a step temperature gradient would occur just below the surface. Evaporation of water from the sea surface by sun and wind leaves the water at the surface saltier. This result is in confirmation with the report that the salinity of seawater decreases with depth [39, 43]

3.6 Conclusion

The thermal blooming technique offers a novel means of measuring thermal diffusivity. The method is simple and accurate. The obvious advantage of this method is only small sample volumes are needed for making such measurements. Also only very short time is needed for the measurements and accurate results can be obtained with TL method.

Thermal diffusivity values of seawater are found to vary with depth of the sea at which the sample is collected. The thermal diffusivity measurements in artificial seawater showed

a decrease in the value of thermal diffusivity with increasing dilution of the sample. Thus salinity does appear to be important in determining the thermal diffusivity.

3.7 References

[1] G. Langer, J. Hartmann and M. Reichling, *Rev. Sci. Instrum.*, **68**, 1510 (1997).

[2] B. Bonno, J. L. Laporte and R. Tascon, *Rev. Sci. Instrum.*, **67**, 3616 (1996).

[3] S. S. Raman, V. P. N. Nampoori, C. P. G. Vallabhan, G. Ambadas and S. Sugunan, *Appl. Phys. Letts.*, **67**, 2939 (1995).

[4] J. R. Lalanne and E. Sein, *Appl. Phys. Letts.*, **36**, 973 (1980).

[5] R. T. Bailey, F. R. Cruickshank, D. Pugh, S. Guthrie, A. Mcleod, W. S. Foulds, W. R. Lee and S. Venkatesh, *Chem. Phys.*, **77**, 243 (1983).

[6] M. Bertolotti, V. Dorgan, G. Liakhou, R. L. Voti, S. Paoloni and C. Sibilia, *Rev. Sci. Instrum.*, **68**, 1521 (1997).

[7] A. J. Angstrom, *Phil. Mag.*, **26**, 161 (1863).

[8] J. G. Parker, *Appl. Opt.*, **12**, 2974 (1973).

[9] Y. S. Touloukian, *Thermal diffusivity*, IFI/Plenum New York (1973).

[10] G. Koren, *Phy. Rev. A*, **13**, 1177 (1976).

[11] J. J. Healy, J. J. de Groot and J. Kestin, *Physica C*, **82**, 392 (1976).

[12] W. J. Parker, R. J. Jenkins, C. P. Butler and G. L. Abbott, *J. Appl. Phys.*, **32**, 1679 (1961).

[13] M. J. Adams and G. F. Kirkbright, *Analyst*, **102**, 281 (1977).

[14] T. Yamane, Y. Mori, S. Katayama and M. Todoki, *J. Appl. Phys.*, **82**, 1153 (1997).

[15] P. Nath and K. L. Chopra, *Thin Solid Films*, **20**, 53 (1974).

[16] C. A. Paddock and G. L. Eesley, *J. Appl. Phys.*, **60**, 285 (1986).

[17] D. G. Cahill, H. E. Fisher, T. Klitsner, E. T. Swartz and R. O. Pohl, *J. Vac. Sci. Technol. A*, **7**, 1259 (1989).

[18] R. E. Taylor, *High Temp. High Press.*, **11**, 43 (1979).

[19] H. W. Deem, W. D. Wood, *Rev. Sci. Instrum.*, **33**, 1107 (1962).

[20] R. T. Bailey, F. R. Cruickshank, D. Pugh, S. Guthrie, A. Mcleod, W. S. Foulds, W. R. Lee and S. Venkatesh, *Chem. Phys.*, **77**, 243 (1983).

[21] R. T. Bailey, F. R. Cruickshank, D. Pugh, A. Mcleod and W. Johnstone, *Chem. Phys.*, **68,** 351 (1982).

[22] P. Calmettes and C. Laj, *J.de Physique*, **C1,** 125 (1972).

[23] M. Rhode, *Thin Solid Films*, **238**, 199 (1994).

[24] M. J. Adams and G. F. Kirkbright, *Analyst*, **102**, 281 (1977).

[25] J. R. Whinnery, *Acc. Chem. Res.*, **7,** 225 (1974).

[26] N. J. Dovichi and J. M. Harris, *Anal. Chem.*, **51**, 728 (1979).

[27] Mool C.Gupta, Su-Don Hong, A. Gupta and J. Moacanin, *Appl. Phys. Letts.*, **37**, 505 (1980).

[28] J. P. Gordon. R. C. C. Leite, R. S. Moore, S. P. S. Porto and J. R. Whinnery, *J. Appl. Phys.*, **36**, 3 (1965).

[29] A. J. Twarowski and D. S. Kliger, *Chem. Phys.*, **20,** 259 (1977).

[30] C. V. Bindhu, S. S. Harilal, R. C. Issac, V. P. N. Nampoori and C. P. G. Vallabhan, *Mod. Phys. Letts.*, **9,** 1471 (1995).

[31] C. V. Bindhu, S. S. Harilal, R. C. Issac, V. P. N. Nampoori and C. P. G. Vallabhan, *J. Phys. D*, **29**, 1074 (1996).

[32] K. Daree, *Opt. Commn.*, 4, 238 (1971).

[33] A. J. Twarowski and D. S. Kliger, *Chem.Phys.*, **20**, 253 (1977).

[34] J. H. Brannon and D. Magde, *J. Phys. Chem.*, **82**, 705 (1975).

[35] K. Raznjevic, *Hand book of Thermodynamic Tables and Charts*, (Hemisphere publishing corporation, Washington, 1976).

[36] R. C. Weast *CRC Handbook of Chemistry and Physics*, (CRC press. inc. Florida, 1987).

[37] W. S. Pegau, D. Gray and J. R. V. Zaneveld, *Appl. Opt.*, **36**, 6035 (1997).

[38] M. Ravisankar, A. T. Reghunath, K. Sathianandan and V. P. N. Nampoori *Appl. Opt.*, **27** 3887 (1988).

[39] R. W. Fairbridge (ed.) *The Encyclopedia of Oceanography* (Van Nostrand Reinhold Company, 1966).

[40] H. U. Sverdrup, M. W. Johnson and R. H. Fleming, *The Oceans*, (Englewood Cliffs, N.J., Prentice-Hall, Inc., 1942).

[41] F. D. Ott, *Virginia J. Science*, **16**, 205 (1965).

[42] A. T. Regunath, Ph.D thesis, Cochin University of Science and Technology (1988).

[43] E. Adrian Gill, *Atmosphere-Ocean Dynamics*, International Geophysics Series: Vol.30 (Academic press, London 1982).

Chapter 4

Multiphoton Absorption Studies in Rhodamine 6G and Rhodamine B Laser Dyes in Different Solvents Using Transient Thermal Lens Technique

Dual beam transient thermal lens studies were carried out in aqueous, alcoholic and ethylene glycol solutions of the laser dyes Rhodamine 6G and Rhodamine B using 532 nm pulses from a frequency doubled Nd:YAG laser. Analysis of thermal lens signal shows the existence of different nonlinear processes like two and three photon absorption phenomena along with one photon as well as excited state absorption. Concentration of the dye in the solution has been found to influence the occurrence of the different nonlinear processes in a significant way.

4.1 Introduction

Xanthene dyes like Rhodamine 6G (Rh6G) and Rhodamine B (RhB) are a class of organic molecules which show lasing action under appropriate conditions of excitation. Dye lasers are among the most useful types of lasers because of their easy tunability, wavelength coverage and simplicity. Dyes can be used in solid, liquid, gaseous phase and their concentration and hence their absorption and gain can be readily controlled. Dye doped polymers can also be successfully employed as lasing media [1]. Solutions of dyes are especially convenient for experimental studies of various type. Different scintillators, coumarines, xanthenes and polymethines can be conveniently chosen to cover a wide range of the spectrum [2].

The laser dyes possess a strong absorption generally in the visible and UV regions of the electromagnetic spectrum with fluorescence emission from the first excited singlet state at Stokes - shifted wavelengths. The variety of organic dyes available to cover the spectrum and the broad tunability for each particular dye make the dye laser a versatile research tool. The ultimate utility of these lasers will depend in large measure upon the photophysical properties of the dye available. Absorption by the upper level of the laser transition is one of the most important parameters determining the suitability of a molecule as a gain medium. As the state S_1 has a radiative lifetime which is longer than the non-radiative relaxation times of the higher excited singlet electronic states, dye molecules in the S_1 state can undergo absorptive transitions in addition to stimulated emissive transitions in the presence of a pump beam. Excited state absorption (ESA) can have three deleterious effects. Absorption which occurs in the same spectral region as fluorescence directly reduces the effective gain. This increases threshold and reduces slope efficiency. If ESA is sufficiently strong, it precludes lasing altogether. Absorption which occurs at shorter wavelengths interfere with optical pumping. Depending upon the pump source, it wastes photons that could otherwise be used to populate the emitting level. This becomes progressively more important for operation well above threshold. If return from higher singlet states to the emitting level is delayed significantly, additional considerations arise [3]. This, however, should be noticeable only in exceptional circumstances, such as when picosecond amplifiers are synchronously pumped by very high power picosecond pulses. Thermal problems frequently do limit dye laser performance. There exists no real laser for which ESA can be completely neglected. ESA is an extremely important factor in all laser dyes under all excitation conditions, since it is a property of the upper level of the laser transition itself. Unlike triplet-triplet absorption, it can never be neglected under any excitation conditions.

The influence of absorptions from the first excited singlet state upon dye laser operation has first been observed by Wieder [4] and several aspects of the problem have since been analyzed. With the prominent contributions by Teschke et al. [5, 6] for quasi-continuous lasers, and by Sahar and Treves [7] for short pulse lasers, the significance of ESA has been widely recognized. Magde [3] reported ESA spectrum for laser dyes like POPOP, coumarins and rhodamine 6G. Sahar and Treves [8] examined ESA in the region from 460 nm to 610 nm while Dolan and Goldschmidt [9] measured the region from 360 to 520 nm. They observed a large peak at 440 nm and a shoulder below 400 nm. Aristov and Shevandin [10] showed a maximum at 435 nm. Falkenstein et al. [11] offered values for the ESA cross section at two particular wavelengths. Hammond [12] studied the ESA in the region from 400 to 670 nm.

The other process which affects the lasing efficiency of dyes is the multiphoton absorption processes. A multiphoton (MP) process is one which occurs through the simultaneous absorption of two or more photons via virtual states in a medium. These processes require high peak powers which are now easily available from pulsed lasers. MP processes have been extensively studied both theoretically and experimentally. In fact as early as 1931, Goppert-Mayer [13] realized that an atom or molecule could absorb two photons simultaneously. The selection rules for two photon absorption (TPA) are quite different from those of one photon absorption (OPA). The prediction of TPA processes opened up a the possibility for a new kind of spectroscopy to probe those transitions that were forbidden under one-photon excitation. One can expect to observe nonlinear optical effects in a medium when the optical field and the electric field within a molecule are comparable. Since the advent of pulsed high power lasers, there has been extensive work in the field of TPA [14-16].

There has been a renewed interest in the field of upconversion lasing in recent years, due to several applications such as high density optical data storage and under sea optical communication. This uses sequential step wise absorption of two (or more) photons through intermediate real states to achieve population inversion. By contrast, two photon pumped lasing in organic dyes involves a direct absorption of two photons through virtual states. Since its first observation in 1971, several papers have been published about upconverted stimulated emission in solutions of commercial dyes such as Rh6G, RhB etc. [17-21]. The advantage of two photon pumped lasing in dyes as compared to conventional single-photon pumped lasing is that the pump wavelength can be shifted to longer wavelengths where dyes are relatively photostable unlike in the UV or visible region. Also since the absorption of the pump beam in the medium is low, it is possible to extract gain from the bulk rather than a thin layer of the medium. However due to the relatively small TPA cross section of the

commonly used laser dyes, efficiency of two photon pumped lasing reported so far have been rather low.

The free electron model proposed by Kühn [22, 23] suggests broad delocalization of the π electrons over the molecular chains, leading to large optical nonlinearities in dye molecules. According to this model the electrons can move freely along the chromophore group. The hectro atom (O for xanthenes) contributes to the energy levels by adding a potential well which modifies the energy of all symmetrical levels, but not the wave functions. The depth of the well depends on the nature of the hectro atom. This prediction has been verified by various reports testifying to the large values of third order nonlinear susceptibility, $\chi^{(3)}$ in dye [14-16]. Since laser dyes are usually pumped at an optical frequency corresponding to or greater than the $S_0 \rightarrow S_1$ transition frequency and if nonlinear processes like two photon absorption (TPA) or ESA occur at the pump wavelength, in general the dye molecules will be excited to a higher singlet state $S_n (n > 1)$. The singlet (S_1) to triplet (T_1) state intersystem crossing will decrease the net available excited singlet state population for stimulated emission, thus affecting the lasing efficiency of dyes, particularly in the cw mode of operation. It is well known that the nonlinear processes like TPA can occur only at intense laser fields, corresponding to pump intensities of the order of 10^8 W cm^{-2} or higher. The detailed study of these two processes (ESA and TPA) is of great significance because of the widespread use of such dyes in tunable lasers.

TPA is one of the important nonlinear optical processes which becomes relevant in laser dyes at high pump intensities. TPA processes in dye solutions have been employed for the time duration measurements of picosecond laser pulses by fluorescence trace analysis [24], for the investigation of third harmonic generation processes etc.[25]. The study of TPA and higher order multiphoton excitations has been mostly based on the observation of radiative transitions induced by the same from a higher excited electronic state usually at a shorter wavelength than the pump wavelength [26, 27]. These emissions have been referred to as anti-Stokes fluorescence (ASF), short wavelength luminescence, nonlinear fluorescence etc. by different authors [28, 29]. Different variation of the ASF technique have been applied to study the two photon characteristics of dye solutions [30]. However in organic dyes the fluorescence quantum yield of ASF is low since higher excited states are depopulated through strong nonradiative coupling to lower levels, thus making the radiative transition between higher and excited singlets and the lower levels. Along with this, there exists the problem of discrimination of Stokes fluorescence at the detector end, for largely fluorescing samples. Thus in general, a radiometric estimate of MP processes can lead to highly erroneous results

(particularly so in weakly absorbing media) as discussed in an earlier report taking the dye anthracene as a typical example [30]. Further, ASF resulting from different orders of MP excitation (2-photon, 3-photon etc.) can cover a broad wavelength region extending from the red end of the spectrum to the UV, thereby limiting the suitability of the ASF technique, often necessitating sophisticated detection schemes. Also these radiative relaxation processes are not very sensitive especially at higher concentrations. In organic dyes, ASF from higher excited singlets is extremely weak since these short lived states primarily relax nonradiatively to the S_1 state, prior to $S_1 \rightarrow S_0$ fluorescence [31]. The ESA can be observed by resultant quenching of dye fluorescence since this is more sensitive than the ASF technique [32, 33]. However, since the highly efficient nonradiative relaxations $S_n \rightarrow S_1$ release a large amount of thermal energy into the medium, such phenomena should be easily detectable by photothermal techniques like thermal lensing [34-37] or photoacoustics [38]. It is in this context that the applicability of TL technique for studying MPA processes becomes significant. In this chapter, the relaxation from the higher excited singlets following TPA or ESA in Rh6G and RhB laser dyes in three solvents *viz.*, methanol, ethylene glycol and water conveniently studied by monitoring the photothermal effect due to nonradiative transition is discussed. A special emphasis is also given to the effects due to aggregates formation in these dyes in three different solvents. Pulsed dual beam thermal lens method is effectively used for these measurements since it is highly sensitive compared to photoacoustic method.

Methods classified as TLS are based upon a thermal change in the optical properties of a sample on the absorption of laser energy which leads to a temperature rise in the sample and consequently to the formation of an inhomogeneous spatial profile of the refractive index. It has been demonstrated that the thermal lensing is a versatile and viable technique for exploring the different processes taking place in laser dyes. TL method gives valuable information and can be more sensitive than absorbance and fluorescence to detect dimer formation. Georges [39, 40] presented a theoretical study of dimerization equilibrium for fluorescent dyes in aqueous solutions. He demonstrated the aggregation equilibrium and its effect on the concentration dependence of absorbance as well as on the photophysical properties of certain laser dyes. Terazima et .al [41] have reported that the thermal lens signal intensity may depend on the solute even after correction for fluorescence and photochemical reactions. These authors have suggested that the solute dependence of the signal comes from the vibrational-mode dependence of the vibration to translation energy transfer etc. The dissipation of the excess of vibrational energy of the solute into the solvent would depend on the solute-solvent interactions and on the frequency of the vibrational modes.

4.2 Experimental

Details of the experimental set up are given in chapter 2. Briefly, the experimental set up consists of a frequency doubled Q-switched Nd:YAG laser which acts as the heating source and an intensity stabilized He-Ne laser as the probe beam. The sample solution taken in a quartz cuvette having pathlength 5 mm was placed in the pump beam path. The pump and probe beams were focused onto the sample cell and made to pass collinearly through it using suitable convex lenses and by the use of a dichroic mirror. The excitation beam was blocked beyond the sample cuvette by a filter. The polished tip of graded index optical fiber placed at 90 cm away from the centre of the sample cuvette serves both as an aperture and as a light guide for the probe beam to the detector consisting of a monochromator - PMT assembly. Using optical fibres to transmit the laser beams makes the thermal lens technique amenable to remote, in situ analysis. It also reduces the influence of mode and pointing variations in the laser. Here we used a multimode fibre which minimize alignment procedures and noise problems encountered with single mode fibres. The monochromator - PMT assembly tuned to the probe beam wavelength (632.8 nm) provides further filtering of the signal. The TL signal was recorded using a digital averaging oscilloscope which provides a complete time domain representation of the signal. The oscilloscope was triggered by a synchronous trigger pulse from the Nd:YAG laser operated at 5 Hz.

4.3 Principle of TL detection of MP processes

The energy conservation involved in the present case is illustrated in fig. 4.1. The laser power incident on any sample P_0 must be equal to the sum of the power transmitted P_t plus the power emitted as luminescence P_f plus the power degraded to heat P_{th}.

$$P_0 = P_a + P_t \tag{4.1}$$

where P_a is the absorbed power given by

$$P_a = P_f + P_{th} \tag{4.2}$$

Therefore,

$$P_0 = P_t + P_f + P_{th} \tag{4.3}$$

The power absorbed by an analyte P_a is given by [39]

$$P_a = P_0 \alpha_t f_a \tag{4.4}$$

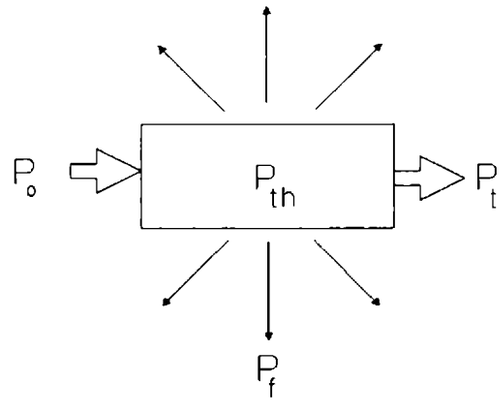

Figure 4.1: Power conservation for luminescence: P_0, incident excitation laser power; P_t, transmitted power; P_f, fluorescence or phosphorescence emission power; P_{th}, thermal power deposited as heat

where α_t is the total absorbance of the solute, α_t=1-10^{-A_t}, f_a is the fraction of the total power absorbed by the analyte which is equal to A_a/A_t (A_a -absorbance of the analyte and A_t - total absorbance of the solution).

The heat released by the nonradiative relaxation processes generates a volume expansion in the sample and a density change within the excitation region. The refractive index caused by the heat evolution due to the radiationless processes, turns in most cases the solution into a divergent lens which defocuses the laser beam. The magnitude S which is the change of irradiance at the beam centre relative to its stationary value, is given by [42, 43]

$$S = \frac{I(t=0) - I(t=\infty)}{I(t=0)} \propto E^n \tag{4.5}$$

where E is the incident laser intensity, n is the number of photons involved in the generation of the thermal lens signal, I(t = 0) and I(t = ∞) are the thermal lens signal strength at time t=0 and t = ∞ respectively. Hence by monitoring the dependence of thermal lens signal amplitude on pump energy, one can identify the occurrence of different processes like one photon absorption (n = 1) and multiphoton absorption processes (n $\geq$ 2).

4.4 Results and discussion

The lasing efficiency and fluorescence yield of a dye medium depend on various parameters like solute-solvent interaction, intersystem crossing, ESA, TPA and radiative and nonradiative relaxation cross sections. Most of the above mentioned phenomena depend critically on dye

concentration and pump intensity. In the present series of experiments transient thermal lens measurements were made from sample solutions of Rh6G and RhB in different solvents at varying concentrations ranging from 10^{-3} to 10^{-7} mol/lt at various input energies. We discuss below the results in these two samples separately.

4.4.1 Rhodamine 6G solutions

In general the absorption and emission of the dyes in various solvents differ from each other due to different kinds of solute-solvent interaction and environmental effects. The spectra for different concentrations in the same solvent also show variations [35]. The absorption spectra of Rh6G in different solvents *viz.*, water, methanol and ethylene glycol at different concentrations (ranging from 10^{-3} to10^{-7} mol/lt) recorded with a UV-VIS-NIR spectrophotometer (Hitachi model 150 - 20) are shown in figs. 4.2-4.4 respectively. Only the absorption spectra taken for low concentration is relevant, since a signal saturation is observed at high concentrations. The samples were taken in a 0.5 cm quartz cuvette. The absorption spectrum of Rh6G in methanol shows maxima at 18875, 29000 and 37000 cm^{-1} corresponding to the excited singlets S_1, S_2 and S_3 respectively. For Rh6G in water system, the maxima corresponding to these excited levels are at 18770, 28845, 36000 cm^{-1} while these maxima for the excited singlet levels are found to be at 18820, 28500, and 35970 cm^{-1} for Rh6G: ethylene glycol solutions. From the absorption studies it is clear that absorption of the probe at 632 nm (probe laser wavelength) is negligibly small and hence any perturbations due to the probe beam can be safely neglected. We have measured TL signal produced from sample solutions of Rh6G in methanol, water and ethylene glycol at different concentrations and for various input energies. As the laser energy increases the TL signal gradually increases. For solutions of low concentrations the increase in signal intensity is gradual and steady irrespective of the solvent used. As the concentration increases the signal intensity also increases. At low concentrated solutions the relation between TL signal and laser energy is linear. As the concentration of the solution and incident energy increases, the amount of energy absorbed increases and nonlinear processes begins to occur in the dye solution. Hence the dependence of TL on pump intensity no longer remains linear. A saturation behaviour is observed in the laser energy vs TL signal intensity curve in our results at high irradiance levels. At very high radiation intensities of pump laser, the amount of energy absorbed decrease, because the population of the ground state is significantly depleted. This may be the reason for the saturation in thermal lens signal intensity at high irradiance levels. Apart from these, the

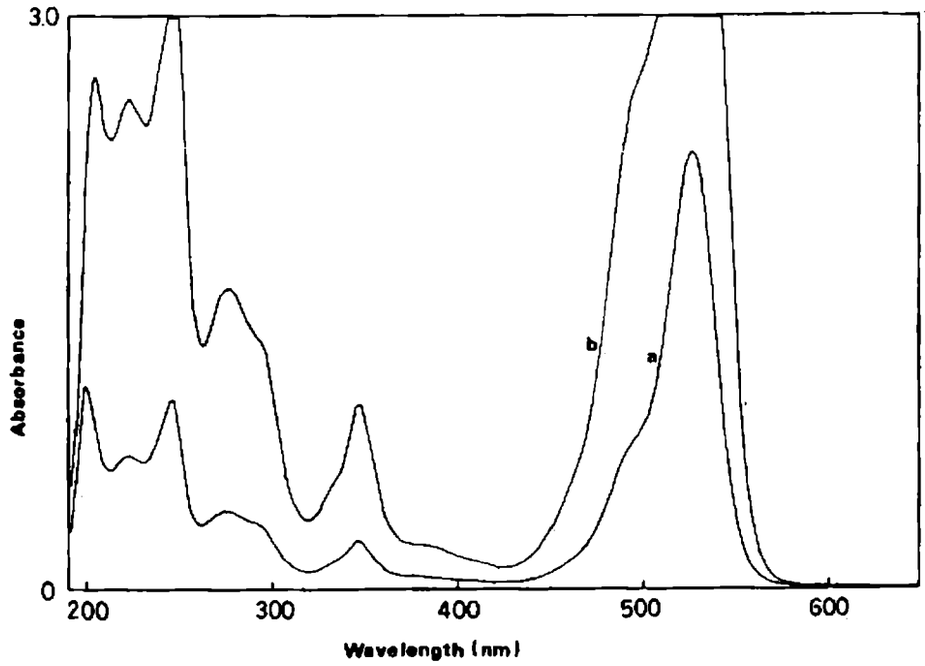

Figure 4.2: Absorption spectra of Rh6G in methanol (a - 2.14 $\times 10^{-5}$ mol/lt and b - 8.55 $\times 10^{-5}$ mol/lt).

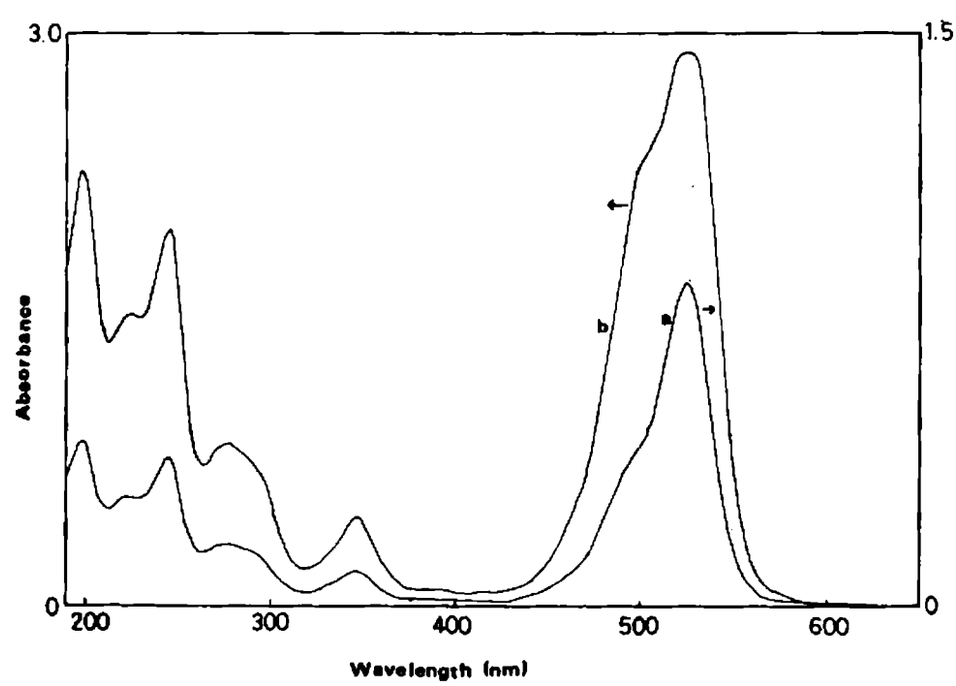

Figure 4.3: Absorption Spectra of Rh6G in water (a - 2.14 $\times 10^{-5}$mol/lt and b - 8.55 $\times 10^{-5}$ mol/lt)

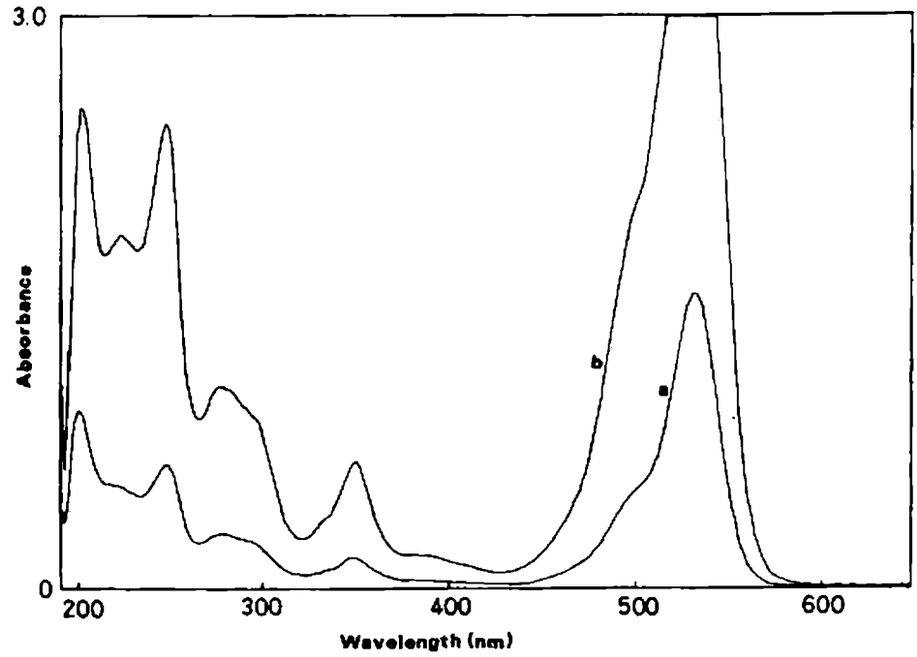

Figure 4.4: Absorption Spectra of Rh6G in ethylene glycol (a - 2.14 $\times 10^{-5}$ mol/lt and b - 8.55 $\times 10^{-5}$ mol/lt)

signal saturation may also occur due to lens aberration effects.

Log-log plots of thermal lens signal against laser energy are obtained for each sample. Figs. 4.5 - 4.7 give some of these log -log plots of thermal lens signal strength as a function of laser power in methanol, water and ethylene glycol solutions of Rh6G. From eqn. 4.5, it is clear that the slope of this plot will be numerically equal to the value of n, i.e., the number of photons involved in a multiphoton process. Fig. 4.8 represents the variation of the slope with concentration for these samples.

From fig. 8 it is clear that the slope which directly gives the number of photons involved, varies with respect to concentration and solvent used. For methanol the slope is found to be 0.8 for the lowest concentration studied (4.5 $\times 10^{-7}$ mol/lt). The slope steadily increases with concentration and attains a value of 3 at 2 $\times$ 10^{-4}mol/lt after which it decreases. The concentration dependence of the slope of log -log plots shows somewhat identical behaviour in all the three solvents. For Rh6G: water system, the slope increases to a value of 2.8 at 2 $\times 10^{-4}$ mol/lt and decreases at higher concentrations. Rh6G: ethylene glycol solutions also exhibit similar behaviour. Maximum slope is observed (2.9) at a concentration of 2 $\times 10^{-4}$ mol/lt.

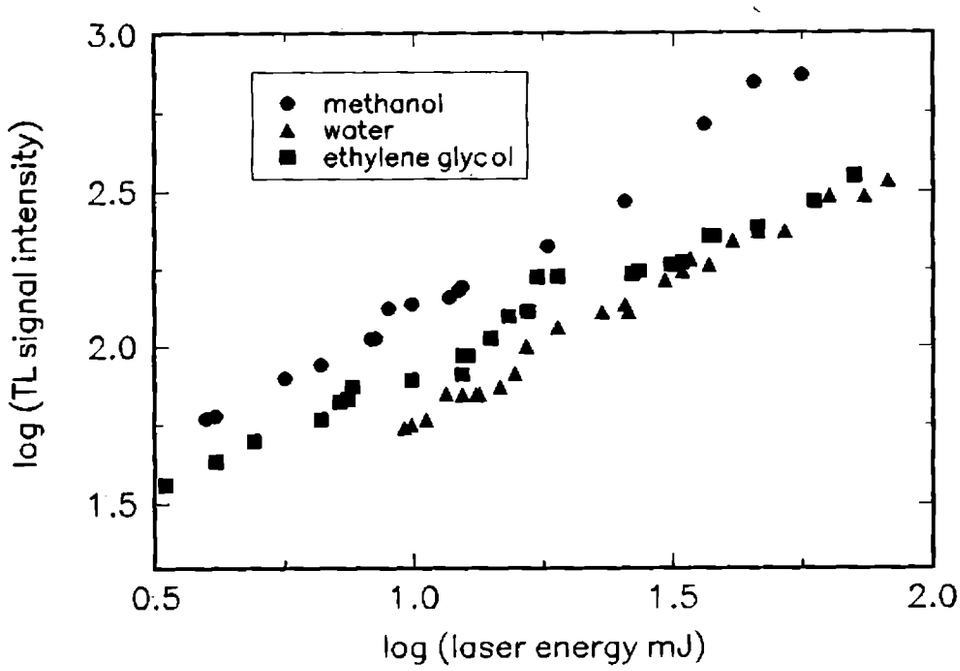

Figure 4.5: Log-log plots of thermal lens amplitude vs incident laser energy for Rh6G in methanol, water and ethylene glycol at a concentration of 2.65 $\times 10^{-6}$ mol/lt

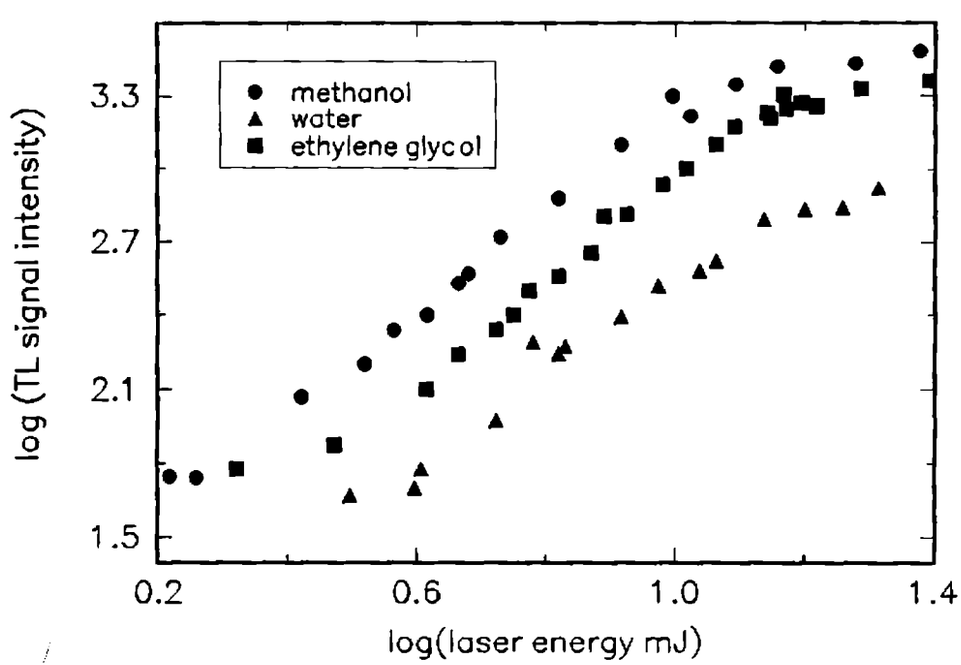

Figure 4.6: Log-log plots of thermal lens signal amplitude vs incident laser energy for Rh6G in methanol, water and ethylene glycol at a concentration of 8.55 $\times$ 10^{-5} mol/lt

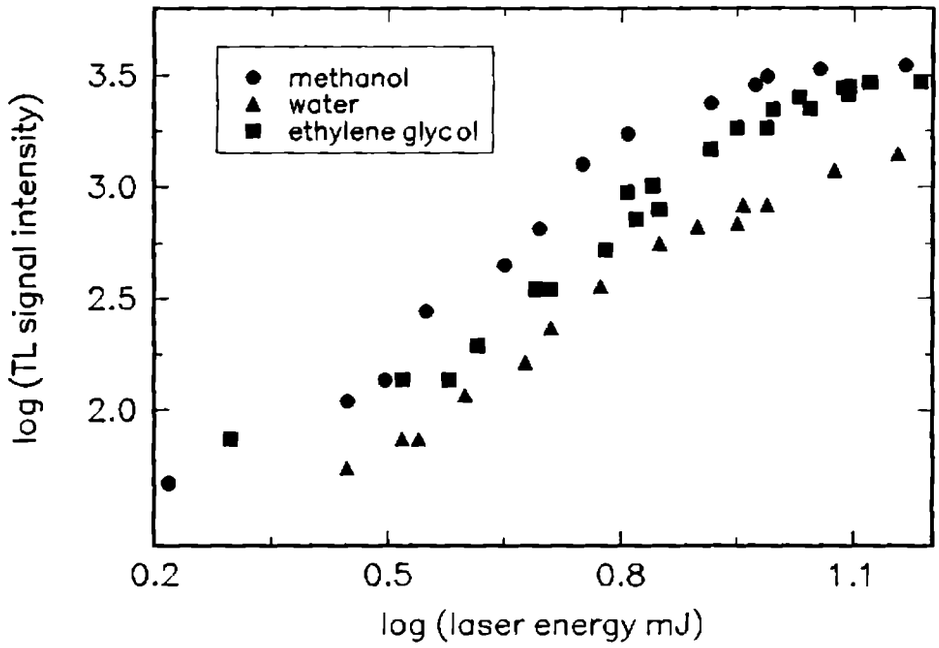

Figure 4.7: Log-log plots of thermal lens signal amplitude vs incident laser energy for Rh6G in different solvents at a concentration of 4.27×10^{-4} mol/lt

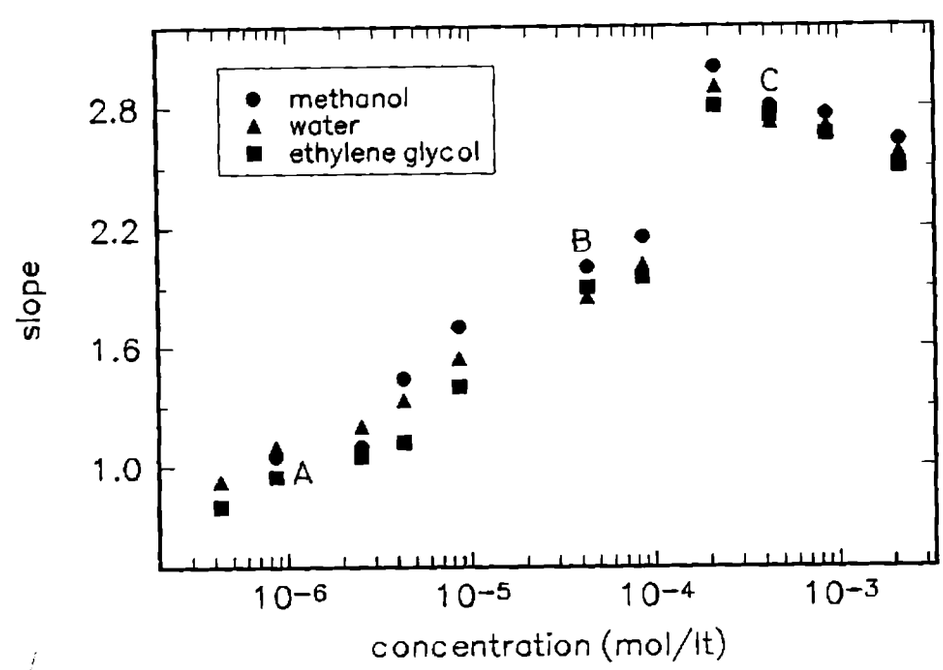

Figure 4.8: Variation of slope with concentration in different solvents. The marked regions (A,B,C) are explained in the text

Fig. 4.8 gives the direct indication of the many photon process involved in the generation of thermal lens transient signal. The curve exhibits three distinct parts with respect to the change in the value of slope:

(a) low concentration region (4.5×10^{-7} to 5×10^{-6} mol/lt), with linear variation of TL signal

(b) mid concentration regime (5×10^{-6} to 5×10^{-5}mol/lt) with quadratic variation of TL signal . In this region the slope value increases steadily with concentration and reaches a value of 2 and

(c) high concentration regime ($\geq 10^{-5}$mol/lt) where the slope attains a value of ~ 3 from where its value decreases with further increase in concentration. These results show that concentration of the dye molecules in different environment has a pronounced effect on the probability of different excitation processes which are taking place in the medium.

In solutions of low concentration (part A of the curve) one photon absorption (OPA) is prominent. The slope varies from 0.8 to 1.45 for Rh6G in aqueous, alcoholic and ethylene glycol solutions. OPA at 532 nm raises the rhodamine 6G molecules to a vibronic level of S_1 state ($\sim$18000 cm^{-1}). Molecules populating the various vibronic levels of S_1 due to OPA will rapidly deexcite nonradiatively to the lowest vibrational levels in the S_1 manifold in accordance with Franck-Condon principle so as to produce TL signals of lesser intensity and with a linear dependence on laser energy. $S_1 \rightarrow S_0$ internal conversion is negligible for Rh6G in the monomer form due to its high quantum yield and comparatively large energy separation between these levels. The possibility for the intersystem crossing to the triplet levels can also be ruled out as shown below. The pulse width of the pump laser t_p is ~ 9 ns in our work such that $t_p << 1/k_{st}$ where k_{st} is the $S_1 \rightarrow T_1$ intersystem crossing rate which is $4.2 \times 10^5 s^{-1}$ in Rh6G (for RhB $k_{st} = 1.7 \times 10^6$ s^{-1}) [44, 45]. Thus intersystem crossing is totally negligible.

The part B of the curve is obtained corresponding to higher concentration. The slope goes on increasing to a value 2 which is an indication of the occurrence of both OPA and TPA. Under intense pumping excitation of Rh6G molecules to higher excited levels ($S_0 \rightarrow S_3$) can take place by means of absorption of two 532 nm photons simultaneously. Subsequent to TPA excitation in the dye, TL signals are generated due to the strong $S_n \rightarrow S_1$ nonradiative coupling. These signals should have a quadratic dependence on laser energy. Along with TPA, ESA can also occur populating the higher excited singlets.

There are few reports regarding the occurrence of TPA in Rh6G laser dye [46-51]. Rulliere and Kottis [46] investigated excited electronic states of rhodamine 6G solutions by means of two photon Spectroscopy. They have explained the existence of TPA via symmetry consid-

erations. TPA can be understood in terms of symmetry allowed transitions; indeed due to the lack of symmetry of the molecule, the one and two photon transitions are always allowed, only the relative magnitude of the two transition moments varies with approximate state symmetry. Therefore state symmetries are mixed up in the case of dyes, leading to rather comparable transition moments for TPA. Recently Sathy et .al obtained similar results using pulsed photoacoustic technique [50, 51]. The ns laser pulse increases the possibilities of ESA as compared to a ps or fs laser sources [46]. Eventhough a ns laser is used, being of high power output it provides good power density, sufficient enough to initiate nonlinear absorption. The peculiar behaviour of the slope of the curve at mid concentration regime can be explained by comparing the cross sections for ground state absorption, excited state absorption and two photon absorption for Rh6G at 532 nm [52]. The absorption cross section ($\sigma_{S_0 \to S_1}(\omega_p) = 3.8\times10^{-16}$ cm^{-2}) and emission cross section ($\sigma_{S_1 \to S_0}(\omega_l) = 1.2\times10^{-16}$ cm^{-2}) are nearly equal and the cross section corresponding to ESA ($\sigma_{s_1 \to s_3}(\omega_p) = 4 \times10^{-17}$ cm^{-2}) is smaller by an order of magnitude for Rh6G. Even though, the cross section corresponding for TPA (for rhodamines the TPA cross section lies between 10^{-48} and 10^{-50} cm^4 sec [53, 54]) is much less in magnitude compared to ESA, it is also a possible mechanism on the basis of symmetry considerations.

In solutions of much higher concentrations we have observed a slope of ~ 3 in the log -log plot for Rh6G. The part C in the curve is thus clearly an indication of three photon absorption or a three step processes. The three photon absorption processes begins to appear almost at the same concentration for aqueous, alcoholic and ethylene glycol solutions of rhodamine 6G. Three step processes like $S_0 \to S_3 \to S_n$ is less probable since the life time of S_3 is so short that the fraction of the molecules excited to S_3 which decay spontaneously to lower singlets is nearly one [53]. After getting excited to S_3 (by two photon process) the molecules depopulate the S_3 level quickly and efficiently through nonradiative transitions before absorption from S_3 can take place. So this type of three photon processes can be safely neglected. The likely process is that the Rh6G molecules in the S_0 state may simultaneously absorb three photons and get excited to S_n levels. Another possible mechanism is that by OPA the Rh6G molecules go to the S_1 level from which by absorbing two more photons simultaneously the molecules gets excited to the S_n levels (excited two photon absorption). Both the above processes are probable at fairly high concentrations. Subsequent to excitation, the molecules deexcite from higher S_n levels nonradiatively giving rise to thermal lens signals of high intensity. Since the three photon absorption processes are more complex and less studied compared to other nonlinear phenomena, much more detailed studies on these aspects are needed to get a clear

picture.

We have also noticed that a decrease in the value of slope in the log -log plot with increase in concentration especially at higher concentrations. This may be predominantly due to the formation of aggregates in the Rh6G laser dye solutions. Usually xanthene dyes like Rh6G forms stable ground state dimers and higher aggregates at concentrations greater than 10^{-4} mol/lt. In general, the formation of aggregates reduces the output of the laser action by a combination of absorption of radiation owing to nonfluorescent aggregates and quenching of the monomer excited state. It has been shown that the strength of the aggregation between two or more dye molecules depends on the structure of the dye, the solvent, temperature, the pH and the presence or absence of electrolytes. The presence of aggregates in concentrated solutions may significantly influence the physico-chemical and biological process after photoexcitation of the system. Aggregates of dye molecules have also found technological application as radiation converters [55] and as sensitizers in the photogaraphic industry [56]. The investigation of the nonlinear optical properties of aggregates is very promising for use of such materials in the field of optical communication and computing [57].

One of the most extensively studied compounds from among xanthene dyes is Rh6G, which shows extremely strong aggregation in aqueous solutions [58]. At first, the aggregates were assigned to the dimers [59, 60]. Then, apart from Rh6G dimers, trimers [61] also were found in concentrated aqueous solutions. Recently, the formation of fluorescent aggregates of higher order than dimers has been shown while investigating photophysical properties of Rh6G aqueous solutions upon high pressure [62]. Scully et .al [63] made a hypothesis on the existence of fluorescent dimers of Rh6G in concentrated ethylene glycol solutions using time correlated single photon counting technique. Bojarski and co-workers [64] studied aggregation of Rh6G in concentrated ethylene glycol solutions. From their measurements of absorption and fluorescence spectra, presence of dimers were confirmed. They have also observed a strong overlaps between all absorption and fluorescence bands in that system enabling forward and reverse energy transport between monomers and dimers. The Rh6G:ethylene glycol solutions possess high bulk viscosities as compared to water and methanol as solvents. The small dependence of the Rh6G fluorescence life time with respect to the solvent viscosity indicates that the rigidity of the molecule, particularly of the amino groups does not affect the efficiency of the nonradiative processes encountered in other rhodamine molecules [65, 66]. Drexhage [67] reported that no aggregation phenomena can occur in alcoholic solutions of xanthene dyes. But several other workers disagree with this claim and has proved the formation of dimers in methanolic or ethanolic solution of these dyes [68-71]. It is also reported that the

spectrum of the dimers in ethanol is red shifted with respect to the monomer, indicating that the geometry of the dimer is also different in ethanol from that formed in water, where the absorption maximum is at shorter wavelength than that of the monomer [70]. Rh6G exists as the monomers in ethanol at concentration $\sim 10^{-4}$m/l and at higher concentrations dimers and trimers have been detected by several workers [71].

The dimer spectrum consists of two visibly separated bands, H and J. The H band of these dyes in water was observed to be larger than the J band while J band is found to be larger than H band in ethylene glycol solutions [74]. Molecules of RhB and Rh6G in water were proved to become nonfluorescent by dimerization [72, 73], since these dimers show strong H absorption [75] where as larger J band absorption was observed in the case of ethylene glycol [74]. It should be noted that the presence of aggregates in concentrated donor-acceptor systems may influence significantly the courses of photophysical and photochemical processes, especially if they are conditioned by the nonradiative excitation transport. In that case fluorescence aggregates play a role of additional acceptors being imperfect traps for the excitation energy [76-79].

Considering the equilibrium between rhodamine monomers (m) and rhodamine dimers (d), at concentrations C_m and C_d respectively, and assuming that each component separately obeys Beer's law, the total absorbance of the solution is given by [39]

$$A_t = A_m + A_d = \frac{l}{2}[\epsilon_d C_t + (2\epsilon_m - \epsilon_d)\frac{\sqrt{1+8K_d C_t} - 1}{4K_d}] \tag{4.6}$$

where l is the optical path length, ϵ_m and ϵ_d the molar absorptivities of monomers and dimers, respectively, at the specified wavelength, $K_d = C_d/C_m^2$, the dimerization constant and

$$C_t = C_m + 2C_d \tag{4.7}$$

the analytical concentration of the dye.

The amount of energy released as light (fluorescence) and as heat (thermal lens) for a solution of monomers and dimers in equilibrium will depend upon the sum of energies absorbed by each component,

$$P_a = P_{a(m)} + P_{a(d)} \tag{4.8}$$

Hence the thermal power liberated by the sample solution P_{th} is given by [39]

$$P_{th} = P_0(1 - 10^{-A_t})[A_m/A_t(1 - Q_{f(m)}\bar{\nu}_f/\nu_a) + A_d/A_t] \tag{4.9}$$

where A_m, A_d, A_t and Q_f are the monomer, dimer, total absorbance and fluorescent quantum efficiency of the laser dye and ν_f and ν_a represent average fluorescence frequency and absorbed

frequency respectively. At higher concentrations we do observe a decrease in slope with increase in concentrations. In order to check the effect of aggregation on the thermal lens signal formation, we have charted thermal lens signal intensity vs concentration curves. It can be noted that there occurs a decrease in thermal lens signal intensity with increasing concentration in the higher concentration regions irrespective of the solvents used.

The TL signal intensity is greatly affected by the dye concentration. Concentration dependence of TL signal strength is monitored for different laser powers. Figs. 4.9 - 4.11 show the variation of the TL signal with concentration at different excitation power levels of the pump beam for different solvents. The curve exhibits a type of concentration dependent variation of TL signal which is independent of the solvent used. As is clear from the figures, the signal intensity goes on increasing with concentration for low power levels. At lower concentrations the TL effect is small. As excitation energy increases the power absorbed by the dye molecules also increases which in turn causes an enhancement in the TL signal. At higher irradiation intensities of incident radiation, TL signal rises up to a particular concentration beyond which it begins to decrease. The signal peaks at a concentration of 4 $\times 10^{-4}$ mole/lt irrespective of the solvent medium. It may be noted here that the photothermal signal amplitude is highly solvent dependent. The intensity of the TL signal is maximum in methanol solutions. In aqueous solutions of Rh6G the signal intensity is weak owing to its low value of dn/dT and high thermal conductivity.

The TL signal also depends on the dimerization constant, the molar absorptivities and the fluorescence quantum yield of the dye solutions through eqn. (4.9.) This fact can be inferred from our present experimental observations. For example, the signal intensity goes on increasing up to a particular concentration and then decreases with increasing concentration. According to eqn. (4.9.) The TL signal is defined by two components: one component corresponding to the energy absorbed by monomers minus the radiant energy, and the other component corresponding to all the energy absorbed by the dimers. Dimerization contributes to decrease the first component in eqn. (4.9) (dimers are nonfluorescent which in turn decreases the value of Q_f and to increase the second component. The ratio A_m/A_t decreases at the same rate as A_d/A_t increases, but the variation of A_m/A_t is weighted by the term $(1 - \phi_{f(m)}\bar{\nu}_f/\nu_a)$ in eqn. (4.9) which is small when the compound is highly fluorescent. The relative amount of energy absorbed by monomers and dimers depends on the dimerization constant and the relative molar absorptivities. In the case of Rh6G at 525 nm, the molar absorptivity of the dimer is more than two times lower than that of the monomer [39, 80]. Therefore as the concentration increases the second component in the square brackets of

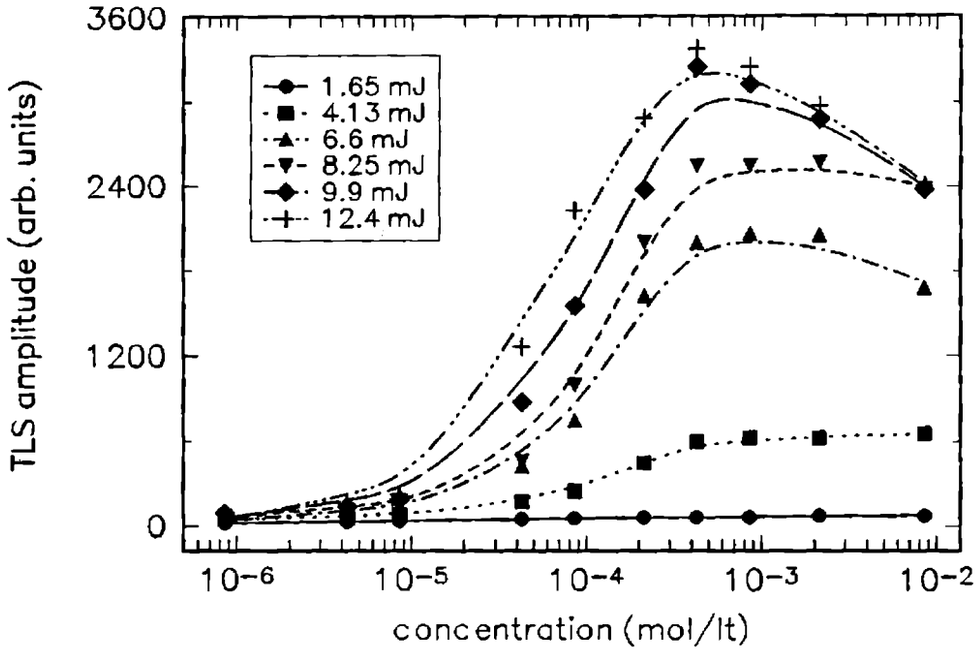

Figure 4.9: Variation of thermal lens signal amplitude as a function of concentration for Rh6G in methanol for different incident energies

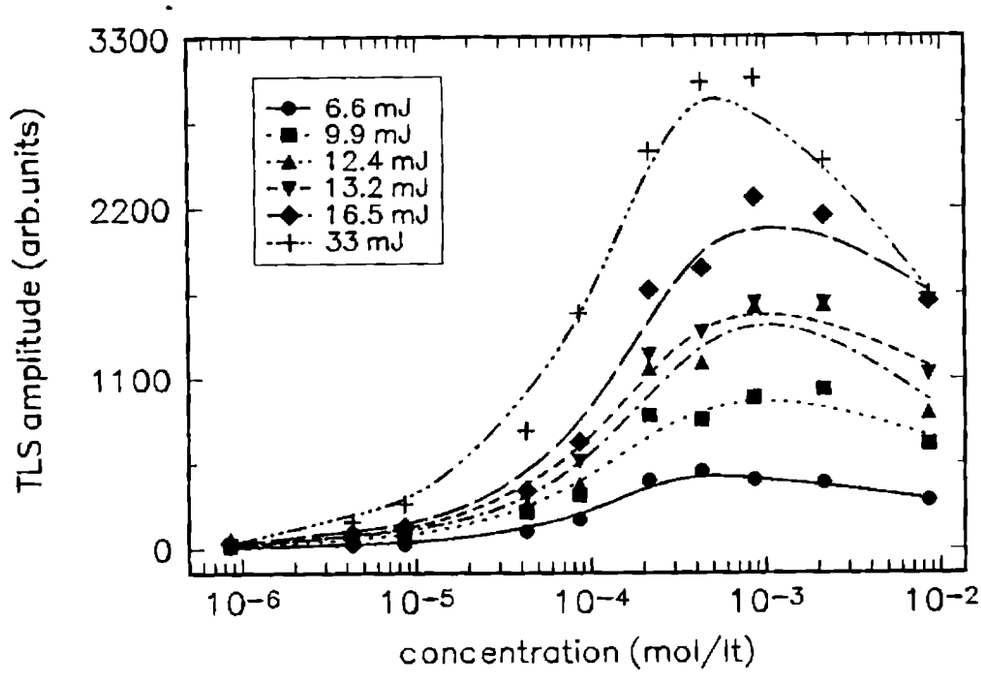

Figure 4.10: Variation of thermal lens signal amplitude as a function of concentration for Rh6G in water for different incident laser energies

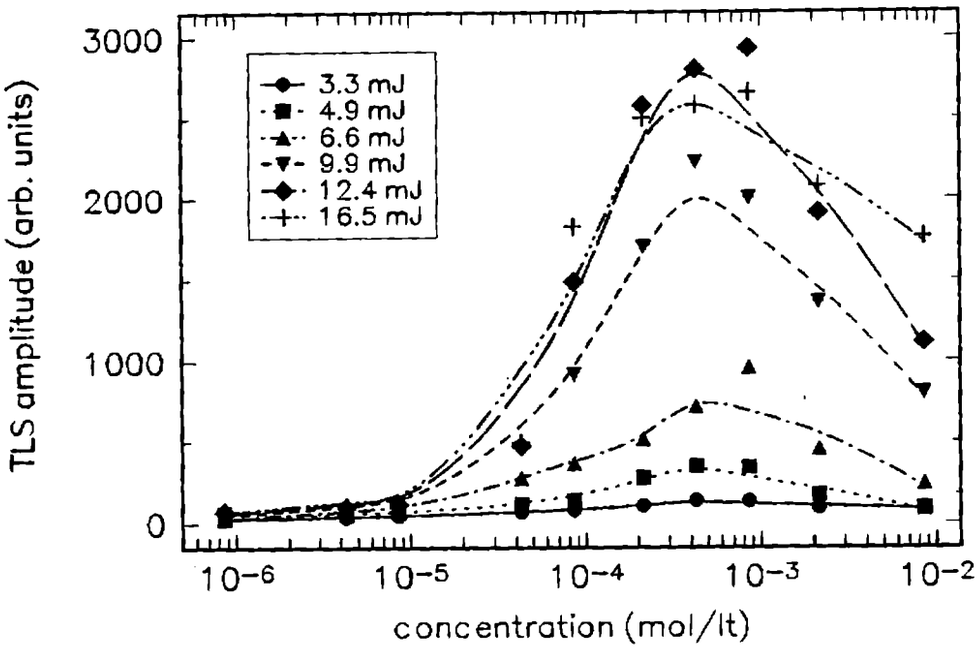

Figure 4.11: Variation of thermal lens signal amplitude as a function of concentration for the Rh6G in ethylene glycol for different laser energies

eqn. (4.9) for P_{th} increases faster and the thermal energy corresponding to the loss of two fluorescent monomers is more than compensated by that provided by the formation of one dimer [39]. Thus the reduction in thermal lens signal intensity at higher concentrations is due to following reasons. (1) The emissive Rh6G monomer can be generated via deaggregation and energetically it can relax nonradiatively through energy transfer to aggregates. (2) With increase in concentration, the concentration of dimer C_d increases. Since a dimer is a combination of two monomers (2m↔d), the effective number density of the absorbing molecules becomes less at higher concentration because of the enhanced aggregation phenomena.

From fig. 4.8 it can be seen that the slope value is higher in alcoholic solutions of Rh6G than in aqueous and ethylene glycol solutions at the concentration range studied. It is reported that the two photon/multiphoton absorption cross section is inversely proportional to the square of the refractive index of the solvent [15] using the equation

$$\delta = \frac{(2\pi)^5\alpha^4}{\lambda^2\mu^2} < (\mid \hat{e}.B.\hat{e} \mid)^2 > g(\omega) \tag{4.10}$$

here δ is the two photon absorption cross section, λ; wavelength of the incident light; μ, refractive index of the solvent; α , a local field correction factor; $g(\omega)$, the normalized one photon line shape and $\hat{e}$ is the unit polarization vector of the electric field and B is a tensor

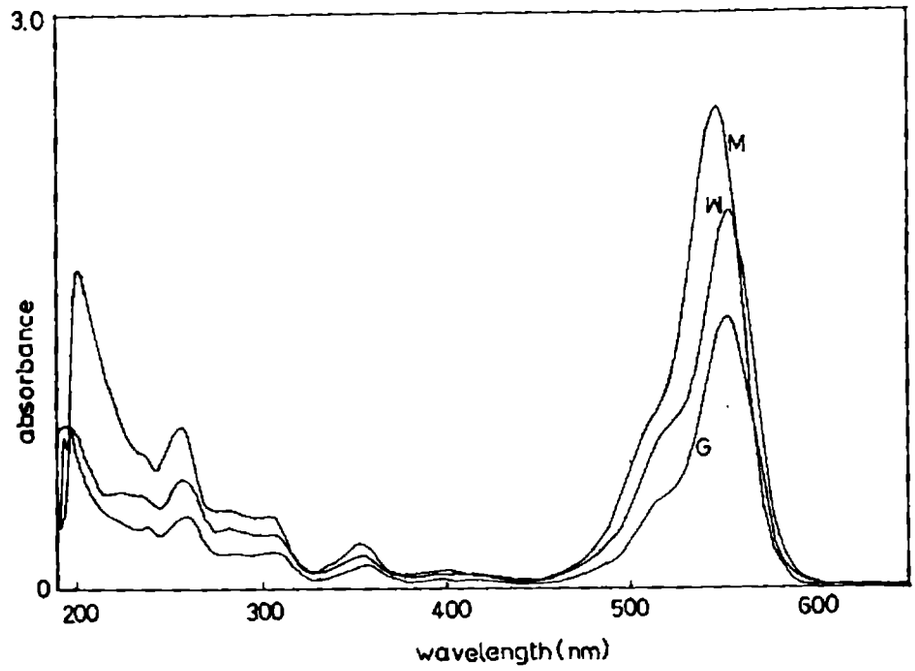

Figure 4.12: Absorption spectra of RhB in methanol (M), water (W) and ethylene glycol (G) (concentration - 2.13 $\times 10^{-5}$ mol/lt)

usually represented by a matrix. Methanol is having a lower refractive index than water and ethylene glycol [81]. So multiphoton absorption processes are more prominent in methanolic solutions than in water or ethylene glycol solutions.

4.4.2 Thermal Lens Studies in Rhodamine B

Rhodamine B (RhB) belongs to the family of xanthene dyes. RhB, one of the most widely used dyes, has been found to lase in alcohol, water, ethylene glycol and PMMA. The appearance of RhB laser dye in the various media mentioned above has stimulated a further study on spectroscopic and structural properties of this dye in relation to the lasing mechanism. Typical absorption spectra for RhB in different solvents are given in fig. 4.12.

In the present work, thermal lens measurements have been performed in aqueous, alcoholic and ethylene glycol solutions of RhB. Thermal lens effect was studied for the concentration range of 8.55 $\times 10^{-7}$ to 8.55 $\times 10^{-3}$ mole/lt and at various incident power levels. Log-log plots of TL signal vs incident intensity were drawn for each sample. Typical log -log plots are given in figs. 4.13-4.15 for different concentration. From these figures it can be seen that the TL effect increases as incident laser power increases due to enhanced absorption of

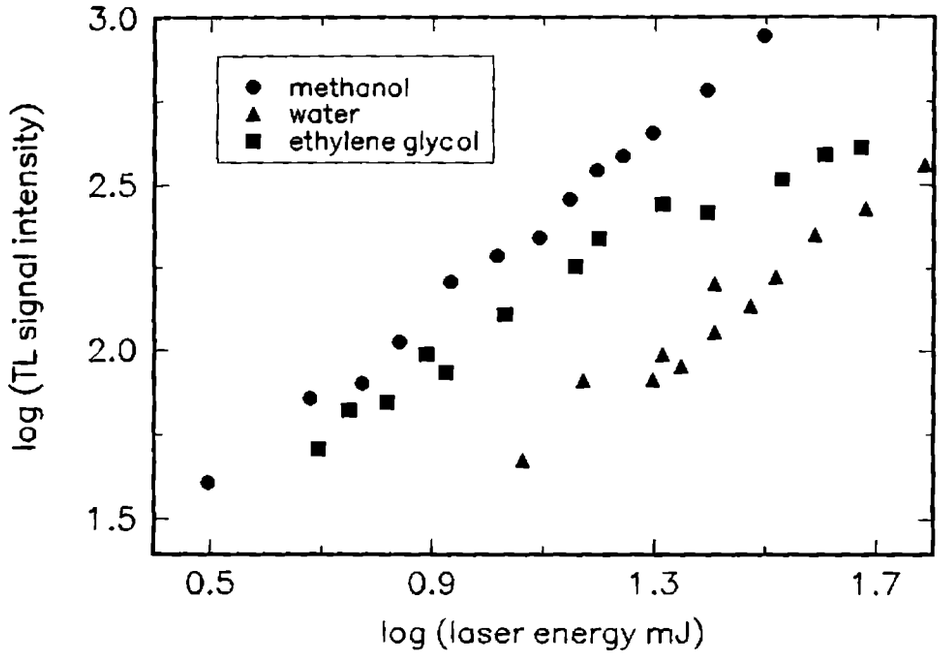

Figure 4.13: Log-log plot of thermal lens signal amplitude and incident laser energy for RhB in methanol, water and ethylene glycol at a concentration of 2.65 $\times 10^{-6}$ mol/lt

the sample solution. At higher illumination the signal tends to saturate due to enhanced depopulation of the ground state. We observed the occurrence of two- and three-photon absorption processes along with one photon absorption in these solutions similar to that observed for Rh6G solutions. The variation of the slope value with solute concentration is given in fig. 4.16 for the three solvents.

From fig. 4.16 the slope is found to $\sim$ 1 at low concentration solutions irrespective of the solvents used. As the concentration increases the slope of the log -log plot also increases and its value reaches $\sim$ 2 at a concentration of 5 $\times 10^{-5}$ mol/lt. At still higher concentration, the slope value becomes $\sim$ 3 beyond which it decreases. The maximum slope is obtained for a concentration of 8 $\times 10^{-4}$ mol/lt for all solvents. The peculiar nature of the slope vs concentration curve indicates concentration dependence of different absorption processes like TPA, 3-PA along with ESA details of which are discussed in the preceding sections. The emission and TPA cross-section for RhB molecules are $\sigma_{S_1 \to S_0}(\omega_l) = 1.9 \times 10^{-17}$ cm^{-2} and $\sigma_{s_1 \to sn}(\omega_p) = 1.2 \times 10^{-48}$ cm^{-2}. Similar to the observations made in the Rh6G solutions, here also maximum slope value is obtained in methanol as a solvent compared to water and ethylene glycol systems.

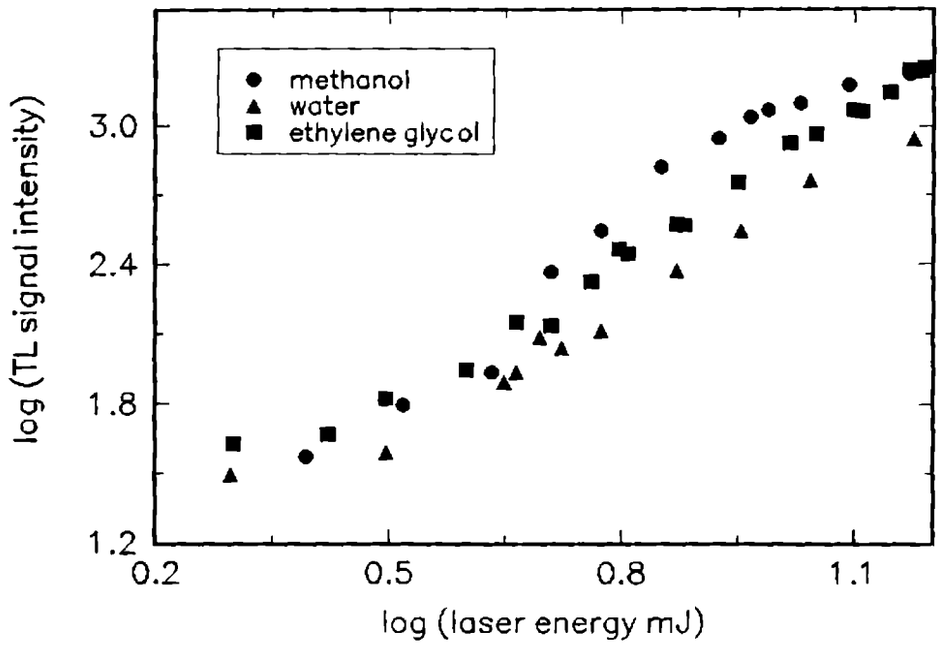

Figure 4.14: Log-log plot of thermal lens signal amplitude and incident laser energy for RhB in methanol, water and ethylene glycol at a concentration of 8.55 $\times 10^{-5}$ mol/lt

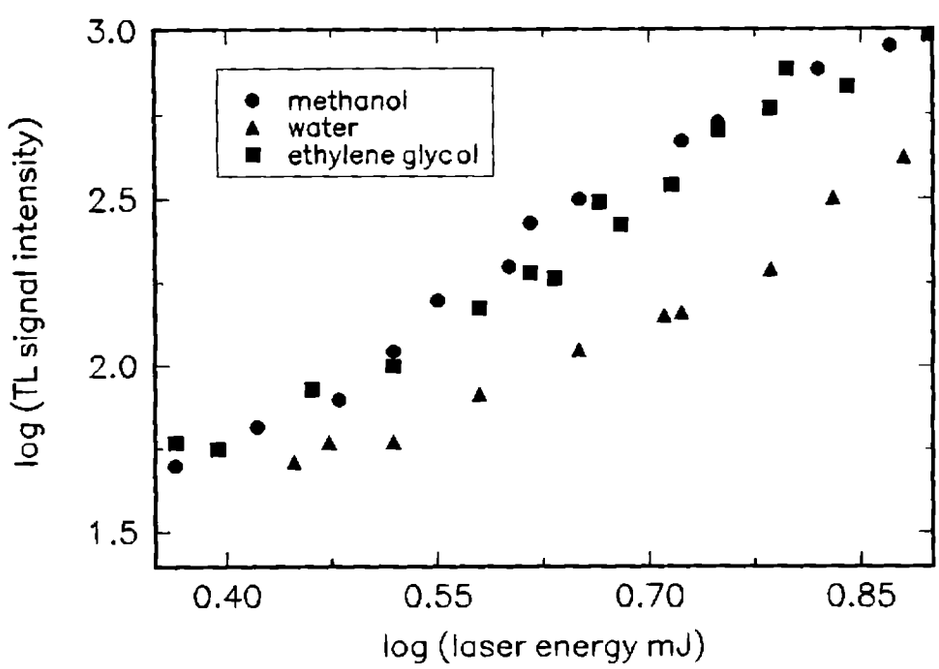

Figure 4.15: Log-log plot of thermal lens signal amplitude and incident laser energy for RhB in different solvents at a concentration of 4.27 $\times 10^{-4}$ mol/lt

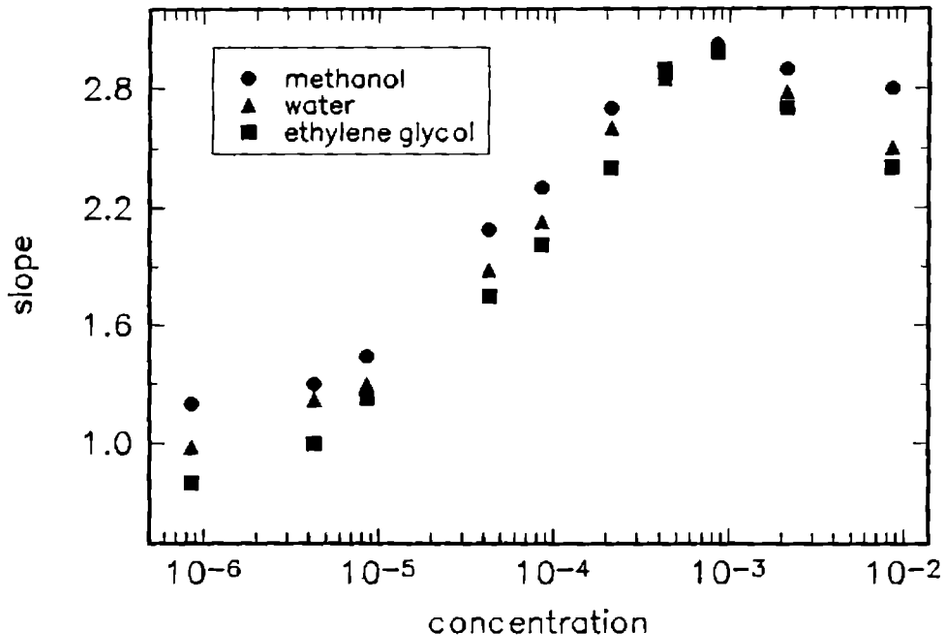

Figure 4.16: Variation of slope with concentration in different solvents for RhB solutions

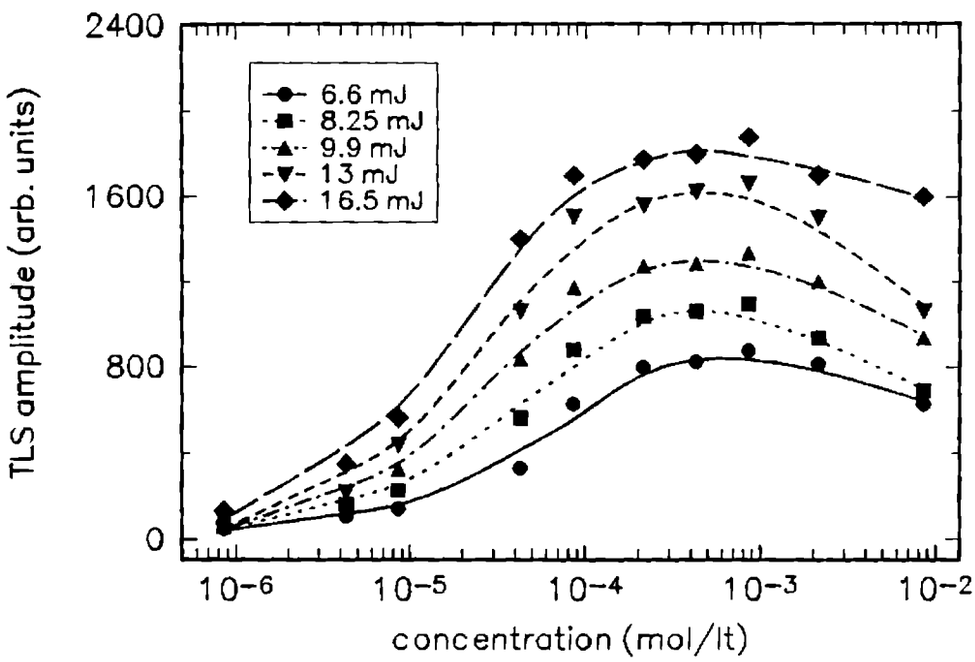

Figure 4.17: Variation of thermal lens signal strength as a function of concentration of RhB in methanol at different incident energy levels

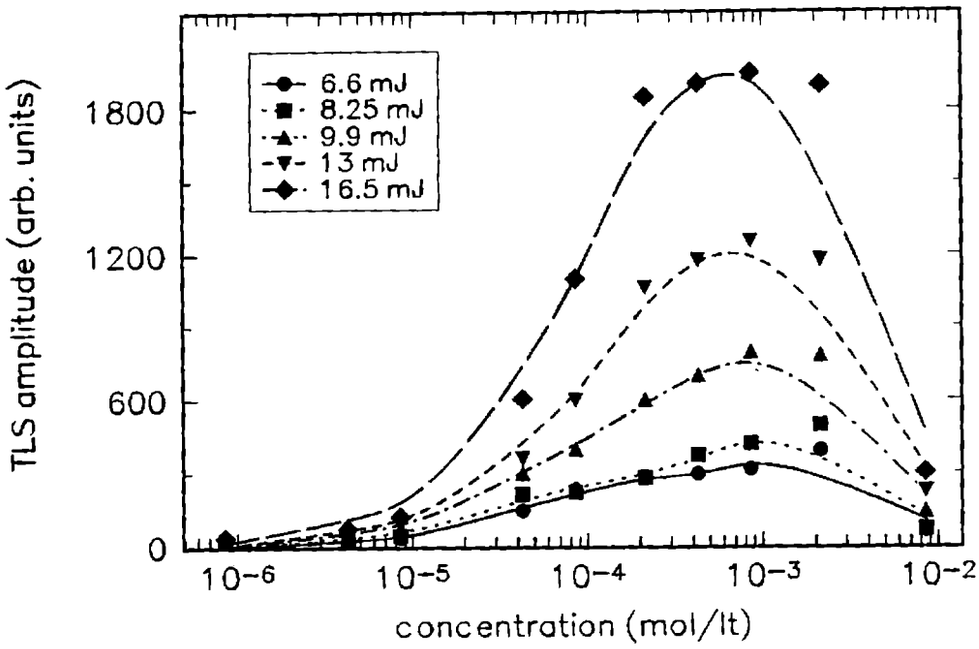

Figure 4.18: Variation of thermal lens signal strength as a function of concentration of RhB in water at different incident energy levels

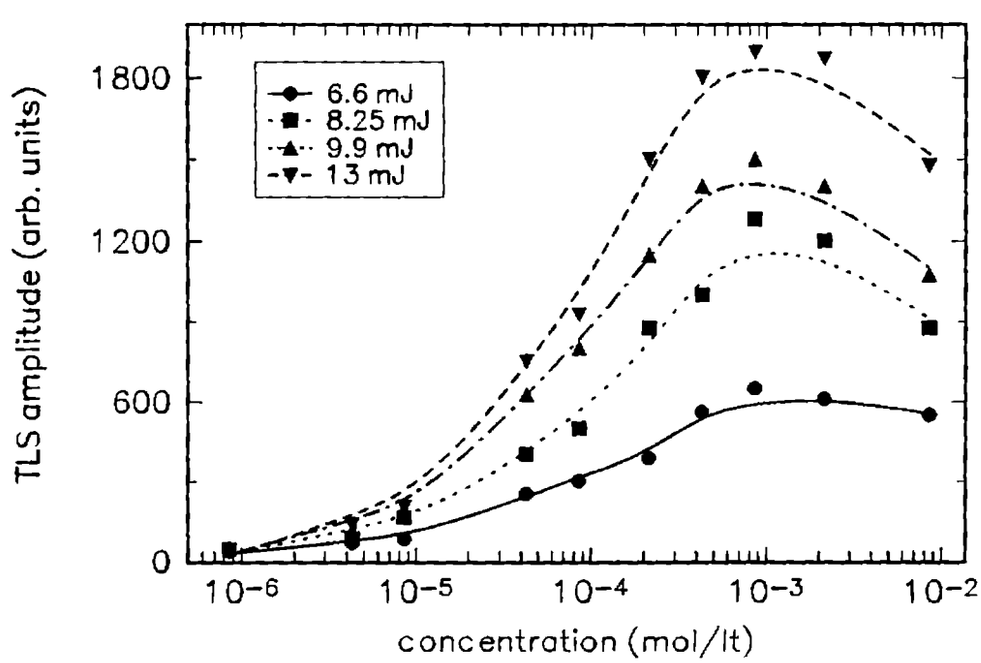

Figure 4.19: Variation of thermal lens signal strength as a function of concentration of RhB in ethylene glycol at different incident energy levels

TL signal strength is plotted by varying dye concentration for different power levels. The variation of TL signal with concentration for different power levels are shown in figs. 4.17-4.19. At low concentration regions the TL effect is comparatively small and it increases as dye concentration increases up to a particular concentration beyond which the signal begins to decrease. This is similar to the observations made in Rh6G solutions. Such peculiar behaviour of TL effect at higher concentrations can be attributed to the formation of dimers and higher aggregates, the details of which are discussed in section 4.4.1.

4.5 Conclusion

The thermal lens technique can be effectively utilized to distinguish between different nonlinear processes that are occurring in the Rhodamine 6G and Rhodamine B laser dyes. The ease of the set up and procedure of the technique are very attractive for such a task and the method appears to be complementary to fluorescent measurements. The nonlinear properties of the dye molecules vary with concentration, and environment. At lower concentrations OPA is prominent in aqueous, alcoholic and ethylene glycol solutions. As the concentration increases occurrence of TPA along with ESA is evident. At higher concentrations three photon processes begin to appear. The decrease in slope at higher concentrations is inferred to be due to the aggregate formation.

It will be very appropriate to use thermal lens spectrometry for analyzing dimerization equilibria because this method sensitive and should be useful over a wide range of concentrations. The thermal lens method is more efficient to detect dimerization equilibria especially because variation of thermal energy involved in such equilibrium is generally more important than the variation of absorbance and fluorescence. We have also noticed a peculiar concentration dependence curve of TL signal strength. With respect to increasing concentration TL signal also increases. At higher concentrations a decrease in TL signal is observed. This is mainly due to the enhancement in aggregate formation which effectively decreases the number density of the absorbing molecule. Both Rhodamine 6G and Rhodamine B solutions exhibit similar behaviour with respect to concentration variations.

4.6 References

[1] M. D. Rahn, T. A. King, A. A. Gorman, I. Hamblett, *Appl. Optics*, **36**, 5862 (1997).

[2] F. P. Schafer in *Dye Lasers*, (Springer Verlag, Berlin 1977).

[3] D. Magde, S. T. Gaffney and B. F. Camplell, *IEEE J. Quant. Elect.*, **17**, 489 (1981).

[4] I. Weider, *Appl. Phys. Letts.*, **21**, 318 (1972).

[5] O. Teschke and D. Dienes, *IEEE J. Quant. Elect.*, **12**, 383 (1976).

[6] O. Teschke and D. Dienes *Appl. Phys. Letts.* **26**, 13 (1975).

[7] E. Sahar and D. Treves, *IEEE J. Quant. Elect.*, **13**, 383 (1976).

[8] E. Sahar, D. Treves and I. Weider, *Opt. Commn.*, **16**, 124 (1976).

[9] G. Dolon and C. R. Goldschmitt, *Chem. Phys. Letts.*, **39**, 320 (1976).

[10] A. V. Aristov and V. S. Shevandin, *Opt. Spectrosk.*, **43**, 228 (1997).

[11] W. Falkenstein, A. Penzkofer, W.Kaiser, *Opt. Commn.*, **27**, 151 (1978).

[12] P. R. Hammond, *IEEE J. Quant. Elect.*, **15**, 624 (1979).

[13] M. Goppert-Mayer, *Ann. Phys. Lpz*, **9**, 273 (1931).

[14] J.P. Hermann, *Opt. Commn.*, **12**, 102 (1974).

[15] J. P. Hermann and J. Ducuing, *Opt.Commn.*, **6**, 101 (1972).

[16] W. Leupacher and A Penzkofer *App. Phys. B*, **36**, 25 (1985).

[17] W. Rapp and B. Gronau, *Chem. Phys. Letts.* **8**, 529 (1971).

[18] M. R. Topp and P. M. Rentzepis, *Phys. Rev. A*, **3**, 358 (1971).

[19] A. N. Rubinov, M. C. Richardson, K. Sala and A. J. Alcock, *Appl. Phys. Letts.*, **27**, 358 (1975).

[20] P. Qui and A. Penzkofer, *Appl. Phys. B*, **48**, 115 (1989).

[21] A. S. Kwok, A. Serpenguzel, W. F. Hsich, R. K. Chang and J. B. Gillespie, *Opt. Letts.*, **17**, 1435 (1992).

[22] H. Kuhn, *Fortschr. Chem. Org. Natürstoffe*, **16**, 1 (1959).

[23] H. Kuhn, *Fortschr. Chem. Org. Natürstoffe*, **17** 4 (1959).

[24] J. A. Giordmaine, P. M. Rentzepis, S. L. Shapiro and K. W. Wecht, *Appl. Phys. Letts.*, **11**, 216 (1967).

[25] J.C. Diels and F.P. Schäfer, *Appl. Phys.*, **5**, 197 (1974).

[26] G. C. Orner and M. R. Topp, *Chem. Phys. Letts.*, **36**, 295 (1975).

[27] A. V. Aristor and V. S. Shevandin *Opt. Spectro.*, **44**, 276 (1978).

[28] I. M. Catalano and A. Cingolani, *Opt. Commn.*, **32**, 159 (1980).

[29] Kh. Vabnits, V. A. Geisenok, A. Slobodyneuk and D. Shubent, *Opt. Spectro.*, **61**, 20 (1988).

[30] J. P. Hermann and J. Ducuing, *Phys. Rev. A*, **5**, 2557 (1972).

[31] P.Sathy, R. Philip, V. P. N. Nampoori and C. P. G. Vallabhan, *J. Phys.D*, **27**, 2019 (1994).

[32] P. R. Hammond, *IEEE J. Quan. Electr.*, **16**, 1157 (1980).

[33] E. Sahar and D. Treves, *IEEE J. Quan. Electr.*, **13**, 962 (1977.

[34] C. V.Bindhu, S. S. Harilal, R. C. Issac, V. P. N. Nampoori and C. P. G.Vallabhan, *Mod. Phys. Letts. B*, **9**, 221 (1995).

[35] C. V. Bindhu, S. S. Harilal, R.C. Issac, V. P. N. Nampoori and C. P.G. Vallabhan, *J. Phys. D*, **29**, 1074 (1996).

[36] M. C. Guptha, S. Hong, A.Guptha and J. Moacanin, *Appl. Phys. Letts.*, **37**, 505 (1988).

[37] K. Daree, *Opt. Commn.*, **4**, 238 (1971).

[38] S. S. Harilal, C. V. Bindhu, R. C. Issac, V. P. N. Nampoori and C. P. G.Vallabhan, *Mod. Phys. Letts. B*, **9**, 871 (1995).

[39] J. Georges, *Spectrochim. Acta A*, **51**, 985 (1995).

[40] M.Fischer and J.Georges, *Spectrochim. Acta A*, **53**, 1419 (1997).

[41] M. Terazima, M. Horiguchi and T. Azumi, *Anal. Chem.*, **61**, 883 (1989).

[42] A. J. Twarowski and D. S. Kliger, *Chem. Phys.*, **20**, 259 (1977).

[43] A. J. Twarowski and D. S. Kliger, *Chem. Phys.*, **20** 253 (1977).

[44] D. N. Dempster, *J. Photo. Chem.*, **2**, 343 (1973).

[45] P. Sperber and A. penzkofer *Opt. Quant. Electr.*, **18**, 381 (1986).

[46] C. Rulliere and P. Kottis, *Chem. Phys. Letts.*, **75**, 478 (1980).

[47] B. Focault and J. P. Hermann, *Opt. Commn.*, **15**, 412 (1975).

[48] H. Lin and M. Topp, *Chem. Phys. Letts.*, **47**, 442 (1977).

[49] D. J. Bradley, M. H. R. Hutchinson, H. Koetser, T. Morrow, G. H. C. New and M. S. Petty, *Proc. R. Soc. Lond. A*, **328**, 97 (1972).

[50] P. Sathy, R. Philip, V. P. N. Nampoori and C. P. G. Vallabhan, *Opt.Commn.*, **74**, 185 (1990).

[51] R. Philip, P. Sathy, V. P. N. Nampoori and C. P. G. Vallabhan, *J. Phys. B*, **25**, 155 (1992).

[52] F. J. Durate and L. W Hillman (eds.) *Dye laser principles with applications*, (New York; Academic 1990).

[53] W. Rapp and B. Gronau, *Chem. Phys. Lett.*, **8**, 529 (1971).

[54] P. Sperber and A. Penzkofer, *Opt. Quant. Elect.*, **18**, 381 (1986).

[55] A. Blum and L. I. Grossweiner, *Photochem. Photobio.*, **14**, 551 (1971).

[56] P. B. Gilman, *Photographic Sci. Engg.*, **18**, 418 (1974).

[57] Y. Wang, *Chem. Phys. Letts.*, **126**, 209 (1986).

[58] K. I. Yuzhakov, *Russian Chem. Rev.*, **61**, 1114 (1992).

[59] V. L. Levshin and E. G. Baranova *Opt. Spectrosco.*, **6**, 31 (1959).

[60] J. E. Selwyn and J. I. Steinfield, *J. Chem. Phys.*, **76**, 762 (1972).

[61] F. L. Arbeloa, P. R. Ojeda and I. L. Arbeloa, *J. Chem. Soc.Tran. II*, **84**, 1903 (1988).

[62] T. Taguchi, S. Hirayama and M. Okamoto *Chem. Phys. Letts.*, **231**, 561 (1994).

[63] A. D. Scully, A. Matsumoto and S. Hirayama, *Chem. Phys.*, **157**, 253 (1991).

[64] P. Bojarski, A. Matezuk, C. Bojarski, A. Kawski, B. Kuklinski, G. Zurkowska, and H. Diehl, *Chem. Phys.*, **210**, 485 (1996).

[65] M. Vogel, W. rettig, R. Sens and K. H. Drexhage, *Chem. Phys. Letts.*, **147**, 452 (1988).

[66] J. C. Mialocq, Ph. Herbert, H. Armand, R. Bonneau and J. P. Morand, *J. Photochem. Photobio. A*, **56**, 323 (1991).

[67] K. H. Drexhage in *Dye Lasers*, (ed) F. P. Schäffer (Springer 1977) p159.

[68] M. M. Wong and Z. A. Schelly, *J. Phys. Chem.*, **78**, 1891 (1974).

[69] C. T. Lin, A. M. Mahloudji, L. Li and M. W. Hsiao, *Chem. Phys. Letts.*, **193**, 8 (1992).

[70] O. V. Aguilera and D. C. Neckers., *Acc. Chem. Res.*, **22**, 171 (1989).

[71] P. R. Ojeda, I. A. P. K. Amashta, J. I. Ochora and I. L. Arbeloa, *J. Chem. Soc. Far. Trans. II*, **84**, 1 (1988).

[72] A. Penzkofer and W. Leupacher, *J. Lumin.*, **37**, 61 (1987).

[73] A. Penzkofer and Y. Lu, *Chem. Phys.*, **103**, 399 (1986).

[74] J. Muto, *J. Phys. Chem.*, **80**, 1342 (1976).

[75] J. Muto, *Jpn. J. Appl. Phys.*, **11**, 1217 (1972).

[76] C. Bojarski, *Z. Natürforsch.* **39a**, 948 (1984).

[77] L. Kulak and C. Bojarski, *J. Fluor.*, **2**, 123 (1992).

[78] L. Kulak and C. Bojarski, *Chem. Phys.*, **191**, 43 (1995).

[79] L. Kulak and C. Bojarski, *Chem. Phys.*, **191** 67 (1995).

[80] J. Georges, N. Arnaud and L.Parise, *Appl. Spectros.*, **50**, 1505 (1996).

[81] R. C. Weast (ed.) *CRC hand book of Chemistry and Physics*, (CRC Press, Florida 1988).

Chapter 5

Measurement of Absolute Fluorescence Quantum Yield of Rhodamine Dyes Using Dual Beam Thermal Lens Technique

Dual beam thermal lens spectrometry is successfully employed for the determination of absolute fluorescence quantum yield of two important xanthene dyes viz. Rhodamine 6G and Rhodamine B. The fluorescence quantum yield values are found to be strongly influenced by different parameters like environmental effects, concentration of the dye solution, mode of excitation of the dye solution, aggregate formation, excited state absorption, multiphoton absorption etc.

5.1 Introduction

When a molecule is excited there are a variety of processes which will return it to the ground state. These are briefly discussed in chapter 1. If we consider three processes for returning to the ground state viz., radiationless energy loss, intersystem crossing through the triplet state, and emission of a photon, then the efficiency of emission will be a function of the competing rates of these processes [1]:

$$q = \frac{k_f}{k_f + k_i + k_x} \tag{5.1}$$

where q is the efficiency or quantum yield and k_f is the rate constant for fluorescence emission; k_x, the rate constant for intersystem crossing and k_i, rate constant for radiationless transitions. The term k_f also relates to the average lifetime τ_0 through the equation, $k_f = 1/\tau_0$. The average lifetime is used since any one molecule can emit light at many probable times, much less or much greater than τ_0.

If there were no other factors involved, the fluorescence emission and absorption should be roughly proportional to one another. For example, if only the $\nu = 0$ to $\nu' = 0$ and $\nu' = 0$ to $\nu = 0$ transitions are considered, the probability of absorption and that of emission should be identical. Therefore the extinction coefficient should be a simple function of the lifetime of the excited state. Molecules with high extinction coefficients should have a high fluorescence efficiency and a short lifetime of the excited state, i.e., k_f should be very large.

The factors that influence the state of radiationless energy loss are not completely understood but certainly are dependent on both the temperature and nature of the solvent, the amount of triplet character of the singlet state as well as on the energy difference between the singlet and triplet states. In general, the greater the energy difference the smaller the rate constant.

For small molecules with well-integrated electronic systems, the competitive reactions from the conversion of excited molecules to the ground state by fluorescent or nonfluorescent processes are from the lowest excited state, no matter how the molecules were excited. Since all of the excited molecules must pass through this state, then regardless of which electrons (or which absorption bands) were excited, this lowest excited state will be formed. Hence it is evident that the fluorescence efficiency is independent of excitation wavelength.

The quantum yield is simply the ratio of the number of quanta emitted to the number of quanta absorbed. It is a dimensionless quantity. The fluorescence quantum yield is one of the key photophysical quantities that are amenable to direct experimental determination. The

quantum yield of fluorescence is a measure of the rate of nonradiative transitions that compete with the emission of light. In efficient laser dyes it approaches unity. Because of its dependence on the basic unimolecular rate constants for excited state decay, the fluorescence yield is of fundamental importance in numerous areas of photochemistry. The fluorescence and phosphorescence techniques have been used as an experimental tool by analytical chemists, biochemists, physical chemists and physicists. This rise in popularity is mainly due to the relatively low cost in instrumentation and a growing appreciation of the power of these methods. Absolute quantum yields are practically important. They are necessary for calculating thresholds for laser action [2] and for judging the suitability of materials as wavelength shifters in optical pumping experiments or for use as energy donors. Quantum yields coupled with luminescence data also allow evaluation of the purity of materials [3]. Absolute quantum yields are of central importance for studies of radiationless processes in molecules [3-6], for correlation of predicted luminescence lifetimes with the observed lifetimes [7] and for making assignments of electronic transitions [8].

Several authors have presented excellent reviews on quantum yield studies. Williams [9] has discussed briefly the methods for obtaining yields of inorganic phosphors. Lipsett [10] has presented an extensive review on quantum yields with particular emphasis on the secondary processes that follow optical excitation (polarization, reabsorption, reemission and apparent lifetime changes). Also, Parker [3] has discussed luminescence instrumentation in detail. Demas and Crosby [11] have discussed various techniques for measuring quantum yields, the advantages and the disadvantages of each experimental method. They also have explained the origins and the magnitudes of the numerous errors which may arise in different fluorescence experimental techniques.

A brief account of the various methods of measuring quantum yields is given in the following sections.

5.2 Methods of Measuring Quantum Yields

5.2.1 MgO_2 as a standard:

The work by Vavilov [12] in 1928 described the first reliable method for measuring absolute luminescence efficiencies of solutions. Basically Vavilov's technique is a substitution method employing a MgO_2 scatterer as a standard. Light from a medium pressure Hg arc is monochromatized by a filter and is focussed by a convex lens to a small spot on element. Either a cuvette containing the luminescent material or a plate coated with a freshly prepared layer

of MgO_2 serves as the element (C). A detector views the scatterer or cuvette normal to the front surface. The experiment consists of two measurements. First the cuvette containing the sample is placed at C and the signal strength from the sample luminescence is recorded by the detector. The cuvette is replaced by a plate coated with MgO_2 which scatters the exciting beams and a second detector reading is obtained. From these data and some additional information, the absolute quantum yield of the sample can be detected.

The most important development has been the introduction of solution scatterers by Weber and Teale [13]. These workers employed optically dilute colloidal solutions as standards, which behave as almost ideal dipole scatterers. These solutions attenuate by scattering a collimated beam of light in the same way as absorbing molecules diminish the intensity. The ideal scatterer, however, behaves as if it were a substance which reemits all the absorbed photons without changing the wavelength. Hence a dipole scatterer may be used as quantum yield standard of unit efficiency.

5.2.2 Comparison with Compounds of Known Quantum Yields

Several simple relative methods have been devised which substitute a compound of known quantum yield in place of a standard scatterer as a reference. Relative measurements fall conveniently into two classes: Optically dense and optically dilute methods. In the former the light is almost completely absorbed and the luminescent spot is near-point source, whereas in the latter, most of the exciting beam emerges unaltered. At intermediate concentrations the two types of measurements overlap and with suitable corrections yield the same results.

5.2.2.1 Optically Dense Measurements

This method uses the Vavilov configuration [12] with the scatterer replaced with a cuvette containing an optically dense solution of a standard compound. The expression for the yields is [11]

$$Q_x = Q_r \frac{K_r}{K_x} \frac{D_x}{D_r} \frac{n_x^2}{n_r^2} \tag{5.2}$$

where Q is the quantum yield of the solution, K is the average detector output per photon over the emission spectrum, D is the detector response and n is the refractive index of the solution. The x and r subscripts refer to the unknown and the standard reference solution, respectively. This equation is applicable provided the absorbed light produces a near point source in both the standard and unknown sample; the detector sees the entire luminescing volume; reflection and transmission effects are the same for both samples; and the refractive

index of each solution is constant over each emission band. Use of this form is restricted to a comparison of compounds which can be excited at a common wavelength. Detailed knowledge of the emission spectra of the standard and the unknown as well as the wavelength sensitivity of the detector must also be known.

5.2.2.2 Optically Dilute Measurements

In this method, a spectrofluorometer is used as the detector. The technique is relatively simple and reasonably accurate. The ready availability of high quality spectrofluorometers and their components adds further appeal. Corrected emission spectra are also obtained. This measurement is based on Beer's law which states that

$$I_0 B = I_0(1 - 10^{-Al}) \tag{5.3}$$

where B = fraction of light absorbed by the sample, I_0 = intensity of the incident light, A = absorbance/cm and l = path length. If the luminescence intensity for each compound is proportional to I_0B, then the expression for the quantum yield becomes [14]

$$Q_x = Q_r \frac{A_r(\lambda_r)}{A_x(\lambda_x)} \frac{I(\lambda_r)}{I(\lambda_x)} \frac{n_x^2}{n_r^2} \frac{D_x}{D_r} \tag{5.4}$$

where D = integrated area under the corrected emission spectrum, $A(\lambda)$ = absorbance/cm of the solution at the exciting wavelength λ. Subscripts x and r refer to the unknown and reference solutions respectively. Many assumptions are inherent in the above equation. For both unknown and reference it is assumed that the integrated luminescence intensity is proportional to the fraction of light absorbed, all geometrical factors are identical, the excitation beams are monochromatic, reflection losses are the same, internal reflection effects are equal, reabsorption and reemission are negligible, and all light emnating from the cuvette is isotropic.

5.2.3 Photothermal methods

Because of formidable difficulties attendant on absolute determinations of fluorescence yields, fluorescence is almost always studied relative to some standard substance [11]. The reliability of such relative determinations is then limited both by the accuracy of the standard yield value and by the confidence that can be placed on the comparison technique. Both of these factors have proved to be restrictive in the past. Very few absolute standards have been assigned reliable yield values. Comparative techniques require close attention to factors such as excitation wavelength, emission spectra, reabsorbance and the refractive index of the solution. Ideally, in a comparative measurement the conditions needed are identical absorbance

throughout the excitation bandwidth, closely similar wavelength distributions of the fluorescence spectra, negligible reabsorbance of the emission and identical refractive indices of the two solutions being compared. With so few reliable fluorescence standards available, it is seldom possible to achieve all of these features; hence it was usually necessary to introduce correction factors (for example, emission response calibration curves, refractive index corrections) which are themselves subject to a degree of uncertainty. As a result, though relative fluorescence quantum yields can be measured relatively easily, they can seldom be reported much better than about 10% reliability.

Rectification of this difficulty requires a whole series of absolute standards encompassing as wide as possible a range of wavelength regions and solvent refractive index and thereby permitting the researcher to select a standard which closely matches the characteristics of the system being studied. Measurements based on photothermal effects are capable of giving fluorescence yields of highly fluorescent solutions with high accuracy and reproducibility. It was for these reasons that photothermal methods such as thermal lensing [15-18], photoacoustic [19-22] and photothermal beam deflection [23, 24] techniques were developed. Even after making various corrections for system geometry, re-absorption, polarization etc., the accuracy of the quantum yield values obtained from photometric measurements is rather poor. In order to evaluate absolute quantum efficiency, we have to consider both the radiative and nonradiative processes taking place in the medium. As the contribution from nonradiative processes is not directly measurable using the traditional optical detection methods, thermo-optic techniques such as photoacoustic and thermal lens methods have been adopted recently for this purpose.

Using thermal lensing and pulsed photoacoustic methods we have determined the fluorescence quantum efficiency of the common laser dyes such as Rhodamine 6G (Rh6G) and Rhodamine B (RhB). The details and results of thermal lensing measurements will be discussed in the present chapter. The photoacoustic determination of fluorescence yields and its advantages will be discussed in the following chapter.

5.3 Q_f Measurements Using Thermal Lens Method

Dual beam thermal lens technique has been found to be very effective for the measurement of fluorescent quantum yield of dye solutions. An advantage of thermal lens is the ease with which it can measure Q_f over a wide range of concentration. The procedure is best known as a sensitive tool able to cope with extremely weak absorptivities. At the same time,

reabsorption-reemission problems are to be much reduced, since photons need only escape from the submillimeter dimensions of a focussed laser beam.

The knowledge of fluorescence quantum efficiency of organic dyes and its concentration dependence are essential for selecting efficient laser media. Fluorescence yield and lasing efficiency of a dye medium depends on various parameters like solute-solvent interaction, intersystem crossing, excited state absorption (ESA), two photon absorption (TPA), radiative and nonradiative relaxation cross section etc. In this chapter a detailed account of the dependence of these parameters on the quantum yield of two important xanthene dyes viz. Rh6G and RhB in different solvents are presented. The effect of excitation source on these important quantities is also verified.

The thermal lens effect [25-28] is one of the thermo-optical methods usually employed for measurements at very low absorption limit. This effect can be observed using moderate laser intensities in media with absorption coefficient as low as 10^{-7} cm^{-1} [29]. Thermal lensing or thermal blooming occurs when energy absorbed from a Gaussian beam produces a local heating within the absorbing medium around the beam axis. In such experiments, the sample is exposed to a laser beam which has gaussian beam profile and it causes excitation of the molecules along the beam path. Thermal relaxation of the excited molecules dissipates heat into the surroundings thereby creating a temperature distribution which in turn produces a refractive index gradient normal to the beam axis within the medium. This acts as diverging lens called thermal lens (TL).

In this chapter we demonstrate that TL technique can be very effectively employed to study the different optical processes in highly fluorescing materials. For fluorescent materials, TL effect is sensitive to fluorescence efficiency which means that any change in the emission characteristics will directly influence the magnitude of TL signal [30]. The variations in quantum yields of highly fluorescent materials can be effectively studied by this method because of the relatively large changes occurring in TL signal compared to that in fluorescence output especially at high concentration limit. Conventional fluorescence quantum yield measurements require the use of accurate luminescence standard samples and comparison of the given sample with a standard, for which the luminescence quantum yield is known. In this kind of experiment it is necessary to introduce corrections for the locations and the shapes of the fluorescence spectra of the sample and the standard. It is a complicated experimental procedure and the accuracy obtained by conventional spectrometric techniques is rather poor. The other disadvantages are the smaller number of standards available, the poor accuracy of the standard yield value, differences in refractive index, polarization effects, differences in

wavelength response of monochromators and detectors and inner filter effects.

Although it is difficult to ascertain whether photothermal methods are more accurate than fluorescence measurements, the former are less sensitive to experimental errors. While fluorescence generally senses a narrow band of wavelengths and only a small part of the emitted photons, the photothermal methods are sensitive to complementary part of the total fluorescence, which means that any change in the emission spectrum will influence the photothermal signal. However changes in the fluorescence spectrum arising from the interaction of the emitted photons with the solution are expected not to affect the photothermal signal.

The TL method offers significant advantages over conventional methods because absolute values of quantum yield can be measured and no standard sample is necessary [16,17,31]. However in strongly absorbing medium there exists an upper limit for pump beam power which gives a noise free TL signal when dual beam TL technique is employed. This method also requires careful attention to all the possible photophysical processes associated with the relaxation of the fluorescent compound.

5.3.1 Theory

The method is based on the principle of energy conservation. If P_0 is the power of the incident excitation beam and P_t is the power of the transmitted beam, the absorbed power is the sum of the luminescence emission power P_f and the thermal power degraded to heat P_{th}, provided that any photochemical reaction is absent. Hence,

$$P_o = P_{th} + P_f + P_t \tag{5.5}$$

so that the transmission ratio is given by

$$T = \frac{P_t}{P_0} \tag{5.6}$$

Absorbance is given by

$$A = 1 - T \tag{5.7}$$

Thus the absorbed power is given by

$$AP_0 = P_{th} + P_l \tag{5.8}$$

Then

$$P_l = AP_0 - P_{th} \tag{5.9}$$

The emission quantum yield is by definition

$$Q_f = \frac{P_f/\nu_f}{(P_0 - P_t)/\nu_0} \tag{5.10}$$

Here ν_o is the laser frequency and $< \nu_f >$ is the mean luminescence emission frequency, evaluated as

$$< \nu_f >= \frac{\int \nu_f dn(\nu_f)}{\int dn(\nu_f)} \tag{5.11}$$

The quantity dn(ν_f) in photons/sec is the number of photons emitted in an incremental bandwidth centered at ν_f. The eqn. (5.10) can be rewritten in the form [31]

$$Q_f = \frac{\nu_0}{< \nu_f >}(1 - \frac{P_{th}}{AP_0}) \tag{5.12}$$

The ratio $\nu_o/ < \nu_f >$ takes into account of the Stokes shift, which entails some deposition of heat in the sample even for a 100% fluorescence quantum yield. The absorption A may be measured with an ordinary spectrophotometer. Brannon and Magde [31] developed a comparison method in which thermal lensing measurements are made on both the fluorescent sample and nonluminescent reference absorber. The concentrations of sample 's' and reference 'r' are carefully adjusted to give identical photometric transmission. With identical incident light levels, the fluorescent sample, of course, produces less solution heating. A measurement is also made on the pure solvent blank. For the reference sample,

$$A^r P_0^r = P_{th}^r \tag{5.13}$$

Brannon and Magde [31] used the equation

$$Q_f = \frac{\nu_0}{< \nu_f >}\left(1 - \frac{A^r P^r}{A^s P^s}\frac{P_{th}^s}{P_{th}^r}\right) \tag{5.14}$$

where A^s = absorption coefficient of the luminescent sample A^r = absorption coefficient of the nonluminenscence reference P_{th}^s = thermal power generated in the sample P_{th}^r = thermal power generated in the reference absorber The absorption coefficient A may be measured with an ordinary spectrophotometer and P_{th} can be measured using thermal lens technique. The reference absorber is a non-luminescent material which is not necessarily strictly non-luminescent [31]. Eqn. (5.14) assumes that the same solvent and the same excitation laser wavelength are used for the sample and the reference, the optical properties of the solute are dominated by the solute and the thermal properties of the solution are determined by the solvent.

When using this method, one has to pay attention to maintaining the ratio A^rP^r/A^sP^s near unity and work with reasonably dilute solutions. Otherwise a systematic error occurs when the sample and the reference solutions are of considerably different optical densities [32]. Another problem is concerned with measuring light absorption coefficient A^s using spectrophotometer. Since a small amount of the fluorescence will be received by the detector when a fluorescent sample is measured, a high apparent transmittance will often result [17], which causes an uncertainty in the quantum yield.

If a quenched luminescent sample is used as the reference absorber, the problems can be solved because the quenched sample has the same light absorption coefficient as the luminescent sample. In the case of a totally fluorescence quenched sample we can consider entire excitation energy to be converted into nonradiative relaxation process and hence the fluorescence quantum yield (Q_f) is given by [31],

$$Q_f = \frac{P_f}{AP_0}\frac{\lambda_f}{\lambda} = \left(1 - \frac{P_{th}}{P_\alpha}\right)\frac{\lambda_f}{\lambda} \tag{5.15}$$

where

$$P_\alpha = AP_0 \tag{5.16}$$

and the ratio of the fluorescence peak wavelength λ_f to excitation wavelength λ takes account of the Stokes shift. P_{th} is directly proportional to the TL signal η and P_α is proportional to TL signal η_α corresponding to the concentration at which the fluorescence intensity is quenched completely. By knowing λ_f, η and η_α one can directly calculate the quantum efficiency Q_f from equation

$$Q_f = \frac{\lambda_f}{\lambda}(1 - \frac{\eta}{\eta_\alpha}) \tag{5.17}$$

The thermal lens signal η has been measured using the standard technique available in the literature [29]. The TL signal is taken as variation of light intensity at the center of the probe beam (He-Ne laser beam) arising due to the thermal lensing effect in the medium.

In order to circumvent uncertainities originating from the measurement of the absorbance of the fluorescent sample and its comparison with that of the reference absorber, a second method has been proposed, using quenched fluorescence samples as references. The signal for a fluorescent sample is compared with that obtained with the same compound, the fluorescence of which has been completely quenched with a quencher. The use of fluorescence quenching eliminates the need for an external reference; the method is therefore more accurate provided the absorbance characteristics are not modified by the fluorescence quencher, but is restricted because not all systems can be totally quenched.

5.4 Experimental

The details of the experimental set up are given in chapter 2. For cw excitation mode, the 514 nm from an argon ion laser was used as the pump source to generate the TL in the medium. For pulsed mode excitation 532 nm radiation from a frequency doubled Nd:YAG laser was used. Radiation of wavelength 632 nm from a low power intensity stabilized He-Ne laser source was used as the probe beam. Samples solutions were taken in a quartz cuvette (0.5 cm) which was kept in the pump beam path. The He-Ne laser beam (probe beam) is made to pass collinearly with the pump through the sample with the help of a dichroic mirror. A filter was placed in the path of the emergent beams which allowed only the 632 nm wavelength to reach the detector where the tip of an optical fibre serves as the detector head with a finite aperture. After passing through the fibre the signal enters a monochromator-Photomultiplier tube (PMT) assembly and the signal was processed using a digital lock-in amplifier in the cw mode excitation. For pulsed mode output of the PMT is directly coupled to a digital storage oscilloscope which gives transient thermal lens signal.

For fluorescence studies, the front surface emission was collected and focused by a lens on to the aperture formed by the tip of another optical fiber attached to the entrance slit of a 1 metre Spex monochromator which is coupled to a PMT having S20 cathode. The PMT output is fed to Lock-in amplifier/boxcar averager for further processing. The emission shows the characteristic fluorescence spectrum.

5.5 Results and Discussion

Fluorescence yield and lasing efficiency of a dye medium depends on various parameters like solute-solvent interaction, intersystem crossing, ESA, TPA, radiative and nonradiative relaxation cross section etc. Most of the above mentioned phenomena depend critically on dye concentration and pump intensity. The values of absolute luminescence yield also influenced by the mode of excitation used. We have carried out luminescence quantum yield determination of xanthene dyes viz. Rhodamine 6G (Rh6G) and Rhodamine B (RhB) in different solvents like methanol, water, ethylene glycol using cw dual beam thermal lens technique.

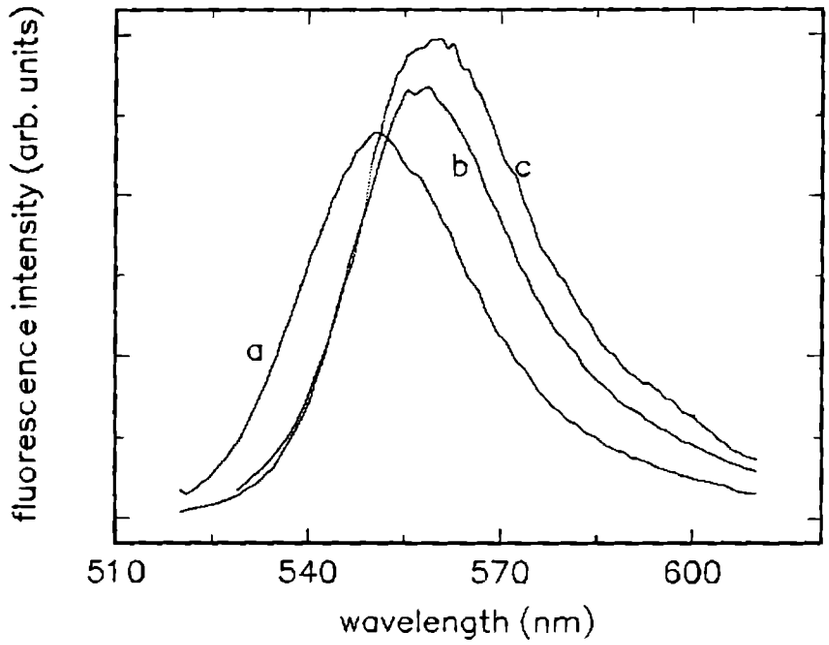

Figure 5.1: Typical fluorescence spectra obtained for Rh6G in methanol during 514 nm Ar^+ excitation for different concentration (a - 4.3×10^{-6} mol/lt, b - 4.3×10^{-5} mol/lt, c - 8.5×10^{-5} mol/lt)

5.5.1 Solvent Effects on Fluorescence Spectra

Fluorescence studies are carried out for Rh6G and RhB laser dyes. For these measurements the emission from the front surface geometry is utilized. Typical fluorescence spectra for Rh6G molecules (recorded using Ar ion laser excitation) in different solvents for various concentrations are given in figs. 5.1-5.3. From these figures it is clear that a concentration dependent change in the fluorescence spectra does occur in these dyes. The fluorescence spectrum of the highest concentration differs strongly from that recorded at lowest concentrations. The difference between these are significant in the case of red shift of fluorescence and enhancement of the half width of the fluorescence spectrum with increasing concentration. A knowledge of possible environmental effects on spectra and quantum yields of fluorescence is necessary for the utilization of fluorescence technique at its maximum potential. A list of the environmental factors that affect fluorescence phenomena includes interactions with solvent and other dissolved compounds, temperature, pH and the concentration of the fluorescence species. The effects that these four parameters have upon fluorescence vary from fluorescent species to species. Both the absorption and emission spectra as well as the quantum yields of fluorescent molecules are influenced by these parameters. Before discussing the results for flu-

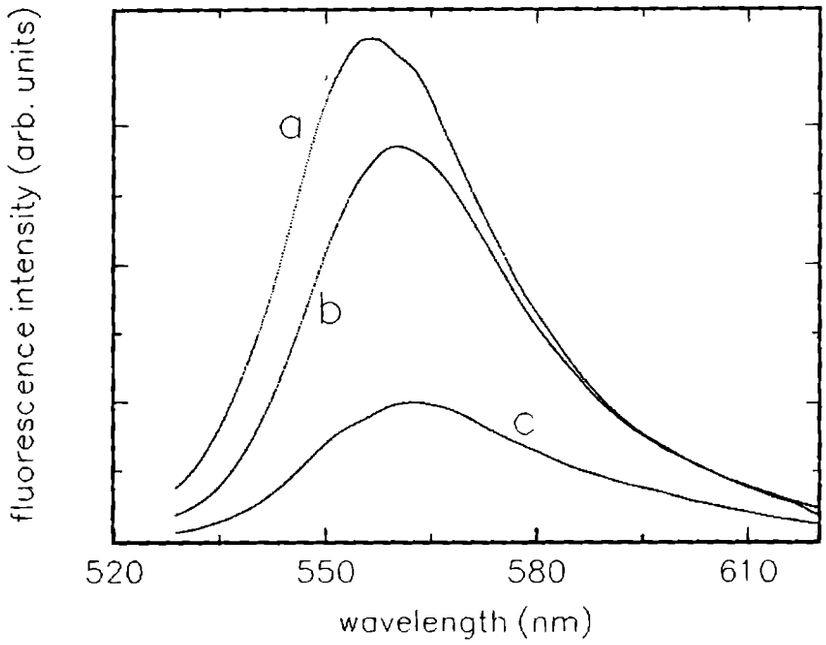

Figure 5.2: Typical fluorescence spectra obtained for Rh6G in water during 514 nm Ar^+ excitation for different concentration (a - 4.3 × 10^{-6} mol/lt, b - 4.3 × 10^{-5} mol/lt, c - 2.12 × 10^{-4} mol/lt)

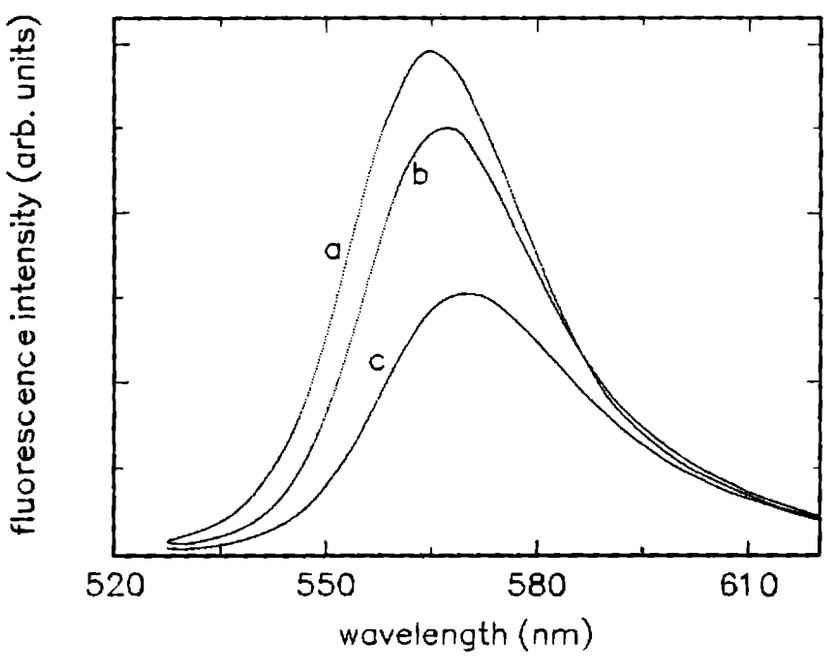

Figure 5.3: Typical fluorescence spectra obtained for Rh6G in ethylene glycol during 514 nm Ar^+ excitation for different concentration (a - 4.3 × 10^{-6} mol/lt, b - 8.5 × 10^{-5} mol/lt, c - 2.12 × 10^{-4} mol/lt)

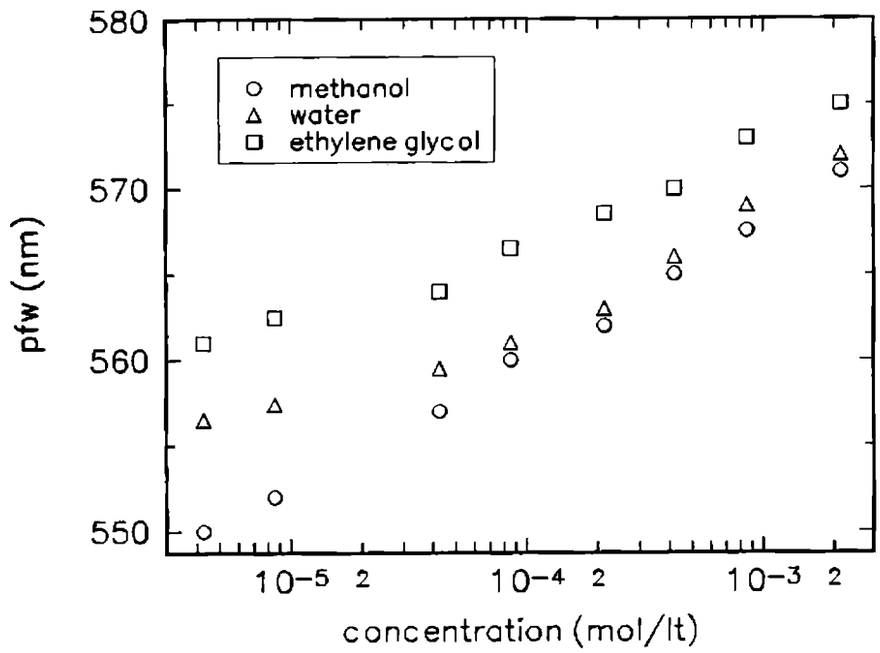

Figure 5.4: The change in peak fluorescence wavelength (pfw) with concentration of Rh6G

orescence efficiency values of Rh6G there are a number of other aspects of the measurements that should be considered.

Fig. 5.4 represents the peak fluorescence wavelength (pfw) of Rh6G as a function of concentration in alcoholic, aqueous and ethylene glycol solutions. It can be seen that the peak fluorescence wavelength (pfw) increases with concentration. In other words the fluorescence spectrum of the dye is shifted to smaller energies when the dye concentration is increased. To determine the emission of the aggregates produced, Arbeloa et al. [33] carried out these experiments with varying optical pathlength of the sample and they found that the fluorescence spectrum of concentrated solutions recorded using very short optical path has the same shape as that observed in dilute solutions. Therefore the aggregates do not emit at room temperature and the spectral shift is a consequence of the reabsorption and reemission phenomena [3,11,24,34-37]. Solvent effects on the absorption and emission spectra of various dyes have been investigated by several authors [38-43]. The absorption and emission characteristics of Rhodamine dyes in several water/ethanol mixtures have been investigated by Arbeloa et. al [44]. Mataga et. al [45, 46] interpreted the red shift of indole and its derivatives in terms of a generalized dipole-dipole interaction between the solute and the solvent in the excited state. Greater solute-solvent interaction in the excited state than in the ground state leads to a red

shift of the spectrum. The spectral shifts observed can be used as a guide to the interaction of the dye with the solvent media.

The solvent parameters, dielectric constant and refractive index can be correlated with the Stokes shift (the shift between the ground and excited state transitions of R6G). A variety of equations have been proposed [47, 48] to describe the effects of the physical properties of the solvent upon the emission spectra of fluorophores. In all these treatments the solvent is regarded as a continuum in which the fluorophore is contained. Of course, this simplifying assumption eventually limits the applicability of the equations since specific fluorophore-solvent interactions between fluorophores and their surroundings can have substantial effects upon the emission spectra. However the general solvent effects are always present, and a quantitative prediction of the expected effects provides a frame work within which one can analyze the experimental data.

The interactions between the solvent and fluorophore molecules affect the energy difference between the ground and the excited states. This energy difference is a property of the refractive index (n) and dielectric constant (ϵ) of the solvent. Within the zeroth order approximation the solute-solvent interaction is considered to be primarily of dipole-dipole nature including dispersion interactions. Equations have been proposed (neglecting short-range hydrogen bonding interaction) by Lippert [47], Kawski [48], Babakhshiev [49] and Chamma and Viallet [50]. The relation proposed by Chamma and Viallet [50] is

$$\frac{\overline{\nu_a} + \overline{\nu_f}}{2} = -\frac{2\Delta\mu^2}{a^3hc}F \tag{5.18}$$

where ν_a and ν_f are the 0-0 absorption and emission frequencies respectively,

$$\Delta\mu^2 = (\mu_e - \mu_g)^2 \tag{5.19}$$

where μ_e and μ_g are the permanent dipole moments in the excited and ground states respectively, h is the Planck's constant, c is the speed of light in a vacuum and a is the Onsager cavity radius assuming the solvent to be a medium of continuous dielectric constant and refractive index. F is given by the equation

$$F = \frac{2n^2+1}{2(n^2+2)}\left[\frac{D-1}{D+2} - \frac{n^2-1}{n^2+2}\right] + \frac{3}{2}\frac{n^4-1}{(n^2+2)^2} \tag{5.20}$$

where n and ϵ are the refractive index and dielectric constant of the solvent medium respectively.

The sensitivity of a fluorophore to solvent polarity is expected to be proportional to $\Delta\mu$ [51]. This term is expected to be constant for a given fluorophore [51]. The slope of the plot

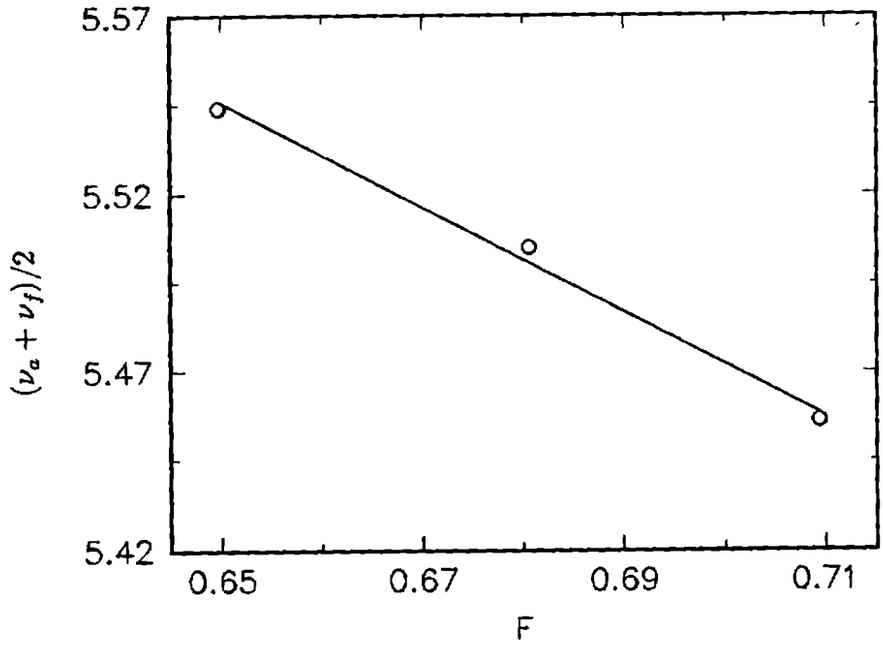

Figure 5.5: The plot of $(\nu_a + \nu_f)/2$ vs F

of the left-hand side of the eqn. (5.18) vs F (fig. 5.5) yields the value of $\Delta\mu = 0.88$ Debye. The Stokes shift in the ground and excited state spectra can be explained using the Franck-Condon Principle. Several workers [52, 53] have correlated the solvent polarity parameter involving the dielectric constant with the Stokes spectral shift as in equation.

The emission spectra clearly contain a good deal of information concerning the fluorophore-solvent interaction which occurs between absorption and emission. No single physical property of the solvent such as orientation polarizability, viscosity, polarity, dielectric constant or refractive index can fully explain this peculiar emission properties. The important physical constants of the three solvents used in the present study are given in table 1. From the magnitudes of F one may judge that spectral shifts will be larger in ethylene glycol. Our experimental observations also indicate that pfw shift is found to be greater in Rh6G: ethylene glycol system and lower in Rh6G: methanol system. Thus our observed results are well consistent with the value of F. It has been reported that the fluorescence quantum yield increases and the emission maximum shifts to shorter wavelengths as the solvent polarity decreases [51]. Jones et. al [40] also observed a large red shift of absorption and emission wavelength with increasing solvent polarity in selected coumarine dyes. They also observed a general broadening of the emission band in more polar media [42]. Similar shifts in emission wavelength have been observed for a number of aminocoumarines and interpreted in terms of solvent polarity-polarizability, hydrogen bonding and cohesion parameters [54].

Table 5.1 Important physical constants f the solvents used.

parameter	Methanol	Water	Ethylene Glycol
refractive index	1.326	1.332	1.429
dielectric constant	32.63	78.54	37
dipole moment	1.7 Debye	1.85 Debye	2.28 Debye
F	0.64	0.68	0.71

In many cases not only a shift in the fluorescence spectrum is observed but this is often accompanied by a shift in the absorption spectrum of the compound. However a shift in one does not necessarily require a shift in the other. It is common for a shift in fluorescence to occur with no shift in the absorption spectrum. For numerous dyes such as Rh6G, the small Stokes shift makes self-absorption an important effect, because absorption and emission spectra overlap so that emission from one dye molecule can excite another.

The half width ($\Delta\lambda_{1/2}$) of the fluorescence band increases distinctly with increase in concentration. For example taking the case of Rh6G: methanol system, the half width of the fluorescence spectrum for the highest concentration studied (8.5 $\times 10^{-3}$ mol/lt) is 52 nm which is greater that for the lowest concentration studied ($\Delta\lambda_{1/2} = 31$ nm at 8.7 $\times 10^{-7}$ mol/lt) where almost only monomers exist. These regularities are also observed for coumarin dyes by Jones et.al, indicating the presence of fluorescence aggregates in the most condensed solutions [42]. Bojarski et. al [55] treated these concentration changes as evidence for the presence of fluorescent dimers of Rh6G in concentrated solutions. The formation of fluorescent dimers of Rh6G with a very low quantum yield has been found in water and in methanol [56-61]. Scully et.al [62] made a hypothesis on the existence of fluorescent dimers of Rh6G in concentrated ethylene glycol solutions. The changes in the $\Delta\lambda_{1/2}$ for the concentrated solutions confirm the hypothesis on the presence of higher aggregates in the solution. Fluorescence measurements were also carried out in rhodamine B laser dye in different solvents as mentioned above. Typical fluorescence spectra for RhB solutions in methanol, water and ethylene glycol are shown in fig. 5.6. The concentration dependence of peak fluorescence wavelength (pwf) shift for these solutions are given in figure 5.7. Similar to Rh6G solutions in these solvents, RhB:ethylene glycol system showed more redshift compared to RhB: methanol and RhB:water systems.

5.5.2 Q_f Measurements in Rhodamine 6G Using CWTL Technique

Absorption spectra of methanol, water and ethylene glycol show that they have negligible or zero absorption at 514 nm and hence any TL effect due to these solvents is neglected. The absorption spectra of Rh6G in methanol, water and ethylene glycol are given in chapter 4

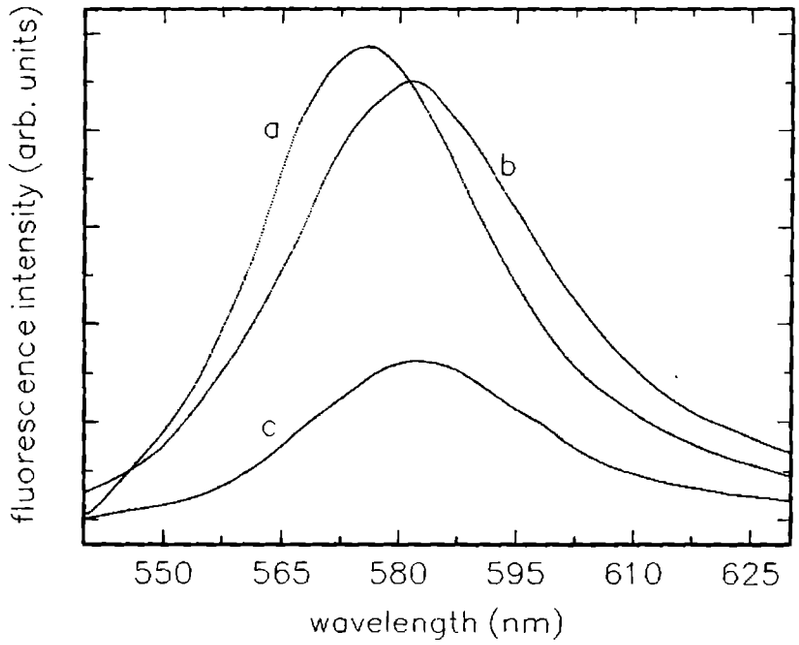

Figure 5.6: Typical fluorescence spectra obtained for RhB during 514 nm Ar^+ excitation for a concentration of 4.3×10^{-5} mol/lt (a-methanol, b - ethylene glycol, c - water)

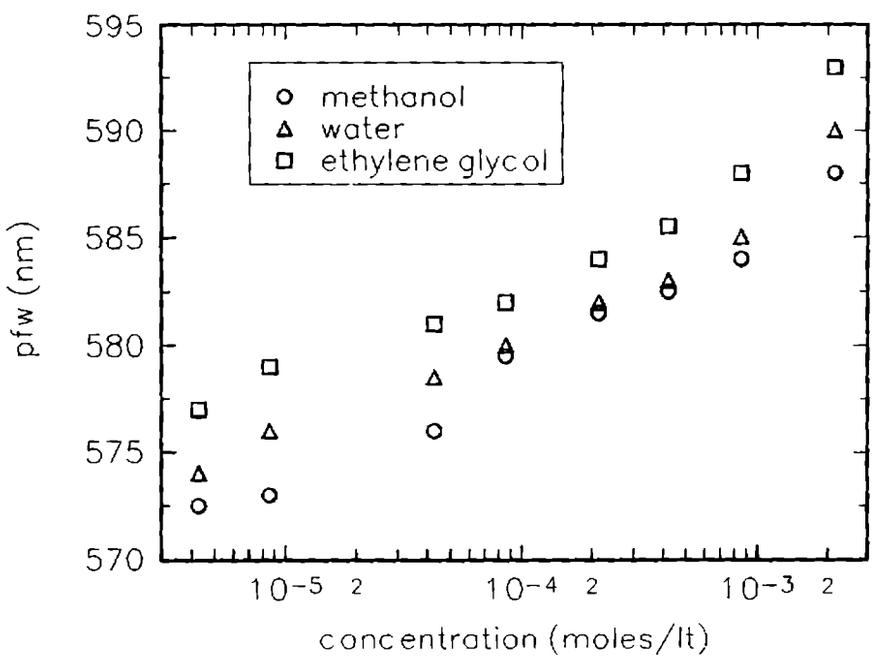

Figure 5.7: The concentration dependence of pfw of RhB in three different solvents

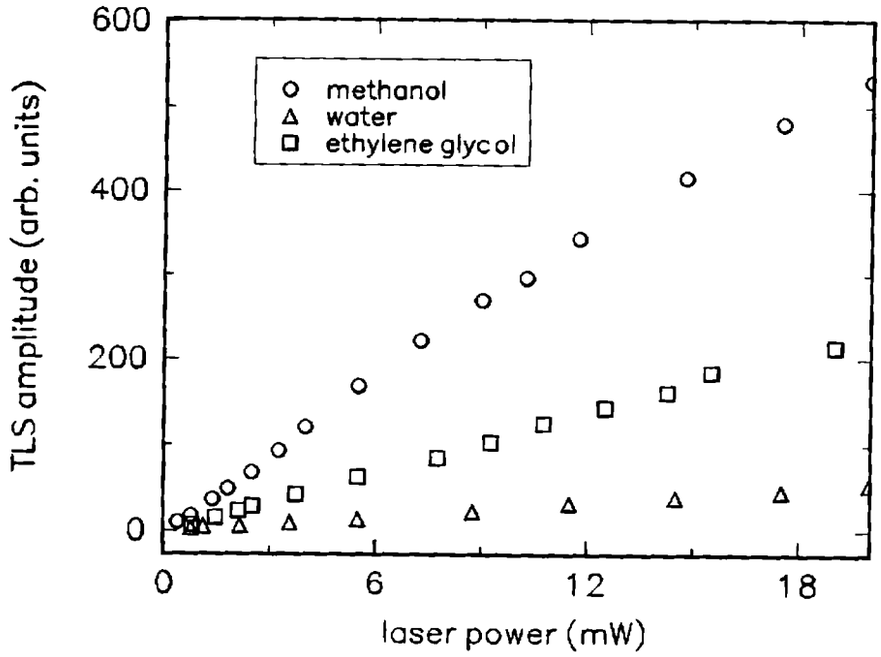

Figure 5.8: The variation of thermal lens signal amplitude on laser power for Rh6G in three solvents. (concentration 4.3 $\times$ 10^{-6} mol/lt)

for different concentrations. From these spectra it is clear that absorption at 632 nm is very small and hence any perturbation due to the probe beam can be neglected.

The TL signal measurements were carried out in the dye solution in the concentration range of 3.47 $\times 10^{-3}$ to 8.7 $\times 10^{-6}$ mole/lt. Dependence of TL signal on laser power for Rh6G: methanol, Rh6G:water and Rh6G :ethylene glycol systems are given in fig. 5.8 and these plots show thermal lens signal intensity varies linearly with laser power. The dependence of TL signal at powers greater than 20 mW has not been studied since aberrational effects begin to appear at these power levels. The aberrational effects in thermal lens are found to be strongly depended on the dye concentration. With increase in concentration, the aberration of the lens starts at much lower power levels which is an effect mainly due to enhanced absorption of the medium.

5.5.2.1 Concentration Dependence of Q_f

Fig. 5.9 shows the variation of quantum yield obtained in TL measurements using eqn.(5.17) for Rh6G in methanol, water and ethylene glycol as a function of concentration. It clearly reveals a decrease in fluorescence quantum yield Q_f at higher concentrations. This is a direct indication that nonradiative processes become significant at higher concentrations and con-

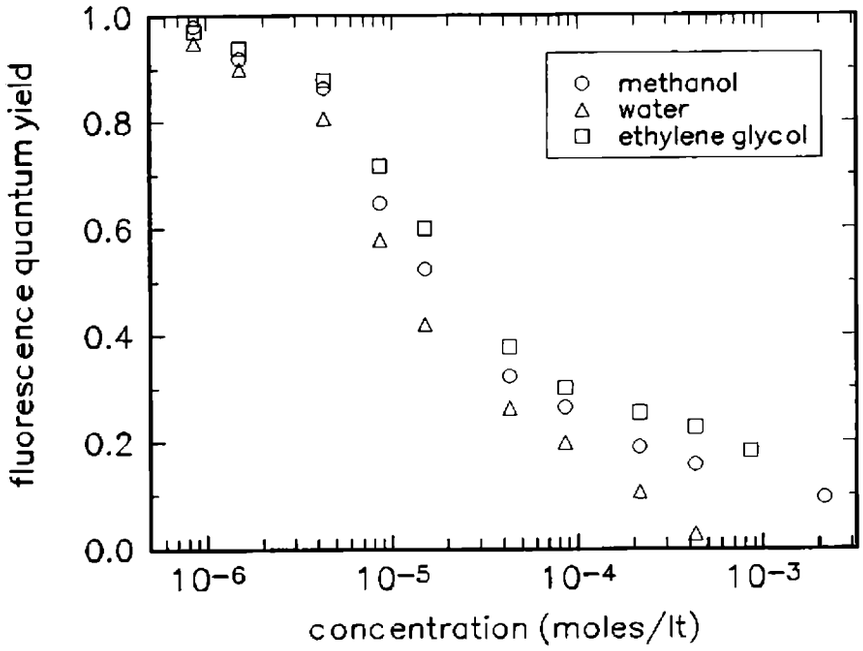

Figure 5.9: Variation of fluorescence quantum yield of Rh6G with concentration

tributes to enhanced thermal lensing. The rapid decrease in Q_f at higher concentrations can be attributed mainly to the formation of dimers and higher aggregates which have zero or very small fluorescence quantum yield. The competition between increasing dimer absorption and decreasing monomer absorption at 514 nm with increasing concentration plays a comparable (or even greater) role than direct self quenching of fluorescence for the decrease in quantum efficiency. The role of triplet state absorption is also important in this connection [63]. The quantum yield obtained using TL method values of 0.98, 0.95 and 0.97 at a concentration of 8.5 $\times 10^{-7}$ mole/lt. For methanol, water and ethylene glycol as solvents which are in good agreement with the reported values of these quantities using other calorimetric methods [64, 18, 65] . The values for Q_f in the aqueous solutions are both lower and apparently more concentration dependent than in the corresponding methanolic and ethylene glycol solutions. Two factors are responsible for the Q_f values obtained. First, the value of Q_f in aqueous solutions can be expected to be less than in methanol and ethylene glycol due to the strong quenching effect of water on fluorescence. Second, as in the case of the methanolic and ethylene glycol solutions, the inner filter effect can be expected to result in a decrease of Q_f with increasing concentration. These two effects would result in a curve for the aqueous Q_f values paralleling those of the methanolic and ethylene glycolic Q_f values.

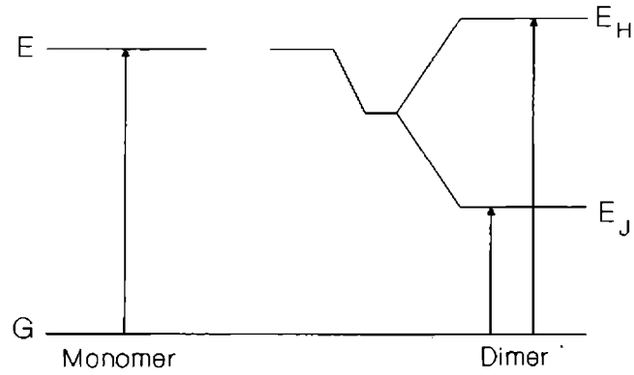

Figure 5.10: The electronic energy diagram of a monomer and for a dimer

This appears to be true in the more dilute aqueous solutions, but at concentrations above $\simeq 5\times10^{-5}$ mole/lt there is a more rapid decrease in the value of Q_f. This rapid decrease is due to considerable formation of dimers in the aqueous solutions.

It must be noted that the quantum yield of the dye solution decreases at higher concentrations irrespective of the solvent used. The major mechanisms that may quench the fluorescence emission at these concentrations are triplet state absorption and aggregate formation. Since we are using cw laser as the excitation source, triplet state absorption is predominant. The formation of dimers and trimers in solutions of higher concentrations lead to fluorescence quenching. Formation of aggregates decreases the emission quantum yield of Rh6G by a combination of monomer-dimer energy transfer and absorption of radiation by dimers. The nature of these aggregates has been extensively studied [66, 67] as a result of this unique property of the dye solutions. The strength of the aggregation depends on the structure of the dye, the solvent, temperature, pressure and other factors. In early studies, the aggregates were attributed mainly to the dimer [35,68,69]. However, it has been proposed recently that higher aggregates consisting of three or more dye molecules exist in concentrated solutions [69]. In the case of Rh6G in ethanol solution, the aggregates are supposed to involve the dimer, trimer and tetramer, whereas only the dimer and trimer are believed to exist in aqueous solution [64]. Typical electronic energy diagram for a monomer and for a dimer is given in fig. 5.10. The dimer spectrum consists of two visibly separated bands, H and J. In that it is similar to the dimer absorption spectrum of Rh6G in methanol [56, 57] as well as in silica gel [70], but differs from that in water where H and J bands overlap partially [71]. The H band of these dyes in water was observed to be larger than the J band while J band is

found to be larger than H band in ethylene glycol solutions [72]. The H class dimer is thought to be nonfluorescent, while the J class dimer is fluorescent [72]. Molecules of RhB and Rh6G in water were proved to become nonfluorescent by dimerization, since these dimers show strong "H" absorption [73, 74] where as larger J band absorption was observed in the case of ethylene glycol. It should be noted that the presence of aggregates in concentrated donor-acceptor systems may influence significantly the courses of photophysical and photochemical processes, especially if they are conditioned by the nonradiative excitation transport. In that case fluorescence aggregates play a role of additional acceptors being imperfect traps for the excitation energy [74-78].

The quantum yield closely depends on the environment of the fluorescing molecule, and the processes like internal nonradiative conversion ($S_1 \rightarrow S_0$), intersystem crossing ($S_1 \rightarrow T_1$), excited singlet state absorption (ESA) and aggregation of dye molecules. These are strongly dependant on excitation source, solvent characteristics as well as concentration of the dye solution [64]. In aqueous solutions Rh6G has a tendency to aggregate and form dimers with increasing concentration. Furthermore, the fluorescence yield of aqueous Rh6G in water were recognized to make little contribution to fluorescence, though they were capable of optical absorption [35, 60]. The trimer has a higher quenching capacity than the dimer; it has both higher quenching constant and a higher equilibrium constant. The decrease of quantum efficiency at higher concentrations is caused by Forster-type energy transfer to dimers. The equilibrium between monomer and dimer shift to the side of the latter with increasing concentration. The dimerization of laser dyes like RhB and Rh6G is severe enough to prevent laser action unless deaggregating agents like hexafluoroisopropanol or ammonyx LO is added to the solution [64]. In the present case no such deaggregating agents were added and hence significant reduction in fluorescence quantum yield can be expected due to aggregate formation at higher concentrations. The role of triplet state absorption is also important in this connection. Penzkofer and Lu are of the opinion that, in Rh6G : methanol solutions, ground state dimer formation is unstable and closely spaced pairs dominate the fluorescence behaviour at higher concentrations [58]. Within the lifetime of the excited monomer, an excited monomer and a ground state monomer come so near together that they interact mutually and form an excited quenching centre. The strong radiationless deactivation of excitation in these quenching centres reduces the fluorescence emissions. Few authors disagree with this argument and claimed that stable state dimes and higher aggregates are found in alcoholic solutions of Rh6G [44]. In the Rh6G-ethylene glycol system, the strong overlaps between all absorption and fluorescence band enable forward and reverse energy transport

between monomer and dimers. This phenomenon affect all the spectroscopic parameters including fluorescence quantum yields [55].

The fluorescence quenching of xanthene dyes produced by their aggregates has been attributed mainly to the transfer of the excitation energy between monomers and aggregates. With rise in concentration, the molecules initially dissolved to monomers come closer together and form more and more centers of low fluorescent quantum yield (quenching centers) which may consist of dimers. The formation of fluorescent dimes of Rh6G with low quantum yield has been found in water (6×10^{-4}), methanol ($8.5\ \times10^{-4}$) and ethylene glycol (0.01) [55, 56, 62, 33]. The presence of fluorescent dimes depends on solvent, dye concentration, viscosity of the medium and temperature. The concentration dependent quenching of fluorescent quantum efficiency is due to transferring excitation energy from primary excitation cites to quenching centers by Forster type energy transfer. The rate k_{EQ} of energy transfer to quenching centers is proportional to the rate of energy transfer between the excited monomer and nonexcited monomer k_{ET} and mole fraction x_Q of the quenching centers [57].

$$k_{EQ} = k_{ET}x_Q = \frac{1}{\tau_F(0)}(\frac{C}{C_0})^2 x_Q \tag{5.21}$$

where $\tau_F(0)$ is the fluorescence lifetime at low concentration without energy transfer, C_0 is the critical transfer concentration given by

$$C_0 = (N_A R_0^3)^{-1}, \tag{5.22}$$

where N_A and R_0 are Avogadro number and critical distance of energy transfer (Forster distance, where energy transfer rate is $k_{ET} = 1/\tau_F(0)$). Here the same energy transfer rate k_{ET} from monomer to monomer and from monomer to quenching center is assumed, i.e., the energy migrates along monomers until it comes close to a quenching center where it is captured and quenched by nonradiative decay. Then the monomer fluorescence lifetime shortens to

$$\tau_{Fm}(C) = \frac{\tau_F(0)}{1+\tau_F(0)k_{EQ}} = \frac{\tau_F(0)}{1+x_Q(C/C_0)^2} \tag{5.23}$$

Then fluorescence quantum efficiency reduces to [57]

$$Q_F(C) = (1-x_Q)\frac{Q_F(0)-Q}{1+(x_Q(C/C_0)^2)} + Q_Q \tag{5.24}$$

A more accurate and detailed description including different absorption cross-sections of monomers and quenching centers as well as energy back transfer is given in ref. [57]. Besides the dimerization process, the concentration dependence of photothermal and fluorescence

signals can be explained by the non-radiative energy transfer from excited monomers to ground state monomers or dimers. The interaction of excited monomers with dimers has been demonstrated by Bojarski and Obermueller [71]. If the quenching requires the close encounter of the two solute molecules, the change in the fluorescence efficiency with concentration should obey the Stern-Volmer law [5]:

$$\frac{Q_0}{Q} = 1 + K_q[D] \tag{5.25}$$

where Q_0 = efficiency at infinite dilution, Q = efficiency at the concentration C (mole/lt), K_q = Stern-Volmer quenching constant, [D] = dimer concentration. It has been considered by many authors that the overlap between excited and unexcited molecules which can cause quenching even when the molecules are separated over several molecular diameters. Self-quenching by this mechanism obeys Stern-Volmer law only over a limited concentration range.

The fluorescence yields reported here demonstrate that it is generally unjustified to assume that fluorescence parameters are minimally influenced by solvent. The absolute yield of Rh6G measured using this method show solvent variations of 1-15%, especially at higher concentrations, indicating that solvent-solute interactions play a measurable role in modifying unimolecular decay constants for excited singlet electronic states. It is interesting to note that the quantum yield of rhodamine 6G is higher in ethylene glycol than in water or methanol. This suggests that the chromophore is fully rigid in the ground state and loosens up only after excitation, provided the solvent is of low viscosity. In ethylene glycol the viscosity is sufficiently high to prevent thermal equilibrium being reached during the radiative lifetime of a few nanoseconds. Hence the planarity of the ground state is not lost before light emission takes place [64].

5.5.3 Q_f measurements in Rhodamine B Laser dye

Absolute luminescence yield measurements were undertaken for RhB laser dye for three solvents using the thermal lens method as mentioned earlier. Fig. 5.11 gives the variation of thermal lens signal strength with laser power for RhB : methanol, RhB : water as well as RhB : ethylene glycol systems. The plots show that a linear dependence is established between thermal lens signal intensity and pump laser power. Fig. 5.12 shows the concentration dependence of absolute quantum yield of RhB. It clearly reveals a decrease in luminescence yield with increase in concentration. A brief description of the comparison of Q_f values of these two members of xanthene family is given at the end of this chapter.

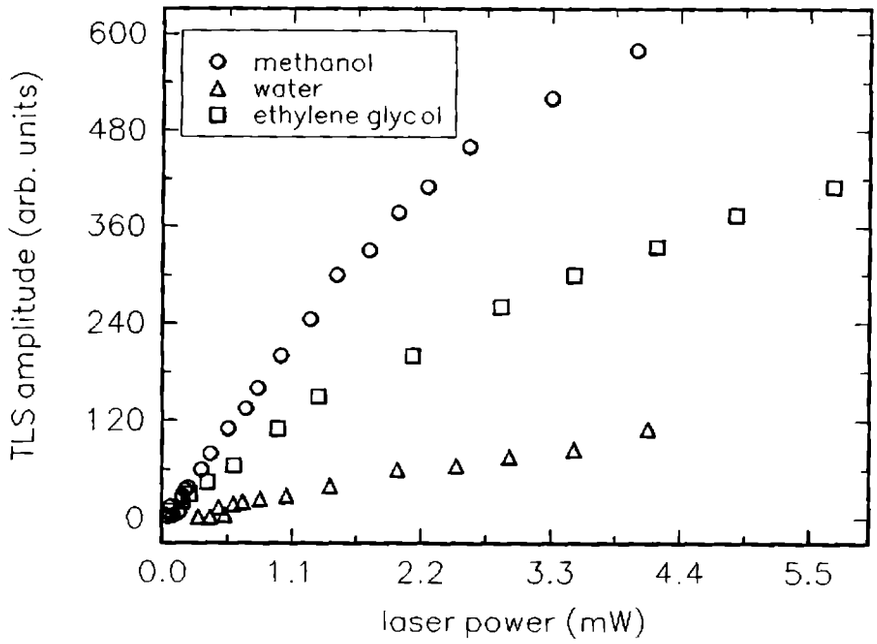

Figure 5.11: Plot showing linear dependence of TLS on laser power for RhB (514 nm Ar^+ excitation, concentration - 4.3×10^{-6} mol/lt)

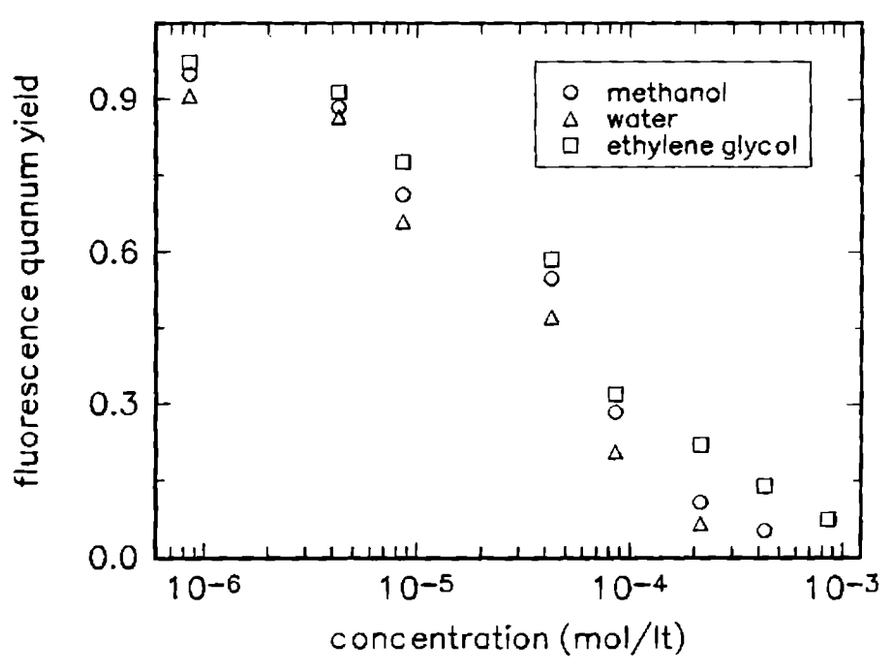

Figure 5.12: Variation of fluorescence quauntum yield with concentration for RhB using cw TL

5.5.4 Q_f Measurements Using Pulsed Thermal Lens

The time resolved thermal lens method has been used to determine the quantum yield of triplet formation and triplet life time or to measure the lifetimes of singlet oxygen produced by energy transfer from the triplet state [79, 80]. In those cases, where slow nonradiative processes occur, the pulsed thermal lens signal consists of a fast rising component, corresponding to fast relaxation processes, followed by a slower component due to slow heat dissipation of the triplet state. Generally, the fast decaying processes, are completed within the lower limit of time resolution which is determined by the acoustic transit time, i.e., the time required for a density change created by the increased temperature to dissipate from the excited region through the beam radius. In our experimental conditions, the time required to reach 90% of the signal is about 0.5 μs. On the contrary, the slower decaying processes are shown if they occur on a time scale which is greater than the acoustic transit time and lower than the characteristic time constant t_c which describes the decrease of the thermal lens signal through dissipation of temperature gradient by thermal conduction. With our experimental values of t_c, about 40 and 60 ms in water and methanol respectively, the longest decay time accessible should be less than a few hundred microseconds. In all cases studied in this work, the rising part of the thermal lens signal was fast and no slow component was detected. This means that the triplet state decay was inoperative because it was fast and no slow component was detected. This means that the triplet state decay was inoperative because it was too long with respect to the time constant t_c or, possibly, faster than the acoustic transit time. Apart from these facts, the pulse width t_p of the pump laser is $\simeq$ 9 ns which is much less than that of $1/k_{st}$, where k_{st} is the intersystem crossing which is of the order of 10^6-$10^7 s^{-1}$ in rhodamine dyes.

The variation of thermal lens signal intensity as a function of excitation energy for Rh6G and RhB in methanol, water and ethylene glycol are given in figs. 5.13 and 5.14. It is noted that at low energy levels thermal lens signals are found to behave linearly with pump energy and at higher energies and at higher concentrations a nonlinear tendency is observed. Fluorescence emission spectra were charted for each samples and typical pfw shift at the fluorescence spectrum with respect to concentration are given in figures 5.15 and 5.16 respectively for Rh6G and RhB. With respect to increasing concentration, the dye system with ethylene glycol exhibited maximum Stokes shift. It is interesting to compare the pfw shift of the dye solutions (in the three solvents presently studied) under different modes of excitation i.e., cw and pulsed. The red shift is found to be large if the fluorescence measurements were made

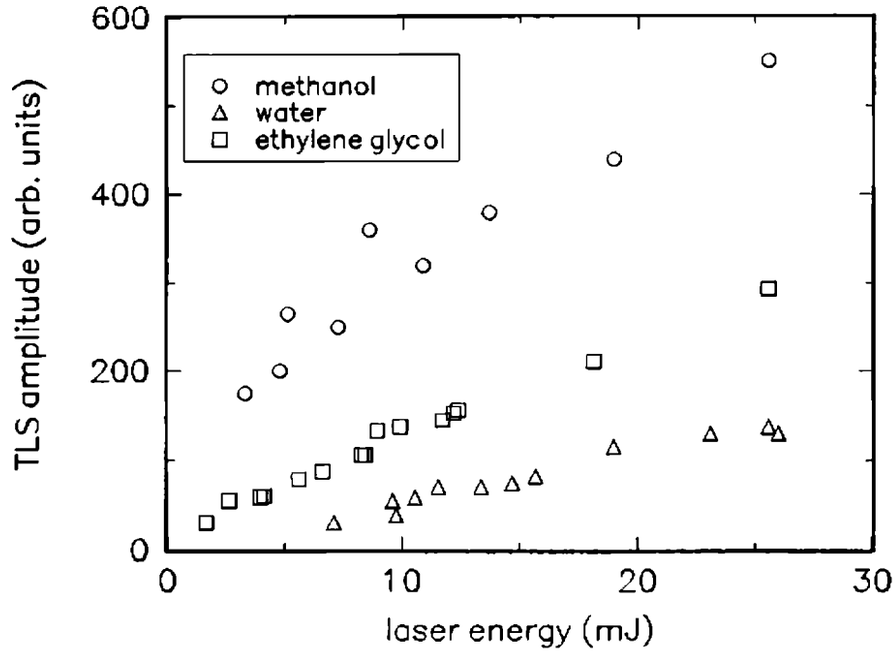

Figure 5.13: Plots showing linear dependence of TLS amplitude on laser energy for [Rh6G] = 8.5×10^{-6} mol/lt

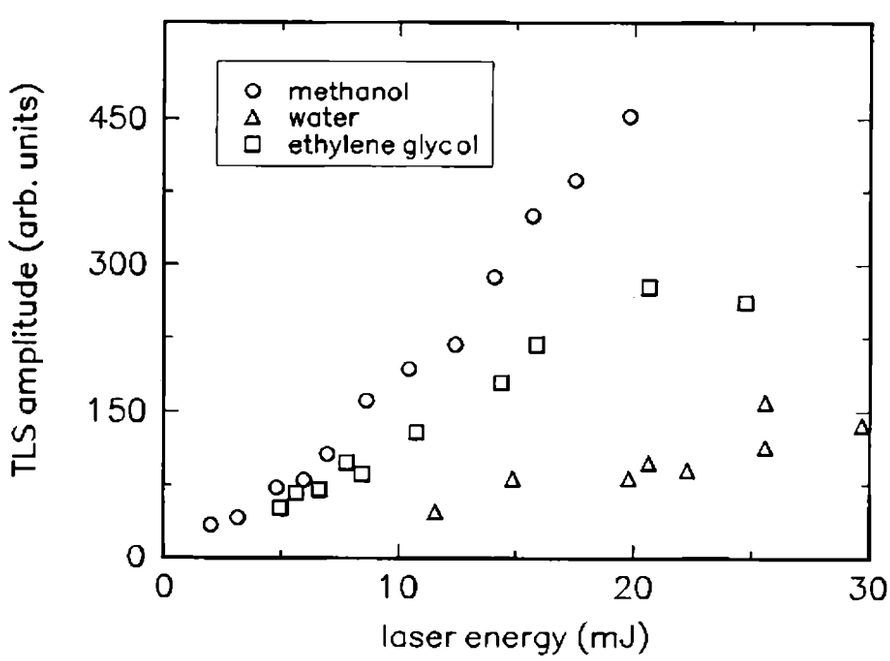

Figure 5.14: Plots showing linear dependence of TLS amplitude on laser energy for [RhB] = 8.5×10^{-6} mol/lt

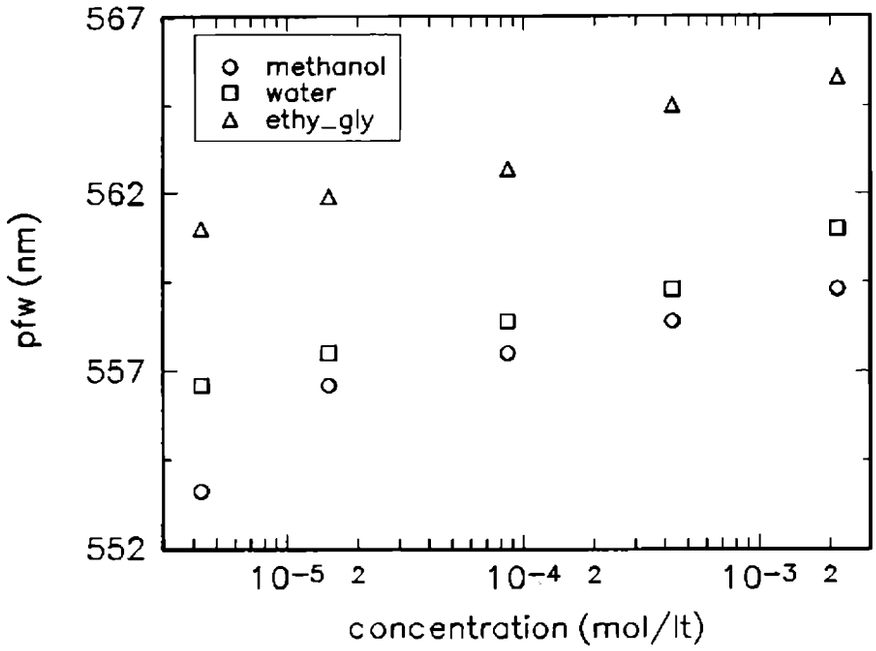

Figure 5.15: The variation of pfw with concentration for Rh6G under pulsed excitation

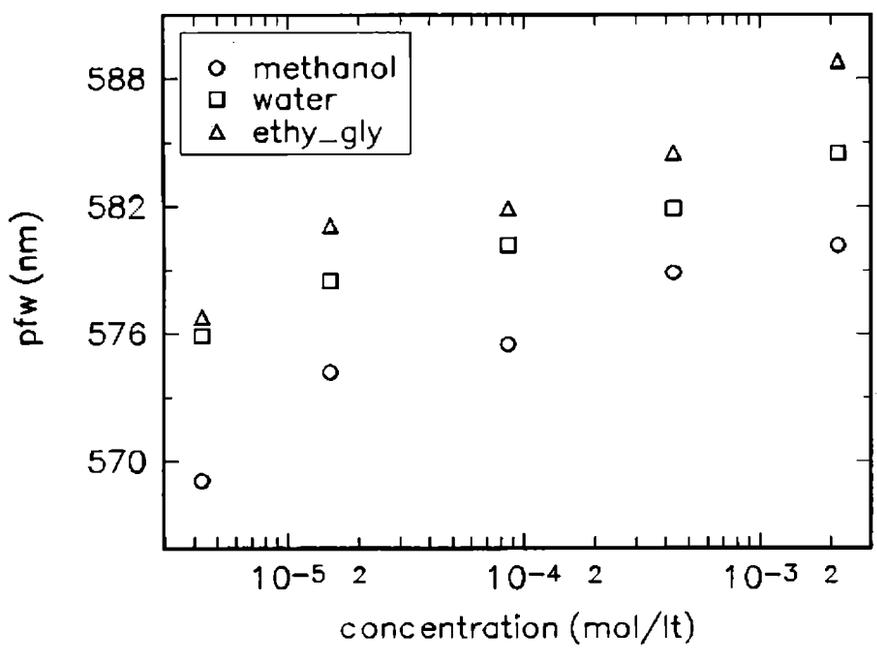

Figure 5.16: The variation of pfw with concentration for RhB under pulsed excitation

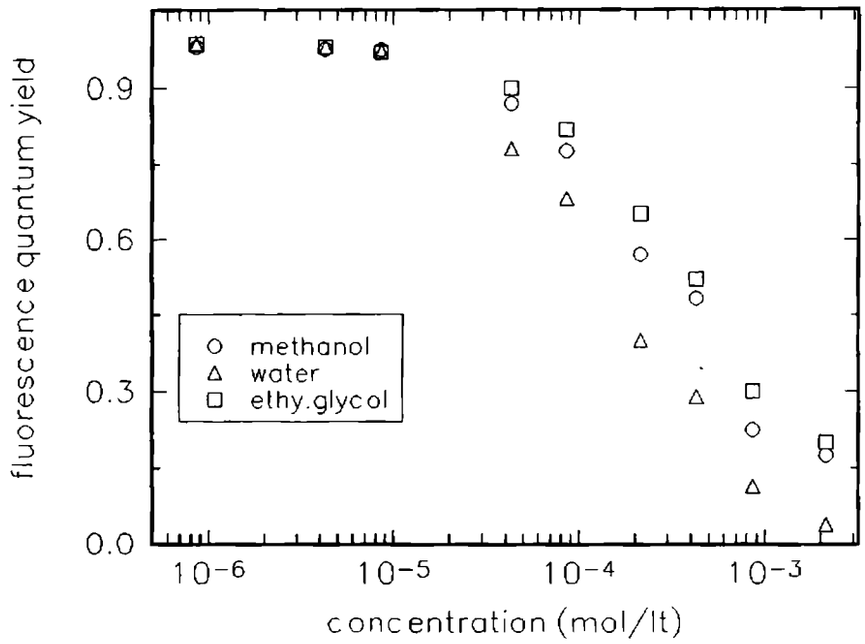

Figure 5.17: The variation of Q_f with concentration for Rh6G under pulsed excitation

with argon ion radiation in comparison with pulsed excitation of the dye solutions. This is because fluorescence reabsorption is more predominant in dye solutions and hence large Stokes shifts are expected when they are illuminated with cw lasers. With rising pump pulse intensity the fluorescence reabsorption is reduced and the pfw shifts to shorter wavelengths as is the case with pulsed laser excitation [81]. The values of Q_f obtained for Rh6G and RhB at different solvents for concentrations ranging from 8.7×10^{-7} to 2×10^{-3} are shown in fig. 5.17 and 5.18. These results show that the absolute fluorescence quantum yield does not vary much over the low concentration range compared to that obtained using cw mode operation. The difference in the method of sample illumination may be one of the possible reasons for the observed anomalies. Indeed, with cw laser illumination, the measurement is made when the thermal lens is in equilibrium, i.e, when the rate of heat input from the relaxation processes is just balanced by the rate of heat conduction out of the illuminated region; constant temperature gradient is achieved and both slow and fast decay processes are in equilibrium. On the contrary, with pulsed excitation, the time scales for the various processes are very different. Thermal lens formation from fast relaxation occurs in a very short time < 1 μs) with respect to subsequent heat conduction (in the order of some tens of milliseconds). If slow decaying processes occur on a time scale which is much greater than the acoustic transit time, the relation between the amount of released thermal energy

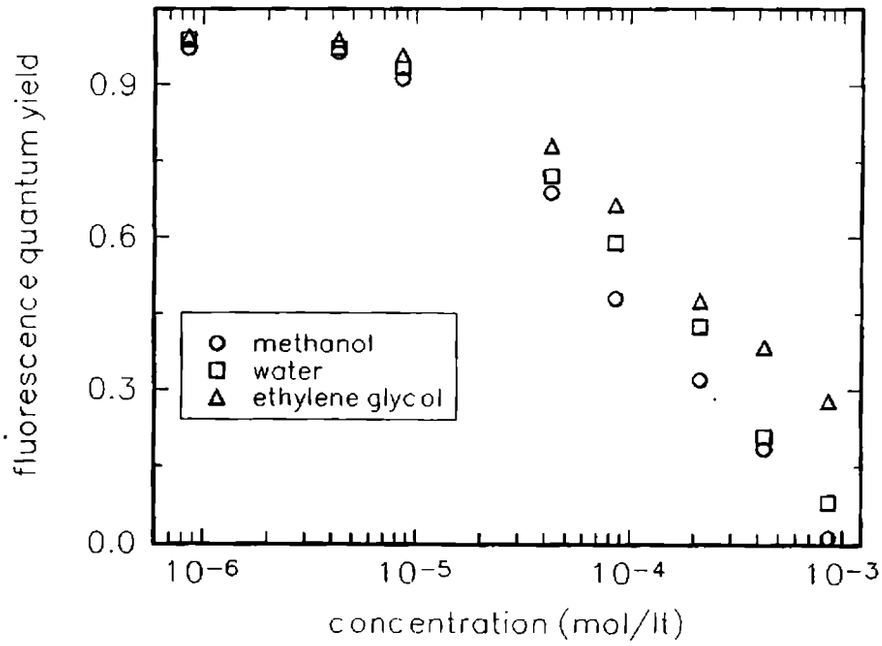

Figure 5.18: The variation of Q_f with concentration for RhB under pulsed excitation

and the magnitude of the thermal-lens signal may no longer be the same. The intersystem crossing is a dominant mechanism in the cw mode illumination, which effectively reduce the luminescence yield values and these processes are absent in the pulse mode operation.

R6G molecules showed high Q_f values for the concentration range studied compared to RhB molecules. Drexhage [64] had earlier distinguished RhB, in which torsional motion of the C=N< group is possible; while for Rh6G molecule the chromophore is rigid and planar. It has been known for a long time that a rigid, planar molecular structure favours high fluorescence efficiency. Rhodamines with rigid amino groups or rhodamines in frozen solutions show Q_fs close to unity [64, 82]. RhB was thought to be characterized by an increase in the nonradiative decay at high temperatures due to increased torsional mobility of the C=N< groups [83]. The precise role of the torsional motion in the nonradiative decay was not well studied. The torsional motion of the diethylamino groups can cause a narrowing of the S_1-S_0 gap thus facilitating internal conversion. In the present case S_1-S_0 is found to be smaller for RhB molecules $\simeq$18000 cm^{-1}) compared to R6G $\simeq$18800 cm^{-1}). The distinction between the rigid and nonrigid structures accords with the observation that the Rhodamines dyes tend to divide into a group with Q_f approaching unity (R6G) and with a group with much lower quantum yield (RhB).

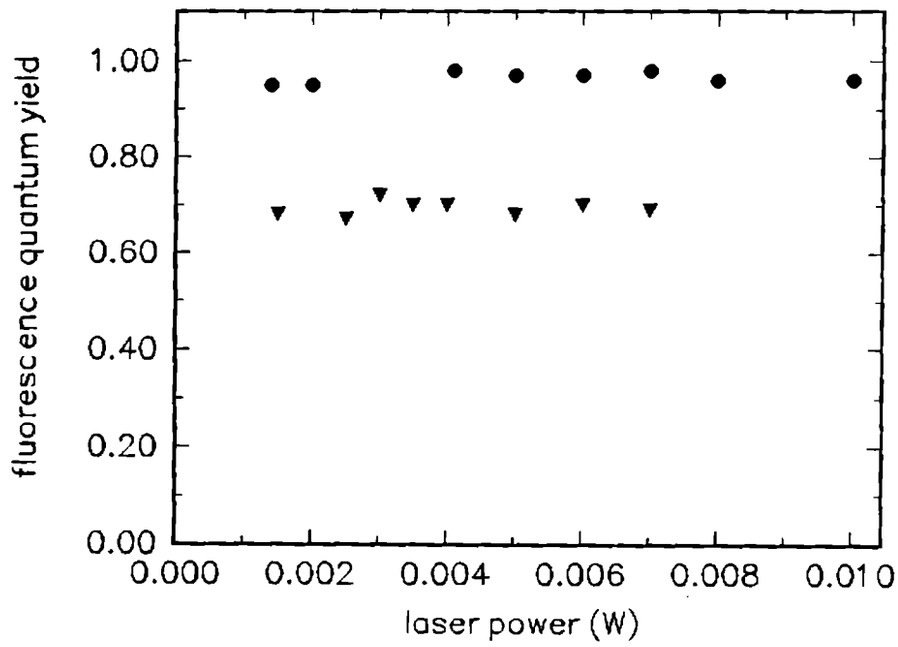

Figure 5.19: The variation of Q_f with laser power for cw TL ([Rh6G] • - 8.5 × 10^{-6} mol/lt, ▼ - 8.5 × 10^{-5} mol/lt)

5.5.5 Energy Dependence of Q_f values

Fig. 5.19 shows the variation of Q_f with laser energy under Argon ion laser excitation. This figure shows that the absolute value of quantum yield measured using thermal lens method is constant irrespective of laser power which is consistent with eqn. 5.5. It can be seen that Q_f is independent of pump laser power. We have also studied dependance of absolute value of fluorescence yield on the laser energy of pulsed excitation source. When the rhodamine dyes are illuminated with the high intense pulses (532nm) from the Q-switched Nd:YAG, nonlinear processes begin to appear [84]. The values of Q_f given in figs. 5.17 and 5.18 were measured at lower energy levels where a linear dependence of thermal lens signal on laser energy was hold good. At higher intensities a deviation from the linearity was observed due to different nonlinear processes like ESA, TPA and/or three photon absorption [85, 86]. This is evident from the observed reduction in Q_f with increasing laser energy(fig.20). As the incident energy increases the dye molecules populate higher excited levels. This in fact decreases the number of absorbing molecules in the ground state, thereby reducing the effective number of emitted photons.

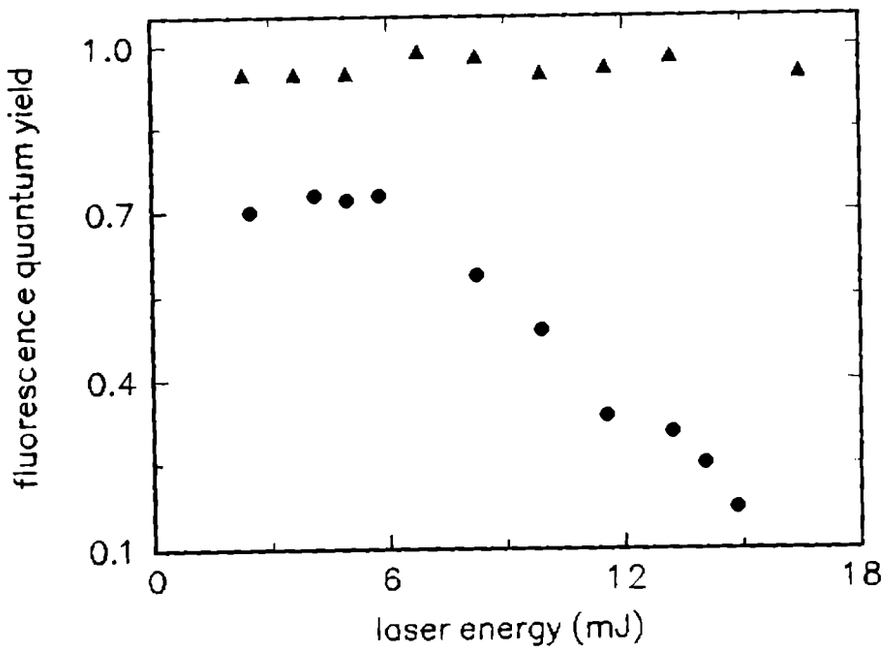

Figure 5.20: The variation of Q_f with laser power for pulsed TL ([Rh6G] ▲ - 8.5 × 10^{-6} mol/lt, • - 8.5 × 10^{-5} mol/lt)

5.6 Conclusion

Dual beam thermal lens technique is successfully employed for the determination of absolute value of fluorescence quantum yield of two important laser dyes Rh6G and RhB. For fluorescing materials like Rh6G and RhB, the thermal lens method is suitable for the evaluation of quantum efficiency since it requires no standard and is very convenient and useful, especially at higher concentrations, namely near the fluorescence quenching regimes. The fluorescence yields reported here demonstrate that fluorescence parameters are influenced by solvent. Our results indicate that a higher fluorescence yield is obtained for rhodamine 6G in ethylene glycol than in methanol or water. This quantum yield variation with solvent indicates that solvent-solute interactions play measurable role in modifying unimolecular decay constants for excited singlet electronic states.

The variation of quantum yield with concentration of the dye solution showed a decreasing tendency irrespective of the solvent used. The decrease in the value of Q_f follows different trajectories for different modes of excitation. With cw excitation the reduction in the Q_f values is found to be more sharper than the pulsed mode excitation. The presence of triplet state absorption plays a major role in these peculiar phenomena.

5.7 References

[1] D. M. Hercules (ed.), *Fluorescence and Phosphorescence Analysis*, (Wiley-Interscience, New York, 1966).

[2] P. P. Sorokin, J. R. Lankard, V. L. Moruzzi and E. C. Hammond, *J. Chem. Phys.*, **48**, 4726 (1968).

[3] C. A. Parker, *Photoluminescence of Solutions,* (Elsevier Publishing Co., New York, 1968).

[4] J. G. Calvert and J. N. Pitts Jr., *Photochemistry*, (Wiley, New York, 1966).

[5] J. B. Birks, *Photophysics of Aromatic molecules,* (Wiley - Interscience, New York, 1970).

[6] A. J. Pesce, C. G. Rosen, T. L. Pasby, *Fluorescence Spectroscopy*, (Marcel Dekker Inc., New York, 1971).

[7] S. J. Strickler and R. A. Berg, *J. Chem. Phys.*, **37**, 814 (1962).

[8] F. E. Lytle and D. M. Hercules, *J. Am. Chem. Soc.*, **91**, 251 (1969).

[9] T. T. Williams, *J. Electrochem. Soc.*, **105**, 173 (1958).

[10] F. R. Lipsett, *Progr. Dielectrics*, **7**, 217 (1967).

[11] J. N. Demas and J. Crosby, *J. Phys. Chem.*, **75**, 991 (1971).

[12] S. I. Vavilov, *Z. Phys.*, **22**, 266 (1924).

[13] G. Weber and F. W. J. Teale, *Trans. Faraday Soc.*, **54**, 649 (1958).

[14] C. A. Parker and W. T. Rees, *Analyst*, **85**, 587 (1960).

[15] M. Mardelli and J. Olmsted III, *J. Photochem.*, **7**, 377 (1977).

[16] D. Magde, J. H. Brannon, T. L. Cremers and J. Olmsted III, *J. Phys. Chem.*, **83**, 693 (1979).

[17] J. Shen and D. Snook, *Chem. Phys. Letts.*, **155**, 583 (1989).

[18] M. Fischer and J. Georges, *Chem. Phys. Letts.*, **260**, 115 (1996).

[19] P. Sathy, R. Philip, V. P. N. Nampoori and C. P. G. Vallabhan, *Pramana - J.Phys.*, **34**, 585 (1990).

[20] Y. Sakai, M. Kawahigashi, T. Minami, T. Inoue, S. Hirayama, *J. Lumin.*, **42**, 317 (1989).

[21] M. G. Rockley and K. M. Waugh, *Chem. Phys. Letts.*, **54**, 597 91978).

[22] I. O. Starobogatov, *Opt. Spectr.*, **42**, 172 (1977).

[23] M. Terazima and T. Azumi, *Chem. Phys. Letts.*, **176**, 79 (1991).

[24] S. J. Isak and E. M. Eyring, *J. Phys. Chem.*, **96**, 1738 (1992).

[25] H. L. Fang and R. L. Swofford in *Ultrasensitive Laser Spectroscopy* (ed.) D. S. Kliger, (Academic Press, new York, 1983).

[26] J. M. Harris in *Analytical Applications of Lasers*, (ed.) E. H. Piepmier, (John Wiley & sons, New York, 1986).

[27] M. Franko and C. D. Tran, *Rev. Sci. Instrum.*, **67**, 1 (1996).

[28] R. D. Snook and R. D. Lowe, *Analyst*, **120**, 2051 (1995).

[29] C. Hu and J. Whinnery, *Appl. Opt.*, **12**, 72 (1973).

[30] D. Cahen, H. Garty and R. S. Becker, *J. Phys. Chem.*, **84**, 3384 (1980).

[31] J. H. Brannon and D. Magde, *J. Phys. Chem.*, **82**, 705 (1978).

[32] M. L. Lesiecki and J. M. Drake, *Appl. Opt.*, **21**, 557 (1982).

[33] F. L. Arbeloa, P. R. Ojeda and I. L. Arbeloa, *J. Photochem. Photobiol. A*, **45**, 313 (1988).

[34] G. G. Guilbault, *Practical Fluorescence*, (Marcel Dekker, New York, 1973).

[35] I. L. Arbeloa, *J.Chem.Soc.Faraday Trans.2*, **78**, 989 (1982).

[36] E. W. Jones and J. Gormally, *Aggregation processes in solutions*, (Elsevier, Amsterdam, 1983).

[37] O. V. Aguilera and D. C. Necckers, *Acc. Chem. Res.*, **22** , 171 (1989).

[38] S. K. Brahma, C. Bandopadhyay and A. K. Chakraborty, *Ind. J. Chem.*, **29A**, 1165 (1990).

[39] J. Griffiths, *Chem.Soc. Rev.*, **1**, 481 (1972).

[40] G. Jones II, W. R. Jackson, C. Y. Choi and W. R. Bergmark, *J. Phys. Chem.*, **89**, 294 (1985).

[41] G. Jones II, W. R. Jackson and A. M. Halperrn, *Chem. Phys. Letts.*, **72**, 391 (1980).

[42] G. Jones II, W. R. Jackson and S. Kanoktanaporn, *Opt. Commn.*, **33**, 315 (1980).

[43] F. J. Durate and L. W. Hillman (eds.), *Dye laser principles with applications*, (New York; Academic 1990).

[44] F. L. Arbeloa, T. L. Arbeloa, M. J. T. Estevez and I. L. Arbeloa, *J. Phys. Chem.*, **95**, 2203 (1991).

[45] N. Mataga, Y. Kaifu and M. Koizumi, *Bull. Chem. Soc. Jpn.*, **29**, 465 (1956).

[46] N. Mataga, V.Toritashi and K. Ezumi, *Theor.Chim.Acta*, **2**, 158 (1964).

[47] V. E. Lippert, *Z. Electrochem.*, **61**, 962 (1957).

[48] A. Kawski, *Acta Phys.Pol.*, **29**, 507 (1966).

[49] N. G. Babakhshiev, *Opt. Spectros.*, **61**, 821 (1964).

[50] A. Chamma and P.Viallet, *C. R. Acad. Sci.Ser.C.*, **II**, 1901 (1970).

[51] J. R. Lakowicz, *Principles of Fluorescence Spectroscopy*, (Plenum, New York, 1983).

[52] L. Crosemans, F. C. de Schryver and A. van Dormael, *Chem. Phys. Letts.*, **65**, 95 (1979).

[53] N. Mataga, Y. Kaifu and M. Koizumi, *Bull.Chem.Soc.Jpn.*, **28**, 690 (1955).

[54] L. Coosemans, F. C. de Schryver and A. van Dormael, *Chem. Phys. Letts.*, **65**, 95 (1979).

[55] P. Bojarski, A. Matczuk, C. Bojarski, A. Kawski, B. Kuklinski, G. Zurkowska and H. Diehl, *Chem.Phys.*, **210**, 485 (1996).

[56] A. Penzkofer and W. Leupacher, *J. Lumin.*, **37**, 61 (1987).

[57] A. Penzkofer and W. Leupacher, *Chem. Phys.*, **103**, 399 (1986).

[58] F. L. Arbeloa, P. R. Ojeda and I. L. Arbeloa, *J. Photochem. Photobiol.A*, **45**, 313 (1988).

[59] P. R. Ojeda, I. A. K. Amashta, J. R. Ochoa and I. L. Arbeloa, *J. Chem. Soc. Faraday Trans. 2*, **84**, 1 (1988).

[60] F. L. Arbeloa, P. R. Ojeda and I. L. Arbeloa, *J. Chem. Soc .Faraday Trans. 2*, **84**, 1903 (1988).

[61] J. E. Selwyn and J. I. Steinfeld, *J. Phys. Chem.*, **76**, 762 (1972).

[62] A. D. Scully, A. Matsumoto and S. Hirayama, *Chem. Phys.*, **157**, 253 (1991).

[63] F. P. Schafer, *Dye laser Principles*, (Springer 1977)

[64] K. H. Drexhage in *Dye laser Principles*, (ed) F. P. Schafer (Springer 1977).

[65] J. Arden, G. D. Seltau, V. Huth, U. Kringal, D. Peros and K. H. Drexhage, *J.Lumin.*, **48-49**, 352 (1991).

[66] O. V. Aguilera and D. C. Neckers, *Acc. Chem. Res.*, **22**, 171 (1989).

[67] V. I. Yuzhakov, *Russian Chem. Rev.*, **48**, 2007 (1979).

[68] . L. Arbeloa and P. R. Ojeda, *Chem. Phys. Letts.*, **87**, 556 (1982).

[69] E. Ghomaschi, A. Ghanadezadeh and M. G. Mahjani, *Spectrochim.Acta A*, **47**, 211 (1991).

[70] S. Blonski, *Chem.Phys.Letts.*, **184**, 229 (1991).

[71] C. Bojarski and G. Obermueller, *Acta. Phys. Pol.*, **A50**, 389 (1976).

[72] J. Muto, *J. Phys. Chem.*, **80**, 1342 (1976).

[73] P. Alexander, K.A. Stacey, *Proc. R. Soc. London, A*, **212**, 274 (1952).

[74] W. J. Malic, P. Chand, *J. Electroanal. Chem.*, **19**, 431 (1968).

[75] C. Bojarski, *Z. Naturforsch.*, **39a**, 948 (1984).

[76] L. Kulak and C. Bojarski, *J. Fluorescence*, **2/2**, 123 (1992).

[77] L. Kulak and C. Bojarski, *Chem.Phys.*, **191**, 43 (1995).

[78] L. Kulak and C. Bojarski, *Chem. Phys.*, **191**, 67 (1995).

[79] M. Terazima and T. Azumi, *Chem. Phys. Letts.*, **153**, 27 (1988).

[80] G. Rossbroich, N. A. Garcia and S. E. Braslavsky, *J. Photochem.*, **31**, 37 91985).

[81] A. Penzkofer, *Appl. Phys. B*, **48**, 115 (1989).

[82] R. F. Kubin, A. N. Fletcher, *J. Lumin.*, **27**, 455 (1982).

[83] M. J.Snare, F. E. Treloar, K. P. Ghiggino and P. J. Thistlethwaite, *J. Photochem.*, **18**, 335 (1982).

[84] See Chapter 4.

[85] E. Sahar, D. Treves and I. Wieder, *Opt.Commn.*, **16**, 124 (1976).

[86] I. Weider, *Appl. Phys. Letts.*, **21**, 318 (1972).

Chapter 6

Pulsed Photoacoustic Determination of Absolute Fluorescent Quantum Yield of the Laser Dye Rhodamine B

Pulsed photoacoustic technique which is found to be a very convenient and accurate method, is used for the determination of absolute fluorescence quantum yield of laser dye rhodamine B. Concentration and laser energy dependence of quantum yield of rhodamine B in methanol is studied using 532 nm radiation from a Q-switched Nd:YAG laser. Results show that there is a rapid decrease in quantum yield as the concentration is increased and finally it reaches the limit corresponding to fluorescence quenching.

6.1 Introduction

Evenafter the incorporation of various corrections for system geometry, reabsorption, polarization etc. the accuracy of the fluorescence quantum yield (Q_f) values obtained from photometric and calorimetric methods are rather poor. A detailed account of different calorimetric methods are given in chapter 5. In order to evaluate absolute quantum efficiency, one has to consider both radiative and nonradiative processes taking place in the medium. As the contribution from nonradiative processes is not directly measurable using traditional optical detection methods, thermo-optic techniques such as photoacoustics and thermal lens have been adopted for this purpose. Details of the measurement of Q_f using thermal lensing techniques are given in the previous chapter. In this chapter we discuss pulsed photoacoustic measurement of Q_f in rhodamine B (RhB) methanol solutions.

Despite the fact that several methods are used for the determination of fluorescence quantum yield of rhodamine B in methanol, the reported ones differ in their values [1-4]. These differences are generally ascribed not only to the method used for the determination but also to concentration effects [5, 6]. For example significant changes in Q_f have been observed for Rh B and Rh 6G over a concentration range 8.7×10^{-7} to 3×10^{-3}m/lt [7].

The advantages of using photoacoustic (PA) technique for characterizing various molecular processes have been extensively discussed by various workers [8-10]. The PA effect is essentially an energy - conversion process. On irradiation with a pulsed laser beam, a part of the absorbed energy is converted into translational energy of the molecules by nonradiative relaxation processes. This deexcitation channel finally results in the production of an acoustic wave. The amplitude of the acoustic signal obviously depends on the amount of energy absorbed [11]. Of the several configurations of PA measurements pulsed PA is the most sensitive as the high power delivered by a pulsed laser can generate acoustic signals of considerable magnitudes. Because of its high sensitivity, pulsed PA is ideally suited for probing the nonradiative relaxations and this technique has recently been used to study two photon absorption processes in certain laser dyes [12] as well as in organic vapours [13].

It may be recalled that for fluorescent materials, PA detection is sensitive to the total fluorescence emission. Any change in the emission characteristics will affect the PA signal [14]. PA detection is very effective if small variations in quantum yield of highly fluorescent materials are to be studied because the change in PA signal will be relatively much larger than that occurring in the fluorescence emissions.

When a material is optically excited it decays to the ground state by fluorescence and/or by

heat generation. The measurement of absolute optical energy absorbed W_0 and the absolute heat energy generated W_h provide the fluorescence efficiency Q_f for a simple 2 level system

$$Q_f = (W_0 - W_h)/W_0 \tag{6.1}$$

In measuring Q_f using the above equation the absolute heat energy is involved; however PA signal generally proportional to the heat energy absorbed, with an unknown proportionality constant. To avoid this difficulty PA measurements have been made for two samples, first with the desired sample where Q_f is to be evaluated and the second with the sample whose Q_f is altered in a known way. This provides two equations with two unknowns and so Q_f can be solved.

There are two methods for evaluating Q_f using PA measurements. The first is the quenching method, which have been employed by several workers [15-17]. Here, after taking the PA signal pure sample first, its fluorescence is quenched by the addition of a small concentration of an efficient 'quencher' molecules and the second reading is taken. In this method care should be taken, such that the addition of the quenching molecule should not affect the physical and chemical properties of the fluorescing molecule.

The second method relies on the possibility of optically exciting higher excited states S_n that decay nonradiatively to the lowest state in S_1. This method was proposed and demonstrated by Rockley and Waugh [18]. Depending upon the wavelength of excitation, the dye molecules can be excited to lowest singlet states S_1 or higher singlet states S_n (where $n > 1$) with corresponding energies E_1 or E_n. For every absorbed photon of energy E_n the fraction of energy corresponding to $(E_n\text{-}E_1)/E$ will appear as heat coming from the sample. A fraction of $(1\text{-}Q_f)$ of all the energies absorbed by $S_0 \rightarrow S_1$ transition also will appear as heat. These heat signals (nonradiative) can be detected by photoacoustic technique. Then using the following equations Q_f values can be evaluated.

$$I^{PAS}(S_n) = k(E_n - E_1 + E_1(1 - Q_f)) \tag{6.2}$$

$$I^{PAS}(S_1) = k(E_1(1 - Q_f) \tag{6.3}$$

where E_n and E_1 are known quantities, $I^{PAS}(S_n)$ and $I^{PAS}(S_1)$ are the measured quantities and k is a constant.

According to Malkin and Cahen [19], for fluorescent samples with quantum yield Q_f, the PA signal can be written as

$$P(\lambda) = \alpha(\lambda)(1 - \frac{Q_f}{\lambda_f}\lambda) \tag{6.4}$$

where λ and λ_f are the excitation wavelength and the fluorescence peak wavelength respectively, α is the fraction of the light absorbed in that part of the sample that participates in the generation of PA signal. In the case of totally quenched sample we can consider the entire excitation energy to be converted to nonradiative relaxation processes and hence

$$P(\lambda) = P_\alpha(\lambda) \equiv \alpha(\lambda) \tag{6.5}$$

such that

$$\frac{P}{P_\alpha} = 1 - \frac{Q_f}{\lambda_f}\lambda \tag{6.6}$$

and if λ_1 is known, Q_f can be obtained directly using the equation

$$Q_f = \frac{\lambda_f}{\lambda}\left(1 - \frac{P}{P_\alpha}\right) \tag{6.7}$$

6.2 Experimental Set up

The details of the experimental set up is given in chapter 2. Briefly, the second harmonic output beam (532 nm) from a Q-switched Nd:YAG laser is focused by a convex lens (focal length 5 cm) into the PA cell containing the sample at room temperature (24^0C). The lens position is adjusted so that the beam focus is at the center of the cell. The laser pulse width (FWHM) is $\simeq$ 9 ns and the pulse repetition frequency is 10 Hz. The incident power is monitored by a laser power meter (Scientech model 362) and the transducer output is observed on a 200 MHz digital storage oscilloscope. The averaged amplitude of the first pulse in the PA signal trace is monitored as a function of laser power.

For the fluorescence study, the front surface emission is collected and focused by a lens on to the aperture formed by the tip of an optical fiber attached to the entrance slit of a 1 meter Spex monochromator which is coupled to a PMT having S20 cathode. The PMT output is fed to a photon counter (SR 400) which is coupled to a PC/AT for data processing. The emission is wavelength scanned in the desired region (540-670 nm) and it shows the characteristic fluorescence spectrum of rhodamine B. The dependence of fluorescence peak wavelength on concentration is given elsewhere and this shows characteristic Stoke's shift.

6.3 Results and Discussion

An accurately weighed amount of rhodamine B (Exciton) is dissolved in spectroscopic grade methanol to give concentration of 3.47 $\times 10^{-3}$ moles/lt. From this stock solution, sample solutions with different concentration were prepared. The PA signal strength from the dye

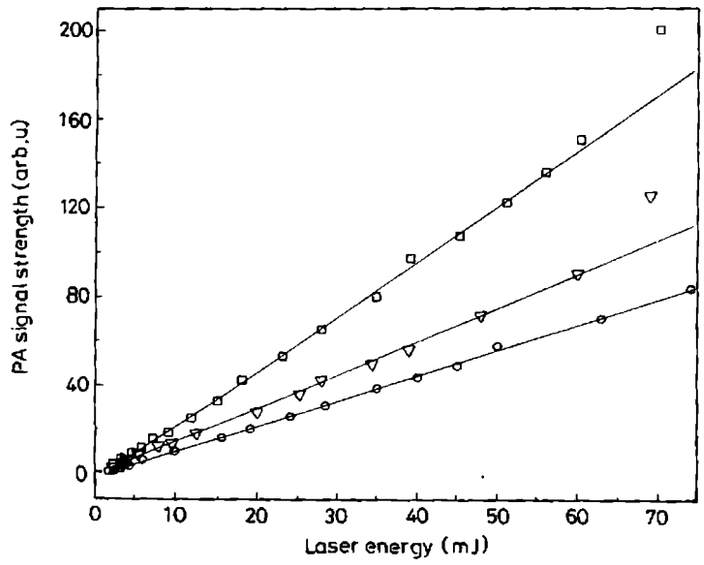

Figure 6.1: The variation of PA signal strength with laser energy for different concentration (□ - 3.47 × 10^{-3} mol/lt, ∇ - 8.7 × 10^{-4} mol/lt and o - 8.7 × 10^{-5} mol/l

solution was measured in the concentration range of 3.47 ×10^{-3} to 1 ×10^{-5} moles/lt. Absorption spectrum of methanol shows that it has very low absorption at 532 nm and hence any PA effect due to methanol is neglected. The quantum yield closely depends on the environment of the fluorescing molecule and the processes like internal nonradiative conversion ($S_1 \rightarrow S_0$), intersystem crossing ($S_1 \rightarrow T_1$), excited singlet state absorption (ESA), two photon absorption, aggregation of dye molecules, radiative and nonradiative relaxation cross section etc. Most of the above mentioned phenomena depend eventually on dye concentration and pump intensity. Role of the excitation source is also important in this context as many of the above mentioned phenomena become significant in the medium when the input energy exceeds certain critical value. The intersystem crossing rate depends on the rise time of the pump pulse. Slowly varying pump light pulse would transfer most of the molecules to the triplet state and deplete the ground state population correspondingly. To a first approximation intersystem crossing to the triplet levels can be ruled out, since the pulse width t_p of the pump laser in our case is only about 9 ns such that $t_p << 1/k_{st}$ where k_{st} is the $S_1 \rightarrow T_1$ intersystem crossing rate which is of the order of 10^6-$10^7 s^{-1}$ in rhodamine B laser dye [20]

We have measured the PA signals produced from sample solutions of Rhodamine B in methanol at different concentrations (ranging from 3.47 ×10^{-3} to 1 ×10^{-5} mol l^{-1}) for various input energies (0-75 mJ). The variation of PA signal amplitude with incident laser energies for different concentrations of dye solution is given in fig.6.1. It is found that the signal increases

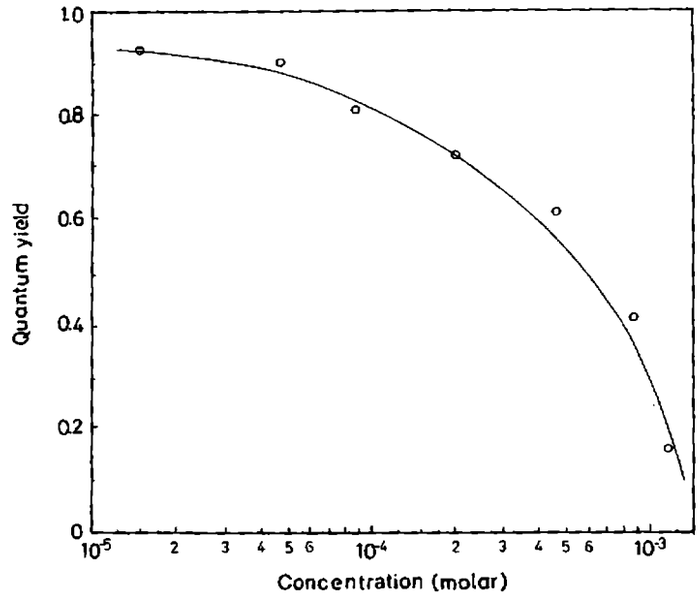

Figure 6.2: Variation of quantum yield of rhodamine B in methanol with concentration

with incident energy for all concentrations, showing a linear dependence on pump intensity.

The quantum yield (Q_f) measurements are carried out using eqn.(6.7) for different concentrations (in the range 3.47 $\times 10^{-3}$ mole/lt- 1×10^{-5} mole/lt) and pump energies (up to 75 mJ). Fig.6.2 shows the variation of Q_f as a function of concentration (laser energy 50 mJ). The plot clearly reveals a decrease in fluorescence quantum yield Q_f at higher concentrations. The calculated value of Q_f at the lowest concentration studied is 0.92 and the yield decreases sharply with increasing concentration. This is a direct indication that nonradiative processes become significant at higher concentrations and contributes to enhanced PA signals.

It is well known that xanthene dyes like rhodamine B form unstable ground state dimers and higher aggregates in alcoholic solutions [21-23]. The rapid decrease in Q_f at higher concentrations is mainly due to the formation of dimers and higher aggregates which have very small fluorescence quantum yield. The decrease in fluorescence quantum efficiency at higher concentrations is caused by Förster-type excitation energy migration transfer from monomers (electric dipole-electric dipole interaction) to weakly fluorescing dimers [24]. A more detailed description of the aggregate formation is given in chapter 5.

In rhodamine B methanol solutions, ground state dimer formation is unstable and closely spaced pairs dominate the fluorescence behaviour at higher concentrations. Within the life time of the excited monomer, an excited monomer and a ground state monomer come so near together that they interact mutually and form an excited quenching center. The strong

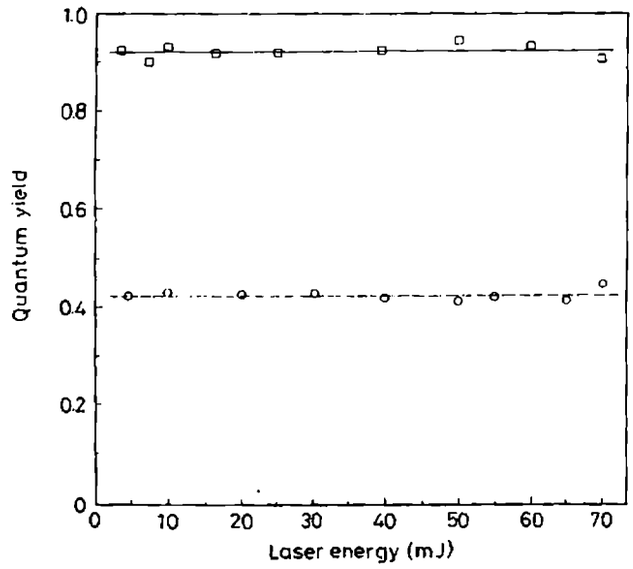

Figure 6.3: Variation of quantum yield of rhodamine B in methanol with laser energy for different concentrations (□ - 1×10^{-5} mol/lt and o - 8.7×10^{-4} moles/lt)

radiationless deactivation of excitation in these quenching centers reduces the fluorescence emissions [24, 25]. Such aggregation/complexing effects alter the absorption characteristics of the solution at different concentrations. The fluorescence can be quenched by dimers only while monomer molecules and statistical traps can fluoresce with respective quantum yields in which the total quantum yield is directly related to the total concentration of the molecules in the solution. The variation of Q_f with laser energy for Rhodamine B in methanol is given in fig.6.3 which shows that Q_f is independent of the pump energy in the range of present studies.

6.4 Conclusion

Fluorescence quantum yield measurements of Rhodamine B solutions have been carried out using pulsed PA technique with 532 nm excitation from a Q-switched Nd:YAG laser. PA method proves to be a viable and versatile tool for quantum yield measurements. The PA technique is highly sensitive since any change in the PA signal will be relatively much larger than fluorescence.

The slight difference between the variation of Q_f values with change in concentration observed for two methods used viz. pulsed thermal lens and pulsed photoacoustics may be due to the difference in cell configurations. It is expected that thermal lens measurements

of Q_f values are more accurate than these PA measurements because the former is more sensitive with respect to nonradiative transitions than the latter. Moreover in thermal lens spectrometry we used a sample cell of length 5 mm only, while in the PA case the length of the sample medium is 45 mm. This factor will affect different experimental anomalies like reabsorption, reemission, attenuation of the laser beam before the focal point.

6.5 References

[1] R. F. Kubin and A. N. Fletcher, *J. Lumin.*, **27**, 455 (1982).

[2] J. Olmsted III, *J. Phys. Chem.*, **83**, 2581 (1979).

[3] R. P. Hammond, *J. Chem. Phys.* , **70**, 3884 (1979).

[4] J. Arden, G. Deltau, V. Huth, U. Kringel, D. Peros and K. H. Drexhage, *J. Lumin.*, **48-49**, 352 (1991).

[5] S. J. Isak and E. M. Eyring, *J. Phys. Chem.*, **96**, 1738 (1992).

[6] J. Georges, N. Arnaud and L. Parise, *Appl. Spectros.*, **50**, 1505 (1996).

[7] *see* Chapter 4 of this thesis.

[8] A. C. Tam and C. K. N. Patel, *Nature*, **280**, 304 (1979).

[9] P. Sathy, R. Philip, V. P. N. Nampoori and C. P. G. Vallabhan, *J. Phys. D*, **27**, 2019 (1994).

[10] C. V. Bindhu, S. S. Harilal, R. C. Issac, G. K. Varier, V. P. N. Nampoori and C. P. G. Vallabhan, *Pramana - J. Phys.*, **45**, 231 (1995).

[11] A. Rosenwaig, *Photoacoustics and Photoacoustic Spectroscopy*, (Wiley, New York 1980) p158

[12] R. Philip, P. Sathy, V. P. N. Nampoori and C. P. G. Vallabhan, *J. Phys. B*, **25**, 155 (1991).

[13] A. V. R. Kumar, G. Padmaja, V. P. N. Nampoori and C. P. G. Vallabhan *Photoacoustic and Photothermal Phenomena -II*, Ed. J. C. Murphy (Springer-Verlag Publ., Heidelberg, 1990) p 360.

[14] N. J. Dovichi and J. M. Harris, *Anal. Chem.*, **53**, 106 (1981).

[15] W. Lahman and H. J. Ludewig, *Chem. Phys. Lett.*, **45**, 177 (1977).

[16] L. M. Hall, T. F. Hunter and M. G. Stock, *Chem. Phys. Lett.*, **44**, 145 (1976).

[17] I. O. Starobogatov, *Opt. Spectro.*, **42**, 172 (1977).

[18] M. G. Rockley and K. M. Waugh, *Chem. Phys. Letts.*, **54**, 597 (1978).

[19] S. Malkin and D. Cahen, *Photochem. Photobio.*, **29**, 803 (1979).

[20] F. P. Schäfer, *Dye Lasers*, F. P. Schäfer, ed., (Springer-Verlag, Berlin 1977) p34

[21] F. Lopez Arbeloa, P. Ruizojeda and I. Lopez Arbeloa, *Chem. Phys. Letts.*, **148**, 253 (1988).

[22] K. A. Selanger, J. Falnes and T. Sikkeland, *J. Phys. Chem.*, **81**, 1960 (1977).

[23] J. E. Selwyn and J. I. Steinfeld, *J. Phys. Chem.*, **76**, 762 (1972).

[24] A. Penzkofer and W. Leupacher, *J. Lumin.*, **37**, 61 (1987).

[25] A. Penzkofer and Y. Lu, *Chem. Phys.*, **103**, 399 (1986).

Chapter 7

Optical Limiting and Photothermal Studies in Fullerenes

Optical limiting as well as thermo-optic properties of C_{60} and C_{70} in toluene are studied using 532 nm, 9 ns pulses from a frequency doubled Nd:YAG laser. Optical limiting studies in these fullerene molecules lead to the conclusion that reverse saturable absorption (RSA) is the major mechanism for limiting properties in these molecules. Thermal lensing and photoacoustic measurements were also performed in fullerene solutions. The quadratic dependence of thermal lens signal on incident energy indicate that enhanced optical absorption by the sample via excited triplet state absorption may play a leading role in the limiting property. Contrary to our expectations, we observed a linear dependence of photoacoustic signal variation with respect to laser energy.

7.1 Introduction

The story of the discovery of C_{60}, otherwise known as Buckminsterfullerene and the birth of Fullerene science started in 1985 when Harold Kroto and co-workers evidenced a self-assembled spontaneous C_{60} molecule from a hot nucleating carbon plasma [1]. The molecule had, however a prehistory: The earliest paper which describes the C_{60} molecule is to be found in Kagaku (in Japanese) [2], where Eiji Osawa in 1970 suggested that it should be stable and the following year the possible aromatic properties of these molecules are discussed in a book in more detail by Yoshida [3].

Fullerenes and their derivatives possess a number of potentially useful physical, biological and chemical properties. The technique developed by Krätschmer *et al.* [4] for preparing and isolating macroscopic quantities of C_{60}, 'a new form of carbon', opened the way for exploring the molecular and bulk properties of these novel species. C_{60}, which was found to be stable, was named buckminsterfullerene after Buckminster Fuller, American architect, engineer and constructor of geodesic dome.

Kroto and co-workers exploited pulsed laser ablation of the graphite in helium ambient as a reliable method for the production of C_{60} and higher fullerenes [5]. Here a pulsed laser beam (Nd:YAG, 532 nm, 9 ns) is directed onto the surface of a rotating graphite disk. The power density delivered by the laser beam on to the target is sufficient to generate a plasma of carbon vapour over the irradiated spot in which temperatures over 10000^0C are readily available [6, 7]. As the carbon atoms and small radicals are cooled in the carrier gas ambient (usually He) clustering reactions occur [8].

After the report of species upto 33 carbon atoms in the carbon arc, Rohfling *et al.* [9] reported that much larger carbon clusters i.e., even numbered C_n wit n=30 to 190 could be produced by vapourization of graphite, among which C_{60} is the most stable one. C_{60} (buckminsterfullerene) and C_{70} (falmerene) and to some extent C_{84} are most accessible members of the family of closed cage molecules known as fullerenes formed entirely of carbon in sp^2 - hybridized state. There is no molecule formed by the same atom in chemistry as big as buckminster fullerene. Elemental carbon has been known to exist in two polymorphic forms, graphite and diamond. Graphite has two-dimensional layers of sp^2 hybridized carbon atoms interlinked by weak van der Waals forces. Since the inter-layer interaction is weak, graphite is used as a lubricant. Diamond, however, is one of the hardest materials known to man. This property arises from the strong three-dimensional bonding in diamond in which each sp^3 hybridized carbon atom is bonded to four other similar atoms. Fullerenes constitute

another allotrope of carbon. Developments in recent years showed that these molecules need not be found only with tens and hundreds of atoms but also with thousands of atoms. These giant molecules of carbon occur as nanometer size tubes and balls which are called carbon nanotubes and onions respectively. Detailed nature of the carbon clusters can be studied using time of flight mass spectroscopy [10-12] and laser spectroscopy [13-15]. Several other interesting studies have shown that laser vapourization of a wide variety of carbonaceous target materials also yield C_{60} [16-20].

The triggering of the activity of these exciting field of research started especially after it became possible to synthesize and isolate them in macroscopic quantities using simple and straight forward methods [4]. These molecules have the unique properties like relatively high temperature superconductivity [21], photovoltaic response [22], high degree of hardness [23], persistent photoconductivity [24], ability to trap anions inside the cage [25] etc.. Following their landmark 1985 paper, Kroto, Smally et. al. explained the abundance of these even-numbered species with the formation of an entire family of carbon cages containing a several cavity called fullerenes [26]. In following vigorous developments, the cage like truncated icosahedral structure of C_{60}, resembling a soccer ball (fig. 7.1), has been firmly established. The stability of C_{60} molecule is due to the structure in which the carbon atoms are arranged at the 60 vertices of a truncated icosahedron composed of 32 faces, a structure analogous to a soccer ball. Specifically it was proposed that each molecule of the fullerene family (C_n) with the composition C_{20+2m} can take the stable form of hollow closed nets composed of 12 pentagons and m hexagons, conforming to the relation m = (n-20)/2 (Euler's theorem). Therefore, C_{60} is composed of 32 faces of which 12 are pentagons and 20 are hexagons.

Kratschmer et al. [4] found that C_{70} was the second most abundant all carbon-molecule formed by resistive heating of graphite, in agreement with the earlier Rice studies which proposed C_{70} to be second most prominent carbon cluster in the molecular beams generated by laser vapourization of graphite [26, 27]. Like C_{60}, the larger C_{70} molecule is also a member of the fullerene family, and its ellipsoidal cage shape of a rugby ball (fig.7.1) has been confirmed by ^{13}C NMR spectroscopy [28-30]. For some of the higher fullerenes beyond C_{60} and C_{70}, structures had been calculated; most theoretical studies did not predict structures for those derivatives that could actually be isolated [31-33].

The optical properties of fullerenes have been demonstrated by numerous investigators [34-38]. These studies have largely centered on the numerical evaluation of the dynamics of optical transitions. It has been found that C_{60} exhibits optical nonlinearities leading to second harmonic generation [39] and optical limiting [40]. Photophysical and excited state

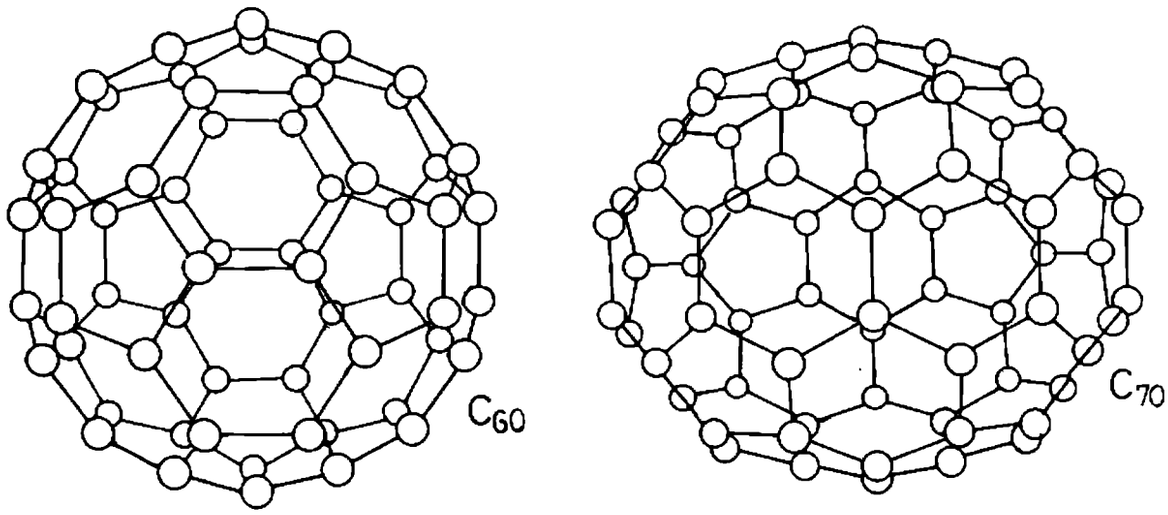

Figure 7.1: Structure of C_{60} and C_{70}

kinetic properties of fullerenes, including fluorescence have been studied at low temperatures [41, 42, 43] as well as at room temperature [44]. Because of the very high rate for intersystem crossing to the excited triplet state at room temperature, the fluorescence emission spectra of these molecules are very weak with an extremely low fluorescent quantum yield of $\simeq 1.45 \times 10^{-4}$ for C_{60} at room temperature [45]. The small singlet-triplet splitting, the very low value of fluorescent rate constant and expected large spin-orbital interaction in these spherical molecules indicate the occurrence of intersystem crossing as a dominant process. Early literature reports [41] revealed that C_{60} had a higher excited state absorption cross section than the ground state absorption cross section over the complete visible spectrum. This information implied that the fullerenes are reverse saturable absorption (RSA) materials and may have application to optical limiting for sensor protection [46]. But few authors reported that apart from RSA some other nonlinear mechanism like nonlinear refraction, nonlinear scattering, two photon absorption etc. also play a major role in the optical limiting properties of these molecules [47-50].

In this chapter an attempt is made to study optical limiting properties of C_{60} and C_{70} in toluene. Firstly a brief description is given for different optical limiting mechanisms viz. RSA, Two photon absorption (TPA), nonlinear scattering and nonlinear refraction. We also employed thermo-optic techniques such as pulsed photoacoustics and transient thermal lens methods for deducing the role of any two photon absorption that may occur in these molecules.

7.2 Optical limiting

The continuing integration of all-optical, electro-optical, acousto-optical and opto-mechanical devices into modern technology has led the development of an ever increasing number of novel schemes for efficiently manipulating the amplitude, phase, polarization or direction of optical beams. The ability to control the intensity of light in a predetermined and predictable manner is one of the most fundamental and important aspect of optical manipulations, with applications ranging from optical communications to optical computing. Although lasers and other high-intensity visible light sources have become more prevalent, the development of materials and devices for protection of solid-state sensors and the human eye has been slow. One desirable approach to sensor and eye protection is to employ an optical power limiter that is passive.

One of the most important applications for optical limiters is eye and sensor protection in optical systems such as direct viewing devices, focal plane arrays, night vision systems etc. All photonic sensors including the eye, have an intensity level above which damage occurs. Using an appropriate optical limiter in the system prior to the sensor extends the dynamic range of the sensor and allow the sensor to continue to operate under harsher conditions than otherwise possible. An ideal optical limiter is one which is perfectly transparent at low intensities up to a predetermined intensity level, above which the transmitted intensity remains clamped at a constant value. Fig. 7.2 shows the response of an ideal optical limiter. Optical limiters can be broadly classified into two categories: active and passive. Active limiting involves the use of an external feedback mechanism to actively control the transmittance, but is too slow for practical applications. On the other hand passive limiting uses the inherent nonlinear optical properties of a material to sense the incident intensity and alter the transmittance.

Several mechanisms have been suggested and used for passive optical limiting. Among these are reverse saturable absorption, multiphoton absorption, free carrier absorption in semiconductors, nonlinear refraction and optically induced scattering. Multiphoton absorption induced optical limiting has desirable features such as low attenuation at low incident intensities and an instantaneous response to the incident light. Two-photon absorption for optical limiting has been studied predominantly in semiconductors [51, 52] and in novel organic molecules [53-55]. However, it is well known that several other organic molecules also posses a large two photon absorption cross section. Three photon absorption and higher order multiphoton absorption could also be used for optical limiting. However, with increasing order of nonlinearity, the probability of the transition drastically reduces and it takes higher

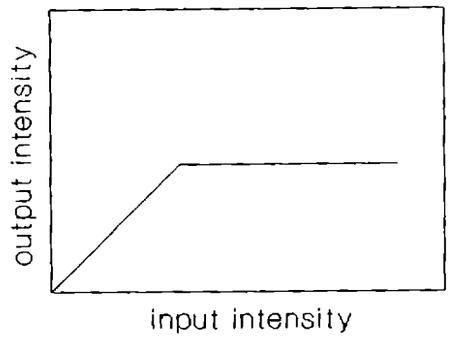

Figure 7.2: The optical response of ideal optical limiter. Here the transmittivity at intensities lower than the threshold is 100%, while the transmitted intensity remains clamped at a fixed value once the incident intensity crosses the threshold

intensities to induce sufficient nonlinear absorption for optical limiting. Our work has been focussed on the study of optical limiting in newly found material like fullerenes.

The optical limiting devices that have been reported in the literature are many and varied, but they all rely on a material that exhibits at least one nonlinear optical mechanism. Such mechanisms include nonlinear absorption, nonlinear refraction, induced scattering and even phase transitions. The origins of such nonlinearities vary widely. For example, nonlinear absorption may be associated with two photon absorption (TPA), excited state absorption (ESA) or free carrier absorption. Nonlinear refraction may arise from molecular reorientation, the electronic Kerr effect, excitation of free carriers, photorefraction or optically induced heating of the material. Induced scattering is typically a consequence of optically-induced heating or plasma generation in the medium. Often, more than one of these processes are operative for an optical limiting property of a given material.

All optical nonlinearities can be broadly classified into two groups: instantaneous and accumulative nonlinearities. For instantaneous nonlinearity, the polarization density resulting from an applied electric field occurs instantaneously. Accumulative nonlinearities arise from interactions with memory, ie., the polarization density generated by an applied field either develops or decays on a time scale comparable to or longer than the excitation duration. Examples of instantaneous nonlinearities include, two photon absorption, multiphoton absorption, electronic Kerr effect etc. and examples of accumulative nonlinearities include nonlinear absorptive processes such as excited state absorption, free carrier absorption and nonlinear refractive processes. An important example of accumulative nonlinearity with applications to optical limiting is the photorefractive effect. Accumulative nonlinearities can,

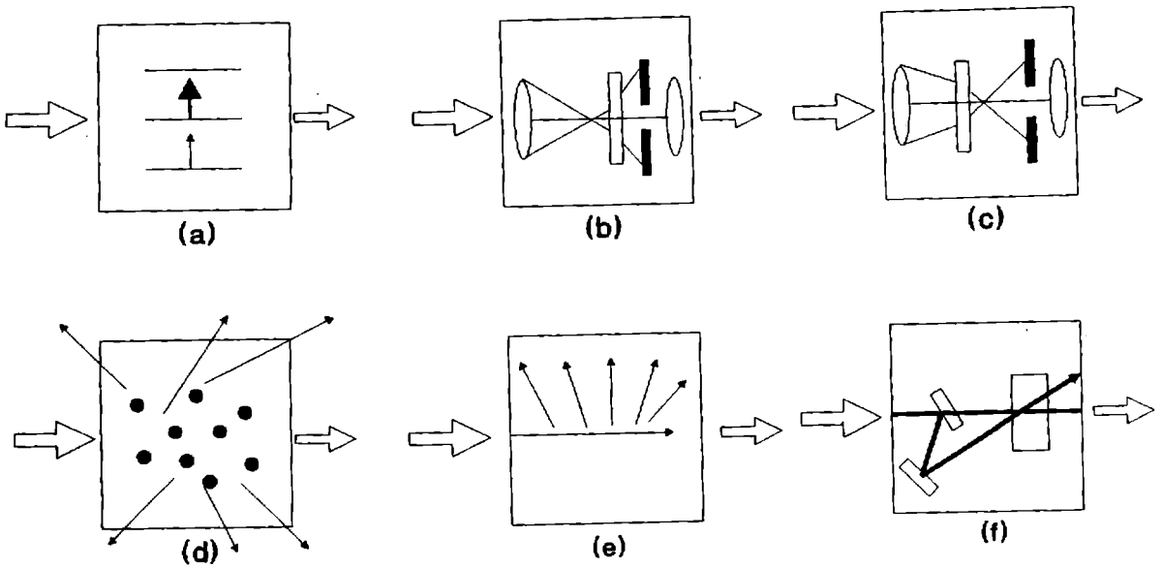

Figure 7.3: Some optical limiters based on different mechanisms (a) an induced absorption limiter, (b) self defocusing limiter, (c) self focusing limiter, (d) induced scattering limiter, (e) beam fanning limiting and (f) photorefractive excisor device

in principle, depend only on the fluence (as opposed to the intensity) in the incident pulse and therefore, can be used to construct optical limiters with responses that are insensitive to incident pulse duration. The resonant nature of the accumulative nonlinearities, however, frequently results in a narrow bandwidth of operation for devices utilizing these mechanisms. By contrast, optical limiters that rely on instantaneous nonlinearities can be very broad band. These broad band usually require high intensities. All of the nonlinear phenomena discussed above can be used for limiting applications. Fig. 7.3 schematically represents the applications of some of these processes in several of the optical limiting configurations. A brief description of the different nonlinearities that lead to optical limiting which is important in the present context is given below.

7.2.1 Reverse Saturable absorption

Reverse Saturable Absorption (RSA) generally arises in a molecular system when the excited state absorption cross section is larger than ground state absorption cross section. A detailed theoretical approach on RSA [56] and its applications [57] are given elsewhere. RSA can be understood by considering a system that is modeled using three vibronically broadened electronic energy levels as shown in fig. 7.4. Here σ_1 and σ_2 represent absorption cross section from the ground and first excited state and τ_1 and τ_2 represent lifetimes of these

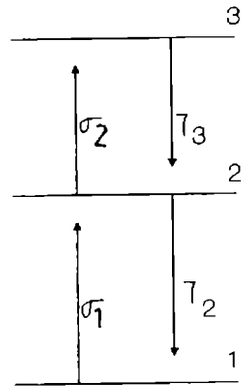

Figure 7.4: Three level model for RSA

levels respectively. As light is absorbed by the material, the first excited state begins to become populated and contributes to the total absorption cross section. If σ_2 is smaller than σ_1, then the material becomes more transparent and this is the case of saturable absorber. If σ_2 is larger than σ_1, then the total absorption increases and the material is known as the reverse saturable absorber. The change in intensity of the beam as it propagates through the material is given by

$$\frac{dI}{dz} = -[N_T\sigma_1 + N_2(\sigma_2 - \sigma_1)]I \tag{7.1}$$

where z is the direction traversed, N_T is the total number of active molecules per unit area in the slice dz, N_2 is the population of the level 2 and the population of the level 3 has been neglected. Initially the material obeys Beer's law when level 2 is unpopulated, and transmission is constant as the incident fluence is increased. The slope is given by T = $10^{-\sigma_1 N_T L}$. At a sufficiently higher fluence the first excited state 2 becomes substantially populated and in the limit of complete ground state depletion, the slope again becomes constant at a new value of $10^{-\sigma_2 N_T L}$. The optical limiting action is not truly limiting, as the fluence which is transmitted is still increasing with increasing incidence fluence, but it does so more slowly. If the ratio σ_2/σ_1 is sufficiently large, the transmission will be small and in a properly designed system the dynamic range of the sensor will be greatly extended.

The three level model describes the simplest case for RSA material but can generally be applied for subnanosecond pulses and under circumstances such that transitions from the second excited state are negligible. For pulses with larger time scales, significant intersystem crossing to other states can occur from the first excited state. In this case a three level model is inadequate and a five level model is applicable (fig. 7.5). The excited state 4 is usually a

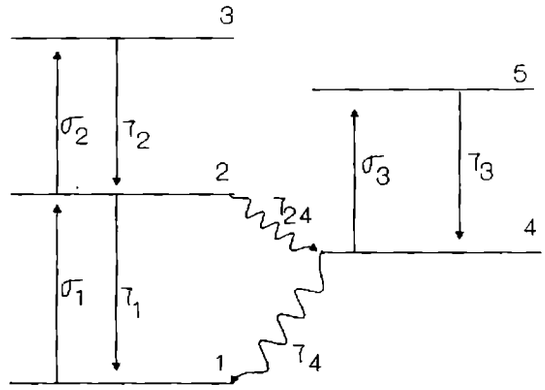

Figure 7.5: Five level model for RSA

triple state or any other long lived state, and for long pulses it can act as a metastable state that accumulate population within the duration of the pulse. The life time of level 4 shows an indication of the maximum pulse width for which the material is efficient to act as an optical limiter. The rate equation for a five level model can be written as

$$\frac{\partial I}{\partial z} = -\sigma_1(N_T - N_2 - N_3 - N_4 - N_5)I - \sigma_2 N_2 I - \sigma_4 N_4 I \tag{7.2}$$

In this case for maximum optical limiting efficiency, the ratio of the excited state absorption to the ground state, $\sigma_2/\sigma_1, \sigma_4/\sigma_1$ should be large to minimize the transmission of the limiter at high incident intensity and the life time of the triplet state and the intersystem crossing rate $1/\tau_{24}$ should be large to populate the triplet state and maintain the population throughout the pulse.

7.2.2 Two Photon Absorption

Two photon absorption (TPA) is one of the effective technical approaches that can be used to accomplish optical limiting. Compared with other optical limiting mechanisms, the TPA mechanism possesses two distinct advantages. First the linear or initial transmittivity can be high because, for relatively weak input signals, TPA can be neglected and the nonlinear medium can be almost completely transparent. Second, the temporal response of the nonlinear medium can be fast because of the instantaneous nature of the TPA process. Based on the second advantage, the TPA mechanism is suitable not only for power limiting but also for reshaping optical pulses and stabilizing fast peak-power fluctuations.

According to the basic considerations of a TPA process, the beam intensity change along

the propagation direction (z axis) can be represented as

$$\frac{dI}{dz} + \alpha I + \beta I^2 = 0 \tag{7.3}$$

where α is the attenuation coefficient that is due to linear absorption and scattering and β is the nonlinear attenuation coefficient that is due to TPA. The solution of eqn.(7.3) is

$$I(z) = \frac{I(0)\exp(-\alpha z)}{1 + (\beta/\alpha)I(0) - (\beta/\alpha)I(0)\exp(-\alpha z)} \tag{7.4}$$

where I(0) is the initial intensity. In the case $\alpha z << 1$, eqn. (7.4) reduces to

$$I(z) = \frac{I(0)\exp(-\alpha z)}{1 + \beta z I(0)} \tag{7.5}$$

and the transmittivity of the nonlinear medium can be written as

$$T(z) = \frac{I(z)}{I(0)} = \frac{\exp(-\alpha z)}{1 + \beta z I(0)} - \frac{T_0}{1 + \beta z I(0)} = T_0 T_i \tag{7.6}$$

Here T_0 is the linear transmittivity and T_i is the nonlinear transmittivity and can be written as

$$T_i = \frac{1}{1 + \beta z I(0)} \tag{7.7}$$

The nonlinear absorption coefficient β (in units of cm/GW) for a given medium can be expressed as

$$\beta = \sigma_2 N_0 = \sigma_2 N_A d_0 \times 10^{-3} \tag{7.8}$$

where σ_2 is the TPA cross section (in units cm^4/GW) of the absorptive molecules, N_0 is the number of these molecules in unit volume, N_A is the Avagadro number, and d_0 is the concentration of the solute in the solution (in units of m/l).

According to eqn. (7.7), for a given nonlinear medium with a given optical path length z = L, the nonlinear transmittivity T_i is a function of the input intensity of $I(0) = I_0$. The value of T_i decreases as the value of I_0 increases. This is the principle of using a TPA process to reach optical limiting performances. From eqn.(7.7) it is also clear that for a given nonlinear absorptive medium, the nonlinear transmittivity T_i can be determined by the product of the input intensity I_0 and the optical path length L. This means that, to reach the same optical limiting performance, a much lower input intensity level is required if the effective interaction length L can be greatly increased.

7.2.3 Nonlinear Refraction

Optical limiters based on self focusing and defocusing form another class of promising devices. The mechanism for these devices may arise from the real portion of $\chi^{(3)}$. Both self focusing and defocusing devices operate by refracting light away from the sensor as opposed to simply absorbing the incident radiation. Compared to strictly absorbing devices, these limiters can potentially yield a larger dynamic range before damage to the limiter itself. Typical device configurations of self-focusing and defocusing limiters are given in figs.(7.3b) and (7.3c). A converging lens is used to focus the incident radiation so it passes through the nonlinear medium. This lens provides optical gain to the system, allowing the device to activate at low incident intensities. The output passes through an aperture before impinging on the detector. At low input levels, the nonlinear medium has little effect on the incident beam, and the aperture blocks an insignificant portion of the beam, thus allowing for a low insertion loss for the device. When nonlinear refraction occurs, the nonuniform beam profile within the medium results in the generation of a spatially uniform refractive index. This acts as either negative or positive lens, depending on the sign of the nonlinear refractive nonlinearity, causing the incident beam to either defocus or focus. In a properly designed system, the self-focusing results in significant energy blocked by the system aperture, thereby protecting the sensor.

Theoretical details of these devices may be found in the work of Herman [58, 59]. While there is a large number of experimental work based on the application of the nonlinear refraction to optical limiting, perhaps first such demonstration was reported by Leite et. al [60], who used thermal lensing in a thick cell of nitrobenzene, in combination with spatial filtering to achieve optical limiting.

7.2.4 Induced Scattering

Scattering is a mechanism that has been extensively studied, as it occurs in many circumstances where reduced optical thoughput is not acceptable. Scattering is caused by light interacting with small centers that can be physical particles or simple interfaces between groups of nonexcited and excited molecules. The scattering can be highly directional or fairly uniform depending on the size of the scattering centers. It is obvious that, if an optical signal induces scattering centers in a given medium, the transmission of the medium, measured in a given solid angle, will decrease. Hence optically induced scattering can be used in optical limiters for sensor protection. Induced scattering limiters usually rely on liquid

media, because the process in such media is often reversible. That is, if chemical or structural decomposition has not occurred, the excited liquid can readily return to equilibrium. A number of methods have been devised that can induce scattering centers. The simplest method of generating such centers is to utilize absorbing molecules in solution. The optical energy is initially absorbed and heats the liquid until the local boiling point has been exceeded [61]. When this occurs, bubbles are generated. The vapour liquid interface is very good for scattering since the refractive index discontinuity is large.

7.3 Optical limiting in C_{60} and C_{70}

The discovery of optical limiting in fullerenes evoked considerable attention because of its comparatively lower threshold limiting fluence [46, 62, 63]. Optical limiting property in these new found materials was first reported by Tutt and Kost [40] using 532 nm, 8 ns pulses. These authors attributed the limiting action mainly to RSA in C_{60} resulting from the higher absorption from the photoexcited triplet state compared with that from the ground state. Transient excited state absorption spectroscopy measurements of higher lying singlets and triplet states of these molecules lend support to the RSA hypothesis. Joshi et. al. [47] did a numerical analysis of a simple model incorporating the effect of higher excited state absorption and found that this model cannot explain their observations. They also observed a reduction in pulse width and steepening of the falling part of the pulse for input energies well into the saturation region and suggests that the multiphoton absorption from the excited state rather than the ground state might be operative. A similar conclusion was reached by Mclean et al. [49], who found that their nonlinear transmission measurements with 8 ns and 30 ps, 532 nm pulses departed from the results of a rate equation analysis for input fluences greater than 1 J cm^{-2} indicating initiation of some other limiting mechanism. According to them, RSA yields a reasonable explanation of the low fluence behaviour in both ns and ps cases, but unusual large nonradiative relaxation rates for higher lying singlet states must be assumed in the picosecond case. Kost et. al [63] reported that nonlinear transmission of C_{60} in PMMA was in agreement with the RSA mechanism and suggested the stronger limiting in C_{60} solutions could be due to nonlinear scattering. Eventhough large attention has been given for the limiting property of these fascinating molecules, a clear cut picture for the underlying physics behind this phenomenon has not yet emerged.

Molecules of fullerenes have a nm scale and can be modeled as a sphere or pseudo sphere, where electrons are delocalized on the surface. In that case they are something like a con-

jugated polymers with delocalized π electrons and have been predicted to exhibit nonlinear optical behaviour similar to that of conjugated polymers. Few authors have reported the third order nonlinear susceptibility $\chi^{(3)}$ of C_{60} and C_{70} solutions in various solvents [65, 66]. Koudoumas and co-workers [67] calculated these nonlinear susceptibilities of C_{60} up to $\chi^{(7)}$.

C_{60} and C_{70} used in our experiment was prepared by following Krätschmer-Huffman technique [15] and the sample was further purified by employing high purity liquid chromatography. The extract of C_{60} and C_{70} have the characteristic colour (magenta for C_{60} and reddish yellow for C_{70}) and its electronic absorption spectrum (figs. 7.6a and 7.6b) was identical with that reported in the literature [68]. We have carried out measurement of optical limiting properties in C_{60} and C_{70} in toluene sample solutions. The solution was taken in quartz cuvettes of path lengths 5 mm and 10 mm. The cuvette was kept slightly away from the focal spot and a long focal length lens was used so that the spot size inside the cuvette remains constant and was about 500 microns in radius. The input and output pulse energies were measured using a laser energy meter. The set up essentially avoids nonlinear refraction as only the nonlinear absorption is important in this case contrary to the measurements done with a point detector to measure the transmitted laser energy. The optical limiting is obtained by varying the input energy and measuring the transmitted energy. The variation of transmitted energy with input energy is given in fig. 7.7 for different concentrations of C_{60} in toluene for an optical path length of 5 mm. At very low laser energies the transmission obeys Beer-Lambert law and the transmitted intensity varies with increasing input energy with a slope equal to $\exp(-N_0\sigma_1 L)$ where σ_1 is the absorption cross section of the ground state, N_0 the number density of the C_{60} molecules and L the cuvette length. At high input intensity the transmittance decreases with input intensity and we observe an optical limiting property with saturated or clamped output intensity. With solutions showing low intensity linear transmittance of 46% and 38% the outgoing laser intensities are saturated at energy levels of 6 mJ and 4.5 mJ respectively. This data show that as the concentration increases, a reduction in linear transmittance as well as the clamping level is observed. It is also noted that the saturated output intensity decreases with increase in length of the optical path. Fig. 7.8 gives the optical limiting properties of these solutions with 10 mm cell path length. In this experiment the low intensity linear transmittance of the solutions in a 10 mm path length cell are 27% and 19% with clamping energies at 4.6 and 3 mJ respectively. This indicates that the number density of C_{60} in the laser beam is the main factor affecting the clamped level. From the threshold intensity for optical limiting for each sample it can be seen that the threshold is inversely proportional to the concentration. We also investigated the optical

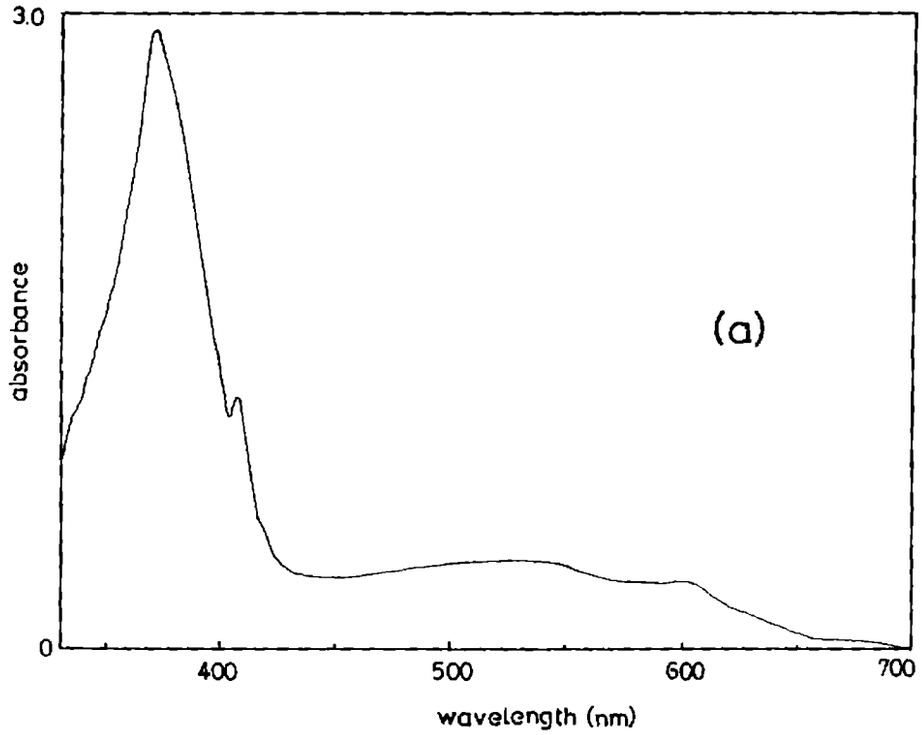

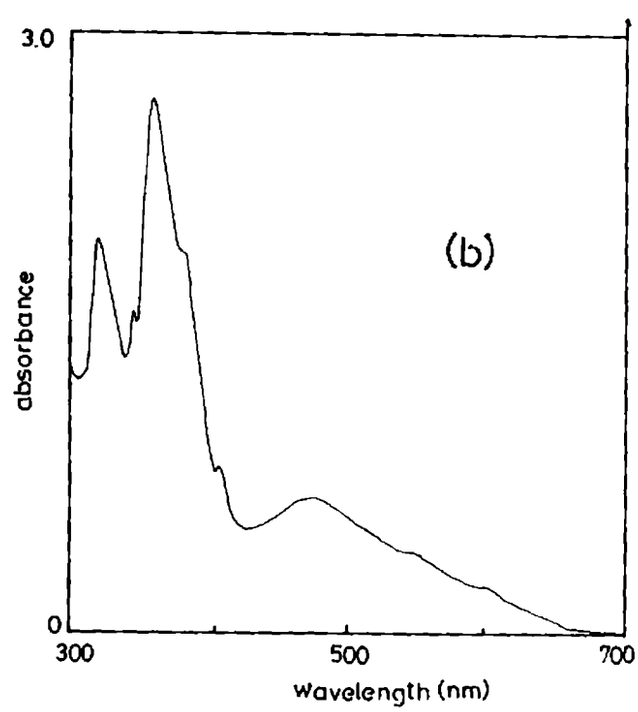

Figure 7.6: Electronic absorption spectrum for (a) C_{60} and (b) C_{70}

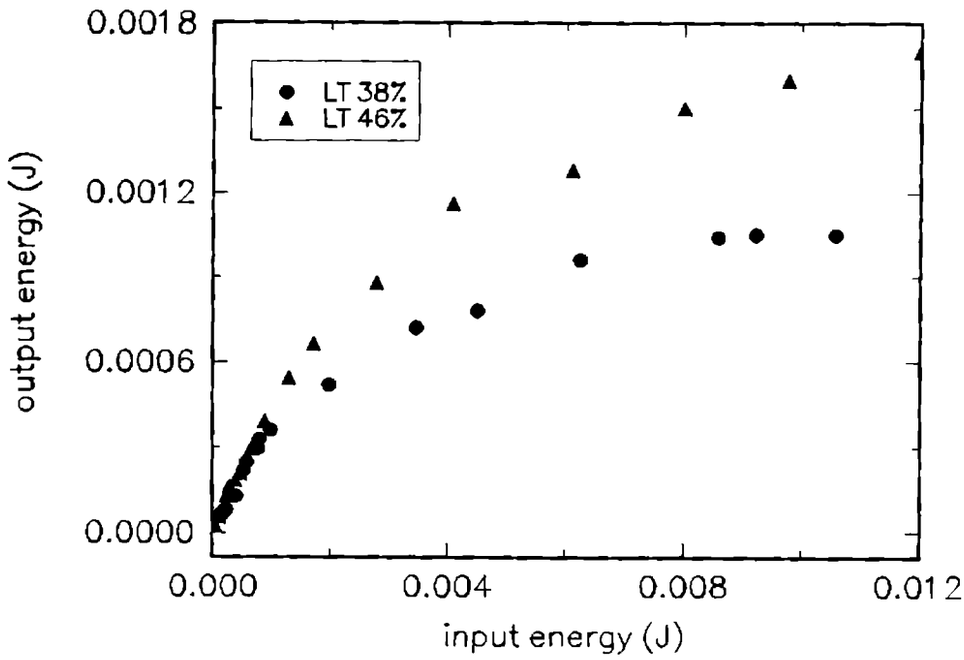

Figure 7.7: Variation of transmitted energy with respect to input laser energy for C_{60} for an optical pathlength of 5 mm for a linear transmittance (LT) of 46 % and 38 %

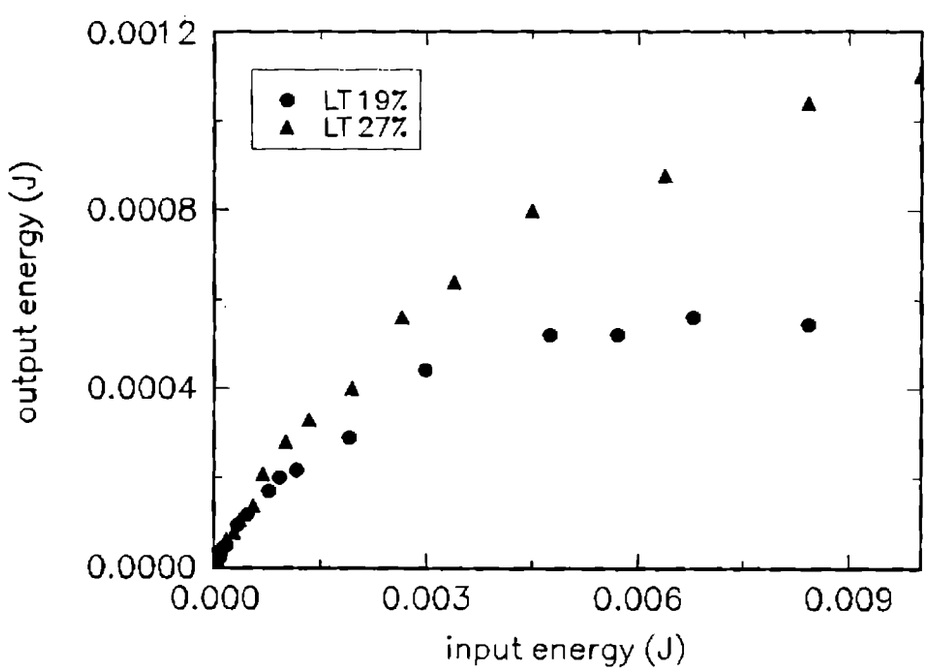

Figure 7.8: Variation of output energy vs input energy for an optical pathlength of 10 mm for C_{60} with a linear tansmittance of 27 % and 19 %

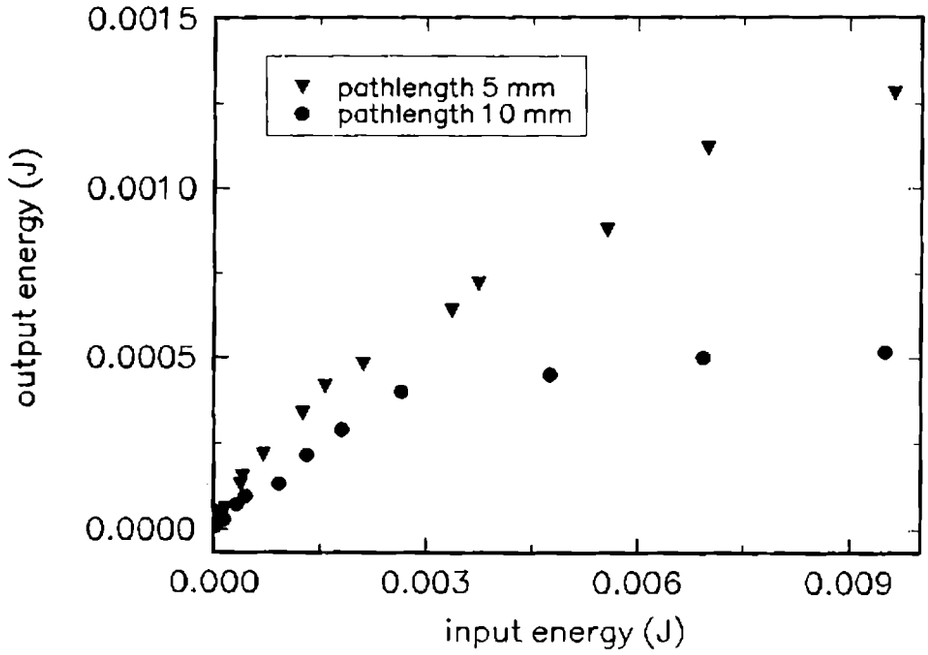

Figure 7.9: Optical limiting properties in C_{70} toluene solution (low LT solution)

limiting properties in C_{70} - toluene solutions. Fig. 7.9 and 7.10 show the input - output response for C_{70} in toluene solution for different low intensity linear transmittance and for different cell path lengths. For an optical path length of 5 mm, the 48% linear transmitting solution gets clamped at 7.5 mJ and the 30% linear transmitting one is clamped at 6 mJ. The clamping levels for these solutions with 10 mm optical path length are 6 mJ for 30% and 3.3 mJ for 16% linear transmittance. It is observed that solutions of C_{60} in toluene provided lower output energies at a given input energy than solutions containing the larger molecule C_{70}. It is also noticed that for the same low intensity linear transmittance solutions, the clamped level of laser energy is higher for C_{70} solution compared to C_{60}. These results are in qualitative agreement with previous reports [69]. The reddish - orange C_{70} solutions have a higher absorption at 532 nm than the magenta C_{60} solutions. Hence the higher ground state absorption of C_{70} results in a smaller ratio of excited state to ground state absorption and a higher threshold for optical limiting. The molar absorption coefficient for the triplet state of C_{60} is significantly larger than that of C_{70}, while the ground state absorption cross section in the visible region is much larger for C_{70} than for C_{60}. It is thus expected that the optical limiting capability of C_{60} should be higher than that of C_{70} as found experimentally. Several mechanisms have been proposed for optical limiting in C_{60} and C_{70} including RSA, nonlinear scattering, multiphoton absorption, cyclic multiphoton absorption etc. The RSA by a 5 level

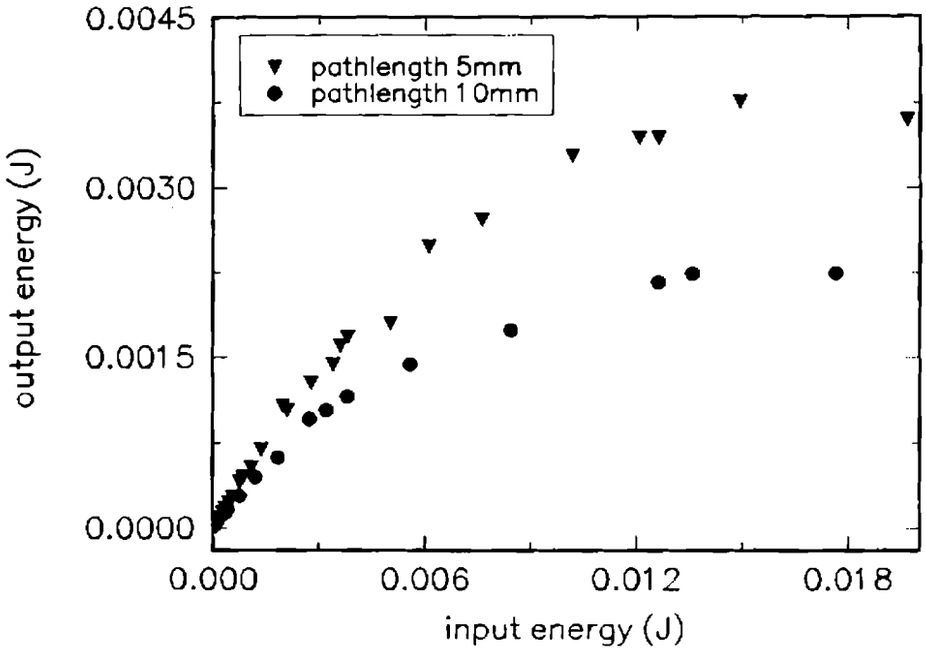

Figure 7.10: Optical limiting properties in C_{70} toluene solution (high LT solution)

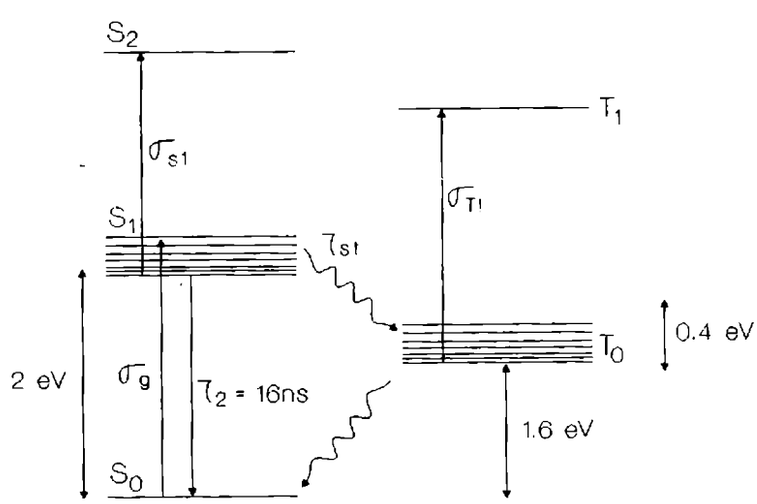

Figure 7.11: Five level diagram for C_{60}

energy diagram yielded a reasonable explanation for optical limiting in the ns regime of a π - electron conjugated system such as C_{60} and C_{70} below the input fluence of 1 Jcm^{-2}. A typical 5 level model for C_{60} is given in fig. 7.11. The initial absorption is from the ground state (S_0) to an excited singlet state (S_1). This excited state can relax nonradiatively to its original ground state, or be excited to a higher singlet state (S_n) or transfer to the lower level of triplet state (T_1) by intersystem crossing. The triplet state absorption takes place from level T_1 to T_n. To obtain an optical limiting property by RSA, the upper singlet (S_1) and lower triplet (T_1) should have larger absorption cross sections σ_{S1} and σ_{T1} than the ground state σ_g. It is also assumed that relaxation times between S_n and S_1 and between T_n and T_1 are extremely fast. When a C_{60} molecule is photoexcited using 532 nm, 9 ns pulse, it gets excited from the ground state S_0 (σ_g=1.21 $\times 10^{-18}$ cm^2) into one vibrational rotational state of the first excited singlet state S_1. The molecule relaxes rapidly ($\approx$1 ps) into an equilibrium state S_1 which releases 0.33 eV energy. This level relaxes either to the ground state with τ_0=16 ns, or to the triplet state T_1 in τ_{st} = 650 ps. The reported fluorescence quantum yield [41] for C_{60} in toluene is 1.45 x 10^{-4}. But the triplet production yield is found to be nearly unity (0.96±0.04) at 532 nm excitation for C_{60} molecules (0.9 ±0.1 for C_{70}). Hence excited singlet state transfers dominantly to the lower level of the triplet state due to high triplet yield and small S-T splitting of 9 Kcal/mol for C_{60}. The molecule in the S_1 and T_1 states can be excited to higher S_n and T_n states (σ_{s1}=8.07 $\times$ $10^{-18}cm^2$ and σ_{T1}= 5.35 $\times 10^{-18}cm^2$). Relaxation from these S_n and T_n states is in the form of heat and extremely short (< ps). The relaxation to T_1 to S_0 is forbidden and therefore very slow. The triplet state which has long life time (40 ± 4 μs for C_{60} and 130 ±10 μs for C_{70}) [70] and higher absorption cross section than that of the ground state will accumulate significant population and eventually become the dominant absorption source. At very low laser energies the transmission increases with increasing input energy with a slope equal to exp(-$N_0\sigma_g L$) where N_0 the number density of the C_{60} molecules and L the optical path length. At higher laser energies, taking into account the ground state absorption as well as ESA the transmission varies at a rate exp-($N_0\sigma_{s1}$+$N_1\sigma_{T1}$)L where N_1 is the population density for the photoexcited triplet state. It has been found that $\sigma_2 \simeq 2.9\sigma_1$ [41]. Using the above expressions we estimate N_1 and it is plotted as a function of the input laser energy in fig. 7.12. For lower laser energies the population at the excited state grows faster than that in the power limiting region which means that at higher laser energies most of the molecules are in the excited state and the dominant process involved in optical limiting arises mainly from the excited state.

Kojima et al. [71] while explaining the optical limiting property of a polyacene based

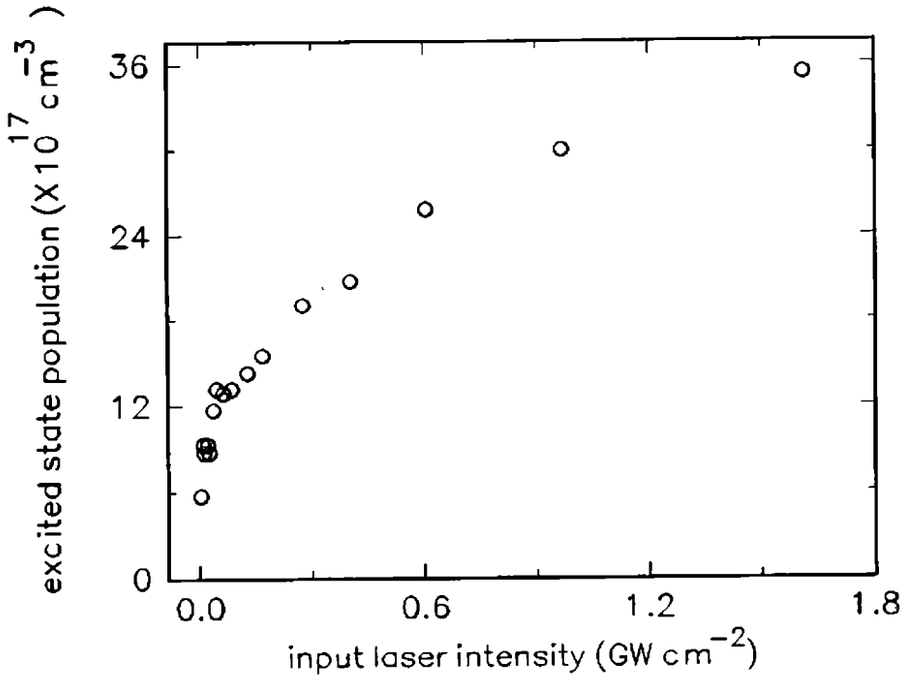

Figure 7.12: Plot showing variation of excited state population of C_{60}

oligomer have shown that in the case of pure RSA the incident laser fluence I_0 and the transmitted laser fluence I obeys the relation,

$$\ln(\frac{I_0}{I}) = k(I_0 - I) + A_g \tag{7.9}$$

where k is a constant which depends on the absorption cross sections and life times of the ground, excited singlet and excited triplet states and A_g is the ground state absorbance. The above equation says that the plot of $\ln(I_0/I)$ vs $(I_0\text{-}I)$ should be a straight line with slope k and intercept A_g. Figs. 7.13 and 7.14 show such a plots for C_{60} and C_{70}. The plot of $\ln(I_0/I)$ vs $(I_0\text{-}I)$ looks almost linear for both cases in the desired energy ranges of interest. This is a clear indication that RSA is one of the limiting mechanism in the case of C_{60} and C_{70}. Eventhough there are many reports exploring nonlinearities and fluorescence of C_{60} and C_{70} molecules, its nonradiative relaxations in solutions are not well investigated. Apart from that there is a controversy existing in the optical limiting mechanism of these molecules. Kost et. al [63] studied optical limiting with C_{60} in solid polymer matrix like polymethyl methacrylate. They observed higher threshold for optical limiting in polymer matrix as compared to solutions and attributed this to increase in light scattering cross section in solid matrices. McLean et. al [49] suggested various mechanism other than RSA for the observation of optical limiting in C_{60}. Joshi et. al [47] have found that the optical limiting in C_{60} deviates from theoretical model based on large excited state absorption cross section alone and they have attributed the

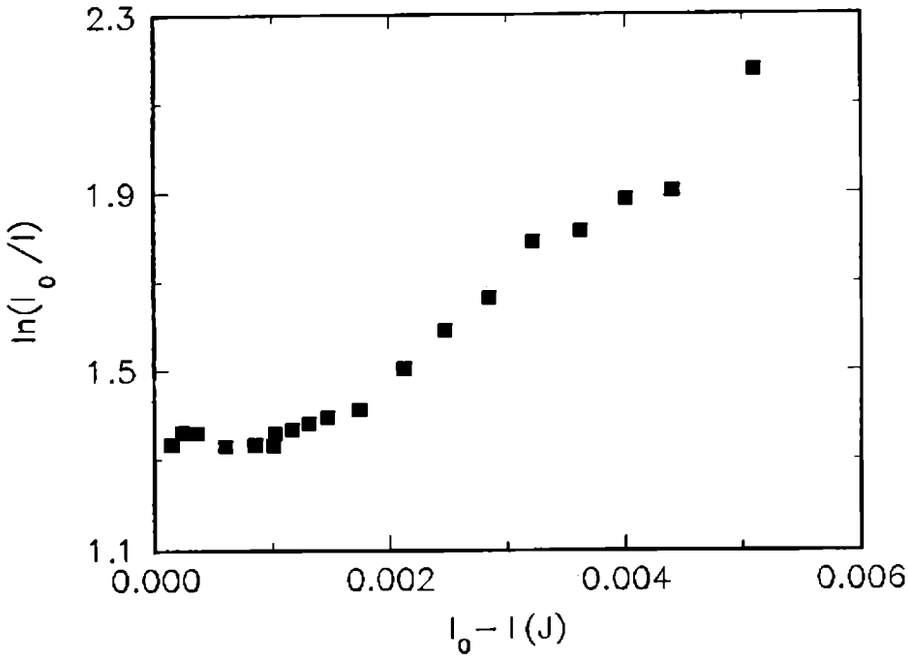

Figure 7.13: Plot of $\log(I_0/I) vs (I_0 - I)$ for C_{60} toluene solution showing linearity in the entire energy range studied

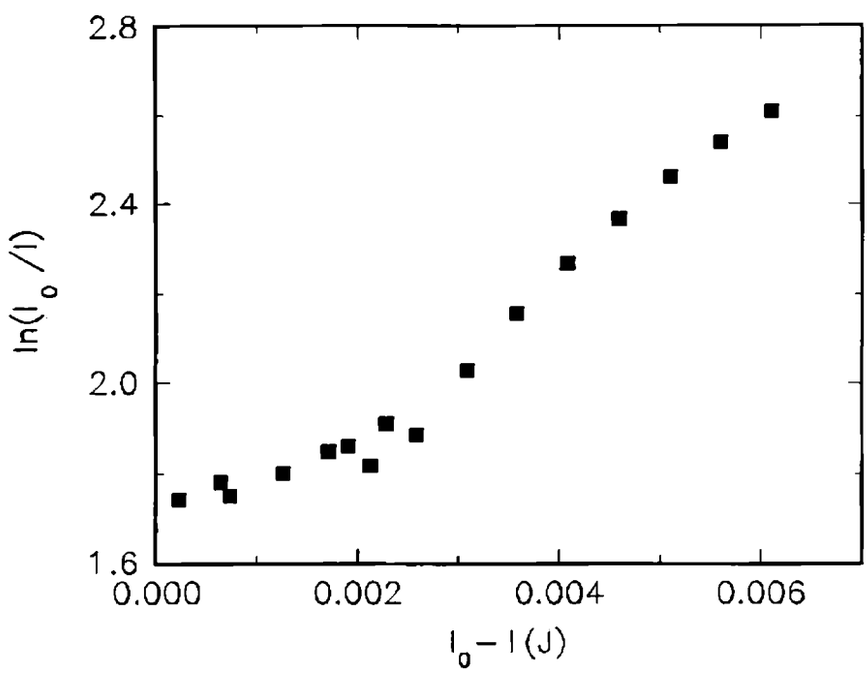

Figure 7.14: Plot of $\log(I_0/I) vs (I_0 - I)$ for C_{70} in toluene showing linearity

discrepancy to the possibility of multiphoton absorption (MPA) apart from ESA. The study of MPA in absorbing media can very effectively be carried out using pulsed photoacoustic (PA) technique [72, 73, 74] or transient thermal lens technique [75, 76]. We have explored the nonradiative relaxations in C_{60} and C_{70} in toluene solution using pulsed photoacoustics and thermal lens techniques. The results obtained in C_{60} and C_{70} using these thermo-optic techniques are described in the following subsections.

7.4 Thermal lensing in C_{60} and C_{70} toluene solutions

Thermal lens spectroscopy is an effective and efficient method to monitor nonradiative relaxations in a medium. Very weak optical absorption processes can be studied using this method. Recently, thermal lens technique is successfully used for the determination of nonlinear properties like two photon absorption and three photon absorption in a dye medium [77]. Terazima and Azumi [78-80] have demonstrated that thermal lens technique is very powerful in investigating the properties of the excited state. Terazima and co-workers [81] have also used this method for studying photophysical properties of triplet states of C_{60} clusters. They investigated time dependence of the thermal lens signal by considering the quenching and decay of the triplet state and triplet-triplet absorption process.

Even though few reports are available in literature on the thermo-optic properties of C_{60} and C_{70}, a more detailed study of thermo-optic properties of these fullerene molecules is not undertaken yet. In this section, thermal lensing studies in C_{60} and C_{70} are given. Experimental details of the thermal lens spectrophotometer is given in chapter 2. Briefly, 532 nm, 9 ns pulses from a Nd:YAG laser operated at 5 Hz was used as the heating source and a low power intensity stabilized He-Ne laser was used for probing the thermal lens. The samples were taken in a quartz cuvette having an optical path length of 5 mm. The transient thermal lens signal thus obtained was monitored using a 100 MHz Tektronix digital storage oscilloscope.

We have measured thermal lens signal produced from solutions of C_{60} and C_{70} in toluene at different concentrations and various input energies. Log$-$ log plots of thermal lens signal against laser energy is plotted for each sample. Figs. 7.15 and 7.16 give some of the typical log$-$log plots for C_{60} and C_{70} in toluene. As is clear from the figure that for a linear transmittance of 30% C_{60} toluene solution gives a slope value of ~ 2. Similar experiments were conducted in C_{70} :toluene solutions and a slope value of two was observed in this case too. Fig. 17 gives the dependence of slope on the concentration of C_{70} :toluene solution. From this

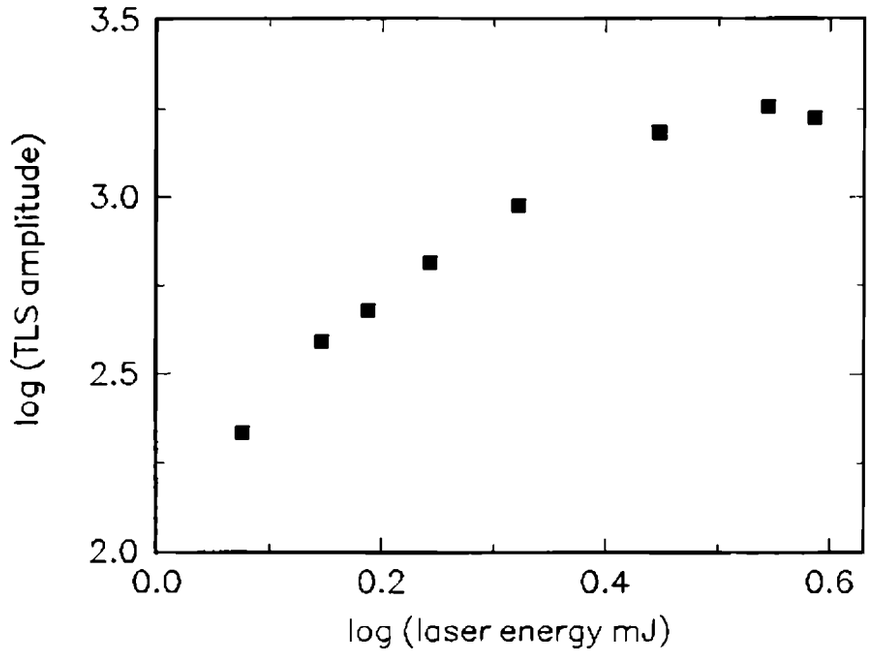

Figure 7.15: Log-log plot of TL signal strength as a function of input laser energy for C_{60}

graph, the slope value is found to be more or less constant in the concentration range 10^{-5} to 5×10^{-4}m/l and decreases at higher concentrations. From fig. 7.17 it is clear that the slope which directly gives the number of photons involved, varies with respect to concentration. The occurrence of slope 2 in these curves is an indication of two photon absorption. However, the optical limiting action of C_{60} and C_{70} can be explained in terms of transient reverse saturable absorption, although some other mechanisms like nonlinear refraction, nonlinear scattering etc. may also play a role under certain experimental conditions. The participation of instantaneous or simultaneous TPA in C_{60} or in C_{70} has not yet been demonstrated under laser excitation in the nanosecond range. The two photon absorption from the triplet state in these molecules is less likely since considerable triplet-triplet absorption cross-section is reported at 532 nm [81]. Another potentially effective nonlinearity is sequential two-photon absorption where the excited state absorption cross section is larger than the ground state absorption cross section. The observation of slope 2 in the double logarithmic plot of these molecules could be due to sequential two photon absorption. That is, instead of simultaneous absorption of many photons and exciting the molecule to a higher level which is multiphoton resonant, the photons are absorbed one after the other. In the power limiting region, leading part of the laser pulse excites most of the molecules to the vibrational levels of the excited singlet state S_1. It rapidly decays nonradiatively to the lowest vibrational level of S_1. The

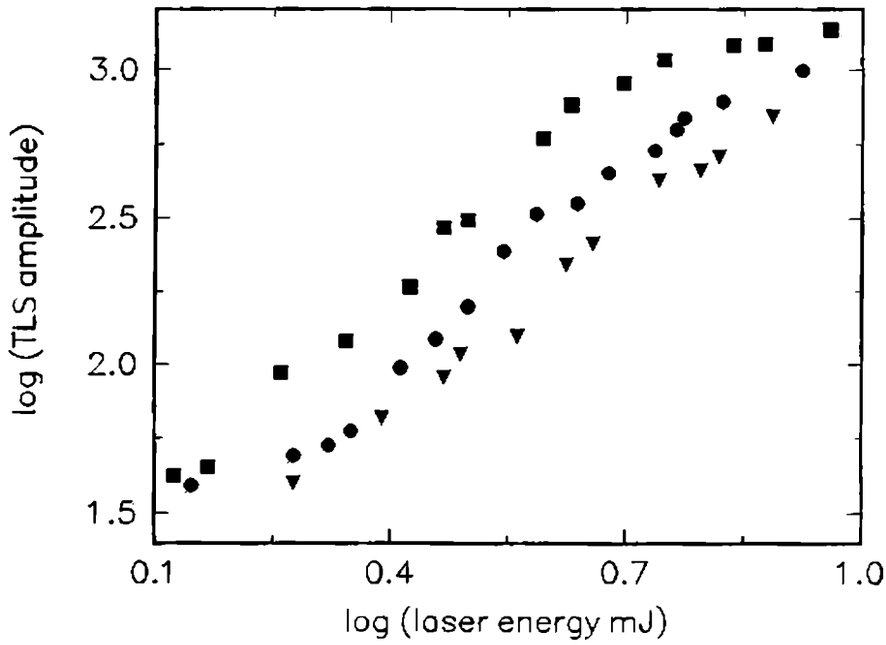

Figure 7.16: Log-log plots PA signal strength as a function of input laser energy for C_{70} at different concentrations (■ - 1.14×10^{-4} mol/lt, • - 8.5×10^{-5} mol/lt and ▼ - 2.8×10^{-5} mol/lt)

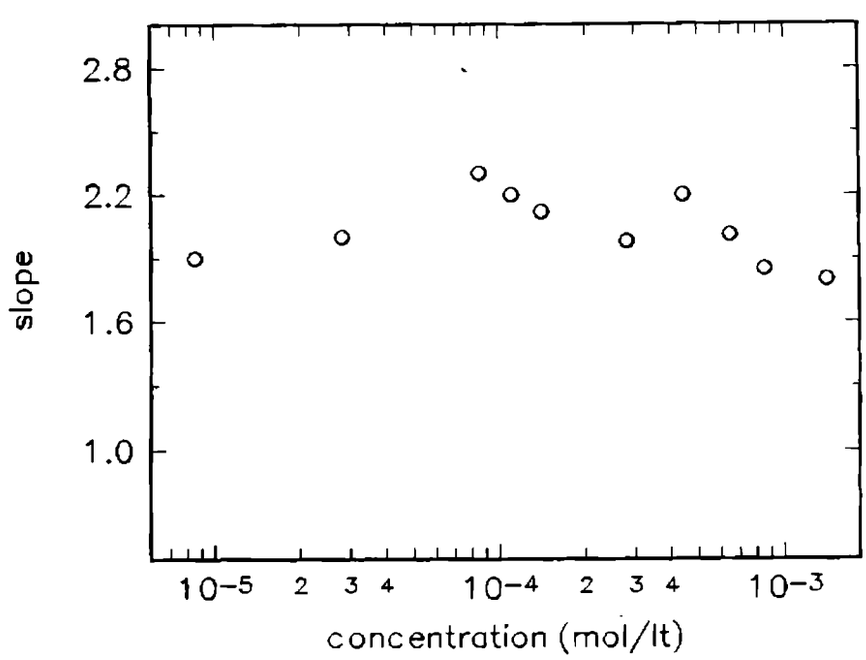

Figure 7.17: The slope as a function of concentration of C_{70} in toluene

reported quantum yield for intersystem crossing rate to the lowest triplet T_1 for C_{60} and C_{70} are equal to nearly unity [70]. As the intersystem crossing is very fast for C_{60} and C_{70} ($\ll$ ns) for ns pulses, the triplet state T_1 gets populated rapidly. The triplet state T_1 has a long life time (40 μs for C_{60} and 130 μs for C_{70} [41]) and higher absorption cross section than that of the ground state. After resonantly absorbing a single photon, the molecule in the triplet state goes to a higher excited state (T_n), the life time of which is considered to be in the picosecond region due to fast internal conversion. The molecule can relax to the lower excited triplet level by collissional energy transfer to the surrounding solvent molecules. This process occurs within the duration of the nanosecond laser pulse. Thus the nonradiative decay from T_n gives rise to appreciable thermal lens signals with quadratic dependence on laser energy.

The time dependence of the TL signal of the system can be given by the following scheme:

$$C_{60}(S_0) + h\nu \rightarrow C_{60}(S_1^*) \tag{7.10}$$

$$C_{60}(S_1^*) \rightarrow C_{60}(S_1) \tag{7.11}$$

$$C_{60}(S_1) \rightarrow C_{60}(T_1) \tag{7.12}$$

$$C_{60}(T_1) + h\nu \rightarrow C_{60}(T_n) \tag{7.13}$$

$$C_{60}(T_n) \rightarrow C_{60}(T_1) \tag{7.14}$$

$$C_{60}(T_1) \rightarrow C_{60}(S_0) \tag{7.15}$$

where S_1^* represents the higher vibrational level of S_1.

For C_{60} and C_{70}, the absorption from the excited singlet states is negligible for ns pulses, the variation of light intensity $I(\lambda)$, at laser wavelength λ, along the beam propagation direction in a cell containing these solutions will be given, at an instant t during the laser pulse, by the following expression [64]:

$$\frac{dI(\lambda)}{dz} = -\alpha_0[S_0]I(\lambda) - \alpha_1[T_1]I(\lambda) \tag{7.16}$$

where S_0 and T_1 are the ground and triplet state concentrations respectively, at instant t, and α_0 and α_1 are the linear absorption coefficients from the S_0 and T_1 states respectively.

The triplet state concentration at instant t is, to a good approximation, given by

$$[T_1] = \alpha_0[S_0]I(\lambda)\Phi_{isc} \tag{7.17}$$

where Φ_{isc} is the intersystem crossing yield. For C_{60} and C_{70}, $\Phi_{isc} \approx 1$, so that

$$\frac{dI(\lambda)}{dz} = -\alpha_0[S_0]I(\lambda) - \alpha_1\alpha_0[S_0]I(\lambda)I(\lambda) = -\alpha I(\lambda) \tag{7.18}$$

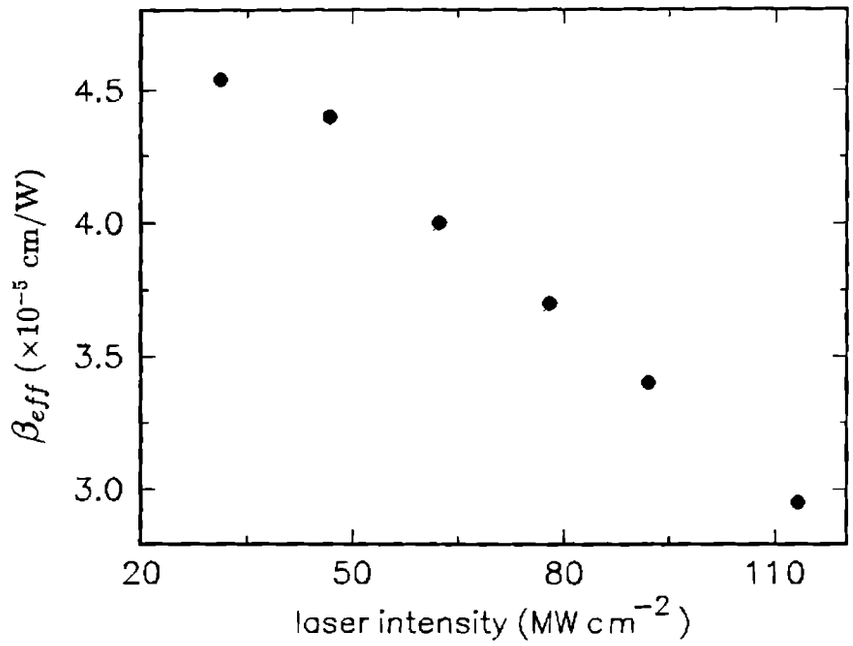

Figure 7.18: Effective STPA parameter β_{eff} as a function of the incident laser intensity for C_{60}

where α = -α_0[S_0] - $\alpha_1\alpha_0$[S_0]I(λ) can be considered as an intensity dependent absorption coefficient. This α represents the absorption coefficient for the sequential two photon absorption (STPA) with effective STPA parameter β_{eff} = $\alpha_1\alpha_0$[S_0]. The above equation is formally similar to $\alpha = \alpha_0 + \beta I$ for the case of instantaneous two photon absorption (ITPA).

Eqn.(7.18) will remain unchanged after temporal integration over the laser pulse duration and integration over the spatial duration of the pulse; the final result will be average values of α and β_{eff}. However, the quantity β_{eff} is intensity dependent through the [S_0] term while in the ITPA case β is constant. The dependence of the effective TPA parameter β_{eff} as a function of the incident intensity I_0 is depicted in figures 7.18 and 7.19. for C_{60} and C_{70}. It is noted that the value of β_{eff} decreases with respect to increasing intensity of radiation. The fall-off of β_{eff} with increasing I_0 is a consequence of STPA. With increasing intensity the total absorption of the C_{60} and C_{70} approaches asymptotically the value of α_1, ie. the absorbance of the triplet state [49]. We remark that a decrease of β_{eff} with increasing incident intensity has also been reported that for the optical limiting action of thiophene oligomers, where it is attributed to saturation of ITPA [82] and in p-toluene sulfonate crystal [83]. The triplet-triplet absorption spectrum [81] shows that both C_{60} and C_{70} have an absorption at 632 nm. During the thermal lens measurements the absorption of the He-Ne laser light by the T-T

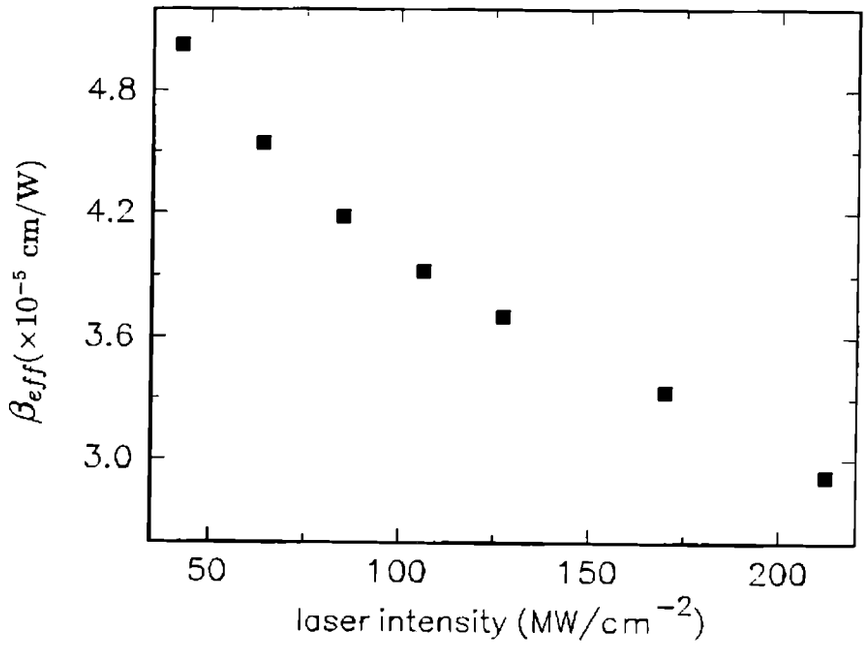

Figure 7.19: Effective STPA parameter β_{eff} as a function of the incident laser intensity for C_{70}

absorption of C_{60} (or C_{70}) may take place. Hence the effect of the T-T absorption by the probe beam should be taken into account. Since the TL signal is detected as the decrease of the probe beam intensity, there is further decrease of the intensity by the T-T absorption. The contribution of this effect is represented by [81]

$$I_{TL}(t) = AI_{ex}I_p\epsilon_{TT}\phi_{isc}\exp(-k_\tau t) \tag{7.19}$$

where A is a constant that depends on an experimental configuration, I_p is the intensity of the probe beam, ϵ_{TT} is an extinction coefficient of the T-T absorption, k_τ is the lifetime of the triplet state. In the present case we expect that triplet - triplet absorption of the probe beam does not affect our experimental observations since we are looking only the signal strength of the thermal lens rather than decay phenomena.

7.5 Photoacoustic Studies in C_{60} and C_{70}

Pulsed photoacoustics (PA) is a very powerful technique for exploring the nonradiative relaxations and multiphoton process in liquids. In this section, we examine the PA signal and optical limiting simultaneously using a suitable PA cell. The schematic diagram and other details of the experimental set up used for PA measurements are given in the chapter 2.

Solution of C_{60} or C_{70} is taken inside the PA cell. The 532 nm radiation from a Q-switched frequency-doubled Nd:YAG laser was focused into the center of the PA cell containing the solution using a convex lens (f = 5 cm). The laser pulse width was 9 ns with pulse repetition frequency of 16 Hz. The length of the photoacoustic cell was 4.5 cm. The pump pulse energy was monitored using a laser powermeter and the strength of PA signal was measured using a 200 MHz digital storage oscilloscope. The average amplitude of PA signal was monitored as a function of pump pulse energy. The pulse energies were measured after averaging over 16 pulses and the correction for the reflection losses at window and lens surfaces are made. The transmitted energy from the PA cell was measured with an energy meter to study optical limiting in the solution. This experimental set up enables us to make simultaneous measurement of the PA signal as well as transmitted energy.

In general the pulsed PA signal amplitude q(ν) generated in an absorbing liquid media at input laser frequency ν can be written as [84]

$$q(\nu) = \frac{A}{\pi\omega_0^2}\sigma(\nu)L_{eff}N\tau\eta(\nu_m)I^m(\nu) \tag{7.20}$$

i.e. $q(\nu)$ is proportional to the mth power of the incident laser power density I(ν), m being the number of photons involved in the process. In the above equation A is a constant determined by calibration factors which include cell geometry, acoustic transducer property etc., $\sigma(\nu)$ the absorption cross section at laser frequency ν, N the density of absorbing molecules, L_{eff} the effective optical path length in the cell given by $L_{eff} = (1\text{-}e^{-\alpha L})/\alpha$ where α is the absorption coefficient in units of cm^{-1} and ω_0 is the beam waist radius at the focal spot. Therefore assuming the dominance of m photon absorption, the slope of the plot of logq(ν) vs log I(ν) will give an indication of the number of photons involved in the process. Simultaneous measurement of the transmitted intensity of the excitation beam at 532 nm show optical limiting in C_{60}. Optical limiting studies using 4.5 cm long PA cell gives a linear transmittance of 8 percentage of transmission is evidently due to the longer pathlength of laser light through the solution.

The graph of PA signal as a function of laser energy for C_{60} - toluene solution is shown in fig. 7.20 which exhibits a tendency of saturation at higher laser energies. The radiative deexcitation cross section of the excited molecules should be small as seen from very low fluorescence quantum efficiency of fullerenes [45]. Therefore one expects enhanced nonradiative deexcitation probability, particularly at higher laser energies. This should logically result in a major enhancement in the PA signal amplitude in the range of laser energies exhibiting optical limiting. However the experimental results as given in fig. 7.20 do not show any

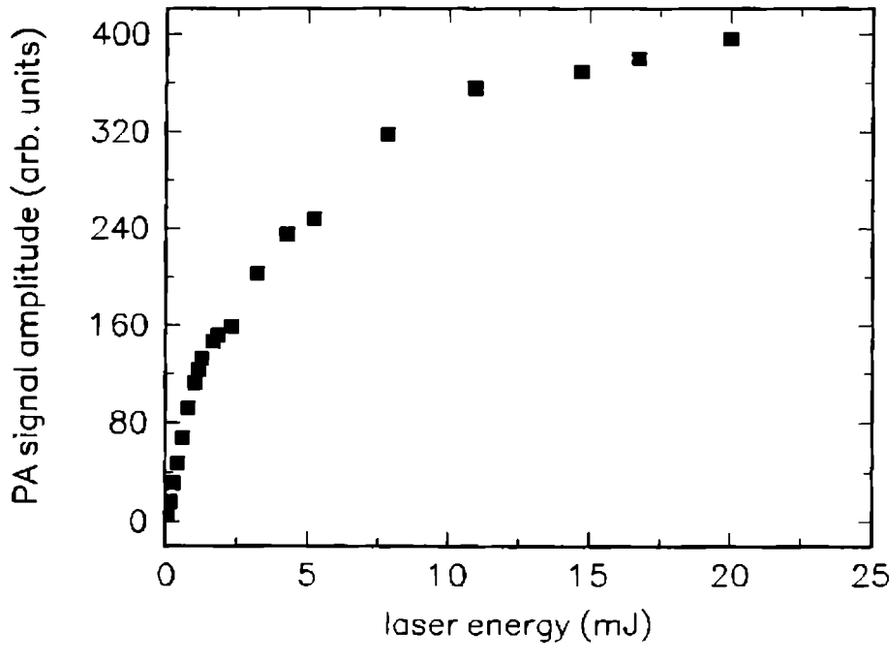

Figure 7.20: Change in PA signal amplitude with input laser energy for C_{60} in toluene

indication of such a major enhancement of PA signal amplitude though a slight increase is observed at the limiting threshold followed by a saturation. Log– log plots of PA signal as a function of laser pulse energy for C_{60} is given in fig. 7.21. Contrary to the observation gathered from the thermal lens measurements, we observed a linear dependence of PA signal strength on the pump laser energy. In the case of pure toluene [73] the initial linear dependence of PA signal on the input laser energy changes into a quadratic dependence after a threshold laser energy thus giving evidence of two photon transition corresponding to the (one photon) absorption band at 266 nm due to the transition $^1A_1 \rightarrow {}^1B_2$. But after C_{60} is dissolved in toluene the intensity dependence of PA signal is found to be linear and there is no tendency for it to change over to a higher order dependence. Since single photon absorption alone is involved in these cycles the PA signal exhibits only a linear dependence on the laser pulse energy. Similar experiments are also undertaken for C_{70} toluene solutions. Fig. 7.22 shows the variation of transmitted laser energy and PA signal as a function of input laser energy for a solution having a low intensity transmission of 16%. In this case one can see that the PA signal saturation threshold and limiting threshold clearly separates out. Fig. 7.23 shows a log-log plot of laser energy and photoacoustic signal for the C_{70} solution which show a linear dependence of PA signal on incident laser energy. We also noticed that strength of the PA signal as well as the slope of plot showed a decreasing tendency as trace amounts of

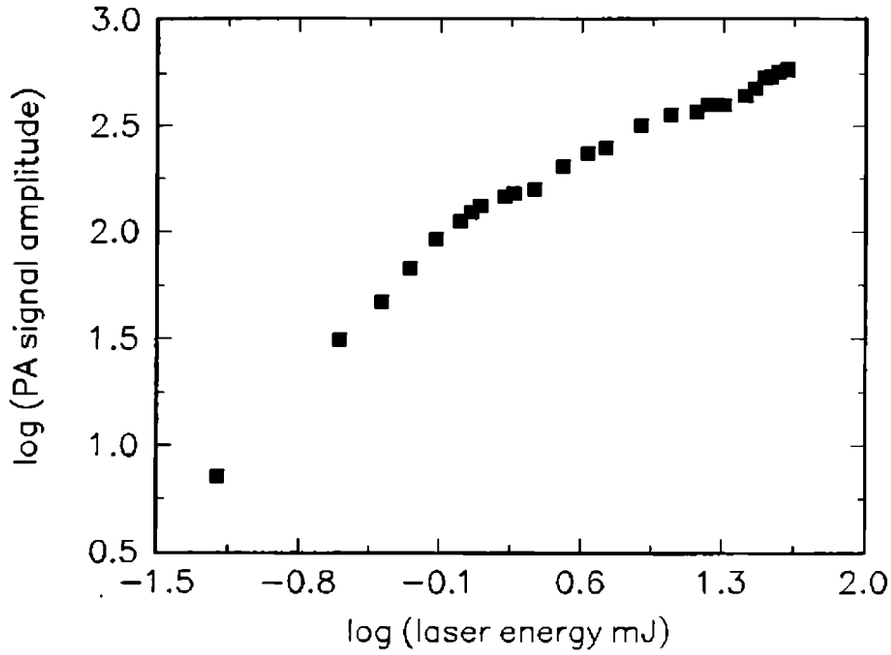

Figure 7.21: Log-log plot of PA signal strength as a function of input laser energy for C_{60}

C_{60} or C_{70} into toluene solution.

We expect that the observed PA signal saturation at high energies may be due to our PA cell configuration. The PA cell used in the present work is having a path length of 4.5 cm. During the PA measurements the laser beam was focused in the center of the PA cell by using a short focal length lens (5 cm). The optical limiting measurements of C_{60} and C_{70} discussed in the previous sections were done by using 5 mm and 10 mm cuvettes. For these studies the sample cell was kept slightly away from the focal spot and a long focal length lens with f = 50 cm is used so that the spot size inside the cuvette is more or less constant. But in the former case the spot size inside the PA cell varies drastically since we are using a short focal length lens and the optical path inside the PA cell is $\sim$ 4.5 cm. Usually, the nonlinear properties are expected to be maximum at the focal point due to higher laser fluence. But before reaching the focal point the absorption of the laser photons by C_{60} or C_{70} may happen which effectively reduces the laser energy coupling at the focal spot. The measured PA signals are due to the pressure variations occurring at the focal spot and these acoustic signals are measured using a PZT transducer. The absorption of the laser photons before the focal region considerably reduces the effective laser fluence at the focal spot which in turn saturates the PA signal. This fact is supported by the following observation. Usually the amplitude of the first peak in the oscilloscope trace (peak to peak voltage) (fig. 7.24) which originates directly from the focal spot is measured as the PA signal. As the laser energy increases the amplitude of

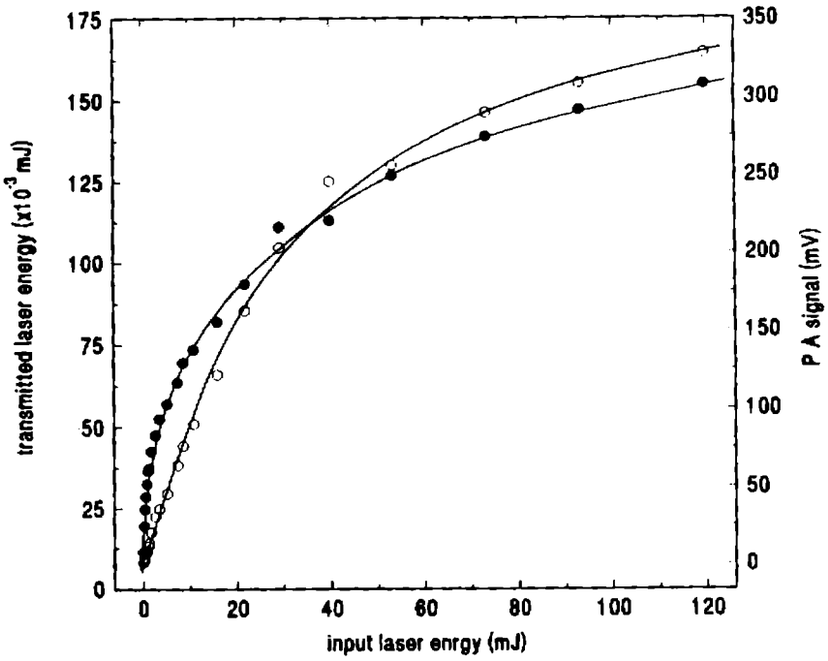

Figure 7.22: The variation of transmitted laser energy (•) and PA signal (o) as a function of input laser energy in a C_{70} - toluene solution with a low intensity transmission of 24 %

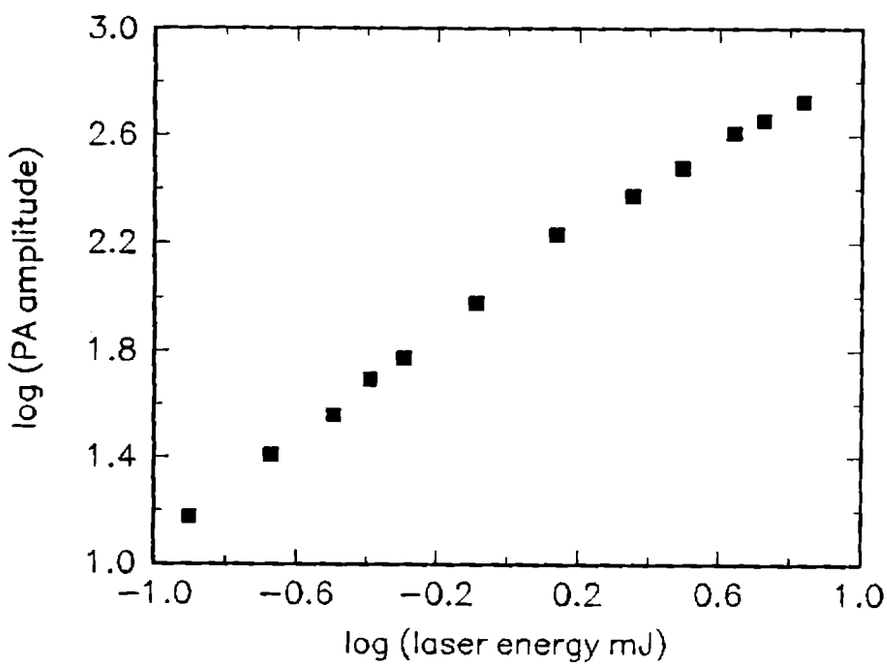

Figure 7.23: Log-log plot of PA signal with laser energy for C_{70}

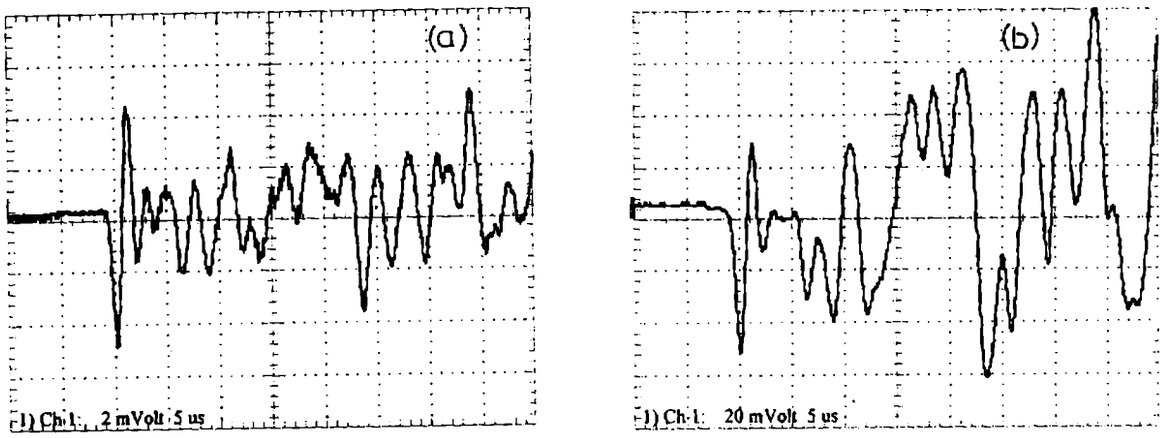

Figure 7.24: Typical oscilloscope trace PA signal (a) low energy levels and (b) higher energy levels

this peak gets saturated due to enhanced absorption by the fullerene molecules in the laser beam path before the focal spot. At the same time the amplitude of the delayed peaks, (see fig. 7.24) originating from the region before the focal point, begins to increase due to increased absorption in that regime. Due to these reasons a saturation is observed in the PA signal. Since the PA signal from fullerene solutions saturate, we were unable to detect any multiphoton processes taking place in these solutions.

7.6 Conclusions

Optical limiting properties of C_{60} and C_{70} molecules in toluene are studied using 532 nm, 9 ns pulses from a frequency doubled Nd:YAG laser. Because of large excited singlet as well as triplet absorption cross sections compared to ground state absorption cross section, the major mechanism for this limiting behaviour of these molecules is reverse saturable absorption. The limiting properties of C_{60} toluene solution is found to be better than that of the C_{70} toluene solutions. A higher limiting threshold is found in C_{70} solution compared to C_{60} toluene solution. This is attributed to higher ground state absorption of C_{70} resulting in a smaller ratio of excited state to ground state absorption of C_{70} and a higher threshold for optical limiting.

Thermal lensing studies in these solutions show a quadratic dependence of thermal lens signal strength vs input laser energy. The occurrence of instantaneous TPA is less probable in

the present context, since we are using ns laser pulses for pumping. So triplet state absorption via sequential two photon absorption is the process behind the observation of slope 2 in the log – log plots. Hence thermal lensing studies in fullerenes lead to the conclusion sequential TPA (RSA), which gives a value of slope 2 is playing the leading role in the optical limiting properties of C_{60} and C_{70}.

Contrary to expectations, pulsed photoacoustics studies show a linear dependence of PA signal as a function of laser energy. This leads to the conclusion that two step processes are absent. We expect that the unpredictable observation of linearity in PA signal with laser energy is due to our PA cell configuration. Being of a path length 4.5 cm, and due to nonuniformity of the spot size in the optical path in the sample solution, measured PA signals could be misleading.

7.7 References

[1] H. W. Kroto, J. R. Heath, S. C. O. Brien, R. F. Curl and R. E. Smalley, *Nature* **318**, 162 (1985).

[2] E. Osawa, *Kagaku (in Japaneese)* **25**, 854 (1970).

[3] E. Osawa, *Chem. Abstr.*, **74**, 75698v (1971).

[4] W. Krätschmer, L. D. Lamb, K. Fostiropoulos and D. R. Huffmann, *Nature*, **347**, 354 (1990).

[5] S. S. Harilal, R. C. Issac, C. V. Bindhu, V. P. Nampoori and C. P. G. Vallabhan, *Pramana - J. Phys.*, **49**, 317 (1997).

[6] S. S. Harilal, C. V. Bindhu, R. C. Issac, V. P. Nampoori and C. P. G. Vallabhan, *J. Appl. Phys.*, **82**, 2140 (1997).

[7] S. S. Harilal, C. V. Bindhu, V. P. Nampoori and C. P. G. Vallabhan, *Appl. Phys. Letts.*, **72**, 167 (1998).

[8] S. S. Harilal, R. C. Issac, C. V. Bindhu, V. P. Nampoori and C. P. G. Vallabhan, *Jap. J. Appl. Phys.*, **36**, 134 (1997).

[9] E. A. Rohlfing, *J. Chem. Phys.*, **89**, 6103 (1988).

[10] C. P. Safvan, F. A. Rajgara, V. Bhardvaj, G. R. Kuamr, D. Mathur, *Chem. Phys. Letts.*, **255**, 25 (1996).

[11] S. W. McElvany, M. M. Ross, and J. H. Callahan, *Acc. Chem. Res.*, **25**, 162 (1992).

[12] R. E. Smalley, *Acc. Chem. Res.*, **25**, 98 (1992).

[13] S. S. Harilal, R. C. Issac, C. V. Bindhu, V. P. Nampoori and C. P. G. Vallabhan, *J. Appl. Phys.*, **80**, 3561 (1996).

[14] S. S. Harilal, R. C. Issac, C. V. Bindhu, V. P. Nampoori and C. P. G. Vallabhan, *J. Appl. Phys.* **81**, 3637 (1997).

[15] S. S. Harilal, R. C. Issac, C. V. Bindhu, V. P. Nampoori and C. P. G. Vallabhan, *Plas. Sour. Sci. Tech.*, **6**, 317 (1997).

[16] W. R. Creasy and J. T. Brenna, *J. Chem. Phys.*, **92** 2269 (1990).

[17] W. R. Creasy and J. T. Brenna, *Chem. Phys.*, **126** 453 (1988).

[18] E. E. B. Cambel, G. Ulmer, B. Hasselberger, H. G. Busmann, and I. V. Hertel, *Chem. Phys.*, **93**, 6900 (1990).

[19] B. Hasselberger, H. G. Busmann, and E. E. B. Cambel, *Appl. Surf. Sci.*, **46**, 272 (1990).

[20] E. E. B. Cambel, G. Ulmer, H. G. Busmann, H. G. Hertel and I. V. Hertel, *Chem. Phys. Lett.*, **175** 505 (1990).

[21] M. J. Rosseinsky, A. P. Ramirez, S. H. Glarum, D. W. Murphy, R. C. Haddon, A. F. Hebbard T. T. M..Palstra, A. R. Kortan, S. M. Zahurak and A. V. Makhija, *Phys. Rev. Lett.*, **66**, 2830 (1991).

[22] C. H. Lee, G. Yu, D. Moses and A. J. Heeger, *Appl. Phys.Lett.*, **65**, 664 (1994).

[23] V. Blank, M. Popov, S. Buga, S. Davydov, V. N. Denisov, A. N. Ivlev, B. N. Mavrin, V. Agatonov, R. Ceolin, H. Szwarc, A. Rassat, *Phys. Letts. A* **188**, 281 (1994).

[24] A. Hamed, H. Rasmussa and P. H. Hor, *Appl. Phys. Lett,* **64**, 526 (1994).

[25] L. Zhu, S. Wang, Y. Li, Z. Zhang, H. Hou and Q. Qin, *Appl. Phys. Lett.*, **65**, 702 (1994).

[26] R. E. Smalley, *Chem. Eng. News,* **63**, 20 (1985).

[27] R. F. Curl, and R. E. Smalley, *Sci. Amer.*, (October) 32 (1991).

[28] H. W. Kroto, A. W. Allaf and S. P. Balm, *Chem. Rev.*, **91**, 1213 (1991).

[29] P. M. Allemand, A. Koch, E. Wudl, Y. Rubin, F. Dieddrich, M. M. Alvarez, S. J. Anz, and R. L. Whetten, *J. Amer. Chem. Soc.*, **113**, 1050 (1991).

[30] R. D. Johnson, G. Meijer, J. R. Salem, and D. S. Bethune, *J. Amer. Chem. Soc.*, **113**, 3619 (1992).

[31] P. W. Fowler, J. E. Cremona and J. I. Steer, *Theor. Chim. Acta,* **73**, 1 (1988).

[32] T. G. Schmalz, W. A. Seitz, D. S. Klein and G. E. Hite, *J. Amer. Chem. Soc.*, **110**, 1113 (1988).

[33] D. Bakowies and W. J. Thiel, *Amer. Chem. Soc,* **113**, 3704 (1991).

[34] K. C. Rustagi, *Ind.J.Phys.,* **67**A, 493 (1993).

[35] R. V. Bensasson, E. Bienvenue, M. Dellinger, S. Leach and P. Seta, *J. Phys. Chem.*, **98**, 3492 (1994).

[36] Y. Sun and C. E. Bunker, *J. Phys. Chem.*, **97**, 6770 (1993).

[37] Z. H. Kafafi, J. R. Lindle, R. G. S. Pong, F. J. Bartoli, L. J. Lingg and J. Milliken, *Chem. Phys. Letts.*, **188**, 492 (1992).

[38] E. Shin, J. Park, M. Lee, D. Kim, Y. D. Suh, S. I. Yang, S. M. Jin and S. K. Kim, *Chem. Phys. Letts.*, **209**, 427 (1993).

[39] X. Kwang, T. G. Zhang, W. P. Lin, S. Z. Liu, G. K. Wong, M. M. Kappes, R. P. H. Chang and J. B. Ketterson, *Appl. Phys. Letts.,* **60**, 610 (1992).

[40] L. W. Tutt and A. Kost, *Nature* **356**, 225 (1992).

[41] J. N. Arbogast, A. P. Darmanyan, C. S. Foote, Y. Rubin, F. N. Diedelich, M. M. Alvarez, S. J. Anz and R. L. Whetten, *J. Phys. Chem.*, **95**, 11 (1991).

[42] R. J. Sension, C. M. Philips, A. Z. Szarka, W. J. Romanow, A. R. Mcuhie, J. P. McCauley Jr., A. B. Smith III and R. M. Hochstrasser, *J. Phys. Chem.*, **95** 6075 (1991).

[43] S. D. Sibley, S. M. Argentine and A. H. Francis, *Chem. Phys. Letts*, **188**, 187 (1992).

[44] A. Andreoni, M. Bondoni and G. Consolati, *Phy. Rev. Letts.*, **72**, 844 (1994).

[45] D. Kim and M. Lee, *J. Amer. Chem. Soc.*, **114**, 4429 (1992).

[46] L. W. Tutt and T. F. Boggess, *Prog. Quant. Elect.*, **17**, 299 (1993).

[47] M. P. Joshi, S. R. Mishra, H. S. Rawat, S. C. Mehendale and K. C. Rustagi, *Appl. Phys. Letts.*, **62**, 1763 (1993).

[48] S. R. Mishra, H. S. Rawat, M. P. Joshi, and S. C. Mehendale, *Appl. Phys. A*, **63**, 223 (1996).

[49] D. G. McLean, R. L. Sutherland, M. C. Brant, D. M. Brandelik, P. A. Fleitz and T. Pottenger *Opt. Lett.*, **18** 858 (1993).

[50] S. R. Mishra, H. S. Rawat, M. P. Joshi, and S. C. Mehendale, *J. Phys. B.* **27**, L157 (1994).

[51] E. W. V. Stryland, E. Vanherzeele, K. A. Woodall, M. J. Soilleau, A. L. Smirl, S. Guha, T. F. Boggess, *Opt. Engg.*, **24**, 613 (1985).

[52] E. W. V. Stryland, Y. Y. Wu, D. J. Haga, M. J. Soilleau, and K. Mansour, *J. Opt. Soc. Amer.*, B5,1980 (1988).

[53] G. S. He, G. C. Xu, P. N. Prasad, B. A. Reinhardt, J. C. Bhatt and A. G. Dillard, *Opt. Letts.*, **435**, 20 (1995).

[54] G. S. He, J. D. Bhawalkar, C. F. Zhao and P. N. Prasad, *Appl. Phys. Letts.*, **67** 2433 (1995).

[55] G. S. He, L. Yuan, J. D. Bhawalkar, and P. N. Prasad, *Appl. Phys. Letts.*, **67** 2433 (1995).

[56] D. J. Harter, M. L. Shand and Y. B. Band, *J. Appl. Phys.*, **56**, 865 (1984).

[57] K. P. J. Reddy, *Curr. Sci.*, **61**, 520 (1991).

[58] J. A. Hermann, *Opt. Acta*, **32**, 541 (1985).

[59] J. A. Hermann and P. B. Chapple, *Proc. SPIE*, **1307**, 401 (1990).

[60] R. C. C. Leite, S. P. S. Porto and T. C. Damen, *Appl. Phys. Letts.*, **10**, 100 (1967).

[61] S. S. Harilal, R. C. Issac, C. V. Bindhu, V. P. Nampoori and C. P. G. Vallabhan, *Mod. Phys. Letts. B*, **10**, 1103 (1996).

[62] Y. Sun, Q. Gong, S. Yang, Y. H. Zou, L. Fei, X. Zhou and D. Qiang, *Opt. Commn.*, **102**, 205 (1993).

[63] A. Kost, L. W. Tutt, M. B. Klien, T. K. Dougherty and W. E. Elias, *Opt. Letts.*, **18**, 334 (1993).

[64] S. Couris, E. Koudoumas, A. A. Ruth, and S. Leach, *J. Phys. B.*, **28**, 4537 (1995).

[65] Z. Zhang, D. Wang, P. Ye, Y. Li, P. Wu, and D. Zhu, *Opt. Letts.* **17**, 973 (1992).

[66] D. Neher, G. I. Stegeman, F. A. Tinker, and N. Peyhambarian, *Opt. Letts.*, **17**, 1491 (1992).

[67] E. Koudoumas, F. Dong, M. D. Tzazadaki, S. Couris and S. Leach, *J. Phys. B.*, **29**, L773 (1996).

[68] F. N. Diederich and R. L. Whetten, *Acc. Chem. Res.*, **25** 119 (1992).

[69] V. V. Golovlev, W. R. Garrett and C. H. Chen, *J. Opt. Soc. Amer. B*,**13**,2801(1996).

[70] J. W. Arbogast and C. S. Foote, *J. Amer. Chem. Soc.*, **113**, 8886 (1991)

[71] Y. Kojima, T. Matsuoka, N. Sato and H. Takahashi, *Macromolecules*, **28**, 2893 (1995).

[72] P. Sathy, R. Philip, V. P. N. Nampoori and C. P. G. Vallabhan, *J. Phys. B.*, **25**, 155 (1992).

[73] C. V. Bindhu, S. S. Harilal, R. C. Issac, V. P. Nampoori and C. P. G. Vallabhan, *Pramana - J. Phys.*, **44**, 231 (1995).

[74] S. S. Harilal, R. C. Issac, C. V. Bindhu, V. P. Nampoori and C. P. G. Vallabhan, *Mod. Phys. Letts.*, **9**, 871 (1995).

[75] A. J. Twarowski and D.S. Kliger, *Chem. Phys.*, **20**, 253 (1977).

[76] A. J. Twarowski and D.S. Kliger, *Chem. Phys.*, **20**, 259 (1977).

[77] *See* Chapter 4 of this thesis.

[78] M. Terazima and T. Azumi, *Chem. Phys. Letts.*, **141**, 237 (1987).

[79] M. Terazima and T. Azumi, *Chem. Phys. Letts.*, **153**, 27 (1988).

[80] M. Terazima and T. Azumi, *Chem. Phys. Letts.*, **173**, 327 (1990).

[81] M. Terazima, N. Hirota, H. Shimohara and Y. Saito, *J. Phys. Chem.*, **95**, 9081 (1991).

[82] J. Hein, H. Bergner, M. Lenzner and S. Rentsch, *Chem. Phys.*, **179**, 543 (1994).

[83] B. L. Lawrence, W. Cha, S. Baker and F. Kajzar, *Appl. Phys. Lett.*, **64**, 2773 (1994).

[84] A. M. Bonch-Bruevich, T. K. Razumova and I. O. Starobogatov, *Opt. Spectrosc.*, **42** 45 (1977).

Chapter 8

Use of Pulsed Photoacoustic Technique for the Study of Nonlinear Processes in Liquids

Pulsed photoacoustic measurements have been carried out in toluene, benzene and carbon disulphide liquids using 532 nm radiation from a Q-switched frequency doubled Nd:YAG laser. The present chapter deals with the detection and analysis of the photoacoustic effect in certain organic liquids in the visible region. The variation of photoacoustic signal amplitude with incident laser power indicates the involvement of the multiphoton absorption in the generation of photoacoustic signal. The studies made here demonstrate that pulsed photoacoustic technique is a simple and effective toll for the investigation of multiphoton processes in liquids.

8.1 Introduction

INTERNATIONAL SCHOOL OF PHOTONICS LIBRARY

The term two photon absorption (TPA) is used to designate a process in which a molecule simultaneously absorbs two photons, neither of which is resonant with a transition to an accessible stationary state, and reaches a state whose energy is the sum of the energies of the two photons. The existence of such processes was predicted theoretically by Maria Goeppert-Mayer in 1931 [1]. However,the experimental observation requires very intense light sources, and did not become practical until the invention of the laser. Also the advancement in the area of signal processing and data acquisition techniques has given further impetus to these studies. Much more extensive studies of TPA as a useful spectroscopic phenomenon took place since dye lasers have become available. These are able to provide both the high intensities required for TPA absorption and the tunability over a wide range of wavelengths necessary for spectroscopy. A good review by Peticolas [2] summarizes the early work on two-photon processes such as Raman spectroscopy, three-photon absorption, and harmonic generation.

Direct optical absorption measurements, so common in one photon spectroscopy, are not quite suitable in these investigations due to the extremely small values of multiphoton absorption cross section. Multiphoton processes are usually investigated using alternate techniques like two/three photon induced fluorescence emission. Manyphoton phenomena in liquids and solids are much less investigated as compared to these in gases. Phenomena like multiphoton ionization (MPI) in condensed phase are of considerable importance not only as a means of detecting nonlinear absorptions, but also because it describes charge separation mechanism in condensed media.

The identification and analysis of multiphoton absorption (MPA) in nonlinear optical media have been mostly based on either the observation of radiative transitions [3-5] or on the variation in the transmitted beam intensity [6, 7]. However, the latter technique is not very sensitive in all cases especially where variation in transmitted intensity due to MPA is small, while the former is useful only in samples having large fluorescence quantum yield. Measurements of thermo-optic effect is an alternate method to identify MPA in nonlinear media where probability of nonradiative relaxation of excited molecules is large. Of the various thermo-optic phenomena, photoacoustic (PA) and thermal lens effects are the two widely employed tools to detect very weak processes like manyphoton absorption [8-12].

There has been considerable interest in the possibility of using photoacoustic technique for investigating optical absorption processes in liquids. This interest is stimulated by two

problems that cannot be effectively studied by conventional spectrofluorometry: (i) the accuracy in the measurement of a weakly absorbing solution and (ii) the analysis of highly light scattering liquid systems such as suspensions. The problem of dealing with low absorption solutions has been partially resolved by the use of fluorescence techniques [13]. However, in trace analysis, the analytical procedure often involves the use of a nonfluorescent highly absorbing indicator for the substance to be measured. Here fluorometry is not possible, and conventional spectrophotometric analysis permits a sensitivity of $10^{-3}cm^{-1}$. In the mean time the problem of highly scattering solutions is still not well resolved.

PA effect can provide useful information regarding the multiphoton processes [10]. The advantages of employing PA technique for characterizing various molecular processes have been extensively discussed earlier [14, 15]. The method relies essentially on the study of acoustic waves generated in the sample due to nonradiative transitions following the absorption of light energy. Eventhough PA approach has become an accepted method to study thermal and optical properties of materials [16, 17] during the last two decades, not much work has been reported in utilizing this effect to investigate multiphoton processes, especially in organic molecules, where efficient nonradiative relaxations $S_n \rightarrow S_1$ release a significant amount of thermal energy into the medium [18, 19].

Of the several configurations of PA measurements it has been demonstrated that pulsed PA technique [20-22] is very effective to detect such optical phenomena since one can have sufficient photon flux to induce nonlinear effects in the medium and the pulsed PA technique is found to have higher sensitivity as compared to the continuous wave (cw) modulation schemes. Because of higher average powers, finer spectral resolution and sensitivity advantages of lock-in detection, chopped cw sources are most often used for linear absorption spectroscopic measurements. However, there are certain advantages that occur from using a pulsed light source coupled with real-time detection of the acoustic signal. One advantage is built-in discrimination against window background signals. With proper positioning of the detector, sample signals arrive before those generated by the windows, which in turn can be discriminated with a gated integrator (boxcar averager). Pulsed excitation sources seem to enhance the detection sensitivity when dealing with condensed phases. Shorter excitation pulses minimise the loss of heat from a solid sample through conduction. Another advantage is that nonradiative relaxation rates can be measured using excitation pulses of sufficiently short duration. The rise of the acoustic signal gives a direct measure of the rate of energy transfer into translational degrees of freedom.

High light intensities are normally required to observe nonlinear interactions of electro-

magnetic radiation with matter. This requires the use of an intense pulsed laser source for PA measurements of nonlinear phenomena [23] like two photon absorption processes. Because TPA is a second order process, absorption cross sections are small, making PA detection, with its high sensitivity, ideal for such nonlinear optical phenomena. PA detection of several nonlinear optical processes have been reported, including two-photon (and higher order) electronic absorption, IR multiphoton absorption and stimulated Raman scattering. Several other workers have performed work on multiphoton absorption spectroscopy with PA detection, like Fukumi in ethylene [24], Brenner et al in propynal [25], Webb et al in syntriazine [26], Weulersse and Geneir in CF_3I [27], Chin et al in gases [28] and Bass et al in solids [29]. In their pioneering experiments, Tam and Patel [30] measured the TPA cross-sections in benzene for the first time. Also pulsed PA technique has recently been used to study two photon absorption (TPA) process in certain laser dyes [8, 18] as well as in organic vapours [9]. Since organic liquids like toluene, benzene and carbon disulphide (CS_2) are extensively used for various technical applications such as solvents for fullerenes etc., the nonlinear properties of these solvents become a subject of great importance. Considerable interest exists in the study of multiphoton processes in these molecules as it throws much light on the nature of energy levels and other aspects like interstate coupling and molecular relaxations.

If the laser intensity is sufficiently high, multiphoton absorption can occur, and the PA signal q(ν) generated in an absorbing liquid due to multiphoton absorption is given by [31]

$$q(\nu) \propto [I(\nu)]^m \tag{8.1}$$

where I(ν) is the incident laser intensity and m is the number of photons absorbed. If the photoacoustic signals are generated in a sample due to two photon absorption and the subsequent nonradiative relaxation, then these signals will have a quadratic dependence on pump intensity. Hence by monitoring the dependence of PA signals on pump laser power one can identify the occurrence of nonlinear absorptions taking place, if any, in the sample.

8.2 Experimental Setup

The details of the experimental set up are given in chapter 2. Briefly, the second harmonic output beam (532 nm) from a Q-switched Nd:YAG laser was focused by a convex lens (focal length 5 cm) into the PA cell containing carbondisulphide (spectroscopic grade) liquid at room temperature (24^0C). The lens position is adjusted so that the beam focus is at the centre of the cell. A dichroic filter oriented at 45^0 to the beam axis separates the fundamental

frequency component (1064 nm) from the second harmonic. The laser was operated at a repetition frequency of 10 Hz. The incident power is monitored by a laser power meter and the transducer output was observed on a 200 MHz digital storage oscilloscope. The averaged amplitude of the first pulse in the PA signal trace is monitored as a function of the laser power.

8.3 Results and Discussion

The present studies deal with the multiphoton absorption processes in liquid benzene, toluene and carbon disulphide using pulsed PA technique. The PA effect is a phenomenon where acoustic waves originate from the nonradiative part of the energy released in the decay of a molecule from an excited state induced by the laser pulses. It must be noted here that none of the above organic liquids has any absorption at 532 nm. However two photon absorption and higher multiphoton absorption is a possibility at this wavelength in these liquids. The PA effect has been utilized to investigate multiphoton processes in these organic molecules where efficient non-radiative relaxations $S_n \rightarrow S_1$ release a significant amount of thermal energy into the medium.

It may be relevant here to note that pulsed PA generation in liquids is rather a complex phenomenon, which might have its origin from different mechanisms, of which the prominent ones are thermoelastic expansion, vapourization and dielectic breakdown [31,32]. While the relative probabilities of each of these mechanisms depend on the input laser flux, it has been shown that the temporal profile of resulting acoustic pulse differs in each case permitting identification of the particular process. Secondly, the variation of optical absorptivity of the sample with concentration results in a change of the 'acoustic source geometry so that the distribution of the acoustic energy in the PA cell can be spherical, cylindrical or planar in different situations. However, in all these cases it is shown that the thermoelastic generation will result in the radiation of a dipolar acoustic pulse [33]. For all the samples we studied the PA signal profile was essentially dipolar nature.

8.3.1 TPA Studies in Toluene

Eventhough TPA in toluene has been reported earlier [34], in this section we demonstrate pulsed PA as an effective and versatile technique to study MPA in liquids. Fig. (8.1) shows the oscilloscope trace of the PA signal produced in toluene. The acoustic signal exhibits a delay of 12 μs with respect to the pump pulse which corresponds to the propagation time

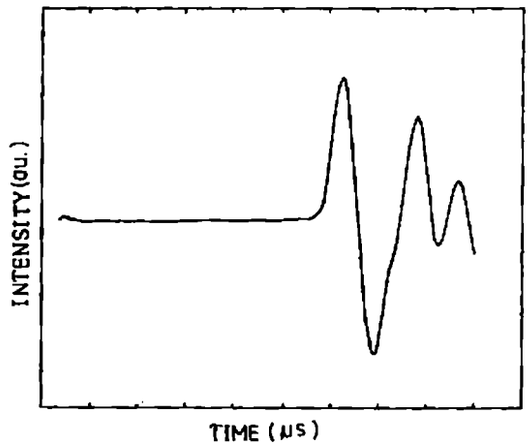

Figure 8.1: A typical PA signal trace observed on the oscilloscope for toluene. The horizontal scale is $2\mu s/div$

of the acoustic signal from the focal region to the piezoelectric detector. This time interval corresponds to the velocity of 1275 m s^{-1} which is comparable with the reported value (1300 m s^{-1}) of ultrasonic velocity [35] in toluene. From eqn. (8.1) it is clear that TPA process requires a slope two for the log -log plot of PA signal strength against laser energy. Fig. (8.2) shows such a plot obtained in the present case. As is clear from figure (3), the slope of log -log plot is nearly unity at low laser energy region whereas the slope changes to $\simeq 2$ at higher laser energies. This shows that at lower laser energies, the optical absorption phenomenon is essentially mediated by one photon process (OPA) while at higher laser energies TPA is favoured.

One photon process in toluene can be explained on the basis of overtone excitation of toluene molecule. CH stretching vibration in toluene has a fundamental frequency (ω_e) at 3100 cm^{-1} with anharmonicity parameter ($\omega_e x_e$) 65cm^{-1}. The sixth overtone corresponding to $\Delta v=7$ in toluene lies at 529 nm which is very near to the pump wavelength 532 nm. Thus at lower laser energy excitation of 6th overtone of CH vibration in toluene takes place through OPA resulting into a PA signal which varies linearly with incident laser energy.

Electronic spectrum of toluene shows a sharp UV band at 274 nm corresponding to $^1A_{1g}$-$^1B_{2u}$ transition which nearly coincides with two photon energy at 532 nm radiation [36]. At

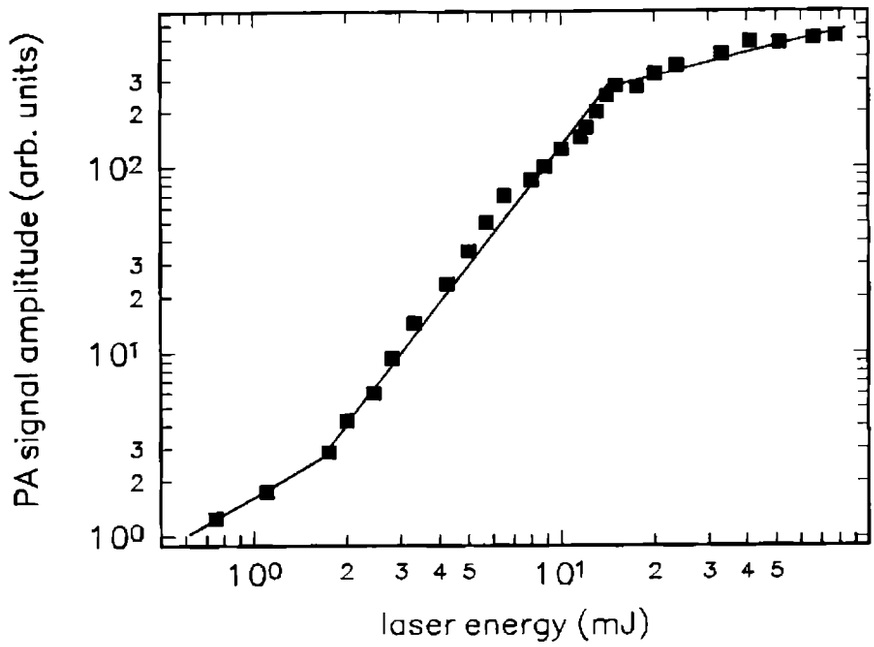

Figure 8.2: Log - log plot of laser energy against PA amplitude for toluene solution

higher laser energies, toluene molecules are excited to $^1B_{2u}$ state through TPA. The nonradiative relaxation which follows this process produces the PA signal with characteristic slope two in the log - log plot.

8.3.2 TPA Studies in Benzene

The multiphoton absorption of benzene with incident laser radiation in the near UV has been examined in a number of studies [38, 39, 40]. Nonlinear absorption studies had been performed in benzene by means of multiphoton ionization (MPI) [38]. An initial report of its MPI appeared in 1978 although the mechanism was not examined in detail. This was followed by work by Scott et al. [39, 40] where it was shown how blue and near UV light ionizes pure liquid benzene by a three photon path in which a TPA is followed by a one photon ionization of a real metastable state of the liquid. It is well known that the PA signal q αI^m where I is the incident photon energy. Log-log plot of q vs I will give the slope n corresponding to the number of photons taking part in the multiphoton process. The log -log plot of photoacoustic signal against laser energy for benzene is given in fig.(2.3).

Two separate break points are distinctly observed in the log -log plots. From the nature of these log-log plots, the role of many photon processes in the generation of PA signal in the sample becomes clearly evident. It is obvious that the various photophysical and

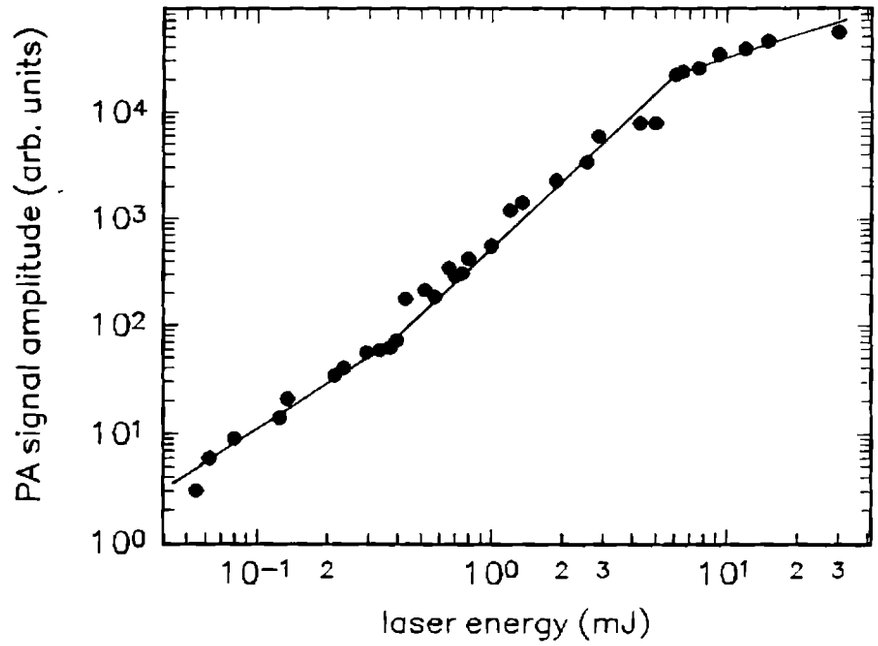

Figure 8.3: Log-log plots of photoacoustic signal strength against laser energy for benzene

photochemical processes involved are distinctly different for various ranges of incident pulse energies. The PA signal increases moderately at low laser energies and rises abruptly at the first break point. The threshold laser energy density for the process is found to be different for toluene (1.8 mJ) and for benzene (0.4 mJ). We have observed that the threshold for benzene is lower than that for toluene while reverse in the case reported by Tsuboi and co-workers [19]. This is because two photon absorption cross section for benzene is larger than that for toluene at 532 nm, while reverse is the case for one photon process at 248 nm. The slope of the log-log plot of the PA signal vs pulse energy after the first break point is found to be $\simeq 2$ for benzene which shows the involvement of two photon processes in the media. A second break point after which the PA signal increase gradually is found in the case of polymer ablation [37].

8.3.3 Multiphoton Absorption Studies in CS_2

Since the initial report of multiphoton ionization (MPI) in benzene by Vaida et. al. [38] many more studies have appeared in literature, mostly pertaining liquid benzene [39, 40]. Some works on MPI of CS_2 are also available in literature [41-44]. All the above studies on CS_2 have been carried out using molecular beam and excimer laser as excitation source. Also they use either multiphoton fluorescence technique or microwave absorption by free radical

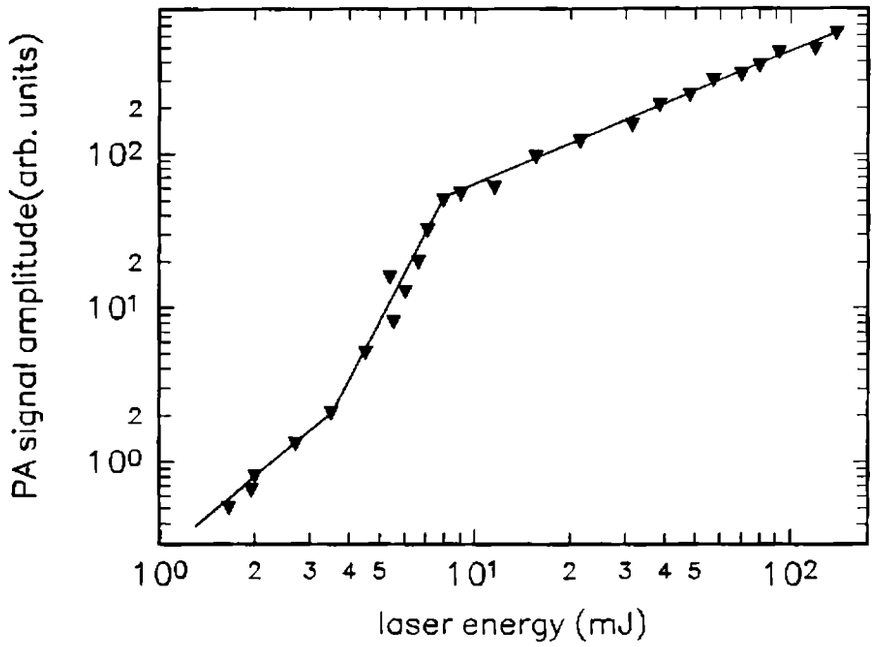

Figure 8.4: Log-log plot of PA signal strength with laser energy for carbon disulphide

produced due to ionization. The multiphoton process in CS_2 are even more diverse and less clearly understood. The photochemistry of CS_2 is sensitive to wavelength of photolysis.

The photodissociation dynamics of CS_2 molecule have been investigated in the VUV-UV wavelength regions using various techniques. These include the conventional flash photolysis technique [45, 46, 47] and ArF laser photolysis with product analysis by time of flight mass spectrum [48, 49], laser induced fluorescence [50] and atomic resonance fluorescence. Photodissociation of CS_2 with 308 nm is reported with the products S atoms in various energy states [51]. Sapers and Donaldson [52] have studied the CS radical ground state vibrational energy distributions which they found to be inverted and bimodal. It has been observed in the 193 nm photodissociation of CS_2 molecule that S atom is formed in the ground and excited $^1D_2$ states [42]. Photodisscociation of CS_2 in the region 285-305 nm have shown the formation of S atoms in the 3P, ^1D and ^1S states [44]. The nature of two photon excited states and the dissociation mechanism has also been reported. Here we present photoacoustic observation of multiphoton induced photodissocition of CS_2 liquid. Log-log plot of PA signal strength vs laser energy for CS_2 is given in fig. 8.4. The plot has three parts (a) lower power region in which slope is $\simeq 2$, (b) medium power region in which slope is $\simeq 4.5$ and (c) high power region where the slope comes to a value below 2 and saturates. The above results clearly indicate the role of many photon processes in the generation of PA signal from the sample

(CS_2). Thus we can attribute two, four and five photon process in the generation of PA signal from CS_2 with 532 nm excitation. A nonradiative component of de-excitation is essential for the generation of PA signal in a sample following the multiphoton absorption. Accordingly, ionization or dissociation of molecules can lead to thermo-optic effect and hence a PA signal. We may consider the following as the most likely processes taking place in the present case.

In the low laser energy region, CS_2 dissociation can be attributed to breaking of SC-S bond following the scheme [42]

$$CS_2 + 2h\nu \rightarrow CS(X^1\Sigma^+) + S(^3P_2) \tag{8.2}$$

corresponding to 4.46 eV which matches with two photon energy of 532 nm radiation. Absorption of two photons at 532 nm excites the CS_2 molecules leading to production of $CS(X^1\Sigma^+)$ and sulphur atoms in the $^3P_2$ states ($^3P_2$ being the ground state of sulphur atoms). However, as described by Hardwick et. al. [41], the above process is not a spin allowed process. The first spin allowed process is

$$CS_2 \rightarrow CS(X^1\Sigma^+) + S(^1D) \tag{8.3}$$

which requires 5.687 eV that does not match with either two photon or three photon processes. The present observation of the clear signature of two photon process favours the dissociation of CS_2 into $CS(X^1\Sigma^+)$ and $S(^3P_2)$. It should be remembered that selection rule corresponding to spin conservation are not as strong as other selection rules, especially in the condensed phase.

The observation of slope $\simeq 4.5$ at higher laser energies indicate both four photon and/or five photon processes corresponding to 8.8 eV and 11.3 eV respectively [53].

$$CS_2 + 4h\upsilon \rightarrow CS(a^3\Pi) + S(^3P_2) \tag{8.4}$$

This process is energetically favoured four photon process. By absorbing four photons at 532 nm, CS_2 molecules are excited to 3d Rydberg states $^1\Delta_u^7$ which predissociates giving sulphur atoms in the $^3P_2$ state and CS in the excited state ($a^3\Pi$).

At higher incident laser energies CS^+ can be produced by ionizing CS by absorbing five photons. *ie.*,

$$CS + 5h\nu \rightarrow CS^+ + e^- \tag{8.5}$$

This corresponds to an energy of 11.3 eV.

Decrease in the value of slope at still higher laser energy region indicates a saturation effect. Similar saturation effect was observed by Siomons and co-workers [54] in the study of pyrene solution in hexane.

8.4 Conclusions

Pulsed Photoacoustic studies have been carried out in toluene, benzene and carbon disulphide liquids using 532 nm, 9 ns pulses from a frequency doubled Nd:YAG laser. In this chapter we have demonstrated the effectiveness and utility of pulsed PA technique for the study of nonlinear optical processes in these liquids. We have also demonstrated the occurrence of different multiphoton processes in liquid CS_2 using pulsed PA techniques. The nature of variation of PA signal amplitude with laser power clearly confirms the occurrence of multiphoton absorption in these liquids at 532 nm. PA technique is an effective tool to investigate the spectroscopy of atoms, molecules as well as condensed matter. The high sensitivity of the technique helps in studying very weak processes like overtone absorption, multiphoton absorption, forbidden transitions, trace detection etc.

8.5 References

[1] M. Göppert-Mayer, *Ann. Phys. Lpz.*, **9**, 273 (1931).

[2] W. L. Peticolas, *Ann. Rev. Phys. Chem.*, **18**, 233 (1967).

[3] N. Mikami and M. Ito, *Chem. Phys. Letts.* **31**, 472 (1975).

[4] H. L. B. Tang, R. J. Thrash and U. E. Luoi, *Chem. Phys. Letts.*, **57**, 59 (1978).

[5] C. Rulliere and P. Kottis, *Chem. Phys. Letts.*, **75**, 478 (1980).

[6] A. Penzkofer, W. Falkenstein and W. Kaiser, *Appl. Phys. Letts.*, **28**, 319 (1979).

[7] P. R. Monson and W. M. McClain, *J. Chem. Phys.*, **53**, 29 (1970).

[8] P. Sathy, R. Philip, V. P. N. Nampoori and C. P. G.Vallabhan, *Opt. Commn.*, **74**, 313 (1990).

[9] A. V. Ravi Kumar, G. Padmaja, V. P. N. Nampoori and C. P. G. Vallabhan, *Pramana - J. Phys.* **33**, L621 (1989).

[10] P. Sathy, R. Philip, V. P. N.Nampoori and C. P. G. Vallabhan, *J. Phys. D*, **27**, 2019 (1994).

[11] A. J. Twarowski and D. S. Kliger, Chem. Phys., **20**, 253 (1977).

[12] A. J. Twarowski and D. S. Kliger, Chem. Phys., **20**, 259 (1977).

[13] W. M. Fairbank, T. W. Hansch and A. L. Schalow, *J. Opt. Soc. Amer.*, **65**, 199 (1975).

[14] A. C. Tam, *Rev. Mod. Phys.*, **58**, 381 (1986).

[15] D. J. Moll, G. R Jr Parker and A. Kupperman, *J. Chem. Phys.*, **80**, 4800 (1984).

[16] S. S. Raman, V. P. N. Nampoori and C. P. G Vallabhan, *Mat. Sci. Letts.*, **15**, 230 (1996).

[17] S. S. Raman, V. P. N. Nampoori and C. P. G Vallabhan, *Appl. Phys. Letts.*, **67**, 2939 (1995).

[18] R. Philip, P. Sathy, V. P. N. Nampoori and C. P. G. Vallabhan, *J. Phys. B*, **25**, 155 (1991).

[19] . Y. Tsuboi, K. Hatanaka, H. Fukumura and H. Masuhara, *J.Phys.Chem.*, **98**, 11237 (1994).

[20] C. K. N. Patel and A. C. Tam, *Rev.Mod.phys.*, **53**, 517 (1981).

[21] W. Lahman and H. J. Ludwig, *Chem. Phys. Letts.*, **45**, 177 (1977).

[22] C. K. N. Patel and A. C. Tam, *Nature*, **280**, 302 (1979).

[23] A. C. Tam, *Rev. Mod. phys.*, **58**, 381 (1986).

[24] T. Fukumi, *Opt.Commn.*, **30**, 351 (1979).

[25] D.M. Brenner, K. Brezinsky and P.M. Curtis, *Chem.Phys.Letts.*, **72**, 202, (1980).

[26] J.D. Webb, K.M. Swift and Bernstein, *J.Chem.Phys.*, **73**, 4891 (1980).

[27] J.M. Weulersse and R. Genier, *Appl.Phys.*, **24**, 363 (1981).

[28] S.L.Chin, D.K. Evans, Mc Alpine and W.N. Selander, *Appl. Opt.*, **21**, 65 (1982).

[29] M.Bass, E.W. Van Stryland and A.F. Steward, *Appl.Phys.Letts.*, **34**, 142 (1979).

[30] A.C.Tam and C.K.N. Patel, *Nature*, **280**, 304 (1979).

[31] A. Rosencwaig, *Photoacoustics and photoacoustic spectroscopy*, Wiley, New York (1980).

[32] D. A. Hutchins, *Can. J. Phys.*, **64**, 1247 (1986).

[33] D. A. Hutchin and A. C. Tam, *IEEE Trans. Ultrason. Ferroelec. Frew. Control*, **33**, 429 (1986).

[34] R.L. Swofford and J.A. Morrell, *J.Appl.Phys.*, **49**, 3667 (1978).

[35] E. G. Richardson, *Ultrasonic Physics*, (ed) A. E. Brown, Elsevile publishing company, New York (1962).

[36] C. N. R. Rao, *Ultraviolet and Visible Spectroscopy - Chemical Applications*, Butterworth and company, London (1967).

[37] A. D. Zweig, V. Venugopalan and T. F. Deutsch *Laser ablation in material processing : Fundamentals and Applications*, B.Baren, J.J.Dubowski, D.P.Norton (Ed.) (Material Research Society, Pennsylvania 1993).

[38] T. Vaida, M. Robin and N. A. Kuefler, *Chem. Phys. Letts.*, **58**, 557 (1978).

[39] T. W. Scott, A. J. Twarowski and A. C. Albrecht, *Chem. Phys. Letts.*, **66**, 1 (1979).

[40] T. W. Scott and A. C. Albrecht, *J. Chem. Phys.*, **74**, 3807 (1981).

[41] J. L. Hardwick, Y. Ono and J. T. Moseley, *J. Phys. Chem.*, **91**, 4506 (1987).

[42] S. C. Yang, A. Freedman, M. Kawasaki and R. Bersohn, *J. Chem. Phys.*, **72**, 4058 (1980).

[43] T. V. Venkitachalam and A. S. Rao, *Appl. Phys. B*, **52**, 92 (1991).

[44] T. V. Venkitachalam and A. S. Rao, *Spectrochim. Acta*, **48A**, 1555 (1992).

[45] A. B. Callear, *Proc. R. Soc.*, **276 A** 401 (1963).

[46] F. J. Wright, *J.Phys. Chem.*, **64**, 1648 (1960).

[47] M. De Sorgo, A.J. Yarwood, O.P. Strausz and H.E. Gunning, *Can. J.Chem.*, **43**, 1886 (1965).

[48] S.C.Yang, A. Freedman, M. Kawasaki and R. Bersohn, *J. Chem. Phys.*, **72**, 4058 (1980).

[49] V. R. McCravy, R. Lu, D. Zakheim, J. Halpern, J. Russel and W. Jackson, *J. Chem. Phys.*, **83**, 3481 (1985).

[50] J. E. Butler, W. S. Drozodoski and J. R. McDonald, *Chem. Phys.*, **50**, 413 (1980).

[51] P. Brewer, N. Van Veen and R. Bersohn, *Chem. Phys. Letts.*, **95** 126 (1982).

[52] S. Sapers and D. J. Donaldson, *Chem. Phys. Letts.*, **198**, 341 (1992).

[53] K. P. Huber and G. Herzberg, *Constants of diatomic molecules* (Van Nostrand - Reinhold, New York, 1979).

[54] K. Siomos and L. G. Christophorou, *Chem. Phys. Letts.*, **72**, 43 (1980).

Chapter 9

Summary and Conclusions

Application of thermal lens and photoacoustic phenomena have been the main theme of the present thesis. Both thermal lensing and photoacoustic technique are indirect absorption measurements. One feature which should be noted in this context is that they are both excitation techniques: that is, the net amount of energy absorbed is measured, rather than a decrease in transmitted light. Therefore, short of saturation, the signals will scale linearly with power of the incident light, indicating that high intensity light sources are most useful for thermal lensing spectroscopy. In fact, thermal lensing spectroscopy was virtually unknown until the advent of high power lasers, and photoacoustic spectroscopy has undergone an enormous resurgence since lasers have come into popular usage. It is true that both thermal and fluorescence spectroscopy are fundamentally excitation techniques. In this sense, photothermal spectroscopy is quite similar to fluorescence spectroscopy. In fact, they are complementary: thermal spectroscopy measures the photon energy which has been converted to heat, while fluorescence spectroscopy observes re-emitted photons.

Unlike conventional transmission or reflection measurements, the sensitivity of these thermo-optical methods depends on the power of the radiation used for excitation and the thermophysical properties of the sample. Solvents which exhibit a large change in refractive index with temperature, dn/dT, are advantageous since a given increase in temperature produces a large change in optical path. For continuous wave (CW) excitation, solvents of smaller thermal conductivity produce larger temperature gradients at steady state, where the rate of heating is balanced by the rate of thermal diffusion.

One of the novel applications of the thermal blooming is a new means of measuring thermal diffusivity. The method is simple and accurate. The obvious advantage of this method is that only small sample volumes are needed for making such measurements. Also only very short time is needed for completing the measurements and accurate results can be obtained with TL method. Thermal diffusivity is an important parameter in heat flow studies. A knowledge

of thermal diffusivity is useful for calculating thermal conductivity data. In our case the measured values of thermal diffusivity for standard liquids were in good agreement with the literature values. This shows that thermal lens method is very effective for measurement of thermal diffusivity. Moreover, this method presents itself as a nondestructive and noinvasive method and requires samples only in small amounts.

The thermal diffusivity measurements in seawater shows that salinity does appear to be important in determining the thermal diffusivity. Thermal diffusivity values of seawater is found to vary with depth of the sea at which the sample is collected. This observation is further supported by measurements carried out in artificial seawater. A decrease in the value of thermal diffusivity is estimated with increasing dilution of the sample. The temperature of the sea surface is determined by the rate of heat diffused from the upper layers to the deeper region and vice versa. Thus a knowledge of thermal diffusivity of seawater is of great importance in the field of oceanography.

Dye lasers are among the most useful types of lasers because of their easy tunability, wavelength coverage and simplicity. Xanthene dyes like Rhodamine 6G (Rh6G) and Rhodamine B (RhB) are a class of organic molecules which show lasing action under appropriate conditions of excitation. Hence the photophysical properties of these common laser dyes should be extensively understood. Excited state absorption (ESA) from the upper lasing level considerably reduces the number density of fluorescing molecules. ESA is an extremely important factor in all laser dyes under all excitation conditions, since it is a property of the upper level of the laser transition itself. Unlike triplet-triplet absorption, it can never be neglected under any excitation conditions. TPA is another important nonlinear optical processes which becomes relevant in laser dyes at high pump intensities. The study of TPA and higher order multiphoton excitations has been mostly based on the observation of radiative transitions induced by the same from a higher excited electronic state usually at a shorter wavelength than the pump wavelength. In organic dyes, anti-Stokes fluorescence (ASF) from higher excited singlets is extremely weak. It is in this context, the applicability of TL technique to distinguish between different nonlinear absorption processes becomes significant. The ease of the set up and procedure of the technique are very attractive for such a task. The studies presented in this thesis clearly show that the nonlinear properties of the dye molecules vary significantly with concentration and excitation intensity. At lower concentrations one photon absorption is dominant. As the concentration increases occurrence of TPA along with ESA is evident. At higher concentrations three photon processes begin to appear. The decrease in slope of the double log plot at still higher concentrations is inferred to be due to aggregate

formation.

It will be very appropriate to use thermal lens spectrometry for analyzing dimerization equilibria because this method is very sensitive and should be useful over a wide range of concentrations. The thermal lens method is more efficient to detect dimerization equilibria especially because variation of thermal energy involved in such equilibrium is generally more important than the variation of absorbance and fluorescence.

The fluorescence quantum yield values of the laser dyes measured in the present work demonstrate that fluorescence parameters are influenced by solvent effects. Our results indicate that a higher fluorescence yield is obtained for Rhodamine 6G and Rhodamine B in ethylene glycol than in methanol or water. The variation of quantum yield with solvent indicates that solvent-solute interactions play measurable role in modifying unimolecular decay constants for excited singlet electronic states. We noticed that there occurs a drastic reduction in the fluorescence quantum yield in nonlinear absorption region. Under intense illumination, higher excited states get populated via TPA or 3PA or ESA resulting in reduction of effective number of fluorescing molecules. This leads to the conclusion that dyes should be excited with power levels below which nonlinear absorption processes are negligible. For highly fluorescing materials like Rhodamines, the thermal lens method is suitable for the evaluation of quantum efficiency since it requires no standard and is very convenient and useful, especially at higher concentrations, i.e., near the fluorescence quenching regimes.

Present studies clearly reveal that for efficient operation of dye laser, there is an optimum value for the dye concentration. Choice of solvents also plays a major role. Our results indicate that ethylene glycol appears to be more suitable solvent than water or methanol. At the same time, low thermal conductivity of ethylene glycol is a disadvantage since heat dissipation will be poor in the dye solution. In this aspect, the high thermal conductivity of water makes it a fair candidate. But the high capacity for heat dissipation is paid for by the strong dimerization processes in aqueous solutions. For a better efficiency of dye lasers all these factors should be considered.

Optical limiting is one of the interesting nonlinear phenomena.

The general causes for optical limiting are Reverse Saturable Absorption (RSA), Excited State Absorption (ESA), Two Photon Absorption (TPA), Nonlinear Scattering (NLS) etc. In this thesis The optical limiting behaviour of C_{60} and C_{70} solutions in toluene was presented. A higher limiting threshold is found in C_{70} solution compared to C_{60}. The limiting properties of C_{60} is found to be better than that of the C_{70} solution. This is because of the higher ground state absorption of C_{70}. Using PA and TL techniques we have attempted to elucidate

the role of these processes in the case of optical limiting in C_{60} and C_{70}. Thermal lens signal shows a quadratic dependence on incident laser energy indicating the occurrence of nonlinear absorptions such as TPA or ESA. Under nanosecond laser excitation, fullerenes do not show instantaneous TPA so that sequential TPA (i.e., RSA) is mainly responsible for the observed optical limiting in fullerenes. The limiting behaviour was interpreted as due to the rapid $S_1 \rightarrow T_1$ intersystem crossing, in addition to the large cross section for $T_1 \rightarrow T_n$ absorption. Study of the optical transitions from S_1 or T_1 states to higher excited states is important both scientifically and in terms of application.

Contrary to our expectations, pulsed PA analysis of fullerene solutions show a linear dependence of PA signal on laser energy. This observation of linear dependence is due nonuniformity of the spot size in the optical path in the PA cell and hence the measured PA signals could be misleading.

One of the important applications of the photothermal methods finds in the study of multiphoton absorption processes occurring in liquids. By carrying out pulsed photoacoustic studies in toluene, benzene and carbon disulphide liquids using 532 nm, 9 ns pulses from the frequency doubled Nd:YAG laser, we have demonstrated the effectiveness and utility of pulsed PA technique for the study of nonlinear optical processes these liquids. The nature of variation of PA signal amplitude with laser power clearly confirms the occurrence of multiphoton absorption in these liquids at 532 nm. PA technique is an effective tool to investigate the spectroscopy of atoms, molecules as well as condensed matter. The high sensitivity of the technique helps in studying very weak processes like overtone absorption, multiphoton absorption, forbidden transitions, trace detection etc.

In summary, the work presented in this thesis shows that nonradiative processes, which forms the basis of both the thermal lensing and photoacoustic methods are as important as radiative processes. Exploitation of the photothermal techniques under appropriate conditions will be able to throw much better light on the thermal and optical properties of materials and the fundamental processes involved.

****

INTERNATIONAL SCHOOL OF
LIBRARY